



MEDICAL UNIVERSITY
OF VIENNA

A unique Schwann cell subtype contributing to keloid formation

Doctoral thesis at the Medical University of Vienna
for obtaining the academic degree

Doctor of Philosophy

Submitted by

Dr. med. univ. Martin Leopold Direder

Supervisor:

Univ.-Prof. Univ.-Doz. Dr. med. univ. Hendrik Ankersmit, MBA

Department of Thoracic Surgery

Medical University of Vienna

Währinger Gürtel 18-20

1090 Vienna, Austria

Vienna, 11/2022

Dedicated to

Marianne & Franz Preisinger

Declaration

I, Martin Leopold Direder, herewith declare, that the present thesis “A unique Schwann cell subtype contributing to keloid formation” is the result of my own scientific work and has not been submitted for any other degree or academic qualification.

The dissertation was conducted as part of the PhD program “vascular biology” at the Department of Thoracic Surgery of the Medical University of Vienna under the supervision by Univ.-Prof. Univ.-Doz. Dr. med. univ. Hendrik Ankersmit, MBA with co-supervision by Assoc. Prof. Priv.-Doz. Dr. Michael Mildner, in cooperation with the Department of Dermatology (Medical University of Vienna) and the Department of Plastic, Reconstructive and Aesthetic Surgery (Medical University of Vienna). The projects were financed by the Aposcience AG and peer reviewed third party funding as mentioned in the corresponding sections of the manuscripts.

Publications risen from this thesis include the lists of authors and indicate their explicit contribution to the respective study. The entire thesis has been authored by myself.

Table of contents

Declaration	iii
Table of contents	iv
List of figures	v
Abstract	vi
Zusammenfassung	vii
Publications arising from this thesis	viii
Abbreviations	ix
Acknowledgments	xii
1 CHAPTER ONE: INTRODUCTION	1
1.1 The human skin and its functions	1
1.2 Wound healing	3
1.2.1 The haemostasis phase	4
1.2.2 The inflammatory phase	5
1.2.3 The proliferation phase	6
1.2.4 The remodelling phase	8
1.2.5 Treatments to support proper wound healing	8
1.3 A scar is not a scar	9
1.4 Processes affecting the extent of scar formation	10
1.4.1 Contraction, a scar type affecting factor	10
1.4.2 Mechanical stretching affects scar extent	11
1.4.3 Inflammation, the crucial impact of a wound healing phase on the scar formation	12
1.5 The keloid	14
1.5.1 Recent results of single cell RNA sequencing analyses of keloids	21
1.6 The extracellular matrix in skin, scar and keloid	22
1.7 The neuronal system in skin, scar, and keloid	25
1.8 Schwann cells and their role in tissue regeneration	27
1.9 Aims of the thesis	33

2	CHAPTER TWO: RESULTS.....	34
2.1	Prologue.....	34
2.2	Interlude.....	79
3	CHAPTER THREE: DISCUSSION.....	118
	<i>“All that glisters is not gold”</i> (Shakespeare et al, 1823).....	118
	<i>“Love all, trust few, do wrong to none”</i> (Shakespeare, 1813).....	119
	<i>“To be, or not to be, that is the question”</i> (Shakespeare, 1954).....	120
	<i>“Who can control his fate?”</i> (Shakespeare, 1975).....	120
	<i>“Our descent, then, is the origin of our evil passions”</i> (Darwin, 1859).....	122
	<i>“It was the nightingale and not the lark”</i> (Shakespeare, 2000).....	123
	<i>“And where two raging fires meet together ...”</i> (Shakespeare, 1998).....	125
	<i>“We know what we are, but know not what we may be”</i> (Shakespeare, 1954).....	127
	<i>“There is nothing either good or bad ...”</i> (Shakespeare, 1954).....	128
3.1	Conclusion & future prospects.....	131
4	CHAPTER FOUR: MATERIALS & METHODS.....	132
	References.....	133
	Curriculum Vitae.....	155

List of figures

Figure 1:	Anatomy of the human skin.....	3
Figure 2:	Stages of Wound Healing.....	4
Figure 3:	Areas prone to form specific keloid types.....	17
Figure 4:	Schwann cell transformation upon injury.....	32

Abstract

Keloids are diseases of the skin exhibiting features of scars as well as tumours. They are especially characterized by their steady spreading beyond the borders of the original wound. A wide range of studies focusing on the different cell types present in keloids and their potential contribution to keloid formation provided useful insights into the nature of this disease. However, despite many years of research, the pathologic forces driving keloid formation still remain largely undiscovered. In keloids, single cell RNA sequencing revealed a significant increase of a so far neglected cell type, the Schwann cells. Schwann cells are a specialized type of peripheral glia cells ensheathing nerve axons to support their function and to ensure fast stimulus conduction. In the healthy skin, Schwann cells are exclusively identified in contact with tissue-pervading neurons, whereas keloidal Schwann cells exhibit a unique expression pattern and spread through the whole dermal layer without axon attachment. Striking similarities of this keloid-specific Schwann cells with repair Schwann cells, an activated Schwann cell subtype involved in the neuronal regeneration processes upon injury, were observed. In contrast to these repair Schwann cells, keloidal Schwann cells showed a strong contribution to the formation of the extracellular matrix. Numerous matrix-associated genes were identified to be upregulated in keloidal Schwann cells and specific factors, such as insulin-like growth factor binding protein 5 (IGFBP5) and cellular communication network factor 3 (CCN3), were exclusively detected in keloidal Schwann cells suggesting their contribution to the pathologic features of keloids. As Schwann cells have not been associated with keloid formation so far, a comparison of the keloidal Schwann cells with Schwann cells from the cutaneous neurofibroma type 1, a skin disease driven by this cell type, was performed. This joint analysis pointed to distinct pathologic roots and further uncovered the lack of pro-inflammatory factors in keloidal cells. A potential interaction of Schwann cells and macrophages in keloids was identified, suggesting the attraction and M2 polarization of macrophages by keloidal Schwann cells and the enforcement of dedifferentiation and maintenance of in an activated state of Schwann cells by keloidal macrophages. In-depth analysis of independent single cell datasets verified the tissue-specific presence of keloidal Schwann cells and paved the way to define a characteristic transcriptional pattern of twenty-one genes for the identification of this special Schwann cell type in other fibrotic tissues. Together, a novel pro-fibrotic Schwann cell type persisting in keloids was identified, which might be an interesting new target for therapeutic interventions to prevent or reduce keloid formation in the future.

Zusammenfassung

Keloide sind Erkrankungen der Haut, die sowohl Narben- als auch Tumormerkmale aufweisen. Sie sind charakterisiert durch ihre stetige Ausbreitung über die Grenzen der ursprünglichen Wunde. Eine breite Palette von Studien, die sich auf die verschiedenen Zelltypen in Keloiden und ihren möglichen Beitrag zur Keloidbildung konzentrierten, lieferte nützliche Einblicke in die Natur dieser Krankheit. Trotz langjähriger Forschung sind die pathologischen Kräfte, welche die Keloidbildung antreiben, noch immer weitgehend unentdeckt. Bei Keloiden zeigte die Einzelzell-RNA-Sequenzierung eine signifikante Zunahme eines bisher vernachlässigten Zelltyps, der Schwann-Zellen. Schwann-Zellen sind eine spezialisierte Art von peripheren Gliazellen, die Nervenaxone umhüllen, um deren Funktion zu unterstützen und eine schnelle Reizleitung zu gewährleisten. In der gesunden Haut werden Schwann-Zellen ausschließlich im Kontakt mit gewebedurchdringenden Neuronen identifiziert, während keloidale Schwann-Zellen ein einzigartiges Expressionsmuster aufweisen und sich ohne Axonanhaftung durch die gesamte dermale Hautschicht ausbreiten. Es wurde eine auffällige Ähnlichkeit dieser Keloid-spezifischen Schwann-Zellen mit Reparatur-Schwann-Zellen, einem aktivierten Schwann-Zell-Subtyp, der an neuronalen Regenerationsprozessen nach Verletzungen beteiligt ist, beobachtet. Im Gegensatz zu diesen Reparatur-Schwann-Zellen zeigten keloidale Schwann-Zellen einen starken Beitrag zur Bildung der extrazellulären Matrix. Eine Hochregulation zahlreicher matrixassoziierte Gene in keloidalen Schwann-Zellen wurde entdeckt. Zusätzlich wurden spezifische Faktoren wie insulin-like growth factor binding protein 5 (IGFBP5) und cellular communication network factor 3 (CCN3) ausschließlich in keloidalen Schwann-Zellen nachgewiesen, was auf ihren Beitrag zu den pathologischen Merkmalen von Keloiden hindeutet. Da Schwann-Zellen bisher nicht mit der Ausbildung von Keloiden in Verbindung gebracht wurden, wurde ein Vergleich der keloidalen Schwann-Zellen mit Schwann-Zellen aus dem kutanen Neurofibrom Typ 1, einer durch diesen Zelltyp verursachten Hauterkrankung, durchgeführt. Diese gemeinsame Analyse wies auf unterschiedliche pathologische Wurzeln hin und deckte das Fehlen entzündungsfördernder Faktoren in Keloidzellen auf. Eine potenzielle Wechselwirkung von Schwann-Zellen und Makrophagen in Keloiden wurde identifiziert, was auf die Anziehung und M2-Polarisierung von Makrophagen durch keloidale Schwann-Zellen und die Erzwingung der Dedifferenzierung und Aufrechterhaltung eines aktivierten Zustands von Schwann-Zellen durch keloidale Makrophagen hindeutet. Eine eingehende Analyse unabhängiger Einzelzell Datensätze verifizierte das gewebespezifische Vorhandensein von keloidalen Schwann-Zellen und ebnete den Weg zur Definition eines charakteristischen Transkriptionsmusters von einundzwanzig Genen zur Identifizierung dieses speziellen Schwann-Zelltyps in anderen fibrotischen Geweben. Zusammengefasst wurde ein neuartiger pro-fibrotischer Schwann-

Zelltyp identifiziert, welcher in Keloiden persistiert und ein interessantes neues Ziel für therapeutische Interventionen zur Reduktion oder Prävention von Keloiden sein könnte.

Publications arising from this thesis

Direder M, Weiss T, Copic D, Vorstandlechner V, Laggner M, Pfisterer K, Mildner CS, Klas K, Bormann D, Haslik W et al (2022a) *Schwann cells contribute to keloid formation*. Matrix Biol 108: 55-76 [open access CC-BY]

Direder M, Wielscher M, Weiss T, Laggner M, Copic D, Klas K, Bormann D, Vorstandlechner V, Tschachler E, Jan Ankersmit H et al (2022b) *The transcriptional profile of keloidal Schwann cells*. Experimental & Molecular Medicine [open access CC-BY 4.0]

Abbreviations

AP-2 alpha	transcription factor AP-2 alpha
BDNF	brain-derived neurotrophic factor
CALB2	calbindin2
CAMs	cell adhesion molecules
CCL17	C-C Motif Chemokine Ligand 17
CCL2; MCP-1	C-C Motif Chemokine Ligand 2
CCL22	C-C Motif Chemokine Ligand 22
CCL3	C-C Motif Chemokine Ligand 3
CCL5	C-C Motif Chemokine Ligand 5
CCL7	C-C Motif Chemokine Ligand 7
CCL8	C-C Motif Chemokine Ligand 8
CCN3	Cellular Communication Network Factor 3
CD206	mannose receptor
COL12A1	collagen type XII alpha 1
COL1A1	collagen type I alpha 1
COL4A1	collagen type IV alpha 1
COL4A2	collagen type IV alpha 2
COL5A1	collagen type V alpha 1
COL5A2	collagen type V alpha 2
COL5A3	collagen type V alpha 3
COL6A1	collagen type VI alpha 1
COL6A2	collagen type VI alpha 2
COL7A1	collagen type VII alpha 1
COL8A1	collagen type VIII alpha 1
CRYAB	alpha-crystallin B chain
CSRP2	cysteine and glycine rich protein 2
CTGF	connective tissue growth factor
CXCL12	C-X-C motif chemokine 12
CXCL2	C-X-C motif chemokine 2
DAMPs	damage-associated molecular patterns
ECM	extracellular matrix
EGF	epidermal growth factor
ELN	elastin
EMT	epithelial to mesenchymal transition
ENC1	ectodermal-neural cortex 1
endoMT	endothelial to mesenchymal transversion
EphB2	Ephrin type-B receptor 2
ErbB2	receptor tyrosine-protein kinase erbB-2
ErbB3	receptor tyrosine-protein kinase erbB-3
FGF2	basic fibroblast growth factor
FoxD3	forkhead box D3
GAS6	growth arrest specific 6
GDNF	glial cell-derived neurotrophic factor
GFAP	glial fibrillary acidic protein
GPM6B	neuronal membrane glycoprotein M6-b
GPR126	G protein-coupled receptor 126
IFN- γ	or interferon gamma

IGF-1	insulin-like growth factor 1
IGF-2	insulin-like growth factor 2
IGFBP3	insulin-like growth factor binding protein 3
IGFBP5	insulin-like growth factor binding protein 5
IL-10	interleukin 10
IL-13	interleukin 13
IL-17	interleukin 17
IL-1 β	interleukin 1 beta
IL-1 α	interleukin 1 alpha
IL-4	interleukin 4
IL-6	interleukin 6
IL-8	interleukin 8
ITGB1	integrin subunit beta 1
JNK	c-Jun N terminal kinase
JUNB	transcription factor jun-B
KGF	keratinocyte growth factor
Krox20	nearly growth response protein 2
LIF	leukaemia inhibitory factor
LOX	lysyl oxidase
LYPD1	LY6/PLAUR domain-containing protein 1
MAG	myelin-associated glycoprotein
MBP	myelin basic protein
MMPs	matrix metalloproteases
MPZ	myelin protein zero
NCAM	NCAM
NES	nestin
NETs	Neutrophils release neutrophil extracellular traps
NF1	neurofibromatosis 1
NGF	nerve growth factor
NGFR	p75 neurotrophin receptor
NRXN1	neurexin 1
NT3	neurotrophin-3
OLIG1	oligodendrocyte transcription factor 1
PAMPs	pathogen-associated molecular patterns
Pax3	paired box gene 3
PDGF	platelet derived growth factor
pERK	protein kinase R (PKR)-like endoplasmic reticulum kinase
PGP9.5	Protein gene peptide 9.5
PMP22	peripheral myelin protein 22
PPP1R14B	protein phosphatase 1 regulatory inhibitor subunit 14b
PRRs	pattern recognition receptors
S100A16	S100 calcium binding protein A16
S100B	S100 calcium binding protein B
scRNAseq	single cell RNA sequencing
SH3BGRL3	SH3 domain binding glutamate rich protein like 3
Shh	sonic hedgehog
SLUG	snail family transcriptional repressor 2
SNAIL	snail family transcriptional repressor 1

Sox10	transcription factor SOX-10
SOX2	SRY (sex determining region Y)-box 2
SPARCL1	SPARC like 1
STAT3	signal transducer and activator of transcription 3
TAGLN	transgelin
TGFBI	transforming growth factor beta induced
TGF- β	transforming growth factor beta
TGF- α	transforming growth factor alpha
TNFAIP6	tumor necrosis factor alpha-induced protein 6
TNF- α	tumour necrosis factor alpha
TPM2	tropomyosin 2
TSG-6	TNF-stimulated gene 6
TWIST1	twist-related protein 1
VEGF	vascular endothelial growth factor
Zeb1	zinc finger E-box-binding homeobox 1
Zeb2	zinc finger E-box-binding homeobox 2
α -SMA	alpha smooth muscle actin

Acknowledgments

First of all, I would like to thank Prof. Hendrik Jan Ankersmit for his continuous support and inspirational encouragement, which made the realization of this work possible in the first place.

My special thank goes to Prof. Michael Mildner for his scientific and personal support, which has significantly shaped me in recent years.

I would especially like to thank Tamara Weiss, her remarkable fascination with Schwann cells and her attention to detail inspired me to make the most of my work.

My deep gratitude goes to Maria Laggner for her endless patience with my English skills and for her constant encouragement in difficult times.

A big thank you goes also to my PhD siblings Dragan Copic, Katharina Klas and Daniel Bormann, who shared the constant ups and downs of PhD life with me.

I would like to take this opportunity to say thank you to my parents, my grandparents, my siblings, my brother-in-law and my love. You are a constant support in my life that I would not want to miss. Thank you!

1 CHAPTER ONE: INTRODUCTION

1.1 The human skin and its functions

Naturally, an organism living on dry land requires a spatial demarcation from its environment, an integument (Madison, 2003). In case of humans and animals this purpose is served by the skin. An average adult human body is covered by about 2 square metres of skin and comes along with a varying thickness mostly around 2 millimetres (Mosteller, 1987; Wei *et al*, 2017). The skin is often termed as the largest organ of the human body, however, from the surface perspective it ranks third after the lung (50 square metres) and the gut (30 square metres) (Hasleton, 1972; Helander & Fändriks, 2014). In terms of weight the musculoskeletal system, which has to be considered as an organ in this context, is the heaviest organ in the human body before the skin (Sontheimer, 2014). Beside its task as physical barrier for the body, the skin comprises multiple further important functions in different vital areas. It is, for example used as storage area for an oversupply of lipids (Wajchenberg, 2000). The skin controls the body temperature through vasodilatation and vasoconstriction as well as by the production of sweat (Romanovsky, 2014). It is also capable of absorbing specific substances, this skin feature is utilized in medical fields for the application of therapeutics (Leppert *et al*, 2018; Singh Malik *et al*, 2016). The human integument provides a natural barrier to protect the inside of the body from external harm. This implicates not only physical and mechanical damage, but also pathogens and ultraviolet radiation (D'Orazio *et al*, 2013; Lin & Fisher, 2007; Madison, 2003; Nguyen & Soulika, 2019). Furthermore, the skin as a major sensory organ of our environment. Tactile perception, pain, pressure, temperature, and elongation are detected by different specialized receptors spread through the skin (Zimmerman *et al*, 2014). In addition, these sensations also alert the individual to prevent from external harm by temperature or mechanical stress. The skin further serves as an immunological organ to protect the organism from external pathogens through immune cells resident in the skin but also by recruiting immune cells to the required skin site (Kabashima *et al*, 2019).

The human skin is composed of an epidermal, a dermal and a subcutaneous layer. The epidermal layer, as outermost layer, can be divided into four to five layers: stratum corneum, stratum lucidum (solely on palms and soles), stratum granulosum, stratum spinosum and stratum basale. The cellular landscape of the epidermis consists of keratinocytes, Merkel cells, Melanocytes and Langerhans cells, whereas keratinocytes make up the major cell type in the epidermis (95 %). Basal, non-differentiated keratinocytes are located in the eponymous stratum basale (Hsu *et al*, 2014). They continually proliferate and the resulting new keratinocytes move towards the body surface. This migration comes along with cellular differentiation and morphologic transformation called keratinization (Smack *et al*, 1994). The

keratinocytes are connected to each other by desmosomes, get flattened, release their lipids to form a lipid barrier and finally differentiate into anucleated corneocytes (Fuchs, 1990). The stratum corneum is the outermost layer of the epidermis and consists of multiple corneocyte layers. The majority of the barrier function of the skin is provided by the stratum corneum (Murphrey *et al*, 2022). Melanocytes are pigmented cells derived from the neural crest that are responsible for the production of melanin which in turn creates the skin color, supports thermoregulation and protects against detrimental ultraviolet radiation (Adameyko *et al*, 2009). Merkel cells are mechanoreceptors detecting gentle touch sensations. Both cell types, Melanocytes and Merkel cells are located in the stratum basale (Lin & Fisher, 2007; Zimmerman *et al.*, 2014). Langerhans cells are primarily located in the stratum spinosum. They are specialized tissue-resident macrophages and have important functions in immune homeostasis of the skin to prevent infections (Deckers *et al*, 2018).

The dermal layer of the skin can be divided into a papillary and a reticular area. The papillary dermis starts directly beneath the basal lamina of the epidermis. It forms multiple protrusions into the epidermal layer and includes many capillaries and the subepidermal nerve plexus (Reinisch & Tschachler, 2012; Shirshin *et al*, 2017). The reticular part is much thicker and consists to a large extent of extracellular matrix (ECM), such as collagen, proteoglycans, and elastic fibres (Krieg & Aumailley, 2011; Losquadro, 2017). However, the cellular density and the proteoglycan content is higher in the papillary dermis (Mine *et al*, 2008; Smith & Melrose, 2015). Fibroblasts form, together with myofibroblasts, mast cells, lymphocytes, monocytes and macrophages, the cellular part in the dermis (Nguyen & Soulika, 2019). Hair follicles, sebaceous glands, sweat glands as well as various nerve receptors, such as Meissner corpuscle, Pacinian corpuscle and Ruffini endings, are spread through the dermis (Losquadro, 2017; Zimmerman *et al.*, 2014). Vascular-nerve bundles pervade the dermis to supply nutrients and drain waste substances (Losquadro, 2017; Zimmerman *et al.*, 2014). The subcutaneous layer, also known as hypodermis, is used as energy storage for surplus lipids, which simultaneously exerts a heat-insulating effect. The major cell types are fibrocytes, adipocytes as well as macrophages. It consists of solely loose connective tissue, bigger vessels and nerves, and forms a gliding layer to protect the skin (Driskell *et al*, 2014; Geyer *et al*, 2014; Wong *et al*, 2016).

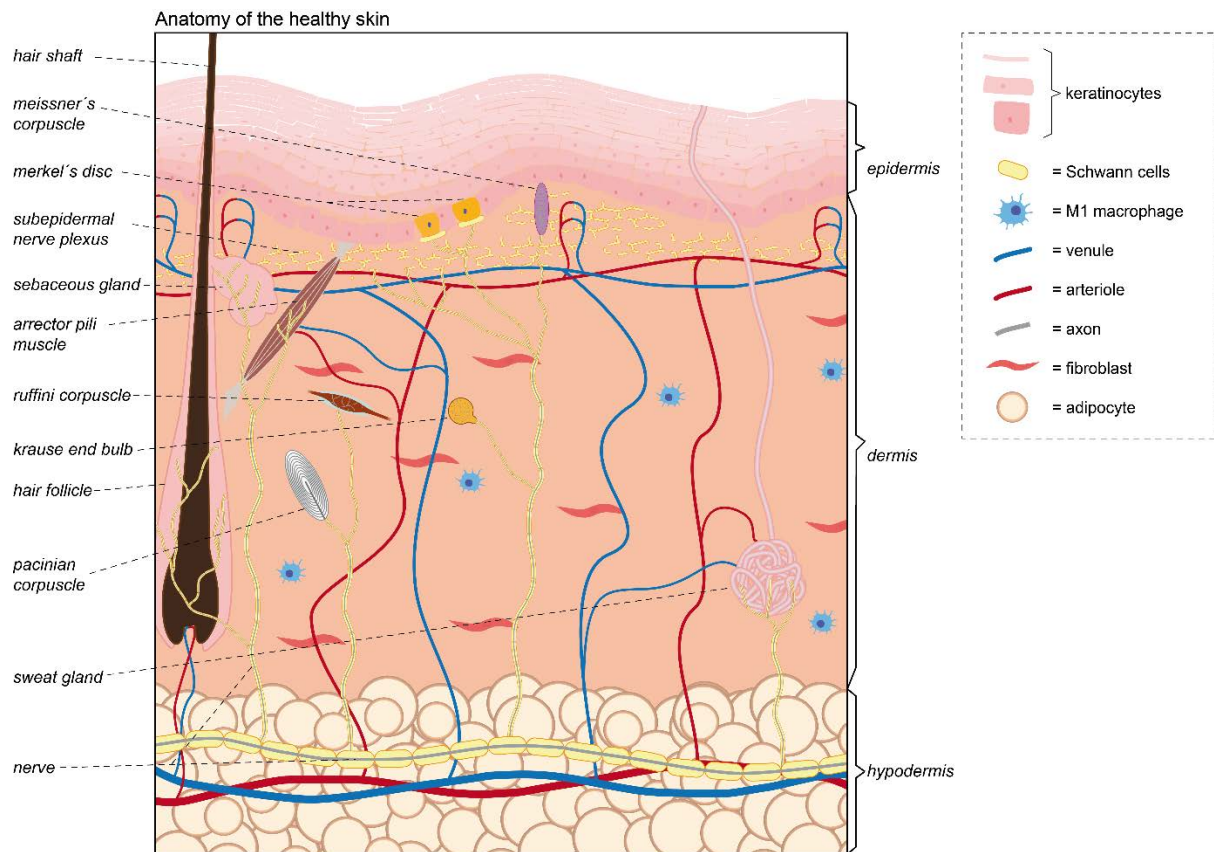


Figure 1: Anatomy of the human skin

1.2 Wound healing

A wound can be defined as a disruption of normal tissue that comes along with a loss of organ functions (Lazarus *et al*, 1994). Two major types of wounds can be distinguished closed/inner wounds and outer/open wounds (Reinke & Sorg, 2012). Inner wounds concern injuries of inner organs, whereas open wounds involve damages of the integument (Reinke & Sorg, 2012). Several cells as well as chemotactic factors and growth factors are involved in the complex process of wound healing in the skin. Ideally, the skin is restored in its previous state, however this regeneration process only occurs in fetal skin or mucosa (Szpaderska *et al*, 2003; Wilgus, 2007). The wound healing of the adult skin can be divided in three up to five partly overlapping phases.

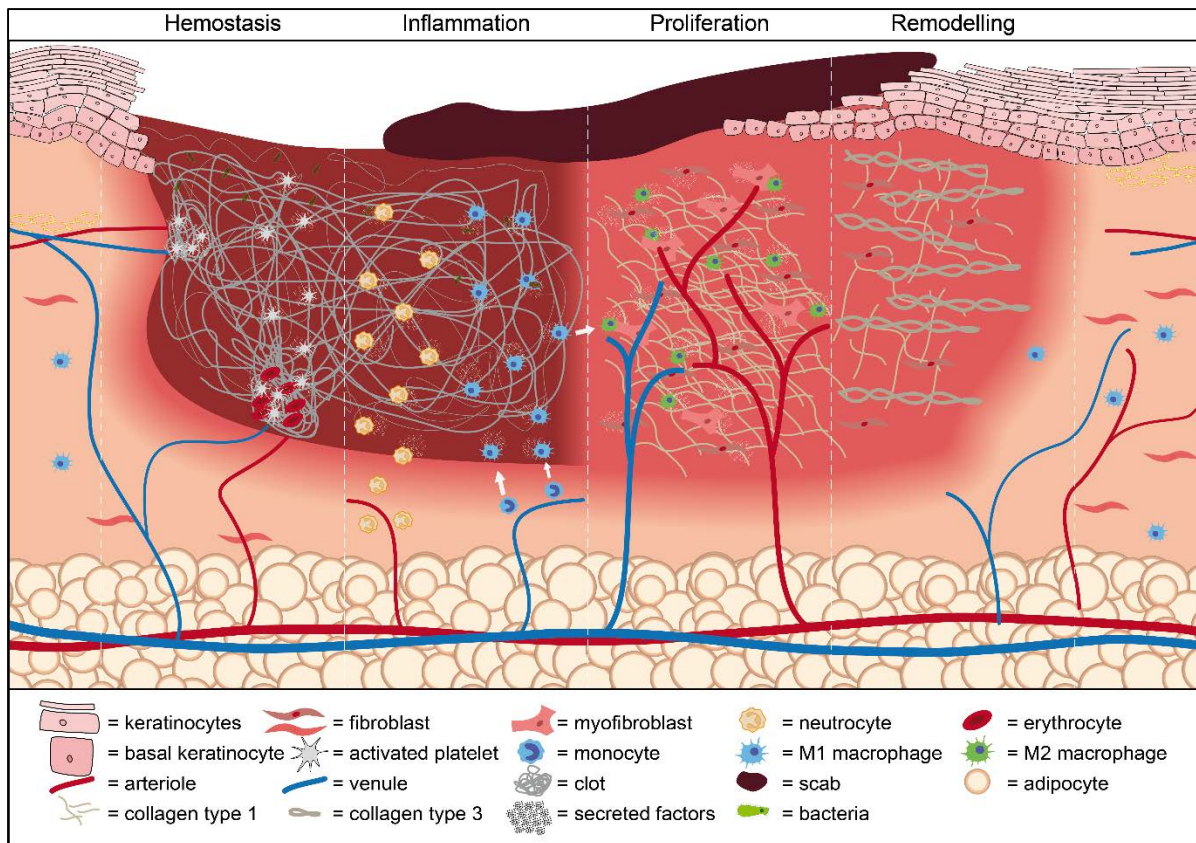


Figure 2: Stages of Wound Healing

1.2.1 The haemostasis phase

The first and initial phase is the haemostasis phase. Haemostasis starts within seconds following damage and lasts for some hours (Ud-Din & Bayat, 2014). The vessel damage induced by an external trauma of the skin causes an abrupt loss of blood and lymph fluid through the wound (Strodtbeck, 2001). The vascular integrity needs to be re-established, but in the beginning it also contributes to the healing process by cleansing potential pathogens and antigens from the wound (Strodtbeck, 2001). To prevent the body from severe blood loss and thereof resulting shock situations, multiple actions start at the same time. Trigger for this activation is the non-physiological contact of blood cells with dermal tissue due to the break of boundaries (Mackman *et al*, 2007). Within seconds, platelets induce vasoconstriction to ensure haemostasis (Martin, 1997). Due to the vasoconstriction, the early wound site is characterized by a low level of oxygen and a decrease of the pH for about 4 days. This state comes along with evident pain behaviour induced by secreted enzymes and mediators (Hunt & Hopf, 1997; Woo *et al*, 2004). Damaged cells further release clotting factors to activate the extrinsic coagulation cascade (Mackman *et al.*, 2007). The contact of platelets with extracellular collagen on the other hand, starts the intrinsic aggregation system (Mackman *et al.*, 2007). Platelets secrete thrombin, a serine protease that supports the aggregation

process and transforms the plasma fibrinogen into an insoluble fibrin clot (He *et al*, 2010). The generated haemostatic clot forms a scaffold that acts as temporal protection and additionally fills the bare inner tissue with a provisional matrix for incoming cells (Martin, 1997). It consists of cells (e.g., erythrocytes, platelets) and proteins (fibrin, fibronectin, thrombospondin, vitronectin, and others) (Martin, 1997). After 5 to 10 minutes, histamine, thrombin and other factors release the constriction of the vessels and induce a vasodilatation that peaks around 10 to 15 minutes later (Mahdavian Delavary *et al*, 2011; Reinke & Sorg, 2012). This change is also the reason for the visible local redness and potential oedema formation at the wound site (Reinke & Sorg, 2012). Beside thrombin, platelets also release several other cytokines and growth factors via granules, such as C-C Motif Chemokine Ligand 5 (CCL5), transforming growth factor beta (TGF- β), vascular endothelial growth factor (VEGF), platelet derived growth factor (PDGF) (Mahdavian Delavary *et al.*, 2011). The coagulation clot acts hereby as a kind of cytokine and growth factor reservoir (Martin, 1997). As it takes some time to establish the required cells and factors for proper wound healing in the wound environment, the haemostasis phase is also known as “Lag”-phase. (Robson *et al*, 2001). The released thrombin stimulates cells such as endothelial cells and peripheral blood mononuclear cells to secrete pro-inflammatory factors as C-C Motif Chemokine Ligand 2 (CCL2, alternatively MCP-1), interleukin 1 beta (IL-1 β), interleukin 6 (IL-6), interleukin 8 (IL-8), tumour necrosis factor alpha (TNF- α), or interferon gamma (IFN- γ) (Mahdavian Delavary *et al.*, 2011; Marin *et al*, 2001). The secreted cytokines induce the attraction of cells like keratinocytes, fibroblasts, endothelial cells and support the transendothelial migration of neutrophils and monocytes to the wound side which is important for the start of the inflammation and proliferation phases (Morton & Phillips, 2016).

1.2.2 The inflammatory phase

The inflammation phase starts already during the haemostasis phase within hours after injury and lasts for at least 2 weeks (Shah *et al*, 2012). It can be divided in two cellular parts, the neutrophil and the monocyte response. Released histamine induces an increased porosity of the dilated vessels, which additionally supports the attraction and migration of leukocytes (Komi *et al*, 2020). Circulating neutrophils get attracted and invade the wound area (Singer & Clark, 1999). They are present for a few days and perform crucial tasks in the early healing process (Eming *et al*, 2007). They defeat microorganisms by phagocytosis or by secretion of proteinases (neutrophil elastase, cathepsin G, urokinase-type plasminogen activator) or antimicrobial substances and remove necrotic and damaged tissue by the release of enzymes as collagenases and others (Eming *et al.*, 2007). Exerted neutrophils are phagocytosed by macrophages or pass into the eschar (Meszaros *et al*, 1999; Thomas *et al*, 1999). Neutrophils produce multiple pro-inflammatory factors as TNF- α , interleukin 1 alpha (IL-1 α), IL-1 β , IL-6 and CCL2 to recruit further neutrophils, monocytes, keratinocytes, and

fibroblasts and additionally to differentiate monocytes (Hübner *et al*, 1996; Werner & Grose, 2003). Three days after wounding, macrophages are the predominate cell type at the wound site and support the healing process by phagocytosis of foreign bodies, organisms and dead neutrophils (Mahdavian Delavary *et al.*, 2011). In response to the increased number of cytokines and other factors (CCL2, C-C Motif Chemokine Ligand 3 [CCL3], transforming growth factor alpha (TGF- α), fibronectin, elastin, p75 neurotrophin receptor [NGFR]) in the wound area, circulating monocytes get in contact with the vessel wall and subsequently, the adhesion cascade is activated monocytes interact with endothelial cells by their glycoprotein ligands (Mahdavian Delavary *et al.*, 2011). Further chemotactic signals promote binding of integrins on the monocyte surface with receptors of endothelial cells leading to an adhesion and transmigration through the endothelium into the tissue (Imhof & Aurrand-Lions, 2004). A chemotactic gradient leads the leukocytes to the avascular area of the wound (Morton & Phillips, 2016). Binding of integrin receptors and selectin to matrix proteins as cell adhesion molecules (CAMs) supports the monocyte movement (Brown, 1995). The early microenvironment of the wound consists of cytokines typical for inflammation (IFN- γ , interleukin 4 [IL-4], interleukin 10 [IL-10]) that support the differentiation of monocytes into macrophages (Stout *et al*, 2009). In general, there are two polarization forms of macrophages that play an important part in the wound healing of the skin. M1 macrophages, driven by IFN- γ , are actively involved in inflammation to defeat pathogens and are characterised by an increase of C-X-C motif chemokine 2 (CXCL2), IL-1 β , CD16, CD32, CD80 and CD86 (Shi *et al*, 2019; Yunna *et al*, 2020). M2 macrophages, driven by IL-4, suppress inflammation and support proper wound healing, tissue formation and angiogenesis (Lawrence & Natoli, 2011). M2 macrophages characteristically express arginase-1, mannose receptor (CD206), IL-10, CD163, C-C Motif Chemokine Ligand 17 and 22 (CCL17, CCL22) (Buechler *et al*, 2000; Yunna *et al.*, 2020). A balance of both polarizations is crucial for successful wound healing. During the inflammation phase, M1 polarization dominates whereas in the later states M2-macrophages prevail (Daley *et al*, 2010; Goerdt & Orfanos, 1999). Macrophages further present antigens to T-cells, release pro-inflammatory proteins, growth factors and cytokines to attract fibroblasts, monocytes and neutrophils and support cell proliferation and matrix production by fibroblasts (Baum & Arpey, 2005). Macrophages that do not contribute to the defence, persist, and presumably change their polarization into M2 later on (Khallou-Laschet *et al*, 2010).

1.2.3 The proliferation phase

The proliferation phase is initiated between 2 to 14 days after the skin damage (Robson *et al.*, 2001). This phase can be divided in three to four parts: fibroplasia and granulation tissue formation, angiogenesis, and re-epithelialization.

During fibroplasia, fibroblasts start to enter the wound site within 2-3 days after injury mediated by PDGF, basic fibroblast growth factor (FGF2), TGF- β and others (Robson *et al.*, 2001). Cellular movement within the fibrin network is enabled by the secretion of matrix metalloproteases (MMPs) which break down fibrin and other matrix components (Yager & Nwomeh, 1999). This proteolytic function is later limited by TGF- β and connective tissue growth factor (CTGF) (Duncan *et al.*, 1999). Fibroblasts adjust to synthesize collagens, elastin, and other proteins of the ECM, as fibronectin, proteoglycans, hyaluronic acid (Eckes *et al.*, 2010). They form the basis for a new matrix and close the wound-induced tissue gap (Martin, 1997). Collagen deposition begins with the invasion of fibroblasts and peaks about 5-7 days after wounding (Morton & Phillips, 2016). The resulting granulation tissue replaces the provisional matrix formed by the clot (Gurtner *et al.*, 2008). The granulation tissue appears red due to the high vascularization and is very vulnerable (Reinke & Sorg, 2012). The ECM is important for development and movement of cells. Balance of matrix production is ensured by a decrease of matrix production by fibroblast with exuberant increasing ECM (Mahdavian Delavary *et al.*, 2011). Wound contraction starts about 4 days after injury (Baum & Arpey, 2005). Triggered by TGF- β 1 and PDGF, fibroblasts differentiate into myofibroblasts, which contract the wound site, restore mechanical strength and produce even more ECM proteins (Werner & Grose, 2003).

Re-epithelialization of the wound surface is important to restore the barrier function of the skin and starts about 3 days after wounding (Reinke & Sorg, 2012). Keratinocytes proliferate and migrate, induced epidermal growth factor (EGF), keratinocyte growth factor (KGF), TGF- α , TGF- β 1, VEGF and others, from the wound margin into the wound bed (Werner & Grose, 2003). This process is further supported by stem cells from sweat glands and from the bulge region of hair follicles (Miller *et al.*, 1998; Taylor *et al.*, 2000). The lack of contact inhibition and physical tension leads to an intracellular reorganization of tonofilaments and induces migration of cells located at the wound borders (Jacinto *et al.*, 2001). Intercellular, desmosomal connections are being released which enables cellular migration of keratinocytes, guided by a chemotactic gradient over the fibronectin-rich matrix of the upper wound site (Clark, 1983; Clark *et al.*, 1982; Wallis *et al.*, 2000). RhoGTPases and small GTPases ensure a structured epithelialization process (Nobes & Hall, 1995, 1999). Plasmin and diverse MMPs pave the way for wound covering keratinocytes (Nussenzweig *et al.*, 1961; Ravanti & Kähäri, 2000). Cellular contact with cells of the opposite wound site induces migration stop and intercellular connection (Santoro & Gaudino, 2005). This re-epithelialization process steadily covers the wound area. Afterwards the basal lamina and epidermal layers are re-established from outside in (Mahdavian Delavary *et al.*, 2011).

The avascular wound area results in a nutrition deficiency. Hence, novel vessels sprout from intact vessels into the undersupplied area (Sorg *et al.*, 2007). Angiogenesis starts with the

activation and migration of endothelial cells from intact vessels induced by pro-angiogenic factors as VEGF, TGF- β , angiopoietin and others (Tonnesen *et al.*, 2000). After being activated, endothelial cells secrete proteolytic enzymes to dissolve their basal lamina and start to proliferate and migrate to form tubular sprouts (Reinke & Sorg, 2012). M2 macrophages are crucial for angiogenesis as they are supposed to stimulate the endothelial cells at the sprouting tips via VEGF and guide them to other sprouts to form vessel loops (Fantin *et al.*, 2010; Tammela *et al.*, 2008). Afterwards, the vessel loops differentiate into capillary networks (Tonnesen *et al.*, 2000). Pericytes and smooth muscle cells are attracted, which support the adaptation and stabilization of the vessel wall (Gao *et al.*, 2021; Teichert *et al.*, 2017). Neovascularization of disrupted skin follows a regular pattern called “*sola cutis se reficientis*”, visually like a shrinking sun, that disappears upon completion (Sorg *et al.*, 2007).

1.2.4 The remodelling phase

The last phase, the so-called remodelling phase, takes weeks up to years upon injury (Gurtner *et al.*, 2008). During the remodelling process, most wound healing processes are downregulated and the majority of cells leave the tissue or undergo apoptosis (Gurtner *et al.*, 2008). The angiogenesis stops and the blood flow subsides due to decreasing nutrient demand (Mahdavian Delavary *et al.*, 2011). A mature scar is characterised as almost avascular and acellular tissue (Gurtner *et al.*, 2008; Sorg *et al.*, 2007). MMPs in combination with inhibitors of metalloproteinases finally rearrange the ECM (Lovvorn *et al.*, 1999). The predominant collagen type III produced in the proliferation phase is replaced by the stronger collagen type I which persists as large, organized parallel fibres (Lovvorn *et al.*, 1999). After wounding the tensile strength increases by the time and reaches 20 % about 3 weeks and 80 % about 12 months of the healthy skin strength (Levenson *et al.*, 1965). However, a scar never reaches the robustness of the intact skin and literature describes 80% strength as maximum outcome (Clark, 1985; Levenson *et al.*, 1965).

1.2.5 Treatments to support proper wound healing

Proper wound healing can be supported by different therapy options. Dressings are the most common ways to support the wound healing as contact layer dressing, semipermeable films, hydrocolloids, foam, or hydrogels (Hawthorne *et al.*, 2021). Antimicrobial dressings are also state of the art to prevent wound infection. Natural substances as honey or aloe vera further show successful treatment effects (Hawthorne *et al.*, 2021; Molan & Rhodes, 2015). In special cases, wound healing is supported by negative pressure wound therapy (Hawthorne *et al.*, 2021). A further approach, especially in chronic wounds, is to provide an environment beneficial for the healing process. This comprises scaffolds, usually composed of ECM components to provide a temporary covering and to promote cellular infiltration (Rodrigues *et al.*, 2019). A further option represents the cell-based therapy, involving cultured epidermal

autografts, artificial skin equivalents consisting of neonatal keratinocytes, scaffolds with neonatal, dermal fibroblasts or allografts of human amnion/chorion membrane (Rodrigues *et al.*, 2019). Beside the cell-based therapy, the acellular, secretome-based therapy as well as platelet-rich plasma showed promising results in the treatment of wounds (Hacker *et al.*, 2016; Mildner *et al.*, 2013; Simader *et al.*, 2017; van der Bijl *et al.*, 2021).

1.3 A scar is not a scar

The wound healing process typically ends up with a scar. In the US, there is an annual \$12 billion market for scar treatment (Sen *et al.*, 2009). Unfortunately, there is no reliable method or instrument to predict abnormal scarring after wounding. Around 100 million patients per year get scars from surgery in the developed world alone (Brown *et al.*, 2008). About 90% of patients with severe burn injury and about half of all operated patients get a hypertrophic scar (Gauglitz *et al.*, 2011). The general prevalence varies, but appears to be higher in Caucasians (Bombaro *et al.*, 2003). Healing- and reepithelialisation-time as well as the injury depth is important for the outcome of scar formation (Kwan & Tredget, 2017). Most of the time, damage of the superficial skin does not end up in a scar (Monstrey *et al.*, 2008). The likelihood of scar formation and the required time for healing increases with increasing harmed skin depth (Monstrey *et al.*, 2008). The quality of the scar is an important parameter to evaluate the outcome of wound healing. Under ideal conditions, the scar presents in the beginning as firm, haemostatic and slightly raised (Bayat *et al.*, 2003). It matures for about 6 to 9 months, afterwards it flattens, gets normotrophic, aesthetic and pale (Burd & Huang, 2005). The final outcome is defined as normal scar. However, external and internal impacts affect the extent of scar formation and its outcome. Possible variants are the caving atrophic, the stretched and the excessive hypertrophic scar (Bayat *et al.*, 2003).

The atrophic scar manifests as a dell in the skin. It may be caused by acne vulgaris and can be subdivided in icepick, rolling and boxcar scars, classified by their depth and form of depression (Jacob *et al.*, 2001). Complications of atrophic scars is the increased burden of disfigurement leading to psychological problems and social stigma, especially when scars occur in the face (Koo & Smith, 1991).

The stretched scar increases its width within 6 months after injury for about one and a half of the normal scar and commonly occurs after surgery (Sommerlad & Creasey, 1978). Especially interventions in the knee or shoulder area lead to this type of soft, pale, and symptomless scar (Bayat *et al.*, 2003).

The hypertrophic scar on the other side appears as firm, rigid, raised, erythematous fibrotic tissue restricted by the boundaries of the original wound and develops within 4-8 weeks after skin damage (Bayat *et al.*, 2003; Gauglitz *et al.*, 2011). In the beginning, the development of

hypertrophic scars is similar to normal scars, but complex and exuberant fibrosis causes worse final outcome (Gabriel, 2011). In addition to the aesthetic aspect, a hypertrophic scar comes along with pain and pruritus (Gauglitz *et al.*, 2011). As hypertrophic scars commonly occur over joints, their increased contraction also leads to restricted mobility (Engrav *et al.*, 1987). Hypertrophic scars may occur following burn injury, surgeries, or fractures (Esselman *et al.*, 2006; Gabriel, 2011). Hypertrophic scars arise especially from wounds in areas of high tension, whereas in areas as scalp, palm, sole or eyelid, the formation of hypertrophic scars is rare (Matsumura *et al.*, 2001). Skin areas frequently confronted with increased mechanical stress are the anterior chest (respiration, limb movement), the shoulder (body bending, limb movement), and suprapubic regions (body bending) (Ogawa, 2011). Sometimes hypertrophic scars regress. They decrease, get softer and almost achieve features of normal scars (Niessen *et al.*, 1999). The occurrence of hypertrophic scars after surgery can be prevented significantly by an accurate wound care and proper tape fixation (Ogawa, 2022). Treatment options for already existing scars, especially for hypertrophic scars, are compression therapy, gel sheets, scar massage, corticosteroids in different regional applications, laser or surgical interventions as excision or, in more complex cases, geometrical techniques to reduce the tension (Ogawa, 2022).

1.4 Processes affecting the extent of scar formation

Scar formation is a sensitive interplay of various mechanisms. Involved processes can be roughly divided in contraction, mechanical stretching, and inflammation. Failure or alterations of one or more steps affect the extent of scar formation significantly.

1.4.1 Contraction, a scar type affecting factor

Scar contraction is primarily conveyed by myofibroblasts and fibroblasts (Nedelec *et al.*, 2000). Myofibroblasts differentiate after 1-2 weeks upon injury by TGF- β , and PDGF from fibroblasts (Kwan & Tredget, 2017; Werner & Grose, 2003). Recent findings additionally reported an involvement of the serine proteases, especially dipeptidyl-peptidase 4 and urokinase, in the differentiation process of fibroblasts into myofibroblasts (Vorstandlechner *et al.*, 2021). They can contract the wound for about 0.75 mm per day and usually disappear gradually afterwards (Marshall *et al.*, 2018). It is supposed, that in hypertrophic scars a high number of myofibroblasts endure and induce the characterizing painful, rigid scar contraction (Marshall *et al.*, 2018). Persistent fibroblasts, in addition, show enhanced production of collagen, TGF- β and CTGF (Wang *et al.*, 2008). They also induce contraction by an increased traction, stronger than required for their movement, whilst they migrate through the matrix of the scar (Harris *et al.*, 1981). Mechanically induced changes of the tissue also

promote differentiation of fibroblasts in myofibroblasts (Ogawa, 2011). High tension also prevents myofibroblasts and other cells from apoptosis through a protein kinase B-dependent mechanism, which furthermore promotes the fibrotic process (Aarabi *et al*, 2007; Derderian *et al*, 2005).

1.4.2 Mechanical stretching affects scar extent

Mechanic impacts on the scar formation can come from outside as compression, shear force, stretching tension or compression, but also from inside as induced by growth, by osmotic or hydrostatic pressure (Demling, 2005; Dunkin *et al*, 2007; Lund *et al*, 1992; Melis *et al*, 2006; Ohura *et al*, 2008). Skin injuries per se cause an acute major change in the field of tension. Wound healing with its tissue altering phases further leads to persistent changes in tension. Mechanisms in the haemostasis and inflammation phase can cause pressure changes due to oedema and changes of circulation in the wound area and the surrounding skin (Orgill *et al*, 2009). During the proliferative and the remodelling phase, the wound gets closed and contracted. The influence of external forces during this time has a significant impact on the quality of the final scar (Ogawa, 2011; Silver *et al*, 2003). Nerve fibre receptors and mechanical sensors and receptors capture mechanical impacts on the integument (Lansman, 1988; Sokabe & Sachs, 1990; Steen *et al*, 1992). These include mechanosensitive ion channels (Mg^{2+} , K^+ , Na^{2+} , Ca^{2+}), cell adhesion molecules, the cytoskeleton but also mechanosensitive nociceptors for the impression of tension or compression (Giamarchi *et al*, 2006; Hamill, 2006; Ingber, 1993; Ingber *et al*, 1986; Inoue *et al*, 2006; Sokabe & Sachs, 1990; Steen *et al.*, 1992). Cell adhesion molecules form the connection between the ECM and the cytoskeleton of the cells and are also in contact with mechanosensitive ion channels (Sokabe *et al*, 1997). Any spatial shift of the tissue impairs the cytoskeleton and in this context the ion channels (Sokabe *et al.*, 1997). This stimulus will be transformed into electrical signals which induce cellular proliferation, as well as epithelium and blood vessel formation (Ogawa, 2011). The mechanical change stimulates TGF- β production and activation, induces G proteins to promote cell growth and increases epidermal growth factor activation through calcium channels (Silver *et al.*, 2003; Wang *et al*, 2006; Wipff *et al*, 2007). Nerve fibre receptors, as mechanosensitive nociceptors, get activated by mechanical stress (Steen *et al.*, 1992). The stimulus is passed through the dorsal root ganglia into the afferent spinal nerves (Scholzen *et al*, 1998; Yamaoka *et al*, 2007). This leads to a release of neuropeptides in the skin through the distal ends of the spinal nerves (Yamaoka *et al.*, 2007). Neuropeptides, as somatostatin, neurokinin A, substance P and others, have a direct impact on skin cells as fibroblasts, endothelial cells or leukocytes and may promote inflammation (neurogenic inflammation), cell accumulation, growth, and proliferation directly at the area of mechanic action (Foreman, 1987a, b, 1988; Holzer, 1998; Liu *et al*, 2006; Senba & Kashiba, 1996). A relationship between hypertrophic scarring and the activity of neuropeptides and

neurogenic inflammation has been discussed (Akaishi *et al*, 2008; Chin *et al*, 2009; Scott *et al*, 2007; Scott *et al*, 2005). In conclusion, skin tension must be balanced, as it is important on the one side for skin growth, expansion, proper wound healing and wound contraction. On the other side, excessive tension seems to promote abnormal extensive scarring.

1.4.3 Inflammation, the crucial impact of a wound healing phase on the scar formation

Inflammation is an important part of proper wound healing. The involved cells and mediators defeat potential pathogens and bacteria to prevent infection and affect the production of ECM. However, prolonged inflammation phase is accompanied with higher risk of either chronic non-healing wounds or excessive scar formation (Niessen *et al.*, 1999; van der Veer *et al*, 2009). The Inflammation extent during wound healing/ scar formation has been reported to correlate directly with the scar size (Mak *et al*, 2009; Ogawa, 2017). Inflammatory cells, mediators and signalling pathways thereby determine the intensity and duration of the inflammation process and therefore the extent of scarring. The inflammatory immune response is initiated by damage-associated molecular patterns (DAMPs) and pathogen-associated molecular patterns (PAMPs) (Tang *et al*, 2012). DAMPs are endogenous molecules secreted or released by cells due to damage or stress (Tang *et al.*, 2012). Typical DAMPs can be metabolites but also proteins that activate immune cells and promote their attraction to the wound site (Tang *et al.*, 2012). The species-specific pattern recognition receptors (PRRs) are present on immune cells as well as tissue cells (Tang *et al.*, 2012). PAMPs, which can be found on pathogen-specific proteins, such as DNA, certain carbohydrates, bacterial cell walls, and others, activate PRRs and thus promote the process of inflammation (Tang *et al.*, 2012). Neutrophils and macrophages, as major cells in the inflammation phase, but also T-cells and mast cells appear to have an important impact on the extent of scar formation. The early inflammatory phase is orchestrated by neutrophils (Singer & Clark, 1999). Neutrophils release neutrophil extracellular traps (NETs) to capture and kill bacteria (Chrysanthopoulou *et al*, 2014). *In vitro* studies reported the ability of NETs to activate pro-fibrotic pathways in fibroblasts and to promote ECM production in myofibroblasts (Chrysanthopoulou *et al.*, 2014). Macrophages have been reported as a crucial cell population for a successful healing process of the skin (Mahdavian Delavary *et al.*, 2011). The balance of M1 and M2 macrophages plays thereby an important part. As previously described are M1 macrophages the predominant cell type in the second part of the inflammatory phase (Daley *et al.*, 2010). Induced by the chemokine CCL2 amongst other factors, monocytes enter the wound site and differentiate in M1 macrophages (Mahdavian Delavary *et al.*, 2011). M1 macrophages further enhance the inflammation by the release of several pro-inflammatory cytokines (Baum & Arpey, 2005). However, an increase of especially M2 polarized macrophages was described in abnormal scars (Butzelaar *et al*, 2016). The pro-fibrotic M2 macrophages are the predominant macrophage type later during

wound healing and even support to dissolve the inflammation (Goerdts & Orfanos, 1999; Greenlee-Wacker, 2016). In a murine depletion model, a lack of macrophages in the inflammatory phase has been shown to be beneficial for a limited scar formation (Lucas *et al.*, 2010). Depletion in the proliferation phase however, promoted severe bleeding of the wound and a lack of macrophages during remodelling revealed even no relevant effect on the scar formation (Lucas *et al.*, 2010). T-cells are divided in cytotoxic T-cells (CD8+) and helper (CD4+) T-cells. Helper T-cells are further subdivided in Th1, Th2, regulatory T cells and others. With regard to scar formation, Th2 cells support fibrotic functions as the collagen formation by the release of interleukin 13 (IL-13) and IL-4 (Trace *et al.*, 2016). Regulatory T-cells also exert fibrotic tasks *in vitro*, as they decreased the collagen production in co-culture of regulatory and other helper T-cells derived from healthy donors with abnormal scar-derived fibroblasts (Murao *et al.*, 2014). However, this effect was reversed when other helper T-cells were excluded from the co-culture-setting (Chen *et al.*, 2019). This phenomenon indicated a direct and an indirect impact on the collagen production of fibroblasts by regulatory T-cells. In contrast, scar-derived helper T-cells have a pro-fibrotic impact on healthy fibroblasts (Wang *et al.*, 2007). In contrast to Th2 and regulatory T cells, Th1 cells rather inhibit scar formation, as they release IFN- γ , which affects fibroblast proliferation and collagen type I and III expression (Wynn, 2004). The amount and activation of mast cells also directly correlate with increased scarring (Bagabir *et al.*, 2012a). A positive effect of mast cells on the collagen secretion and proliferation features of fibroblasts through the release of factors as FGF2, IL4 or VEGF has been reported (Komi *et al.*, 2020). However, the general impact of mast cells on the formation of scars in humans is still uncertain.

During the wound healing process, multiple immune cells and skin tissue cells release inflammatory cytokines to promote the immune response. Later on, the release of anti-inflammatory cytokines supports the phase transition and is crucial for the proliferation and remodelling. Maladjustment of the soluble microenvironment affects regular scar formation. An increase of interleukin 17 (IL-17) for example, is detected in hypertrophic scars (Zhang *et al.*, 2018). The high IL17 concentration is attributed to a release by macrophages and promotes inflammation as well as CCL2, C-C Motif Chemokine Ligand 7 and 8 (CCL7, CCL8) concentration (Zhang *et al.*, 2018). Other cytokines as C-X-C motif chemokine 12 (CXCL12) or CCL2, have also been discussed as major directing factors in scar formation (Ferreira *et al.*, 2006; Nishiguchi *et al.*, 2018). In contrast, anti-inflammatory cytokines have a positive effect on scar formation and support regular scarring (Shi *et al.*, 2016). The anti-inflammatory cytokine IL-10, for example has a limiting effect on the extent of scar formation (Shi *et al.*, 2016). Beside the cytokine-theories, several pathways are involved in scar formation. Especially Wnt/ β catenin, TGF β /Smad, NF- κ B and signal transducer and activator of transcription 3 (STAT-3) signalling are crucial for the formation of normal scars (Ogawa,

2011). It is therefore not surprising that these pathways are also enhanced in abnormal scars (Gabriel, 2009; Ray *et al*, 2013; Wang *et al*, 2020).

In conclusion, the extent and characteristics of a scar depend on a complex interaction of multiple mechanisms during the wound healing process. In general, a prolonged inflammatory phase as well as constant mechanical stress at the wound site increase the possibility for pathologic scar formation.

1.5 The keloid

For many years, keloids have been defined as a type of fibroproliferative abnormal scar, characterised by an excessive continuous growth beyond the original borders of the wound (Tan *et al*, 2019). This definition is debatable as keloids even appear after a minimal trauma, like an insect bite or a vaccination, and even though many mechanisms in the keloid are typical for scarring, the pathology shows some tumour-like features (English & Shenefelt, 1999; Tan *et al*, 2019). About 3000-2500 B.C. the ancient Egyptians already described a kind of large, hard bulging tumour that spreads. This pathologic phenomenon coincides with current descriptions of keloids (Breasted, 1930). However, this knowledge appeared to be forgotten or irrelevant. As late as the early 19th century, the tumor-like scar was re-described by Jean Louis Alibert. In 1817, he coined the term “keloid” in reference to one of the two most common keloidal shapes and its horizontal growth like the laterally movement of a crab (Murray *et al*, 1981). Racial ethnicity has been mentioned as one of the strongest impacts on the incidence of keloids, as people with dark pigmented skin have an increased risk to develop keloids (Burd & Huang, 2005; Wolfram *et al*, 2009). The incidence ranges in the Hispanic and Black population between 4.5 and 16 %, while the Asian and Caucasian population show an incidence below 1 % (Rockwell *et al*, 1989; Seifert & Mrowietz, 2009; Sun *et al*, 2014). More recent findings support this data, with increased levels of keloid development in African American patients following caesarean section or head and neck operations compared to Asian and Caucasian patients (Tulandi *et al*, 2011; Young *et al*, 2014). However, the actual skin colour in Africans appears not to induce keloid formation, as light pigmented Africans have an almost similar increased risk for keloid formation than dark pigmented Africans (Kiprono *et al*, 2015). This might be explained by the higher familial incidence of keloids. First-degree relatives in the Chinese populations showed a heritability of 72 %, followed by second- and third-degree relatives with a risk of 41 % and 17 %, respectively, to develop a keloid (Lu *et al*, 2015). In addition, close relatives are also more likely to develop even more serious keloids (Bayat *et al*, 2005; Lu *et al*, 2015). In addition, a common risk for keloid development was identified in twins (Marneros *et al*, 2001). Although, several signs suggest keloids as a hereditary pathology, related genes have so far not been

identified (Glass, 2017). Gender-specific differences in keloid occurrence have been described with increased levels of keloids in women (Bayat *et al.*, 2005). However, these findings should be considered with caution, as they could be affected by an increased cosmetically and aesthetically awareness of women compared to men (Burd, 2006). There is no age limit for keloid formation, but a striking increased occurrence has been described in individuals between 10 and 30 years of age (Bayat *et al.*, 2005). This age span includes years of significant endocrinological changes in humans, such as puberty or pregnancy, which suggests an impact of increased endocrinologic activity on the pathologic mechanisms of keloids (Seifert & Mrowietz, 2009).

The trigger for the formation of a keloid reaches from minor traumas such as insect bites up to wounds caused by surgical intervention (English & Shenefelt, 1999). Other promoting minimal traumas could be injuries such as abrasions, blunt traumas or lacerations but also tattoos or piercings (English & Shenefelt, 1999). Sometimes, keloids even arise out of an inflammatory area without any injury such as herpes zoster, acne, and others. In case of keloids, the tissue response to these small kind of skin damages is exaggerated and induces, in some cases, subsequently more damage than the initial harming action.

On a histopathologic level, the keloid is mostly characterised by an increased epidermal thickness, thick and loosely cross-linked collagen bundles, reduced number, or absence of rete pegs and increase of fibroblasts, myofibroblasts, fibrocytes, immune and endothelial cells (Limandjaja *et al.*, 2020). Alpha smooth muscle actin (α -SMA) expression and dermal nodules often were described as distinguishing factors between hypertrophic scars and keloids. However, these phenomena have already been proven in both tissue types, whereas the unique collagen bundles remain, at least so far, keloid characteristic (Huang *et al.*, 2014). Typical areas for keloid formation are, like hypertrophic scars, areas of high tension as the shoulder, the sternum, and the neck, but also the earlobes and the upper limbs (Bayat *et al.*, 2005; Bella *et al.*, 2011; Burd & Huang, 2005; Monstrey *et al.*, 2014; Murray *et al.*, 1981).

These areas are additionally characterized by increased levels of sebaceous glands, collagen, and a low number of M1 macrophages (Al-Attar *et al.*, 2006; Butzelaar *et al.*, 2017). Studies on the elastic potential of keloid prone-sites are contradictory as both an increased as well as decreased elasticity has been described (Bux & Madaree, 2012; Sano *et al.*, 2018). Another keloid-specific phenomenon is that patients prone to form keloids do not always develop keloids (Al-Attar *et al.*, 2006). The reason why patients sometimes develop keloids and sometimes normal scars or hypertrophic scars has not been elucidated yet.

Keloids come along with symptoms similar to hypertrophic scars such as disfigurement, pain, and itching (Bijlard *et al.*, 2017; Limandjaja *et al.*, 2020; Murray, 1994). However, keloids reveal a specific perception of pain in the centre and of pruritus in the border area and the surrounding skin (Bijlard *et al.*, 2017; Lee *et al.*, 2004; Limandjaja *et al.*, 2020; Murray, 1994).

In addition, they cause movement restrictions that increase with size (Limandjaja *et al.*, 2020; Ud-Din & Bayat, 2014). The psychologic impairment induced by keloids clearly affects patients in their emotional wellbeing and causes a reduction in quality of life comparable to patients suffering from psoriasis (Balci *et al.*, 2009; Bijlard *et al.*, 2017). The pathogenesis of keloids remains so far unclear, which impairs the development of adequate research models and the identification of successful treatment options. The clinical diagnosis is commonly the preferred way to identify a keloid and to distinguish between keloids and hypertrophic scars (Gulamhuseinwala *et al.*, 2008). The patient interview provides important characterizing information as keloids grow much slower than hypertrophic scars, spread beyond the wound borders into the healthy skin and never regress, whereas hypertrophic scars arise within the wound borders and might regress after a while (Ud-Din & Bayat, 2014). Keloids sometimes occur years after the injury, whereas hypertrophic scars, start to develop directly after an injury, like a normal scar but with ongoing exuberant fibrosis (Burd & Huang, 2005). In general, keloids rarely undergo pathologic analysis (Gulamhuseinwala *et al.*, 2008). However, a study revealed that clinicians were able to accurately identify 81 % of 568 keloids, whereas the wrongly assigned 19 % included normal scars, hypertrophic scar and acne keloidalis (Gulamhuseinwala *et al.*, 2008).

Treatment options for keloids are limited and individual treatments come along with a high rate of recurrence and in worse case scenarios, with an even worse scar formation than before. The most common treatment options of keloids encompass surgical excision, corticosteroids, silicon sheets, radiotherapy, brachytherapy, chemotherapy and targeted therapy, 5-fluorouracil together with triamcinolone and photodynamic therapy (Ogawa, 2022; Tan *et al.*, 2019). However, greatest success has been achieved with combinations of more therapies (Ogawa, 2022; Tan *et al.*, 2019). Treatment by solely surgical excision has a recurrence rate between 45 and 100 % (Mustoe *et al.*, 2002). To better understand the struggle to identify the underlying mechanism(s) driving keloid formation, the next paragraph will give an overview of the current state of knowledge.

Keloids can be subdivided based on different characteristics. They were categorized in regularly and irregularly shaped or in dumbbell, butterfly, and crab's claw shaped scars (Akaishi *et al.*, 2010; Huang *et al.*, 2017). Keloids have further been distinguished by their convexness in raised and flat keloids (Conway *et al.*, 1960). The flat keloid was described as irregularly pigmented and spread with raised, hyperpigmented edges and flat, hypopigmented central areas (Bella *et al.*, 2011). The raised keloid on the other side, has a bulbous appearance and defined borders (Bella *et al.*, 2011). These subtypes indicate a high intralesional heterogeneity within keloids (Bella *et al.*, 2011). In most studies, the description fits the flat keloid as the scar margins are described as active, invading part of the keloid which appear raised and red (Lu *et al.*, 2007; Seifert *et al.*, 2008). The borders are associated

with an increase in cell number, especially fibroblasts, endothelial and immune cells, a general decrease in programmed cell death and an increase in cell activity and proliferation (Huang *et al.*, 2014; Le *et al.*, 2004; Seifert *et al.*, 2008; Suttho *et al.*, 2017; Touchi *et al.*, 2016). The centre, on the other side, mostly exhibits a cellular decrease, limited cellular activity and in general an almost inactive area (Suttho *et al.*, 2017). Interestingly, symptoms of keloids are associated with specific areas, as pruritus occurs more often at the margins, whereas pain is more likely in the central areas (Lee *et al.*, 2004). As heterogeneous the keloid is, as contradictory are sometimes the results in several keloid-studies. Accordingly, there have also been active centres and inactive margins described (Tsujita-Kyutoku *et al.*, 2005). These findings might be set in a frame, as the bulging keloids were suggested to have active centres and in case of flat or better “superficial spreading” keloids the border area forms the active part (Limandjaja *et al.*, 2018). In addition to the horizontal distinction, different active areas were defined going into the deep of the tissue (Chong *et al.*, 2018; Jiao *et al.*, 2017). In case of bulging keloids, the deeper layers were described to form the aggressive part (Chong *et al.*, 2018).

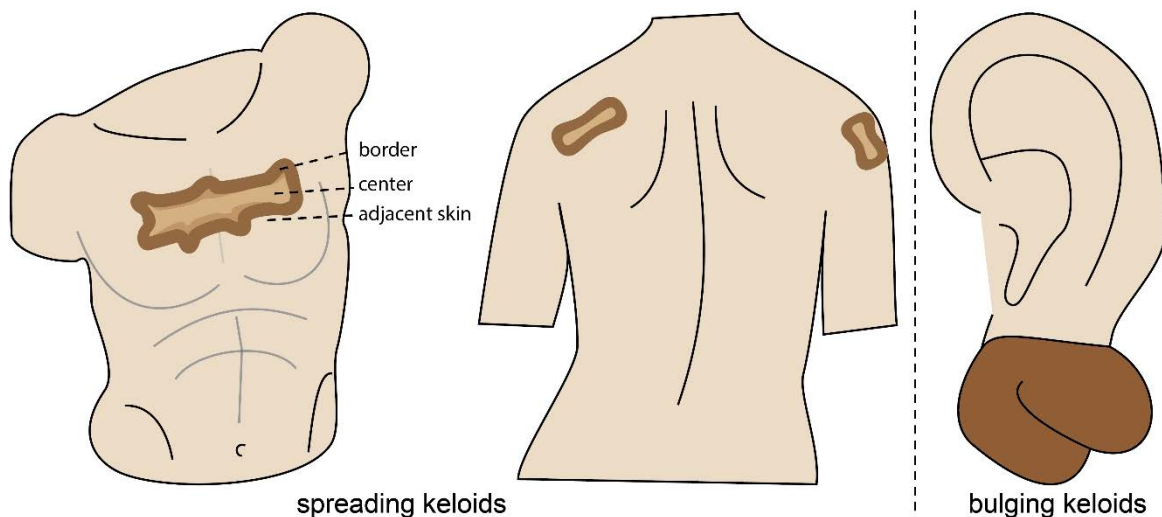


Figure 3: Areas prone to form specific keloid types

The skin next to the keloid represents another quite controversial topic in keloidal research as some research groups define the adjacent skin to be equally to healthy skin (Jumper *et al.*, 2017). This hypothesis has been questioned or better disproved by several studies describing the special features of this intermediate skin phenomenon. Skin adjacent to keloids can even show symptoms typical for the active margins in flat keloids such as pruritus (Lee *et al.*, 2004). An increase of blood circulation and cells, especially lymphocytes has been reported in the surrounding skin (Hahn *et al.*, 2013; Jiao *et al.*, 2017; Liu *et al.*, 2016). The adjacent skin also shows features as keloidal gene expression, enhanced apoptosis, and proliferation, typical for the keloid (Appleton *et al.*, 1996; Hahn *et al.*, 2013). However, there are still differences in the adjacent skin compared to keloids, such as a

higher amount of CD34 positive cells and a less fibrotic matrix formation (Erdag *et al*, 2008). However, keloidal collagen bundles have been reported to trespass from the keloid in the surrounding skin.(Limandjaja *et al.*, 2020) Altogether, the skin adjacent to the keloid has a kind of intermediate state and might play an important role in the pathogenesis, as it is likely to be converted in keloid tissue over time.

Researchers have attempted to decipher the driving force behind the keloid-scar for many years. This effort ended up in numerous studies highlighting the keloid from multiple sides. Special attention was given to the different cell types present in the keloid tissue. In the next passage, major findings about the so far recognized cell types in keloids and their supposed pathology-promoting functions will be described.

Fibroblasts are meant to be the main driver in keloids regarding their production of ECM (Eckes *et al.*, 2010). For this reason, it is no surprise that there is abundant literature on keloidal fibroblasts (Macarak *et al*, 2021). The number of fibroblasts was reported to be increased in keloids (Limandjaja *et al.*, 2020) via increased proliferation and apoptosis-resistance (Wang *et al*, 2018). The telomerase as well as senescence in general appears to be dysfunctional in keloidal fibroblasts, suggesting a pathology supporting ongoing growth (Granick *et al*, 2011; Yu *et al*, 2016). The ECM production and deposition by keloidal fibroblasts appears to be boosted and in contrast, the ability to break down ECM is reduced (He *et al*, 2012; Seifert *et al.*, 2008). Keloidal fibroblasts are more migratory, presumable by an upregulation of TGF- β associated pathways, by CTGF, insulin-like growth factor 1 (IGF-1) receptors, IL-6 and IL-8 and others (Do *et al*, 2012; Fang *et al*, 2016; Hu *et al*, 2014). They express higher levels of matrix-associated genes, such as collagen type I, collagen type III, fibronectin, elastin, glycosaminoglycans, proteoglycans and show higher sensitivity for several wound healing factors (Fang *et al.*, 2016; Lee *et al*, 1991; Suarez *et al*, 2013; Yagi *et al*, 2013; Zhang *et al*, 2009). Interestingly, keloidal fibroblasts express mesenchymal stem cell-associated markers and differentiate into multiple cell types such as osteocytes, smooth muscle cells, neural lineage cells, adipocytes, and others (Iqbal *et al*, 2012; Moon *et al*, 2008; Plikus *et al*, 2017). These multipotent stem cell-like fibroblasts lose their abilities over time in culture. Therefore, it was hypothesized that the keloidal microenvironment supports their undifferentiated state and might be responsible in general for the formation of these cells (Moon *et al.*, 2008).

Fibroblasts and keratinocytes form an effective team in wound healing, as they support each other in their profibrotic and healing functions (Broughton *et al*, 2006). Keloid-derived fibroblasts as well as keloids are known to induce an upregulation of factors important in cellular growth and ECM formation in the healthy counterpart (Chua *et al*, 2011; Lee *et al*, 2016). After injury, keratinocytes are important to cover the integument and to restore the epidermis. The epidermis in keloids however, does not completely fulfil its former functions

as there is a reduced barrier function of the stratum corneum, which comes along with an increased skin conductance and a higher loss of water through the skin (Sogabe *et al*, 2002). Furthermore, keloids are characterized by abnormal expression of involucrin, which is a known marker for terminal differentiation of epidermal cells (Limandjaja *et al*, 2017). A higher amount of involucrin was observed in the thicker epidermal layer of keloids, which indicates impaired cellular differentiation in the stratum corneum (Limandjaja *et al.*, 2017). The keloidal keratinocytes additionally show an altered expression pattern of cytokines and growth factors (Khoo *et al*, 2006; Mukhopadhyay *et al*, 2010; Ong *et al*, 2007). Gene expression studies uncovered a higher cell convertibility and cellular motility (Hahn *et al.*, 2013). Within the last years, the potential of keloidal keratinocytes for epithelial to mesenchymal transition (EMT) has obtained increasing attention (Hahn *et al.*, 2013; Ma *et al*, 2015; Yan *et al*, 2015). EMT, a process of cellular conversion which is characterized by loss of epidermal and acquisition of mesenchymal cellular features, was described to be involved in proper wound healing as one of several sources to increase the number of myofibroblasts at the wound site (Stone *et al*, 2016). This process was reported to constantly occur in keloidal keratinocytes (Yan *et al.*, 2015).

Myofibroblasts enforce the contraction of the wound after a damage of the skin (Werner & Grose, 2003). They display a presence in about 33-81 % of all keloids (Limandjaja *et al.*, 2020). Myofibroblasts can arise from different sources. The most common way is the differentiation from fibroblasts induced by TGF- β 1 or PDGF (Werner & Grose, 2003). Additionally, embryonal stem cell-like cells, which persist in the endothelium of the healthy skin, can be induced by trauma. They migrate into the wound area and differentiate in myofibroblasts and even fibroblasts (Lim *et al*, 2019). The process involved in this cellular change is called endothelial to mesenchymal transversion (endoMT) and describes a cellular conversion similar to EMT but with endothelial cells as cells of origin (Lim *et al.*, 2019). The reported associations of EMT and endoMT suggest an increased cellular transformation potential in keloids. Other discussed sources of myofibroblasts are invading fibrocytes and bone marrow-derived mesenchymal stem cells (Akino *et al*, 2008; Quan *et al*, 2004). The fact that myofibroblasts persist in the fibrotic area might promote the keloid formation, as they support an ongoing contraction and by this increased mechanic tension (Werner & Grose, 2003). One interesting theory for the myofibroblast persistence is the lack of hair follicles in keloids. Hair follicles are important for the conversion of myofibroblasts into adipocytes (Plikus *et al.*, 2017). Missing hair follicles might therefore provoke a backlog of myofibroblasts in the keloid with all its resulting consequences (Limandjaja *et al.*, 2020).

Although the vascular state in keloids has been described inconsistent, the general consent considers keloids as hypoxic tissue (Zhao *et al*, 2017). These contradictory findings can be explained by the high number of small but occluded vessels in hypertrophic scars and

keloids. (Zhao *et al.*, 2017). This phenomenon was explained by the high proliferation rate of endothelial cells (Kischer *et al.*, 1982). As part of the vessels, pericytes were discussed as potential pathologic driving force and an alternative source of keloidal fibroblasts (Kischer, 1984). The vasculature system plays an important role in wound healing and scar formation. An increase of vessels together with a higher permeability was discussed to promote the keloid formation (Ogawa & Akaishi, 2016; Zhao *et al.*, 2017). The “porous” vasculature might support the invasion of fibrosis-inducing immune cells which would consequently also prolong the inflammatory phase (Ogawa & Akaishi, 2016).

As darker pigmentation of the skin was set in context with a higher chance to form a keloid scar, melanocytes are also considered as an important pathologic player (Burd & Huang, 2005; Wolfram *et al.*, 2009). Melanocytes were discussed to support the keloid formation by an interaction with fibroblasts through the damaged basement membrane and by an anti-inflammatory inhibiting behaviour (Gao *et al.*, 2013).

Beside the previously mentioned ethnic, genetic, inflammatory, and cellular hypothesis, there are several other discussed theories about the source of keloid formation. These include viral components, stiffness gaps, nutritional imbalance, metabolic alterations, nitric oxide, hypertension, and psychoneuroimmune-endocrine causes for keloid formation (Alonso *et al.*, 2008; Butler *et al.*, 2008; Cobbold, 2001; Hochman *et al.*, 2015; Huang *et al.*, 2017; Huang & Ogawa, 2013).

One special hypothesis about the keloid as an incomplete malignant formation leads to extensive discussions in the scientific world (Ladin *et al.*, 1998). This hypothesis questions in particular the specification of keloids as an abnormal scar and suggests keloids as a cancer-like pathology (Tan *et al.*, 2019). The main keloid-characterizing features as spreading, uncontrolled expansion, no regression, and a high chance of recurrence upon excision are also considered as typical cancer-specific characteristics (Tan *et al.*, 2019). However, as the keloid does not metastasize it might be more like a non-malignant neoplasia (Tan *et al.*, 2019). The comparison is further supported since multiple tumour biomarkers are also positive in keloids (Tan *et al.*, 2019).

Research in keloids is strongly limited since keloids only occur in humans (Tuan & Nichter, 1998). *In vivo* models comprise computational, invasive, and non-invasive models (Limandjaja *et al.*, 2020). *In vivo* animal models include transgenically implanted keloids as well as single cell implantations or skin equivalents (Limandjaja *et al.*, 2020). The induction of keloids in animals has never been successful so far and the best outcome were hypertrophic-like scars (Khorshid, 2005). *In vitro* models on the other side can be performed as whole explant model of excised keloids, which survive in culture for about 6 weeks (Bagabir *et al.*, 2012b). Other *in vitro* models are the direct cultivation of keloidal cells in monolayers, skin equivalent or seeded in 3D scaffolds (Limandjaja *et al.*, 2020). Co-cultures

of different cell types direct or indirect as in double chamber systems give important information on paracrine interactions (Limandjaja *et al.*, 2020). All models have their limitations, however, so far no successful keloid model has been developed that covers all experimental objectives (Limandjaja *et al.*, 2020).

1.5.1 Recent results of single cell RNA sequencing analyses of keloids

In the last few years, single cell RNA sequencing (scRNAseq) proved as a powerful novel method in the world of basic research. This method provides the chance to get insights in complex pathologies, such as the keloid, by the investigation of their cellular cosmos and their molecular features based on the distinct transcriptomes (Papalexi & Satija, 2018). Numerous important, recently published findings were explored with scRNAseq and the research of keloids already profited from this method (Deng *et al.*, 2021a; Papalexi & Satija, 2018).

The group of Deng *et al.* released the first description of keloids on a single cellular level in June 2021. They compared single cell datasets from the dermal layer of 3 keloids and 3 normal scars. Bioinformatics analysis revealed an increase in endothelial cells, smooth muscle cells and myofibroblasts in the keloid tissue. The relative abundance of fibroblasts however was decreased. The research group of Deng *et al.* further was successful in the characterisation of the identified fibroblasts in secretory-papillary, secretory-reticular, mesenchymal, and pro-inflammatory subtypes, and subsequently demonstrated an increase of mesenchymal fibroblasts in keloids. These mesenchymal fibroblasts appeared to be involved in bone development. Analysis of cell-cell communications identified the mesenchymal fibroblasts as most interacting cells in keloids. They induce collagen expression in other fibroblasts through the secretion of periostin. Their transcriptional analysis further identified the increase of this mesenchymal fibroblasts in scleroderma, another fibrotic skin disease (Deng *et al.*, 2021a).

In December 2021, Xie *et al.* published another study, based on the transcriptional data gained by Deng *et al.* The group of Xie *et al.* first reanalysed the datasets and annotated the mesenchymal fibroblasts as chondrocytes. They identified tenascin-c as novel biomarker for the diagnosis of keloids (Xie *et al.*, 2021).

Xuanyu Liu and his research team published a paper in January 2022 comparing the scRNAseq data of 4 keloids and 4 skins adjacent to keloids. They confirmed the increase in fibroblasts and endothelial cells in keloids. The signalling pathways of TGF- β and Eph-ephrin were associated with the fibrotic process and angiogenesis in keloids. They describe the upregulation of genes involved in pathways associated with tumorigenesis and highlight potential regulatory genes such as collagens, twist-related protein 1 (TWIST1) and others (Liu *et al.*, 2022).

Recently, Shim *et al.* published a paper combining scRNAseq with spatial transcriptomics. They compared keloid with healthy skin and were able to locate the pathology-associated fibroblasts in the deeper layers close to endothelial sites of the keloid. This finding confirms the previously mentioned deep active areas in keloids. Another major finding was the mesenchymal activation of endothelial cells in keloids which was suggested to have a pathology supporting function (Shim *et al.*, 2022).

1.6 The extracellular matrix in skin, scar and keloid

The ECM works as lounge area for cells, as communication and management centre but also as scaffold which defines the tissue. The major components are proteoglycans, collagen and water, but also many other important factors contribute to the matrix and its functions (Meenakshi *et al.*, 2005; Theocharis *et al.*, 2016). Through the matrix, cellular information can be sent to cells and stimulate their growth, differentiation and other physiologic features (Karamanos, 2019). The major amount of matrix components is produced by cells. External stimuli induce the cellular production and secretion of different factors of the extracellular matrix (Baum & Arpey, 2005; Chan *et al.*, 2010). Some of them are entirely released to the extracellular space, others remain bound to the plasma membrane (Manou *et al.*, 2019). Water relates significantly to the presence and concentration of several matrix factors (Comper *et al.*, 1990). The matrix is important to maintain tissue homeostasis but also defines tissue development and morphogenesis. It defines the varying tissue types such as muscle or connective tissue (Manou *et al.*, 2019). This capacity however might also have negative effects in a pathological context (Karamanos, 2019). Biomechanical but also pure mechanical stress constantly shape the ECM, its volume, and its composition (Karamanos *et al.*, 2019).

Proteoglycans as one of the major ECM elements are comprised by core proteins with negatively charged, glycosaminoglycans that are partially esterified with sulfate groups (heparin, heparin sulfate, dermatan sulfate and others) (Karamanos *et al.*, 2018). They support the ECM structure, immobilize and/or store growth factors, and play a key role in mechanical properties such as tissue compression or hydration (Karamanos *et al.*, 2018). According to their location, proteoglycans can be subdivided in an extracellular (hyalectans, small leucine rich), a pericellular (perlecan, agrin), a cell surface (syndecan, glypican) and an intracellular (serglycin) group (Karamanos *et al.*, 2018). They regulate important cellular features such as adhesion, cell death, differentiation, migration, proliferation and survival as well as fibrillogenesis of collagens (Karamanos *et al.*, 2018).

Unbound glycosaminoglycans such as hyaluronic acid are important for the water balance of the ECM and are also involved in tissue repair or regeneration, homeostasis, muscle development or embryogenesis (Garantziotis & Savani, 2019).

Collagens, as the most abundant component within the ECM (30 %), is mainly present as collagen type I, II and III, which make up about 80-90 % of the total ECM collagen (Kirkness *et al*, 2019; Soroushanova *et al*, 2019). They consist of homo- or hetero-trimeric alpha-chains which form of triple-helices (Kirkness *et al.*, 2019). There are 28 different collagen types, some of them are present in many different tissue types (type I, III), others are relatively specific as in basal membrane (col type IV, VII, XV, XVII, XIX), connective tissue (col type II, IX), epithelial tissues (col type XIII, XVII), myotendinous junctions (col type XXII), peripheral nervous system (col type XXVIII), tendons and cartilage (col type X, XI, XII, XX, XXIV, XXVII) (Soroushanova *et al.*, 2019). Collagens provide important scaffold features but also confer tissue stabilization and flexibility (Soroushanova *et al.*, 2019).

Another important component of the ECM are elastic fibres. They are primarily present in tissues of constant mechanical stress such as the lungs, the skin, or arteries (Vindin *et al*, 2019). Tropoelastin, a soluble precursor of elastin, is released by cells and subsequently interconnects with fibrillin, an essential glycoprotein, to form a network of elastic fibres (Vindin *et al.*, 2019). Elastic fibres can interact with other ECM components to support cellular signalling and store growth factors in the matrix (Godwin *et al*, 2019). The amount of elastin in the human body Declines with age (Fhayli *et al*, 2019).

The covalent binding of tropoelastin with collagens is promoted by lysyl oxidase (LOX) and LOX-like proteins (Vallet & Ricard-Blum, 2019). This binding supports the stabilization of the ECM and provides stiffness (Vallet & Ricard-Blum, 2019). LOX and LOX-like protein interact with many growth factors and are also involved in important mechanisms as remodelling, repair and development of tissues (Vallet & Ricard-Blum, 2019).

Another ECM factor important for response to tensions is fibronectin. Fibronectin is an important adhesion molecule for cell migration and is also involved in proliferation, and matrix stabilization (Zollinger & Smith, 2017). Laminins are heterotrimeric glycoproteins consistent of an alpha, beta and gamma chain and are known as important compound of basic membranes (Aumailley, 2013). Tenascins are matricellular proteins (Murdamoothoo *et al*, 2018). They consist of three domains and can be subdivided in tenascin-C, -R, -W and -X (Imanaka-Yoshida & Matsumoto, 2018). Tenascins modulate cell adhesion and specific subtypes are associated with morphogenesis and tissue development (tenascin-C), chronic inflammation and fibrosis (tenascin-C), organogenesis (tenascin-X), neurogenesis (tenascin-R), osteogenesis (tenascin-W), and others (Imanaka-Yoshida & Matsumoto, 2018; Midwood *et al*, 2016; Murdamoothoo *et al.*, 2018; Scherberich *et al*, 2005; Tucker & Degen, 2019; Xu *et al*, 2014).

There are several changes in the composition of the ECM induced by scar or keloid formation in the skin. The amount of ECM is increased in scars and consists of more water (Bailey *et al*, 1975; Kwan & Tredget, 2017). The total collagen in the healthy skin consists of about 80 % type I, 10-15 % type III and a minimal amount of collagen type V (Hayakawa *et al*, 1979; Kwan & Tredget, 2017). In contrast, the hypertrophic scar collagen displays collagen type III percentage of 33 and 10 % collagen type IV (Kwan & Tredget, 2017). Also, the thickness of collagen bundles is altered in hypertrophic scars, compared to the healthy skin. Collagen bundles in the healthy skin are arranged in a nonparallel “basket-weave” way, whereas they are aligned parallel to the scar surface (Verhaegen *et al*, 2009). In keloids, on the other side, significantly thicker, disorganized, loose collagen bundles are described (Verhaegen *et al*, 2009). The ratio of type I collagen to type III collagen in normal scars seems to be about 6:1, whereas in keloids a ratio of 17:1 was reported (Verhaegen *et al*, 2009).

The amount of elastin appears to be decreased which would explain the increased scar stiffness (Amadeu *et al*, 2004). Hyaluronic acid is present in the normotrophic scar in form of a papillary layer (Bertheim & Hellström, 1994). This layer was also identified in hypertrophic scars but much thinner (Bertheim & Hellström, 1994). No information on the relative amount of hyaluronic acid was found in keloids but in comparison with normal scars keloids reveal an equal amount of hyaluronic acid in the epidermis and the dermis (Bertheim & Hellström, 1994).

An increase of versican, biglycan and glycosaminoglycans has been reported in hypertrophic scars and keloids (Carrino *et al*, 2012; Hunzelmann *et al*, 1996).

Decorin, a small leucine-rich proteoglycan, has an antifibrotic effect and reduces contraction (Buraschi *et al*, 2019). It also alters fibrillogenesis and supports a thinner formation of collagen fibers (Reed & Iozzo, 2002). An increase of decorin has been described in hypertrophic scars but not in normal scars or keloids (Garg *et al*, 1996; Hunzelmann *et al*, 1996; Scott *et al*, 1998). The amount of fibrillin-1 is decreased in any scar type compared to healthy skin (Amadeu *et al*, 2004). The amount of periostin, tenascin, chondroitin sulfate and fibronectin is elevated in keloids (Dalkowski *et al*, 1999; Ikeda *et al*, 2009; Kischer & Hendrix, 1983; Maeda *et al*, 2019).

The distinct ECM composition in keloids might be supported by an increase of enzymes affecting collagen production and persistence, such as the matrix metalloproteinases MMP-2, MMP-9 or tissue inhibitors of metalloproteinases -1/-2 (Ulrich *et al*, 2010).

The ECM assumes important functions regarding wound healing and scar formation. Detected alterations in the ECM composition in hypertrophic scars or keloids can be seen as a result of fibrotic processes but also as potential scar-promoting components.

1.7 The neuronal system in skin, scar, and keloid

The human skin is interweaved by numerous nerve fibres of the peripheral nervous system to ensure the sensory and protective function of the skin. Autonomic as well as sensory nerves are present in the skin (Besné *et al*, 2002; Hendriks *et al*, 2018). The skin nerves enter the skin coming from the dorsal root and the sympathetic ganglia and transmit according to their function exogenous stimuli or endogenous stimuli from or to the central nervous system (Abraira & Ginty, 2013; Roosterman *et al*, 2006). Exogenous signals can be set by mechanical forces, temperature, chemicals, electricity, and others (Abraira & Ginty, 2013). Endogenous stimuli detected by the skin comprise physiologic as well as pathophysiologic changes (Abraira & Ginty, 2013). Nerve fibre qualities present in the skin are A β -, A δ - with fast conduction velocity and C-fibres with the slowest velocity (Nolano *et al*, 2013). Between the dermis and the hypodermis is the subdermal plexus, smaller nerve fibres of the skin starting or ending up in this plexus (Zhang *et al*, 2010). The nerve fibres cross through the matrix till they reach their target structure, this can be sweat glands, vessels, the arrector pili muscle, hair follicles but also multiple sensory units as Meissner corpuscles, Merkel discs, Ruffini corpuscles, Krause end bulbs, Pacinian corpuscles or even the subepidermal nerve plexus as a neuronal network close to the epidermis (Gibbons *et al*, 2009; Iheanacho & Vellipuram, 2022; Reinisch & Tschachler, 2012; Siepmann *et al*, 2016; Siepmann *et al*, 2012). Any injury of the skin that includes the dermis comes along with damage in nerve fibres. About one third of all peripheral nerve trauma results in functional limitations and insufficient regeneration (Noble *et al*, 1998). This includes chronic pain, loss of sensation and other limitations (Wang *et al*, 2019). Depending on the extent of a peripheral nerve injury, it can be assigned to one of three different types. The neuropraxia with no structural damage of the nerve, the axonotmesis with disconnection of the axons and the worst case, the neurotmesis, a complete interruption of the nerve fibre (Seddon *et al*, 1943). The effective healing process of axonotmesis including full recovery takes up to 4 months, whereas neurotmesis often requires initial reattachment and, depending on the severity, comes along with a general poor recovery in function (Sunderland, 1951). Insufficient neuronal repair mechanisms can induce fibrotic harm as extraneural, dispersive or intraneural fibrosis which limit a proper neuronal function (Sakurai & Miyasaka, 1986). Damaged nerve fibres release neuropeptide substance P. This neuropeptide promotes inflammation, fibrogenesis as well as cell proliferation and angiogenesis (Pang *et al*, 1996). One potential counterpart of substance P is the neutral endopeptidase, which is bound to the cell membrane and breaks down the neuropeptide (Okamoto *et al*, 1994). Substance P is involved in the remodelling phase of wound healing, as it can regulate MMPs and their inhibitors (Ramos *et al*, 2007). In abnormal scars, an increased amount of substance P has been reported and the concentration of neutral endopeptidase was decreased (Crowe *et al*,

1994; Jing *et al*, 2010). This findings indicated an involvement of substance P in excessive scar formation (Jing *et al.*, 2010).

The nerve fibre density increases by the extent of scarring, as normal scars seem to have a higher density than healthy skin, and hypertrophic scars an even higher density (Crowe *et al.*, 1994).

Literature about the neuronal system in keloids, on the other side, is scarce and inconsistent. In 2008, Hochman *et al.* described a greater number of nerve fibres in keloids compared to normal skin. Their results are based on immunohistochemical staining of S100 calcium binding protein. The described nerve fibres appeared to be present in greater depth of the keloid tissue and should exhibit a much thinner and longer morphology compared to fibres of the healthy skin (Hochman *et al*, 2008).

In 2012, Tey *et al.* reported an insignificant decrease in nerve density in keloids compared to healthy skin. This finding was based on immunofluorescent staining of the pan-neuronal marker Protein gene peptide 9.5 (PGP9.5) in 10 µm-thick sections of itching keloids and healthy skin (Tey *et al*, 2012).

Another study performed by Saffari *et al.* reported similar and described a decrease of nerve fibres in keloids with the highest density in the upper dermis in the border area of keloids (Saffari *et al*, 2018).

The research group of Drummond reported in 2018 an increased expression of alpha1-adrenoceptor in nerve fibres, fibroblasts and blood vessels in keloid tissue compared to healthy skin and burn scars. The alpha1-adrenoceptor was associated with increased inflammation, wound healing, and pain. These staining-based findings were performed using PGP9.5 as marker for nerve bundles. (Drummond *et al*, 2018; Hochman *et al.*, 2008).

An increased response of the previously described neurogenic inflammation induced by mechanic forces was discussed in context with keloid formation by Ogawa *et al* (Ogawa, 2011).

Using scRNAseq, several research groups identified a neural cell cluster in keloid tissue but without any in-depth investigations. Deng *et al.* solely described a neural cell cluster, defined by the marker gene neurexin 1 (*NRXN1*) (Deng *et al.*, 2021a). Liu *et al.* detected a neural and a separate Schwann cell cluster characterised by a strong expression of S100 calcium binding protein B (*S100B*), neuronal membrane glycoprotein M6-b (*GPM6B*), *NRXN1*, alpha-crystallin B chain (*CRYAB*) and transcription factor jun-B (*JUNB*), myelin protein zero (*MPZ*), myelin basic protein (*MBP*), *S100B*, respectively. They described no significant difference in the amount of neural or Schwann cells, comparing keloidal cells and cells from keloid-adjacent skin. However, an increased communication of neural cells with other cells as fibroblasts, vascular endothelial cells and keratinocytes was defined. They also appeared to express a higher amount of *TGF-β1* compared to cells gained from keloid surrounding skin

(Liu *et al.*, 2022). The group of Shim defined a neural cluster by the expression of *S100B* (Shim *et al.*, 2022).

This limited state of knowledge with regard to the neuronal impact on the keloid formation encourages to expand research in the neurologic field of keloids.

1.8 Schwann cells and their role in tissue regeneration

The peripheral nerve system of the human body is structured in three layers. The inner layer, the endoneurium, consists of the nerve fibres/axons, Schwann cells, blood vessels, fibroblasts and macrophages surrounded by ECM (Causey & Barton, 1959; Gamble & Eames, 1964). The embedded nerve fibres are covered with Schwann cell that are in addition enclosed by a basal lamina (Stoll & Müller, 1999). The endoneurium is surrounded by the perineurium, a multi-layered cellular tube (Sunderland & Bradley, 1952). The endoneurium and the perineurium together form a nerve fascicle. In larger nerves, many fascicles are connected by matrix proteins to the third layer, the epineurium (Reina *et al.*, 2020). Not all nerves are multi-fascicular, as there are also small nerves consisting just of a single fascicle (Tan *et al.*, 2014). Schwann cells assume important caregiving functions for the peripheral nerve system (Nave, 2010). Two types of Schwann cells have been described in the healthy adult. The non-myelinating Schwann cells, or Remak cells, cover axons of small diameter which are especially present in the autonomic-, but also in the sensory-nervous system (Jessen & Mirsky, 2019a). One or more axons can be caved in the bodies of non-myelinating Schwann cells (Monk *et al.*, 2015). In contrast, myelinating Schwann cells ensheath multiple layers axons of a larger extent as motor neurons and some sensory axons (Jessen & Mirsky, 2019a). Myelinating Schwann cells produce myelin as part of their cell membrane which forms a kind of insulating layer around the axon (Osso & Chan, 2017). This special feature of myelinating Schwann cells supports a fast conduction of nerve impulses (Lubetzki *et al.*, 2020). Both Schwann cell types, myelinating and non-myelinating, provide important trophic and metabolic factors to the nerve to ensure a proper function and are involved in specific repair mechanisms upon neuronal damage (Jessen & Mirsky, 2019a; Nave, 2010). Schwann cells can be detected by S100, which has been proposed as general Schwann cell marker (Bhattacharyya *et al.*, 1992). Myelinating Schwann cells can be identified by their additional expression of factors associated with myelination, structure, and cholesterol synthesis (early growth response protein 2 [Krox20], MBP, myelin-associated glycoprotein [MAG], MPZ, peripheral myelin protein 22 [PMP22], periaxin), whereas non-myelinating Schwann cells are positive for factors also present in Schwann cell precursor cells, such as NGFR, neural cell adhesion molecule (NCAM), L1 or glial fibrillary acidic protein (GFAP) (Jessen & Mirsky, 2019a).

In the next section, the process of Schwann cell development will be outlined in more detail. Schwann cells evolve out of the neuronal crest in a strictly regulated process. Based on analysis of the neuronal system in rodents, developmental stages have been defined in the early embryonic nerves (Jessen & Mirsky, 2005). In the early embryonal phase, the Schwann cell precursor cells differentiate from neural crest cells (Jessen *et al*, 1994). In contrast to the adult structure, nerves in this early stage are solely composed of multiple packed axons and flat Schwann cell precursors without other cells, basal lamina, or space matrix (Jessen & Mirsky, 2005). Few days later, this structure converts suddenly and the perineurium and the basal lamina evolve (Jessen & Mirsky, 2005). The Schwann cell precursor cells develop into their next stages, the immature Schwann cells, and the ECM, fibroblast and blood vessels become part of the nerve (Jessen & Mirsky, 2005). After this step, the nerve composition is already adequate to the adult nerve (Jessen & Mirsky, 2005). However, the Schwann cell precursor cells are not only precursor cells of immature Schwann cells but also from endoneurial fibroblasts, melanocytes (via melanoblasts) and even parasympathic neurons (Adameyko *et al.*, 2009; Dyachuk *et al*, 2014; Furlan *et al*, 2017). In contrast to neural crest cells, Schwann cell precursor cells are positive for factors associated with differentiation of glia cells (Jessen & Mirsky, 2005). Factors important for the differentiation of crest cells into Schwann cell precursor cells are forkhead box D3 (FoxD3), transcription factor SOX-10 (Sox10), receptor tyrosine-protein kinase erbB-3 (ErbB3), Notch, Neuregulin-1, zinc finger E-box-binding homeobox 2 (Zeb2), endothelin and transcription factor AP-2 alpha (AP-2 alpha) (Brennan *et al*, 2000; Britsch *et al*, 2001; Garratt *et al*, 2000; Morris *et al*, 1999; Quintes *et al*, 2016; Stewart *et al*, 2001; Thomas & Erickson, 2009; Woodhoo *et al*, 2009). FoxD3 diverts lineage development towards Schwann cell development instead of neurons or melanocytes (Thomas & Erickson, 2009). In contrast, Sox10 is important for the Schwann cell precursor development out of neural crest cells and promotes the neuregulin receptors ErbB3 (Britsch *et al.*, 2001). This receptor, in addition, supports indirectly the generation of Schwann cells (Garratt *et al.*, 2000). The contact of Schwann cell precursor cells with axons is vital for the cells as the axons express neuregulin 1 (Garratt *et al.*, 2000). Notch associated precursor – axon interaction has been associated with the time span for Schwann cell differentiation as an increase in Notch signalling enhances differentiation whereas an inactivation of Notch delays Schwann cell conversion (Woodhoo *et al.*, 2009). A connection between Notch, Neuregulin-1 and ErbB3 has also been discussed (Dong *et al*, 1995). Endothelin shows opposite effects as an increase induces a delay in Schwann cell differentiation, whereas an inactivation promotes faster cellular conversion (Brennan *et al.*, 2000). AP-2 alpha has been discussed to support and maintain the precursor cellular state (Stewart *et al.*, 2001). Human nerve development and orientation in the embryo is not dependent on the presence of Schwann cells. However, the Schwann cells are important for the nerve to find its target and

to properly get in contact with it (Meyer & Birchmeier, 1995; Morris *et al.*, 1999; Woldeyesus *et al.*, 1999). Schwann cells precursor cells differentiate into immature Schwann cells which enclose several (Jessen & Mirsky, 2005). While survival of precursor cells is dependent on the contact with axons, immature Schwann cells control their survival by the secretion of autocrine factors as leukaemia inhibitory factor (LIF), lyophosphatidic acid, PDGF, neurotrophin-3, and insulin-like growth factor 2 (IGF-2) (Dong *et al.*, 1995; Meier *et al.*, 1999; Reynolds *et al.*, 1991; Weiner & Chun, 1999). In the next developmental step, the axons are isolated by multiple proliferating and apoptotic Schwann cell to form the final axon bundles covered by single Schwann cells in a non-myelinating or myelinating way depending on their extent (Jessen *et al.*, 2015). Developmental Schwann cell proliferation is driven by Notch, neuregulin-1, TGF- β and laminin, which is a component of the basal lamina (D'Antonio *et al.*, 2006; Garratt *et al.*, 2000; Woodhoo *et al.*, 2009; Yu *et al.*, 2005). Afterwards, myelinating or non-myelinating Schwann cells assume their mature, nerve supporting functions (Webster *et al.*, 1973). In this mature state Schwann cells hardly proliferate (Webster *et al.*, 1973).

Mature Schwann cells, as myelinating and non-myelinating Schwann cells, maintain a high potential plasticity (Boerboom *et al.*, 2017). Their phenotype is related to environmental factors (Boerboom *et al.*, 2017). A potential of myelinating Schwann cells to convert into a non-myelinating state when they get in touch with small nerve fibres and vice versa in case of thick nerve bundles has been suggested (Jessen & Mirsky, 2019a). However, the most impressive transformation of mature Schwann cells has been reported upon peripheral nerve injury. In case of an axonotmesis or neurotmesis, the axon-related Schwann cells undergo a phenotypic and morphologic change to ensure the survival of the damaged axon, to support its regeneration and to conduct reinnervation (Burnett & Zager, 2004; Jessen & Mirsky, 2005).

In case of neurotmesis, the nerve is completely disrupted, the distal part is dysfunctional and degeneration starts within 2-14 days and therefore, a neuronal regeneration coming from the proximal stump is required (Lunn *et al.*, 1989; Tsao *et al.*, 1994). The damaged nerve uses the distal, dying axon part as guiding structure for its regeneration (Rönkkö *et al.*, 2011). For this reason, a reattachment of the proximal and the distal stump is required. The human body facilitates this reconnection by the formation of a tissue bridge which is especially formed by Schwann cells (McDonald *et al.*, 2006). Surgical reconnection and, in severe cases, autografts or nerve conduits, can accelerate and support this process (Battiston *et al.*, 2005). However, misguided targeting, incorrect innervation, and long regeneration times have a negative effect on the outcome of the neuronal repair process (Barrette *et al.*, 2008; Höke, 2006; Jonsson *et al.*, 2013). The neuronal damage leads to a rapid change in the environment of the attached Schwann cells. This environmental change induces a reprogramming/transdifferentiation of mature Schwann cells into repair Schwann cells which

support nerve repair (Arthur-Farraj *et al*, 2012). This reprogramming includes proliferation, migration, cellular dedifferentiation, and activation (Armstrong *et al*, 2007; Chen *et al*, 2007). The injury-induced Schwann cell response comes along with several functional and structural changes, cellular rearrangement in Bungner Bands for neuronal guidance and macrophage attraction, also known as Wallerian degeneration. In the beginning, several factors associated with myelination are downregulated (MBP, MAG, MPZ, periaxin, and others) whereas factors detected in previous Schwann cell states (L1, NCAM, NGFR, GFAP) are upregulated (Jessen *et al.*, 2015). About 50 % of myelin from injury-induced myelinating Schwann cells is removed by themselves through myelinophagy, a type of myelin-specific autophagy (Brosius Lutz *et al*, 2017). In this actin-dependent process, the myelin is broken down into small pieces, that are subsequently digested in lysosomes (Jessen & Mirsky, 2005). The remaining myelin is phagocytosed by macrophages (Hirata & Kawabuchi, 2002; Martini *et al*, 2008). The macrophages are attracted to the injury site by cytokines as TNF- α , IL-1 α , IL-1 β and CCL2 produced by repair Schwann cells (Martini *et al.*, 2008; Shamash *et al*, 2002).

In addition, the upregulation of several factors important for neuronal survival and elongation of axons were identified, including artemin, brain-derived neurotrophic factor (BDNF), glial cell-derived neurotrophic factor (GDNF), nerve growth factor (NGF), neurotrophin-3 (NT3), pleiotrophin, and VEGF (Boyd & Gordon, 2003; Jessen & Mirsky, 2019a). Repair Schwann cells are characterized by an elongated, narrow, spindle shaped, often branched morphology (Gomez-Sanchez *et al*, 2017). Within 4 weeks after trauma, myelinating Schwann cells double in length whereas non-myelinating Schwann cells even obtain the three-fold length (Gomez-Sanchez *et al.*, 2017). They form partly overlapping tracks to target the regenerating nerve to their previous site of innervation (Jessen & Mirsky, 2019a). The transformation process of mature Schwann cells into repair Schwann cells is mediated by Raf/ERK, c-Jun N terminal kinase (JNK), p38 MAP signalling pathways as well as the factors Notch, c-Jun, G protein-coupled receptor 126 (GPR126), signal transducer and activator of transcription 3 (STAT3), Merlin, SRY (sex determining region Y)-box 2 (Sox2), paired box gene 3 (Pax3) and Id4 (Benito *et al*, 2017; Jessen & Mirsky, 2008; Kioussi *et al*, 1995; Mindos *et al*, 2017; Mogha *et al*, 2016). Especially c-Jun has a crucial function in the conversion process (Arthur-Farraj *et al.*, 2012). C-Jun induces the repair program and a lack of c-Jun results in a missing upregulation of factors as artemin, BDNF, GDNF, NGFR, N-cadherin, no proper myelin breakdown and no functional regeneration tracks and neuronal death (Arthur-Farraj *et al.*, 2012). C-Jun, but also STAT3 support the maintenance of the repair state in Schwann cells (Arthur-Farraj *et al.*, 2012; Benito *et al.*, 2017). Increased notch signalling promotes the demyelination process in Schwann cells after neuronal damage (Woodhoo *et al.*, 2009). In addition, H3K27 demethylation, H3K4 methylation and H3K27 deacetylation have also been

set in context with the damage-induced response of Schwann cells (Ma *et al.*, 2016). The migratory function of repair Schwann cells to reconnect the proximal and the distal stump is driven especially by Ephrin type-B receptor 2 (EphB2), Sox2, and N-cadherin (Parrinello *et al.*, 2010). Induced by fibroblast-bound ephrin B, Sox2 promotes N-cadherin induced by EphB2 to get in touch with Schwann cells of the opposite stump (Parrinello *et al.*, 2010). Extensive RNA sequencing analysis proposed several additional proteins and processes involved in the injury-induced response of Schwann cells (Bosse *et al.*, 2006; Weiss *et al.*, 2016). One big limitation of nerve regeneration is the slow regeneration tempo of the nerve in combination with the loss of the cellular repair phenotype of Schwann cells over time (Jonsson *et al.*, 2013).

To be able to distinguish repair Schwann cells from mature or immature Schwann cells, GDNF, oligodendrocyte transcription factor 1 (OLIG1), sonic hedgehog (Shh), artemin and c-Jun have been proposed as repair Schwann cell-specific markers (Jessen & Mirsky, 2016). After regeneration, repair Schwann cells convert back into a myelinating or non-myelinating state, for this reason the repair Schwann cells were only mentioned as a transient state (Jessen & Mirsky, 2016).

The repair response of Schwann cells start within minutes to hours after nerve injury with the activation of JNK-pathway (Parkinson *et al.*, 2008). Within the first day phospholipase A2 immunoreactivity, LIF, IL-6, IL-1 α , IL1 β , TNF- α , receptor tyrosine-protein kinase erbB-2 (ErbB2) neuregulin receptor reach their highest level, whereas IL-1 β , and TNF- α peak within 24 hours and subsequently decrease immediately (Kwon *et al.*, 1997; Rotshenker, 2011). On day 5, the autophagy process peaks. GDNF peaks after 1 week, c-Jun rises for up to 10 days and BDNF peaks after 2-3 weeks (De Felipe & Hunt, 1994; Eggers *et al.*, 2010; Gomez-Sanchez *et al.*, 2015; Jessen & Mirsky, 2019a; Parkinson *et al.*, 2008). Schwann cells proliferate fast within 4 weeks up to the 4-fold amount and are reduced by half after 2-3 months (Jessen & Mirsky, 2019a). However, the level of c-Jun in the distal repair Schwann cells decreases by the time from 4 weeks till 10 weeks after injury (Gomez-Sanchez *et al.*, 2017).

In 2018, the research group of Vadims Parfejevs revealed a functional involvement of glial cells (Schwann cells) in the repair process of damaged skin in rodents. Using genetic lineage tracing, the injury-induced migration of glial cells into the wound side was noticed. The accumulated glial cells were positive for Sox10, had no contact with an axon and steadily increased at the damaged area within two weeks after injury. These wound-associated glial cells were also positive for repair Schwann cell-markers (c-Jun, protein kinase R (PKR)-like endoplasmic reticulum kinase [pERK]) but also for proliferation factors (Ki67), factors typical for Schwann cell precursor cells (NGFR), and negative for MBP, which indicates a dedifferentiation and proliferation process. RNA sequencing analysis revealed a strong

association of the wound-site Schwann cells with ECM production, migration and TGF- β signalling. A lack of these wound-healing associated Schwann cells affected proper wound closure and results in a decrease of myofibroblasts in the damaged area. However, the described Schwann cell function in wound healing has not been investigated in the repair process of the human skin (Parfejevs *et al*, 2018).

In this context, the diversity of repair-associated Schwann cells should be revived (Jessen & Mirsky, 2005).

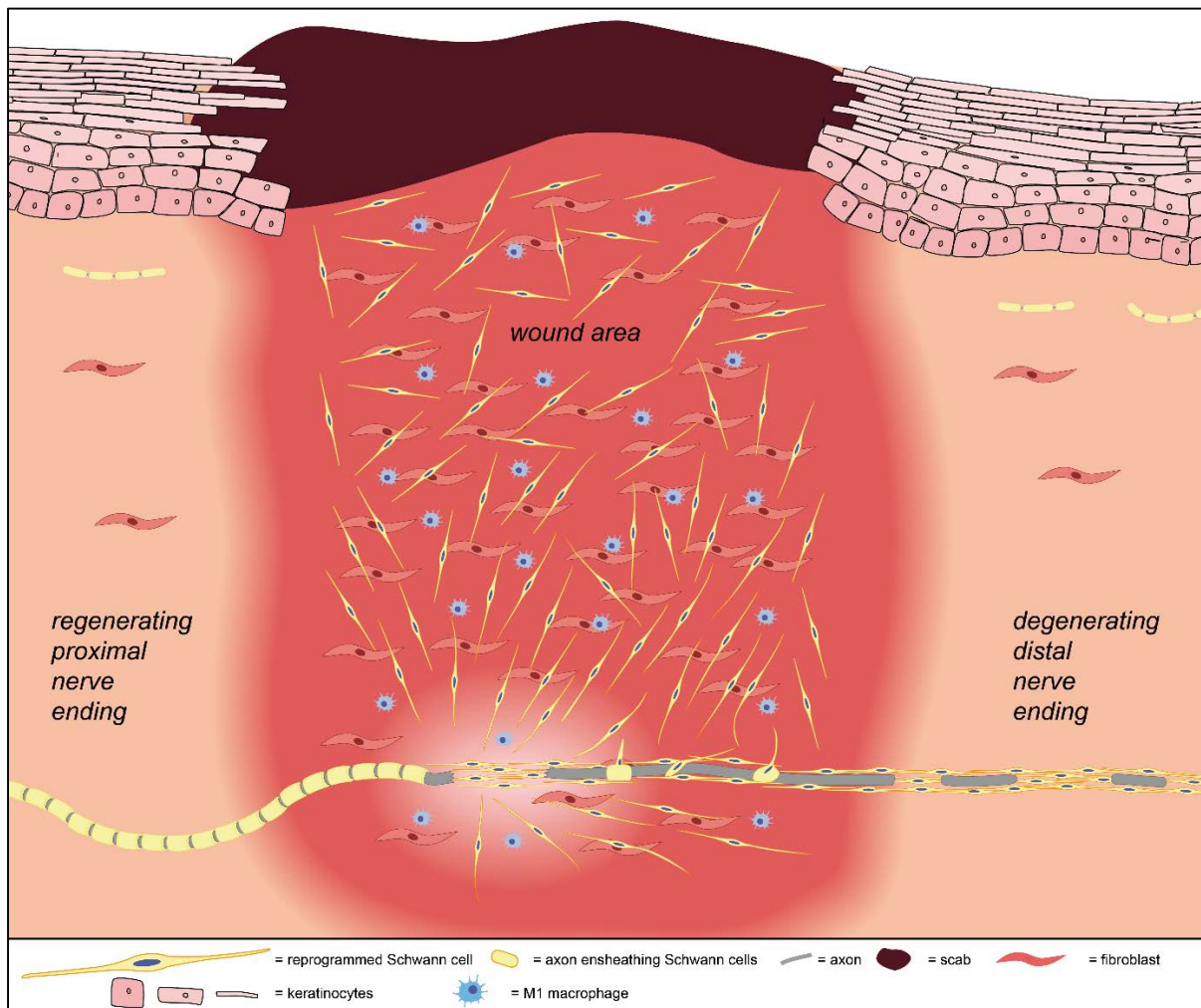


Figure 4: Schwann cell transformation upon injury

1.9 Aims of the thesis

Since the term “keloid” has been mentioned the first time in connection with this continual, border-crossing, fibrotic skin disease, several years of research have passed. Multiple cell types, first of all fibroblasts, have been analysed and various hypotheses are still part of the scientific discourse. The driving force behind the disease, however, still remains unclear.

The first aim of this thesis was to use scRNAseq to uncover so far unrecognized cellular contributions and pathologic mechanisms in keloids and to define novel, promising therapeutic approaches.

The second aim, emerging from the results of the first aim, was to comprehensively investigate the so far unrecognized keloid-specific Schwann cell population, to define their transcriptional pattern and their contribution to the keloidal pathology.

The third aim was to verify the disease specificity of keloidal Schwann cells by the investigation of independent datasets of skin, scars, and keloids.

2 CHAPTER TWO: RESULTS

2.1 Prologue

Multiple theories for the formation of keloids have been mentioned so far, whereby ethnical, hereditary and inflammatory mechanisms are most commonly discussed. However, the initial stimulus for keloid formation has not been elucidated yet. In the first publication of the thesis, the cellular environment of keloid tissue was unravelled applying scRNAseq. Thereby, a so far unrecognized presence of Schwann cells in keloids was identified. These keloidal Schwann cells showed pathology-supporting features and appeared to induce a pro-fibrotic state in macrophages.



Schwann cells contribute to keloid formation



Martin Direder^{a,b}, Tamara Weiss^c, Dragan Copic^{a,b}, Vera Vorstandlechner^c,
Maria Laggner^{a,b}, Karin Pfisterer^d, Caterina Selina Mildner^{a,b}, Katharina Klas^{a,b},
Daniel Bormann^{a,b}, Werner Haslik^{c,e}, Christine Radtke^c, Matthias Farlik^d,
Lisa Shaw^d, Bahar Golabi^d, Erwin Tschachler^d, Konrad Hoetzenecker^f,
Hendrik Jan Ankersmit^{a,b,1} and Michael Mildner^{d,1}

a - Laboratory for Cardiac and Thoracic Diagnosis, Regeneration and Applied Immunology, Department of Thoracic Surgery, Medical University of Vienna, Waehringer Guertel 18-20, Vienna 1090, Austria

b - Aposcience AG (FN 308089y), Dresdner Straße 87/A21, Vienna, Austria

c - Department of Plastic, Reconstructive and Aesthetic Surgery, Medical University of Vienna, Vienna, Austria

d - Department of Dermatology, Medical University of Vienna, Vienna, Austria

e - Department of Obstetrics and Gynecology, Medical University of Vienna, Vienna, Austria

f - Department of Thoracic Surgery, Medical University of Vienna, Vienna, Austria

Corresponding to Michael Mildner: Department of Dermatology, Medical University of Vienna, Waehringer Guertel 18-20, Vienna 1090, Austria.

michael.mildner@meduniwien.ac.at

Corresponding to Hendrik Jan Ankersmit: Laboratory for Cardiac and Thoracic Diagnosis, Regeneration and Applied Immunology, Department of Thoracic Surgery, Medical University of Vienna, Waehringer Guertel 18-20, Vienna 1090, Austria. hendrik.ankersmit@meduniwien.ac.at

<https://doi.org/10.1016/j.matbio.2022.03.001>

Abstract

Keloids are disfiguring, hypertrophic scars with yet poorly understood pathomechanisms, which could lead to severe functional impairments. Here we analyzed the characteristics of keloidal cells by single cell sequencing and discovered the presence of an abundant population of Schwann cells that persisted in the hypertrophic scar tissue after wound healing. In contrast to normal skin, keloidal Schwann cells show a unique, profibrotic phenotype. Our data support the hypothesis that keloidal Schwann cells contribute to the formation of the extracellular matrix and are able to affect M2 polarization of macrophages. Indeed, we show that macrophages in keloids predominantly display a M2 polarization and produce factors that inhibit Schwann cell differentiation. This study suggests the contribution of a Schwann cell - macrophage cross-talk to the continuous expansion of keloids, and that targeting Schwann cells might represent an interesting novel treatment option for keloids.

© 2022 The Author(s). Published by Elsevier B.V. This is an open access article under the CC BY license (<http://creativecommons.org/licenses/by/4.0/>)

Introduction

Keloids are fibroproliferative, protruding scar-like pathologies of the skin [1] characterized by a persisting, gradual growth beyond the margin of the wound

into the surrounding healthy skin. In susceptible individuals even minor skin injuries, such as insect bites or vaccinations, can induce keloid formation [2,3]. Although keloids show some tumor-like behavior, they do not metastasize. Nonetheless, keloids can

cause severe pain, chronic pruritus, psychosocial impairment and movement restriction due to their scar-like character [3–6]. Genetic predispositions as well as chronic inflammatory processes are being discussed in disease etiology [2,6–8]. As keloids are characterized by an increased proliferation of fibroblasts and extensive over-production of ECM components, keloid research has primarily focused on the involvement of fibroblasts in the development of these lesions [1]. Although these studies have identified numerous potentially pathology-related factors, the fundamental patho-mechanistic events driving keloid formation remain unclear [1]. The limited treatment options include steroid injections, g-radiation, and surgery, but the majority of patients still suffer from high recurrence rates [4,9,10], which underline the importance of identifying novel therapeutic approaches.

Due to the pruritic and painful nature of keloids, a neuronal contribution to the pathogenesis is conceivable. The subepidermal nerve plexus of the skin is the largest sensory organ of the human body. There is growing evidence that cutaneous innervation plays an important role in mediating wound healing [11,12]. It is, thus, surprising that a contribution of cutaneous nerves in keloid formation is poorly investigated [13–16]. The major cellular constituents of peripheral nerves are Schwann cells. In the healthy skin, Schwann cells ensheath cutaneous axons and ensure the integrity and function of sensory neurons [17–19]. Previously, increasing attention was drawn to Schwann cells because of their ability to adopt a transient repair phenotype in response to peripheral nerve injury [20,21]. This process involves a de-differentiation step into a proliferative precursor or immature-like Schwann cell state and the acquisition of repair specific functions [22]. These dedicated repair Schwann cells phagocytize myelin debris, express (neuro)trophic factors to support neuronal survival and form regeneration tracks (Bungner bands) to promote axonal outgrowth and guidance [23,24]. Furthermore, repair Schwann cells release a plethora of chemokines and cytokines to attract macrophages, thereby contributing to clear the lesion from myelin debris and remodeling the ECM to facilitate nerve regeneration [25–28]. Previous studies further support that the interaction between Schwann cells and macrophages affect their phenotype. While macrophages are known to regulate repair Schwann cell re-differentiation, Schwann cells promote the induction of M2 polarization of macrophages [29]. Macrophages play a crucial role in cutaneous wound healing by modulating the microenvironment during the different healing stages [30–32]. Especially M2-macrophages are associated with fibrosis and scarring and persist in keloids [31,33,34]. Moreover, a recent study in mice reported that the wound microenvironment is a key determinant of Schwann cell behavior, influencing their proliferation status, re-programming

into mesenchymal-like cells, immune signaling and ECM production [35]. Indeed, Schwann cells have been shown to contribute not only to nerve regeneration but also to wound healing by regulating myofibroblast differentiation, epithelial proliferation and ECM formation [36]. Hence, Schwann cells are important players in cutaneous wound healing processes and might play a yet underappreciated role in fibrotic processes.

In the present study we performed single-cell RNA sequencing (scRNAseq) of keloids to analyze the entire cellular spectrum and the transcriptional landscape at a single cell resolution and identified novel cellular and molecular players involved in keloid pathogenesis. Our analysis revealed that keloids contain a not yet described population of Schwann cells. The vast majority of these keloidal Schwann cells was not associated with axons, displayed a de-differentiated, pro-fibrotic phenotype, and showed key features with a high potential for affecting ECM deposition and macrophage function. Our findings suggest that an abnormal reaction of Schwann cells to skin injuries contribute to keloid pathogenesis.

Results

ScRNAseq reveals enrichment of Schwann cells in keloids

To investigate the cellular composition of keloids, we performed scRNAseq and compared our data with a recently published scRNAseq data set of normal human skin [37]. In total, transcriptomic data of 19,598 cells from normal skin and 47,478 cells from keloids were analyzed. As comparable single cell isolation methods were used in both studies, the differences in cell numbers mainly reflect the differing cellular composition of normal skin and keloids. After unbiased cluster generation (Fig. 1 A), cell clusters were identified with well-established marker genes as well as computed clustermarkers (Supplementary Fig. 1A and 1B; Supplementary Table 1). Cell clusters have been assigned to fibroblasts (FB), smooth muscle cells and pericytes (SMC/PC), keratinocytes (KC), endothelial cells (EC), lymphatic endothelial cells (LEC), T-cells (TC), macrophages (MAC), dendritic cells (DC), melanocytes (MEL) erythrocytes (ERY) and Schwann cells (SC) (Fig. 1 A). Comparison of different cell types between normal skin and keloids revealed a significant increase in cell number of fibroblasts, endothelial cells and lymphatic endothelial cells [1,38] (Fig. 1 A). Immunofluorescence (IF) staining corroborated our scRNAseq data by showing an increase in fibrotic and well-vascularized tissue of keloids compared to healthy skin (Supplementary Fig. 2). Strikingly, the proportion of Schwann cells were strongly increased in keloids (Fig. 1 B). These Schwann cells were characterized by the expression

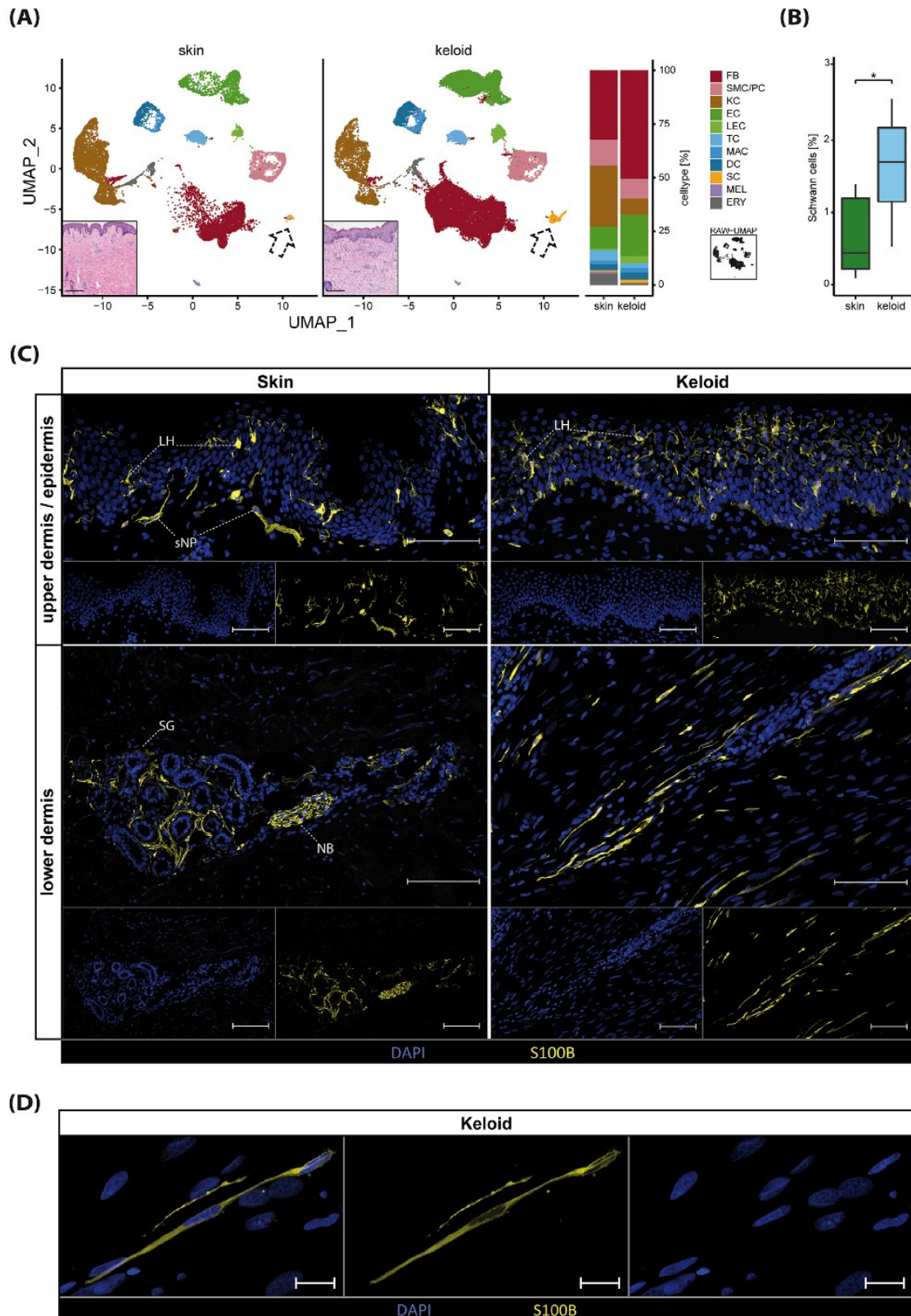


Fig. 1. Single cell RNA sequencing revealed Schwann cell accumulation in keloids compared to healthy skin. (A) Integrated UMAP-plots comparing cells of healthy skin ($n = 7$) with keloid tissue ($n = 4$), split by tissue, identifying fibroblasts (FB), smooth muscle cells and pericytes (SMC/PC), keratinocytes (KC), endothelial cells (EC), lymphatic endothelial cells

of S100 calcium binding protein B (S100B), nerve growth factor receptor (NGFR) (Supplementary Fig. 1B), myelin protein zero (MPZ), proteolipid protein 1 (PLP1), peripheral myelin protein 22 (PMP22), neural cell adhesion molecule 1 (NCAM1), L1 cell adhesion molecule (L1CAM), sodium voltage-gated channel alpha subunit 7 (SCN7A), sry-box transcription factor 10 (SOX10), periaxin (PRX), myelin associated glycoprotein (MAG), desert hedgehog signaling molecule (DHH), fatty acid binding protein 7 (FABP7), growth associated protein 43 (GAP43) and early growth response 2 (EGR2) (Supplementary Fig. 1C). To compare the SC populations between skin and keloid samples, IF staining for the Schwann cell marker S100B was performed. In healthy skin S100B stained epidermal Langerhans cells, melanocytes and dermal Schwann cells of the subepidermal nerve plexus, nerve structures around sweat glands, and larger nerve bundles of the deep dermis (Fig. 1 C). By contrast, S100B staining of keloids showed a scattered distribution of Schwann cells within the keloidal tissue (Fig. 1 C). Morphologically, Schwann cells in keloids showed an elongated, bipolar shape with a spindle-shaped body (Fig. 1 D). To further determine whether Schwann cells were associated with neurons, we stained 100 μ m thick transversal dermal sections of normal skin and keloids with S100B and the neuronal markers PGP9.5 and neurofilament (NF) (Fig. 2 A and B). Throughout all dermal layers of healthy skin, Schwann cells were found to ensheath axons (Fig. 2 A), while the vast majority of Schwann cells in keloids was not associated with axons up to 6 mm depth (Fig. 2 B, Supplementary movies 1–7). Only in the deep dermis of keloids (6000–8500 μ m), neuron-ensheathing Schwann cells were detected. Since axon-free Schwann cells in keloids showed uniform spatial orientation, we performed second harmonic generation microscopy together with S100B staining and found that the majority of Schwann cells were closely aligned with collagen bundles (Fig. 2 C, Supplementary movies 8 and 9).

Several Schwann cell subtypes are present in keloids

To characterize the Schwann cell population in keloids in more detail, we performed subclustering

and detected four Schwann cell subtypes exclusively present in keloids (SC-Keloid, SC-EC, SC-FB and SC-Prolif). In addition, one Schwann cell cluster was exclusively found in normal skin (SC-Skin), while another Schwann cell cluster was present in both normal skin and keloids (SC-Promyel) (Fig. 3 A and Supplementary Fig. 3). A total of 370 genes were differentially expressed between all keloid- and skin-derived Schwann cells (144 up- and 226 down-regulated) (Fig. 3 B). The skin-specific Schwann cell cluster (SC-Skin) expressed several genes characteristic for myelinating Schwann cells (MBP, PLP1, PMP22, MPZ) as well as genes commonly expressed in non-myelinating Schwann cells (NCAM1, L1CAM, SCN7A) [23,39] (Fig. 3 C, D and Supplementary Fig. 4). SC-Promyel, presumably representing promyelinating Schwann cells were characterized by the expression of pou class 3 homeobox 1 (POU3F1), glial fibrillary acidic protein (GFAP) and forkhead box protein O4 (FOXO4), the reduced expression levels of MPZ and PLP1 and the lack of MBP (Fig. 3 C) [40,41]. In line with our scRNAseq data, double staining of S100B with MBP confirmed that myelinating Schwann cells were present in healthy skin but virtually absent from keloids (Fig. 5 A). Schwann cells within keloids showed no or weak expression of previously described marker genes of mesenchymal progenitor cells, skin-derived precursor cells, neural crest cells and Schwann cell progenitor cells (Fig. 3 C) [41,47–49].

The majority of Schwann cells present in keloids is represented by the SC-Keloid subtype characterized by the expression of nestin (NES), insulin-like growth factor-binding protein 3 (IGFBP3), IGFBP5 , transforming growth factor beta-induced (TGFBI) and TNF-alpha induced protein 6 (TNFAIP6) (Fig. 3 A and D) [21,42–44]. To validate our transcriptomics data on the protein level, we performed double staining of S100B and nestin, visualizing that keloidal Schwann cells were highly positive for nestin (Fig. 4 A). Nestin is a known marker for neural precursor cells, involved in neuronal/glial development, which is also upregulated in human repair Schwann cells [45,46]. To characterize the cellular state of keloidal Schwann cells in more detail, we conducted IF staining for SOX10 and NGFR, which are both known to be upregulated in immature/de-differentiated Schwann cells, as

(LEC), T-cells (TC), macrophages (MAC), dendritic cells (DC), Schwann cells (SC), melanocytes (MEL) and erythrocytes (ERY). Bar plot indicates relative amounts of cell types within skin and keloid samples. RAW-UMAP represents unsplit UMAP without cluster coloring. Inserts show representative micrographs of Hematoxylin-Eosin-stained skin and keloid sections. Scale bars: 250 μ m; dashed arrowheads indicate SC-cell clusters. (B) Comparison of relative SC amounts by tissue. * indicates p-value < 0.05. (C) Representative immunostainings of skin (left-side) and keloid (right-side) with S100B-positive SCs in the dermal area. LH = Langerhans cell, sNP = subepidermal nerve plexus, SG = sweat gland, NB = nerve bundle. Scale bars: 100 μ m; (D) Close-up of keloidal SCs; Scale bar: 20 μ m. Tissues of n = 3 donors were analyzed per staining.

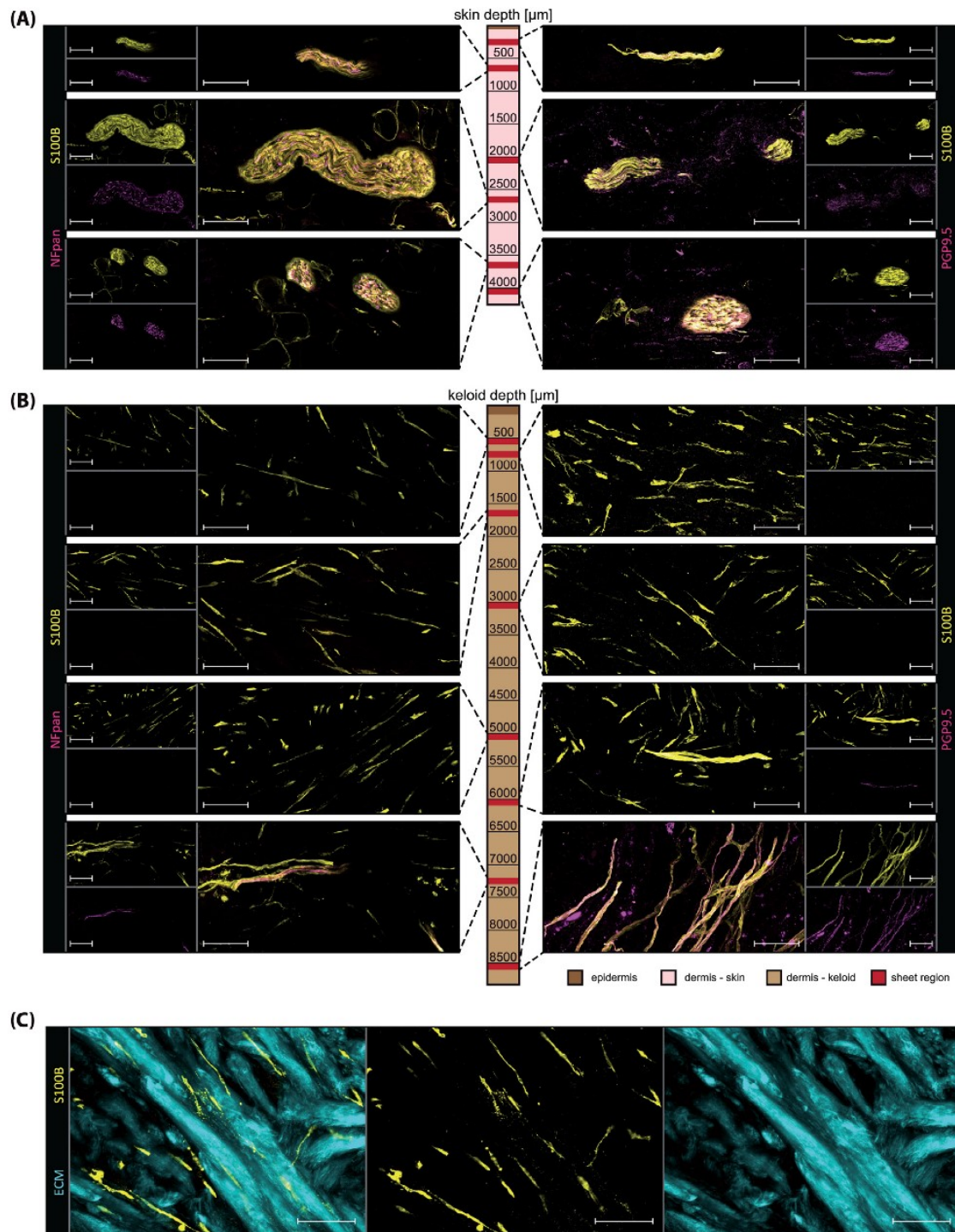


Fig. 2. Nerve-autonomous Schwann cell distribution throughout the whole keloidal dermis. Bird's-eye view of 100 μm -thick sections of (A) healthy skin and (B) keloidal dermal sheets. S100B indicates Schwann cells and PGP 9.5 (right side) or NFpan (left side) nerve fibers. Vertical reference bar illustrates depth of the depicted sheet region below the skin surface. Scale bar: 100 μm . (C) Dermal sheet image (1700-1800 μm depth) of keloids obtained via second harmonic generation (SHG) microscopy in combination with immunofluorescence staining of S100B. cyan: extracellular matrix, yellow: S100B positive cells. Scale bar: 100 μm .

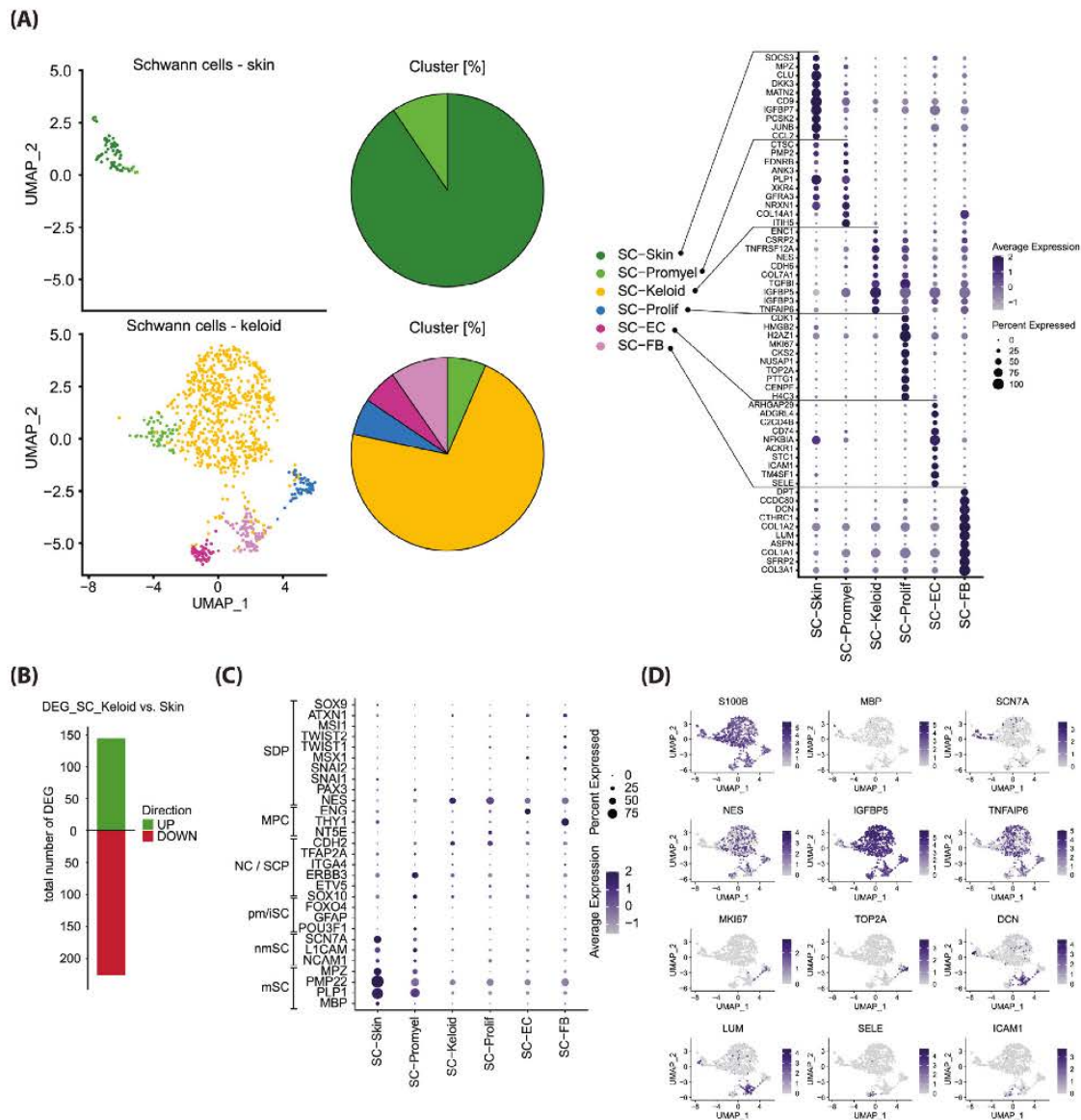


Fig. 3. Identification of keloid-specific Schwann cell subtypes. (A) Analysis of the Schwann cell subset identified 6 distinct Schwann cell subtypes depicted in UMAP-plots split by tissue. Pieplots display cluster percentage of the identified cell subtypes within each condition. Dotplot shows the top 10 genes leading to subcluster formation. Identified Schwann cell cluster: Myelinating and non-myelinating Schwann cells of the healthy skin (SC-Skin), promyelinating Schwann cells (SC-Promyel), keloidal Schwann cells (SC-Keloid), proliferating Schwann cells (SC-Prolif), cells expressing Schwann cell and endothelial cell specific genes (SC-EC), cells expressing Schwann cell and fibroblast specific genes (SC-FB). Color codes indicate average gene expression levels; Dot sizes indicate relative amounts of positive cells. (B) Total amount of differentially expressed genes (DEG) of all keloid- Schwann cells compared to all skin- Schwann cells. Genes with an average foldchange ≥ 2 were included. (C) Mature Schwann cell assignment by validated marker genes; mSC = myelinating Schwann cell marker; nmSC = marker genes for non-myelinating Schwann cells; pm / iSC = premyelinating / immature Schwann cell marker; NC / SCP = Neural crest cells / Schwann cell precursor marker; MPC = Mesenchymal progenitor cell marker; SDP = Skin Derived Precursor Cell marker. Color intensity indicates average gene expression. Dot-size shows percentage of cells expressing the genes. (D) Feature Plots of the integrated Schwann cells from healthy skin and keloids shows the expression of S100 calcium binding protein B (S100B), myelin basic protein (MBP), sodium voltage-gated channel Alpha Subunit 7 (SCN7A), nestin (NES), insulin-like growth factor binding protein 5 (IGFBP5), tumor necrosis factor alpha induced protein 6 (TNFAIP6), marker of proliferation Ki-67 (MKI67), DNA topoisomerase II alpha (TOP2A), decorin (DCN), lumican (LUM), E-selectin (SELE) and intercellular adhesion molecule 1 (ICAM1). Normal log gene expressions are mapped on the UMAP-Plot.

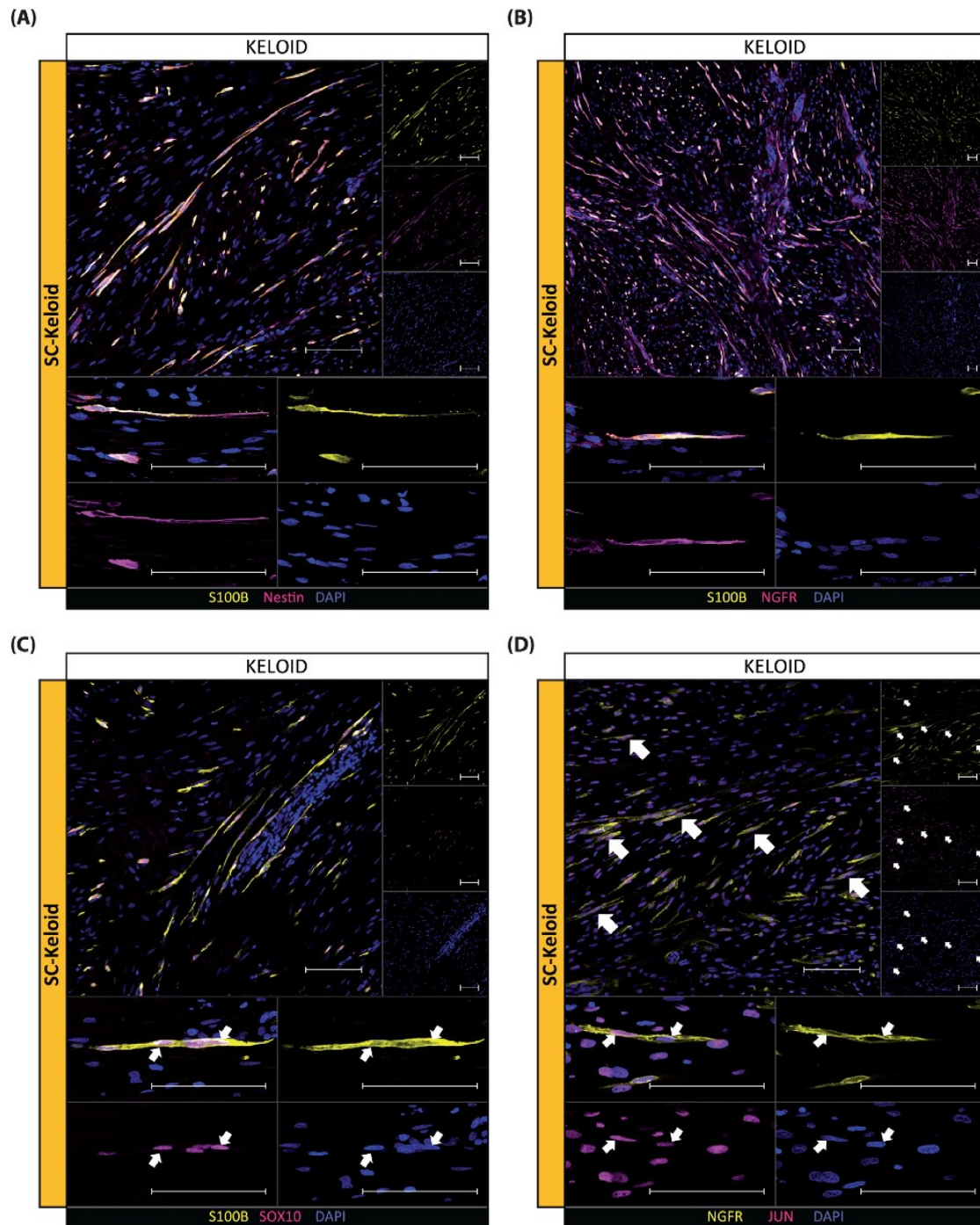


Fig. 4. Immunofluorescence staining confirmed predicted Schwann cell subtypes in keloid tissue. Immunostainings of keloidal Schwann cells for (A) S100B and Nestin, (B) S100B and nerve growth factor receptor (NGFR), (C) S100B and SRY-box transcription factor 10 (SOX10) and (D) NGFR and Jun proto-oncogene (JUN). Scale bar: 100 μ m. One representative micrograph of $n = 3$ donors per condition is shown.

well as the transcription factor JUN, which was demonstrated to be a key factor determining the repair identity of Schwann cells [21]. NGFR was strongly expressed by keloidal Schwann cells and vascular endothelial cells (Fig. 4 B). SOX10

nuclear expression was exclusively found in keloidal Schwann cells (Fig. 4 C). Of note, keloidal Schwann cell nuclei were positive for c-JUN (Fig. 4 D) but c-JUN expression was also found in other cells.

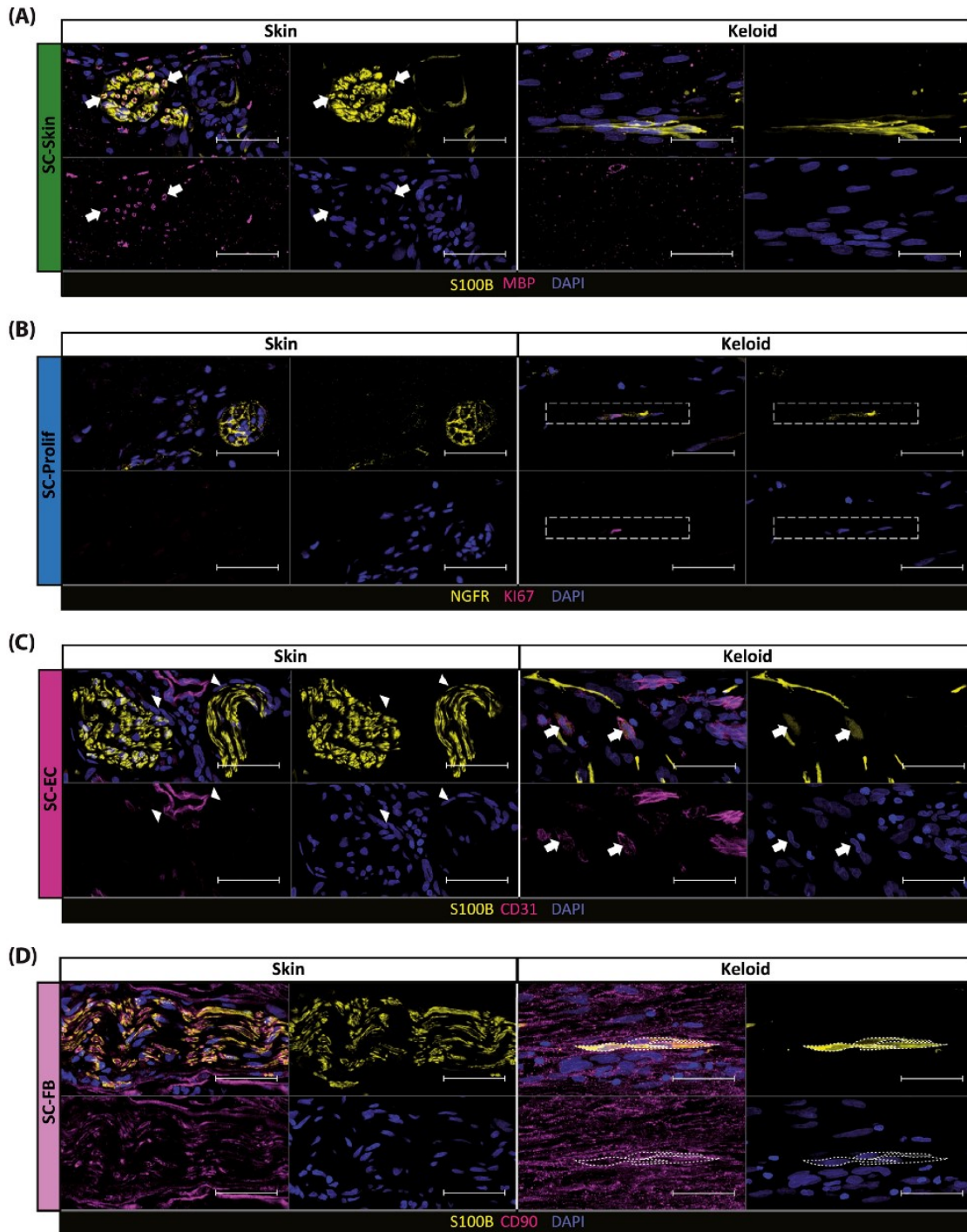


Fig. 5. Immunofluorescence staining confirmed predicted Schwann cell subtypes in keloid tissue. Representative immunofluorescence images of (A) myelin basic protein (MBP) and S100B stained Schwann cells showed double positive cells exclusively in healthy skin. Immunostainings of Schwann cells double positive for (B) nerve growth factor receptor (NGFR) and marker of proliferation Ki-67 (Ki67), (C) S100B and cluster of differentiation 31 (CD31) and (D) S100B and THY-1 cell surface antigen (CD90) in keloid tissue compared to healthy skin. Arrows, frames and rectangles indicate double-positive cells. Arrowheads indicate vessels. Tissues of $n = 3$ donors per condition were stained. Scale bars: 50 μ m.

In addition, we detected a Schwann cell cluster (SC-Prolif) with high expression of genes associated with cell division, such as markers of proliferation Ki-67 (MKI67) and DNA-Topoisomerase 2-alpha (TOP2A) in keloids but not in normal skin (Fig. 3 A and D). IF staining of keloids with Ki-67 in combination with NGFR confirmed the presence of proliferating Schwann cells in situ, indicating that single Schwann cells in keloids re-enter the cell-cycle (Fig. 5 B), corresponding to the increased proliferation rates of Schwann cells reported during wound healing and repair processes [35,36].

Two minor keloid specific Schwann cell populations were characterized in our scRNAseq analysis. The SC-EC cluster showed a combined expression of Schwann cell and endothelial cell markers such as selectin-E (SELE) and intercellular adhesion molecule 1 (ICAM1), and the SC-FB cluster showed a combined expression of Schwann cell and fibroblast markers such as lumican (LUM), decorin (DCN) or CD90 (Fig. 3 A, D and Supplementary Figs. 5 and 6, Supplementary movie 10). IF staining confirmed our single cell data and illustrated double positive cells for S100B and the endothelial cell marker CD31 (SC-EC; Fig. 5 C) as well as S100B and the fibroblast marker CD90 in keloids (SC-FB; Fig. 5 D). In normal skin, CD90-positivity was observed in the connective tissue and axons but not in Schwann

cells (Fig. 5 D) [47]. Compared to all other S100B-positive Schwann cells, SC-EC showed weaker S100B-expression and a different morphology, as they were oval shaped without extensions (Fig. 5 C, Supplementary Fig. 7). The identified SC-FB and SC-EC cell populations might represent a so far not recognized manifestation of Schwann cell plasticity.

In silico analysis of the Schwann cell differentiation behavior in keloids

Upon peripheral nerve injury, non- and myelinating Schwann cells start to de-differentiate, regain migratory and proliferative properties, and perform specific repair functions to support the regeneration of damaged nerves [23,36]. To investigate whether similar processes are ongoing during keloid development, we performed pseudotime trajectory analysis. Pseudotime trajectory suggested that keloidal Schwann cells indeed originate from differentiated myelinated Schwann cells (Fig. 6 A). Moreover, our calculation indicated that some of these keloidal Schwann cells acquired a proliferative state or de-differentiated into fibroblast-like or endothelial-like Schwann cells (Fig. 6 A). We further determined changes in Schwann cell gene expression along the pseudotime axis. While expression of genes associated with myelination [neuroblast differentiation-

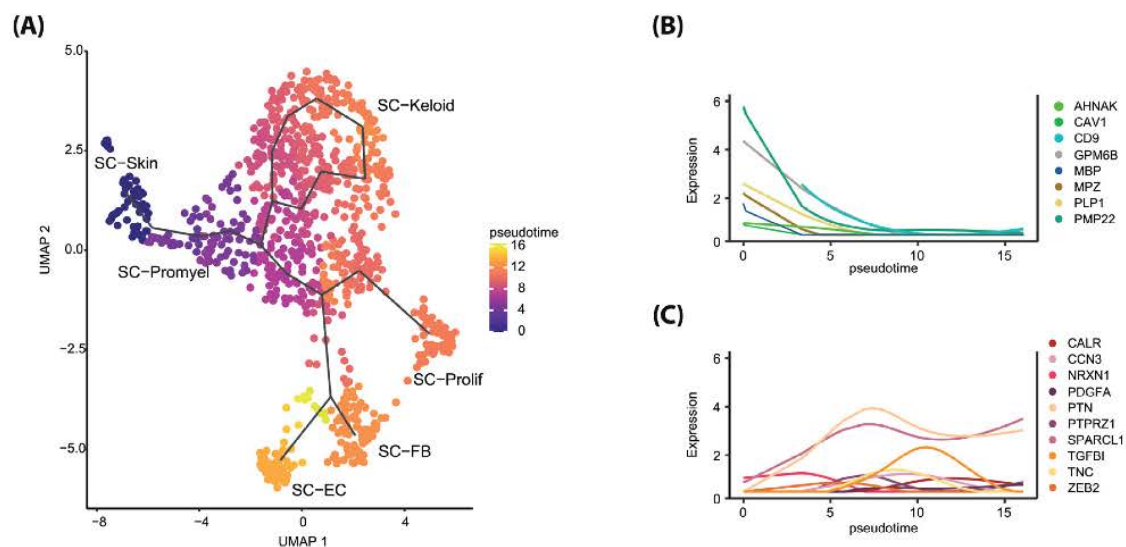


Fig. 6. Pseudotime analysis revealed genetic transformation from healthy SCs to keloidal SCs. (A) UMAP-plot including pseudotime track starting from healthy skin Schwann cells (SC-Skin) to keloidal Schwann cells. Color code indicates cellular moment in the calculated pseudotime. (B) Regulation of the expression of the myelination-associated genes: myelin basic protein (MBP), cluster of differentiation 9 (CD9), myelin protein zero (MPZ), proteolipid protein 1 (PLP1), neuroblast differentiation-associated protein (AHNAK), caveolin 1 (CAV1), neuronal membrane glycoprotein M6-B (GPM6B) and peripheral myelin protein 22 (PMP22) along the pseudotime. (C) Expression of genes associated with Schwann cell precursor cells, keloidal Schwann cells, nerve regeneration and cell migration: zinc finger e-box binding homeobox 2 (Zeb2), neurexin 1 (NRXN1), proliferation-inducing protein 33 (SPARCL1), pleiotrophin (PTN), protein tyrosine phosphatase receptor type Z1 (PTPRZ1), platelet derived growth factor alpha chain (PDGFA), cellular communication network factor 3 (CCN3), transforming growth factor beta –induced (TGFB1), tenascin C (TNC) and calreticulin (CALR). Only SC-Skin, SC-Promyel and SC-Keloid have been included to the pseudotime-expression analysis.

associated protein (AHNAK), caveolin 1 (CAV1), cluster of differentiation 9 (CD9), neuronal membrane glycoprotein M6-B (GPM6B), MBP, MPZ, PLP1 or PMP22] decreased over pseudotime (Fig. 6 B), the expression of genes associated with Schwann cell precursor cells, repair Schwann cells and nerve regeneration, such as cellular communication network factor 3 (CCN3), neurexin 1 (NRXN1), platelet derived growth factor alpha chain (PDGFA), pleiotrophin (PTN), protein tyrosine phosphatase receptor type Z1 (PTPRZ1), proliferation-inducing protein 33 (SPARCL1) and zinc finger e-box binding homeobox 2 (ZEB2) increased (Fig. 6 C) [48–55]. Furthermore, factors associated with cell migration, including calreticulin (CALR), TGFBI and tenascin c (TNC) [56–58], increased along the pseudotime trajectory (Fig. 6 C). A more complete set of genes regulated along the pseudotime trajectory is provided in Supplementary Fig. 8. These findings support the hypothesis that keloidal Schwann cells originate from differentiated myelinated Schwann cells by decreasing the expression of myelin genes while upregulating genes involved in repair mechanisms and migration.

Keloidal Schwann cells contribute to the formation of the extracellular matrix

As the pseudotime trajectory analysis indicated functional changes of Schwann cells in keloids, we further investigated the transcriptional differences and their possible functional consequences. Therefore, we utilized GO-Term enrichment analyses and found that genes highly expressed in normal skin Schwann cells were strongly associated with myelination and neuron development (Supplementary Fig. 9A), as well as membrane assembly, macrophage chemotaxis and dendritic cell differentiation (Supplementary Fig. 9B). GO-terms of the keloid-specific Schwann cell clusters differed significantly from those of Schwann cells present in normal skin. The most prominent GO-terms found in SC-Prolif were associated with cell proliferation processes (Supplementary Fig. 10A). Genes specifically expressed in SC-EC were mainly associated with the regulation of inflammatory response, and response to bacteria but also with vasculature development and regulation of epithelial cell differentiation (Supplementary Fig. 10B). The gene set enriched in SC-FB showed strong association with processes regulating the production and assembly of the ECM (Supplementary Fig. 10C). Interestingly, genes strongly expressed in SC-Keloid were associated with organization of the ECM, response to wound healing and connective tissue development (Fig. 7 A). Overall, the expression of many genes associated with ECM production and assembly [59] was significantly up-regulated in keloids (Supplementary Figs. 11–13) and various matrix-associated

genes were enriched specifically in keloidal Schwann cells (Fig. 7 B). Since inflammatory processes have been reported to be involved in the pathogenesis of keloids, we further investigated the expression of factors related to skin inflammation. However, the expression of inflammatory mediators was even down-regulated in keloids compared to healthy skin (Supplementary Fig. 14) and not regulated in Schwann cells (Fig. 7 C). Together these data indicate a contribution of Schwann cells to the organization of the ECM but not the inflammatory milieu in keloids.

Schwann cells in keloids differ significantly from Schwann cells found in neurofibroma type 1

Since the majority of Schwann cells in keloids were not associated with axons and displayed a dedifferentiated phenotype, we next explored their similarity to Schwann cells of cutaneous neurofibroma type 1 (NF1), a benign skin-tumor originating from Schwann cells [60]. Therefore, we compared our data set with previously published scRNAseq data of NF1 [61]. The re-calculated UMAP (Fig. 8 A) and cluster markers (Fig. 8 B) differed significantly between SC-NF1, SC-Skin and most keloidal Schwann cells. Only the SC-EC cluster showed high transcriptional resemblance with SC-NF1 (Fig. 8 A, left and middle panel; red oval) resulting in a new shared cluster after combined calculation (Fig. 8 A, right panel and Fig. 8 C). Cells of this combined cluster displayed a transcriptional profile associated with inflammatory processes (Supplementary Fig. 15). Importantly, no Schwann cells with SC-Keloid characteristics were found in NF1. In addition, pseudotime trajectory of the combined data set showed that SC-Keloid and SC-NF1 represent two separate branches, both originating from myelinating and non-myelinating skin Schwann cells (Fig. 8 D). Expression of genes associated with matrix formation was decreased in NF1, suggesting that NF1-derived Schwann cells are not involved in tissue remodeling processes (Fig. 8 E). However, expression of several inflammatory mediators, such as interleukin 6 (IL6), interleukin 8 (CXCL8), nuclear receptor 4A1 (NR4A1) and nuclear receptor 4A2 (NR4A2) was strongly upregulated in NF1-derived Schwann cells (Fig. 8 F), indicating that they contribute to tissue inflammation. Hence, our comparison shows that Schwann cells in keloids and Schwann cells in NF1 differ drastically in their ability to affect tissue remodeling and inflammation.

Schwann cells in keloids modulate macrophage function

Since denervated Schwann cells are known to interact with macrophages [26], we next investigated the phenotype of macrophages and how

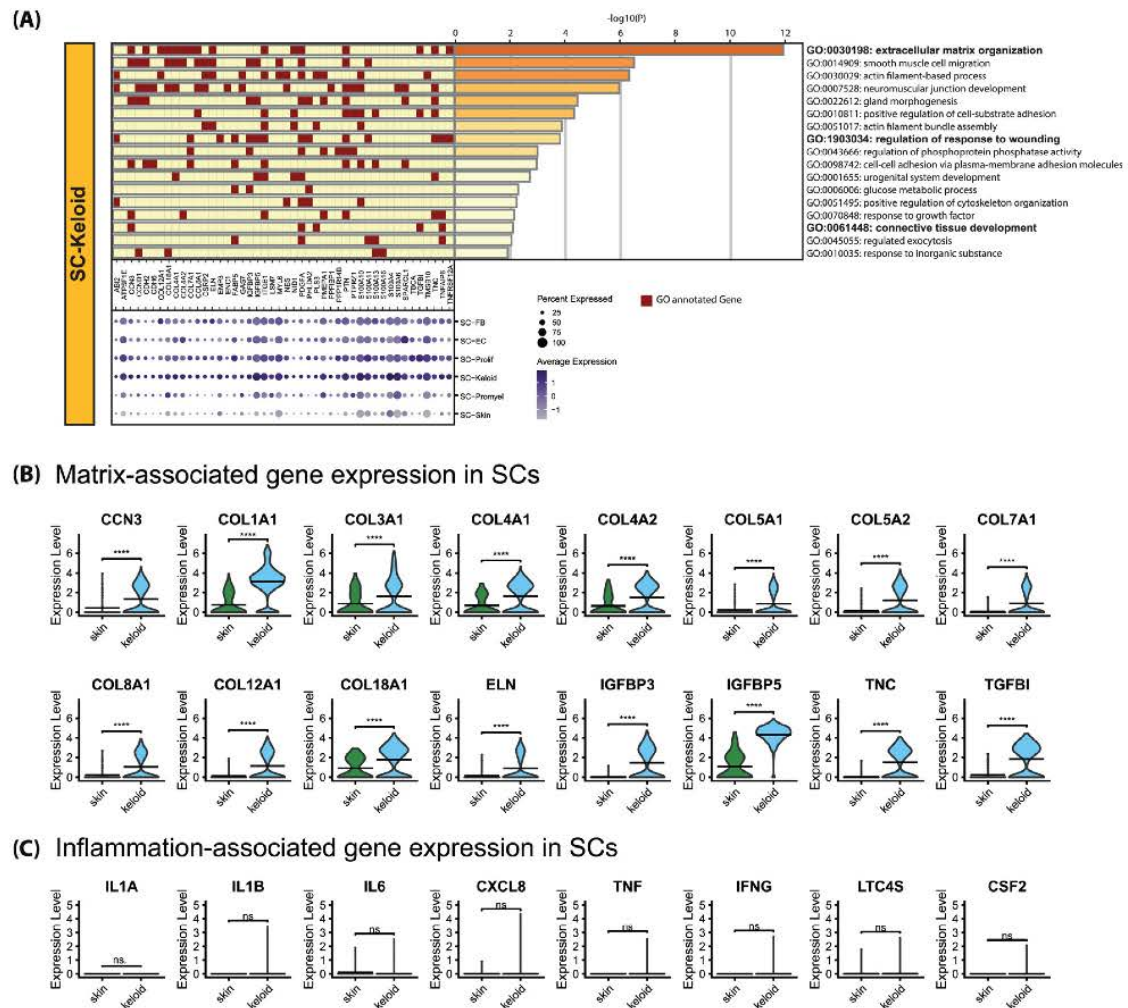


Fig. 7. Keloidal Schwann cells contribute to ECM formation. (A) GO-term enrichment of top-clustermarker genes with average foldchange ≥ 1.5 from SC-Keloid. Bar length represents statistical significance of the annotated term. Genes annotated to the respective term are marked in red. Dotplot depicts expression of the top-clustermarker genes in all Schwann cell subtypes. Color intensity of the dots depicts average gene expression. Dot size symbolizes percentage of cells expressing the respective genes. (B) Expression of the matrix-associated genes cellular communication network factor 3 (CCN3), collagen type I alpha 1 (COL1A1), collagen type III alpha 1 (COL3A1), collagen type IV alpha 1 (COL4A1), collagen type IV alpha 2 (COL4A2), collagen type V alpha 1 (COL5A1), collagen type V alpha 2 (COL5A2), collagen type VII alpha 1 (COL7A1), collagen type VIII alpha 1 (COL8A1), collagen type XII alpha 1 (COL12A1), collagen type XVIII alpha 1 (COL18A1), elastin (ELN), insulin like growth factor binding protein 3 (IGFBP3), insulin like growth factor binding protein 5 (IGFBP5), tenascin c (TNC) and transforming growth factor beta induced (TGFB1) of Schwann cells from the healthy skin and keloid. (C) Expression of the inflammation-associated genes interleukin 1 alpha (IL1A), interleukin 1 beta (IL1B), interleukin 6 (IL6), interleukin 8 (CXCL8), tumor necrosis factor alpha (TNF), interferon gamma (IFNG), leukotriene C4 synthase (LTC4S) and colony-stimulating factor 2 (CSF2) in Schwann cells of healthy skin and keloids. Crossbeam of violin plots depicts mean expression value. Vertical lines show maximum expression. Width represents frequency of cells at the respective expression level; ns. p-value > 0.05 ; **** p-value < 0.0001 .

macrophage function is influenced by the stroma in keloids, especially by Schwann cells. If confirmed a reported increase of macrophages in keloids compared to healthy skin (Supplementary Fig. 16A) [33,34]. We therefore sub-clustered macrophages and classified them according to established M1 and M2 activation markers [macrophage mannose receptor (MRC1) and cluster of differentiation 163

(CD163) for M2-macrophages and interleukin-1 beta (IL1B) and chemokine ligand 2 (CXCL2) for M1-macrophages] (Fig. 9 A). Whereas healthy skin mainly contained M1-macrophages (MAC-M1; 89%) and only few M2-macrophages (MAC-M2; 8%), the majority of macrophages in keloids expressed genes corresponding to M2-macrophages (MAC-M2; 49%). Another large macrophage population in

keloids showed a mixed M1/M2 phenotype (MAC-M1/M2; 36%) and a smaller population was characterized by a combined expression of fibroblast- and macrophage-specific genes (MAC-FB; 15%) (Fig. 9 B and Supplementary Fig. 16B).

We then focused our analysis on Schwann cell-derived factors that are known to influence macrophage function. Expression data of keloidal Schwann cells revealed several genes coding for secreted proteins, which are involved in the regulation of macrophage function. One of the strongest upregulated genes in SC-Keloid was tumor necrosis factor alpha-induced protein 6 (TNFAIP3) (Fig. 9 C), which has been shown to inhibit inflammation [62–64] and promote M2 polarization of macrophages [65,66]. In addition, we found an upregulation of CCN3 in keloidal Schwann cells (Fig. 9 C), a growth factor known to promote macrophage recruitment and differentiation into a M2 phenotype [67]. Interestingly, CCN3 was also upregulated in melanocytes in keloids. In accordance with a M2-promoting environment, CC-chemokine ligand 2 (CCL2), a chemokine important for the recruitment of inflammatory M1 macrophages in wounds [68,69], was almost completely absent in keloids (Fig. 9 C). Furthermore, CC-chemokine ligand 3 (CCL3) expression was strongly downregulated in keloids (Fig. 9 C). Since CCL2 and CCL3 in combination with TNF-alpha (TNF) are known to enhance the production and release of the ECM-degrading enzyme matrix metalloproteinase 9 (MMP9) in monocytes [70], we next investigated MMP9 levels in our data set. While MMP9 was expressed by macrophages and dendritic cells in healthy skin, we detected no MMP9 expression in keloids (Fig. 9 C), and the total release of MMP9 protein was strongly reduced in keloids (Fig. 9 D). Macrophages have been reported to regulate Schwann cell dynamics during nerve regeneration by supporting Schwann cell re-myelination and maturation through growth arrest-specific 6 (GAS6) [71]. Indeed, GAS6 expression was significantly decreased in MAC-M2 and MAC-M1/M2 in keloids (Fig. 9 C). Among the strongest upregulated genes in SC-Keloid was IGFBP5, a known pro-fibrotic factor supporting macrophage migration and conversion of monocytes into mesenchymal cells (Fig. 9 C) [72–74]. IGFBP3, another member of the IGFBP protein family with known anti-inflammatory activity [75] was also significantly upregulated in keloidal Schwann cells (Fig. 9 C). To validate our scRNAseq data, we quantified several of the identified factors in skin and keloid biopsies. We detected elevated CCN3 levels, while

CCL2, MMP9, and GAS6 were significantly decreased in keloids compared to healthy skin (Fig. 9 D). In addition, immunofluorescence staining confirmed increased IGFBP5 in the dermis of keloids compared to normal skin (Fig. 9 E). Together, these data indicate a crosstalk of keloidal Schwann cells and macrophages promoting increased matrix production by Schwann cells whilst inhibiting matrix degradation by macrophages.

Discussion

To date, the pathophysiological processes underlying keloid development are still poorly understood. Thus, we here performed a comprehensive scRNA-seq approach supported by confocal microscopy and second harmonic generation (SHG) imaging to provide insight into yet unknown cellular and molecular drivers of keloid formation. Our findings introduce Schwann cells as novel players involved in keloid pathology and suggest them as promising therapeutic targets.

Unbiased clustering of our scRNAseq data together with IF staining confirmed high amounts of fibroblasts and endothelial cells in keloids compared to normal skin. This finding is in line with the known keloid morphology and a recently published single cell data set of keloids on gene regulation in these cell types [38]. In contrast to the publication by Liu et al., we detected a significantly increased Schwann cell population in keloids compared to healthy skin. Strikingly, the data set by Liu et al. showed a much higher Schwann cell number in the control skin samples as compared to our healthy skin samples. We explain this discrepancy by the different sources of skin control samples. While Liu et al., used samples from skin areas closely adjacent to the keloids [38], we used normal skin from donors not harboring keloids. This observation indicates that the number of Schwann cells is already increased in skin adjacent to keloids and, therefore, already affected by keloid pathology. Since keloids are constantly growing tumors, infiltration of Schwann cells into the surrounding tissue might represent an important driver of the disease. However, further studies are necessary to address this question.

Tumor innervation and the contribution of the nervous system to keloid pathology have been hardly explored so far, and previous publications are contradictory [13–16]. As the major constituents of nerves are axons and Schwann cells, it was striking

highlights cluster with tissue purity below 80%. (D) UMAP-plot including pseudotime track starting from healthy skin Schwann cells (SC-Skin) to Schwann cells from Keloid or NF1. Color code indicates cellular moment in the calculated pseudotime. (E) Expression of matrix- and (F) inflammation-associated genes by Schwann cells of healthy skin, keloids and NF1. Colors indicate average gene expression and size shows percentage of cells expressing the genes in a group.

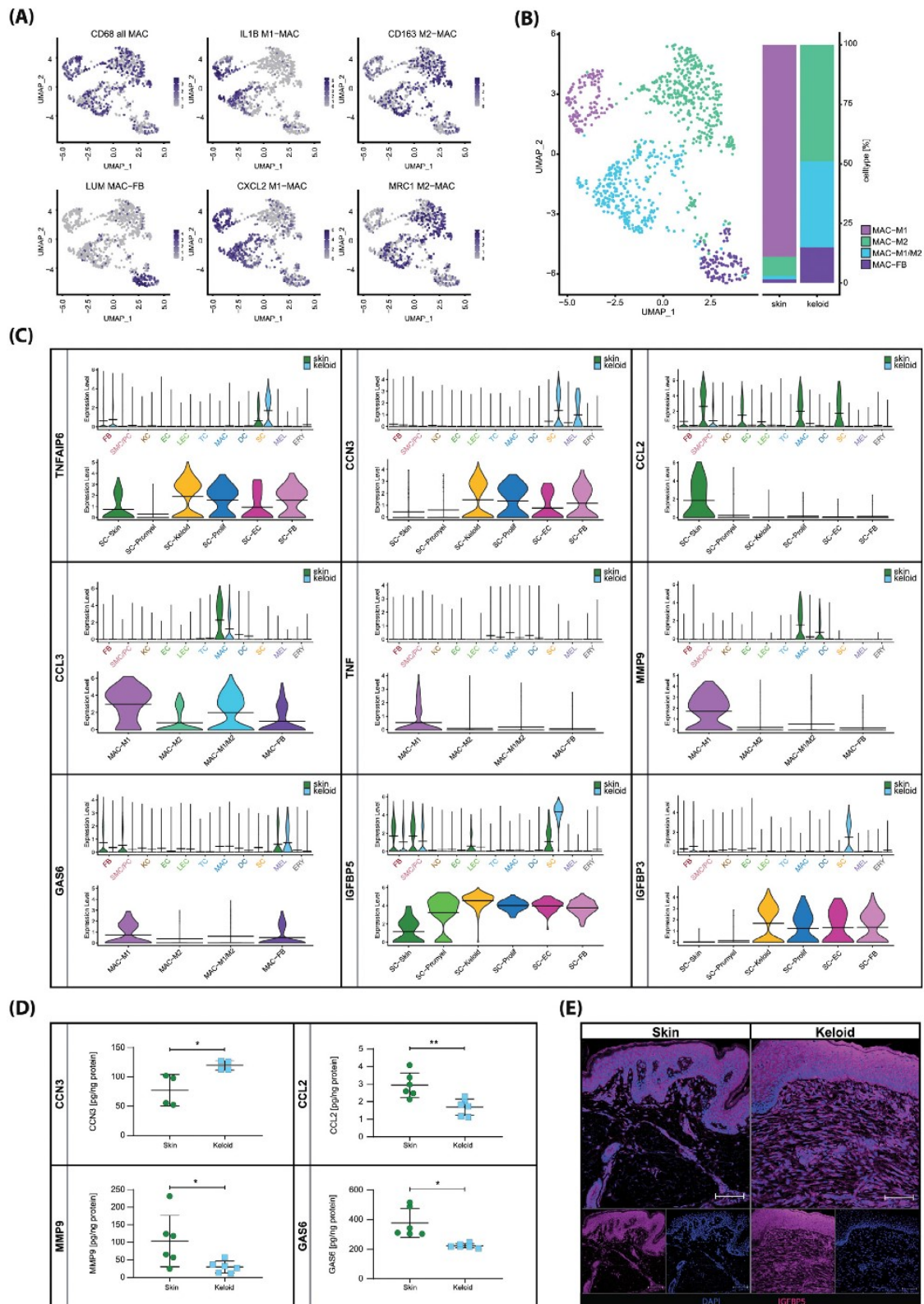


Fig. 9. Predicted Schwann cell - Macrophage interaction in keloids. (A) Macrophage cluster identification by marker genes: cluster of differentiation 68 (CD68), interleukin 1 beta (IL1B), cluster of differentiation 163 (CD163), lumican (LUM), chemokine (c-x-c motif) ligand 2 (CXCL2), mannose receptor (MRC1). Color intensity shows average gene expression. (B) Subset of macrophages detected in healthy skin (n = 4) and keloids (n = 4). Bars depict percentage

that the majority of keloidal Schwann cells were not associated with an axon. These axon-free Schwann cells had a spindle shaped morphology, comparable to that described for repair Schwann cells [20,24]. Repair Schwann cells show a characteristic expression pattern, including the expression of precursor/immature Schwann cell markers, such as SOX10, NGFR and NES, and repair-relevant markers such as JUN [21,42–45], that were all verified in our keloidal Schwann cell cluster. Of note, some previously published marker genes for repair Schwann cells (OLIG1, BDNF or GDNF) were not detected in our data set, arguing against a classical repair phenotype of these cells [20]. The long lasting presence of Schwann cells in keloids might shape the expression of a keloid-specific gene set differing from that of bona fide repair Schwann cells. As a skin injury precedes keloid formation, the manifestation of keloidal Schwann cells might reflect an abnormal wound healing response of dermal repair Schwann cells. Parfejevs et al. recently showed that peripheral glia cells are able to disseminate from the injured nerves into the granulation tissue, de-differentiate and proliferate during wound healing in mice [36]. At the wound site, infiltrating glia cells produce paracrine factors inducing myofibroblast differentiation, thereby promoting wound closure [36]. These findings are in line with our pseudotime trajectory analysis, which supports that keloidal Schwann cells descend from adult Schwann cells. In response to skin injury, an aberrant activation of dermal repair Schwann cells through intrinsic or extrinsic influences could drive the manifestation of keloidal Schwann cells and potential subtypes. We detected cells co-expressing Schwann cell and endothelial cell markers or Schwann cell and fibroblast markers. Future studies are warranted to determine whether these cells indeed represent a trans-differentiation state of Schwann cells. Compared to SC-Keloid and SC-FB, SC-EC exhibited a markedly different morphology and lower expression of S100B. In addition, SC-EC were devoid of SOX10 expression (data not

shown), suggesting vast loss of Schwann cell characteristics. Elucidating the functional relevance of these Schwann cell subsets remains to be evaluated in future investigations.

Interestingly, we found a decreased number of Schwann cells in scar tissue when compared to healthy skin or keloid tissue (Supplementary Fig. 17). This observation suggests that dermal repair Schwann cells do not remain in normal scar tissue after completion of wound healing. Therefore, the high abundance of Schwann cells in keloids led us to hypothesize that the persistence of dermal repair Schwann cells in the injured skin environment contributes to the pathogenesis of keloids. Of note, a connection between Schwann cell density in the skin and impaired wound healing has already been demonstrated in humans [76]. Reinisch et al. showed that the number of Schwann cells in the periphery was strongly diminished in patients with diabetes mellitus, suggesting a role for Schwann cells in the development of diabetic foot ulcers [76]. However, the exact mechanisms underlying this phenomenon remain unclear and need further investigations. Since mice do not develop keloids [1] and currently available in vitro models have several limitations [1], such as the lack of important cell types, including Schwann cells, answering this question is challenging and will require the establishment of new model systems. Nevertheless, we could demonstrate that Schwann cells significantly contribute to the stromal microenvironment of keloids by expressing factors that directly affect the function of other cells and ECM formation (several collagens and members of the IGFBP-family) [59,72–74].

The expression pattern of keloidal Schwann cells demonstrate high disease-specificity, as Schwann cells of NF1, another benign skin tumor with Schwann cell contribution [60], showed only minor similarities to those found in keloids. Whereas keloidal Schwann cells displayed a pro-fibrotic expression pattern with little expression of pro-inflammatory genes, Schwann cells in NF1 had a

distribution of detected macrophage-cluster for each tissue. Identified macrophage cluster: M1-macrophages (MAC-M1), M2-macrophages (MAC-M2), M1-M2 intermediate macrophages (MAC-M1/M2), cells expressing macrophage and fibroblast specific genes (MAC-FB) (C) Expression of TNF-alpha induced protein 6 (TNFAIP6), cellular communication network factor 3 (CCN3), CC-chemokine ligand 2 (CCL2), CC-chemokine ligand 3 (CCL3), TNF-alpha (TNF), matrix metalloproteinase 9 (MMP9), Growth arrest-specific 6 (GAS6), insulin-like growth factor-binding protein 3 (IGFBP3) and insulin-like growth factor-binding protein 5 (IGFBP5) of cells from healthy skin and keloids. Upper panel violin-plots depict gene expression across all celltypes split by tissue; green= skin, blue= keloid; fibroblasts (FB), smooth muscle cells and pericytes (SMC/PC), keratinocytes (KC), endothelial cells (EC), lymphatic endothelial cells (LEC), T-cells (TC), macrophages (MAC), dendritic cells (DC), Schwann cells (SC), melanocytes (MEL) and erythrocytes (ERY); Lower panel violin-plots show gene expression in previously described Schwann cell- or macrophage- types; crossbeam marks mean gene expression; vertical lines show maximum expression, Width represents frequency of cells at the respective expression level. (D) Protein quantifications of CCN3, CCL2, MMP9, and GAS6 in skin and keloids (n = 2 donors for CCN3, n = 3 for all others, measured in duplicate). Whiskers represent first and third quartiles and central bar marks median. * p < 0.05, **p < 0.01; (E) Representative immunostaining of IGFBP5 in skin and keloids. Tissues of n = 3 donors per condition were stained. Scale bars: 100 μm.

prominent pro-inflammatory phenotype, which is in line with a recent publication [77]. Although most of the Schwann cells present in NF1 and keloids are not attached to axons, they develop a remarkably different phenotype. This could be explained by the neoplastic transformation of Schwann cells during NF1 development [78], while the keloidal Schwann cells rather represent deregulated repair cells persisting after an injury. Since a genetic component has been suggested for the development of keloids [2,6–8], it is conceivable that genetic alterations of the expression of one or several genes might directly or indirectly affect Schwann cell functions. A recent study demonstrated that Schwann cells within the acute injury site or the denervated distal nerve segments acquire a different cellular behavior [35], underlining the highly adaptive potential of Schwann cells to their surroundings. Hence, the immediate and extended microenvironment of the wound and/or the forming scar, leading to keloid formation, is likely to be an important determinant for the unique cellular state of keloidal Schwann cells.

Our study also revealed an important cross-talk between Schwann cells and macrophages. Macrophages are known to significantly contribute to the stromal milieu by affecting repair processes, tissue inflammation and matrix remodeling in a macrophage subtype-specific manner [30–32]. Whereas M1-macrophages are pro-inflammatory and matrix-degrading, M2-macrophages contribute to the composition of the ECM [31]. In line with previous publications [33,34], we mainly detected M2-macrophages in our keloids. In addition, we identified one macrophage population with intermediate M1/M2 gene expression pattern and one subpopulation sharing gene sets specific for M2-macrophages and fibroblasts. The ability of macrophages to convert into mesenchymal cells is well documented and IGFBP5, one of the strongest expressed factors in keloidal Schwann cells, has been shown to support this process [74,79]. Although several genes associated with epithelial to mesenchymal transition, such as SNAI1, SNAI2, ZEB1, ZEB2, TWIST1, were not detected in this cell population (partly shown in Fig. 3 C) [80], our data indicate that also macrophages in keloids show a high degree of plasticity. Furthermore, keloidal Schwann cells produce several factors able to affect macrophage function. For example, we detected high levels of TNFAIP6, IGFBP5 and CCN3, all known to regulate migration, activation, and polarization of macrophages [65–67,74]. In contrast to classical repair Schwann cells, CCL2 was strongly down-regulated in keloidal Schwann cells and the overall CCL2 protein level in keloids was low. As CCL2 is one of the most important factors provoking the accumulation of M1-type macrophages in the wound area [68,69], reduced CCL2 levels might represent a crucial step in the development and/or persistence of keloids. CCL3

and TNF- α were also down-regulated in keloids. All three factors together are known to be important for the production of macrophage-derived MMP9 [70]. Indeed, MMP9 protein production was almost completely abolished in keloids. Interestingly, lack of MMP9 does not only contribute to less degradation of the ECM, but also affects Schwann cell function, as MMP9 has been shown to inhibit Schwann cell de-differentiation and proliferation [81].

Together, we show that keloids contain a unique Schwann cell population and suggest that the cross-talk of keloidal Schwann cells and macrophages may represent an important mechanism, leading to increased matrix deposition, which could therefore contribute or be responsible for the infinite growth of keloids. It is tempting to speculate that intervention at any point of this cycle might represent a promising treatment option. Our study opens a new perspective on the pathogenesis of keloids, which could significantly improve the treatment of this skin disease in the future.

Methods

Ethical statement

The use of resected skin and keloid tissue has been approved by the ethics committee of the Medical University of Vienna (votes 217/2010 and 1190/2020) in accordance with the guidelines of the Council for International Organizations of Medical Sciences (CIOMS). Written informed consent was obtained from all donors.

Sample acquisition

ScRNAseq data of skin and neurofibroma were publicly available [37,61]. One additional skin sample was obtained from surplus abdominal skin after elective abdominoplasty. Keloid tissue samples were obtained from the earlobe (3 samples) and the chest (1 sample) after elective therapeutic resection. (donor information – Supplementary Table S1) Previous treatment of the area of interest by laser and/or radiation were defined as exclusion criteria. Diagnosis and surgical procedure were performed by plastic surgeons at the Department of Plastic, Reconstructive and Aesthetic Surgery of the Vienna General Hospital (Vienna, Austria).

Sample dissociation and preparation of the single cell suspension

Tissue samples were washed with sterile Dulbecco's phosphate-buffered saline (PBS, without Ca²⁺ and Mg²⁺, Gibco, Thermo Fisher Scientific, Waltham, MA, USA) under laminar air flow. Six mm punch

biopsies were taken from the intact centre of the keloid and skin tissues, respectively. Biopsies were mechanically minced and enzymatically dissociated in gentleMACS C-Tubes (Miltenyi Biotec, Bergisch Gladbach, Germany) for 2.5 h at 37 °C using MACS Miltenyi Whole Skin Dissociation Kit (Miltenyi). Samples were further processed by gentleMACS Octo-Dissociator (Miltenyi) according to the manufacturer's protocol. Cell suspensions were sequentially passed through 100 and 40 µm cell strainer and washed twice with 0.04% bovine serum albumin (BSA, Sigma Aldrich, St. Louis, MO, USA) in PBS. Cell concentrations and viability were assessed by Acridine Orange/Propidium Iodide (AO/PI) Cell Viability Kit (Logos Biosystems, Anyang-si, Gyeonggi-do, South Korea) and detected by LUNA-FL™ Dual Fluorescence Cell Counter (Logos Biosystems). In case of cell viability < 80%, the samples were treated with Dead Cell Removal Kit (Miltenyi). Cell concentrations were adjusted to 0.7–1.2 × 10⁶ cells/ml. Samples were kept on ice until further processing. Gel beads-in-emulsion (GEM) were generated within 4 h after tissue resection.

Single cell processing and library preparation

GEM generation, barcoding, sample clean-up, cDNA amplification, and library construction were performed according to manufacturer's protocol using Chromium Next GEM Single Cell 3' GEM, Library & Gel Bead Kit v3.1, Chromium Next GEM Chip G Single Cell Kit, and Single Index Kit T Set A (all 10x Genomics, Pleasanton, CA, USA).

Sequencing and matrix preparation

RNA-sequencing, demultiplexing, and counting were carried out by the Biomedical Sequencing Facility (BSF) of the Center for Molecular Medicine (CeMM, Vienna, Austria). Samples were sequenced paired end with dual indexing (read length 75bp) in foursome pools using a HiSeq 3000/4000 (Illumina, San Diego, CA, USA). Raw data were aligned to the human reference genome (GRCh38) and counted by the Cellranger pipelines (Cellranger v3.0.2, except skin 7 v5.0.1, 10x Genomics).

Bioinformatical analysis

Bioinformatics analyses were performed using R (R v4.0.3, The R Foundation, Vienna, Austria), R-studio and Seurat (Seurat v4.0.0, Satija Lab) [82].

All included data sets were aligned by features. Only features detected in all datasets have been included, feature doublets have been excluded and feature names unified. Quality of all single cell data was determined and cells with unique feature counts > 300 and < 2500 and < 5% mitochondrial counts were included in our analyses

(Supplementary Fig. 18). Data were pre-processed by sctransform-normalization supported by the glmGamPoi package and integrated according to Seurat Vignette [83,84]. PCA and UMAP were calculated. All subset analyses have been performed as new calculation based on the raw data of the cells of interest. For cell type identification, clustermarker features were calculated and well-established marker genes were chosen to verify the assignment (marker genes information – Supplementary Table S2). Pseudotime-trajectory calculation was performed using Monocle3 (Monocle3, v.0.2.3.0, Trapnell Lab) [85–89]. The S4 objects of class Seurat were converted to a cell_data_set_object keeping the generated UMAP. Thereby, the principal graphs were calculated based on the cell distribution generated in Seurat. The correlations of the transcriptomic expression pattern of all detected Schwann cells were high enough to form one partition. A total of 20 graph centers (skin-keloid) and 40 graph centres (skin-keloid-NF1) was determined. The Schwann cell cluster of skin samples was defined as the root for pseudotime calculations. Expression changes along the trajectory were calculated for Schwann cells from intact skin to keloids. Gene ontology (GO) enrichment analysis was performed based on gene lists of clustermarker calculations and differentially expressed gene calculations. Only genes above an average foldchange of 2 were included. In case of less than 15 or more than 100 genes with an average foldchange cut-off of 2 or higher, an average foldchange-threshold of 1.5 and 3 was set, respectively. For enrichment analysis, Metascape [<https://metascape.org>] was used [90]. A p-value cutoff of 0.05 and a minimum enrichment score of 2 was set.

Immuno fluorescence

For cryopreservation, tissues were washed with PBS and fixed in 4.5% formaldehyde solution, neutral buffered (SAV Liquid Production GmbH, Flintsbach am Inn, Germany) for 24 h at 4 °C. Specimens were washed with PBS for 24 h and dehydrated by sequential incubation with 10, 25, and 42% sucrose for 24 h each. Tissues were snap-frozen in optimal cutting temperature compound (OCT compound, TissueTek, Sakura, Alphen aan den Rijn, The Netherlands) and stored at -80 °C. Ten µm sections were cut using a cryotome (Leica, Wetzlar, Germany) and dried for 30 min at room temperature. Cryosections were immersed in PBS followed by blocking and permeabilization with 1% BSA, 5% goat serum (DAKO, Glostrup, Denmark), and 0.3% Triton-X (Sigma Aldrich) in PBS for 15 min.

For paraffin embedding, tissues were washed with PBS and 6 mm punches were obtained. Biopsies were cut in a half and each part was fixed in 4.5% formaldehyde solution overnight and embedded in paraffin. After de-paraffinization and hydration,

sections were boiled in Target Retrieval Solution (DAKO) using a 2100 Antigen Retriever (DAKO) followed by three washes with PBS for 5 min.

Antibody details, dilutions, and incubation times are listed in Supplementary Table S3. A washing step consisted of three washes with PBS for 5 min and was performed after each antibody incubation step.

If stained for S100 (DAKO), primary antibodies were diluted in the ready to use S100 antibody solution. For the other staining, antibodies were diluted in the antibody staining solution containing 1% BSA and 0.1% Triton-X in PBS. Sections were incubated with secondary antibodies for 1 h and nuclear stain was performed by adding 50 mg/mL 4,6-diamidino-2-phenylindole (DAPI, Thermo Fisher Scientific) in PBS for 2 min. Sections were embedded in mounting medium (Fluoromount-G, SouthernBiotech, Birmingham, AL, USA) and stored at 4 °C. Micrographs were acquired with a confocal laser scanning microscope (TCS SP8X, Leica) equipped with a 10x (0.3 HCPL FluoTar), a 20x (0.75 HC-Plan-Apochromat, Multimersion), a 20x (0.75 HC-Plan-Apochromat) and a 63x (1.3 HC-Plan-Apochromat, Glycerol) objective using Leica application suite X version 1.8.1.13759 or LAS AF Lite software (both Leica). Confocal images are depicted as maximum projection of total z-stacks. All staining were performed on cryo- as well as paraffin-preserved tissue samples.

Multiphoton microscopy

Six mm punch biopsies were processed for cryopreservation as described above. Whole biopsies were cut in vertical tissue sections of 100 µm thickness. Immunofluorescence was performed as described above with an overnight incubation of the first antibodies and 2 h of incubation of the secondary antibodies. Permeabilization and washing periods were doubled. Images of dermal sheets were obtained as described above. 3D movies were created using Leica Application Suite X (LAS X, Leica). For combined imaging of IF staining with SHG microscopy, samples were sequentially incubated with S100 (DAKO) and goat anti-rabbit Alexa Fluor 647 (#A32733, Invitrogen). Stained tissue sections were placed onto a microscope slide and surrounded by a barrier of industrial grease (Dow Corning, MI USA). The well was filled with 1x PBS and sealed with a borosilicate cover glass (Paul Marienfeld, Lauda-Koenigshofen, Germany). For image acquisition, an upright multiphoton microscope (FluoView FVMPE-RS multiphoton system, Olympus, Tokyo, Japan) equipped with a 25x water immersion objective (n.a. = 1.05; WD 2 mm) for multiphoton excitation with infra-red (IR) laser light was used. A MaiTai IR laser at a wavelength of 880 nm was used to generate SHG signals and signals were detected between 426–477 nm with a non-

descanned transmission GaAsP (NDD) PMT detector. Simultaneously, S100-AF647 was excited with an InSight IR laser (1200 nm) and fluorescence emission was detected between 660–750 nm with a reflection NDD PMT detector. Laser light was split before detection with a dichroic mirror (SDM 570). z-stack images (512 × 512 pixel of 509 × 509 µm) of approximately 100 µm depth (z, 2 µm slices) were captured for all samples. Images were analyzed and 3D projections were generated with Fiji (ImageJ2, Dresden, Germany) [91].

Enzyme-linked immunosorbent assay (ELISA)

Skin- and keloid-derived proteins were quantified by ELISA. 6 mm punch biopsies were collected and cryopreserved at -80 °C until further processing. Tissues were lysed in 0.5 ml of 0.1% Triton X in PBS and homogenised (Precellys 24 Homogenisator, Bertin Instruments, Montigny-le-Bretonneux, France). Homogenization was repeated after overnight incubation at 4 °C. Samples were centrifuged for 15 min at 13,000 g and supernatants were used for protein quantifications. Total protein amounts were determined using Micro BCA™ Protein Assay Kit (Thermo Fisher Scientific) according to manufacturer's protocol. CCL2, MMP9, CCN3, and GAS6 concentrations were determined using commercially available ELISA kits as recommended by the manufacturer (Human CCL2/MCP-1 Quantikine ELISA Kit, Human MMP-9 DuoSet ELISA Kit, Human NOV/CCN3 DuoSet ELISA Kit, and Human GAS6 DuoSet ELISA Kit (all R&D Systems, Minneapolis, MN, USA).

Statistical analyses

For statistical evaluation, GraphPad Prism 8 software (GraphPad Software Inc., La Jolla, CA, USA) was used. Normal distribution within a group was tested by Shapiro-Wilk test. Comparison between two groups with normal distribution was performed with paired t-test. Independent groups without normal distribution were compared by Mann-Whitney-U-Test. Asterisks were used to mark p-values: *p < 0.05, ** p < 0.01, *** p < 0.001, **** p < 0.0001.

Funding

The present study was financed by the FFG Grant "APOSEC" (852748 and 862068; 2015-2019), the Vienna Business Agency "APOSEC to clinic" (ID 2343727, 2018-2020) and by the Aposcience AG under the direction of group leader HJA. The Sparkling Science Program of the Austrian Federal Ministry of Education, Science and Research (SPA06/055) funded MM.

Data availability

Generated scRNASeq data are available in NCBI's Gene Expression Omnibus (GEO) and accessible through GEP series accession number GSE181316 after publication. Acquired scRNASeq data from Brosseau et al. (2021) are accessible in NCBI's Gene Expression Omnibus (GEO) through GSE163028. Sequencing data from Tabib et al. (2018) can be downloaded from https://dom.pitt.edu/wp-content/uploads/2018/10/Skin_6Control_rawUMI.zip and https://dom.pitt.edu/wp-content/uploads/2018/10/Skin_6Control_Metadata.zip.

Disclosures

The authors declare that the research has been performed without any conflict of interest.

Acknowledgment

We would like to thank Hans Peter Haselsteiner and the CRISCAR Familienstiftung for their ongoing support of the Medical University/Aposcience AG public private partnership aiming to augment basic and translational clinical research in Austria/Europe. The authors acknowledge the core facilities of the Medical University of Vienna, a member of Vienna Life Science Instruments. We also thank Matthias Wielscher for his support in bioinformatics issues. We thank Barbara Messner and her team for providing the SMA antibody used in this study.

Supplementary materials

Supplementary material associated with this article can be found in the online version at [doi:10.1016/j.matbio.2022.03.001](https://doi.org/10.1016/j.matbio.2022.03.001).

Received 27 August 2021;

Received in revised form 27 January 2022;

Accepted 4 March 2022

Available online 10 March 2022

Keywords:

Keloid;

Schwann cell;

Single-cell RNA sequencing;

Extracellular matrix;

Macrophage

Abbreviations:

AHNAK, neuroblast differentiation-associated protein;

ATXN1, ataxin-1; BDNF, brain-derived neurotrophic

factor; CALR, calreticulin; CAV1, caveolin 1; CCL2, CC-chemokine ligand 2; CCL3, CC-chemokine ligand 3; CCN3, cellular communication network factor 3; CD163, cluster of differentiation 163; CD9, cluster of differentiation 9; CD90, THY-1 cell surface antigen; CDH2, n-cadherin; CXCL2, chemokine ligand 2; CXCL8, interleukin 8; DC, dendritic cells; DCN, decorin; DHH, desert hedgehog signaling molecule; EC, endothelial cells; ECM, extracellular matrix; EGR2, early growth response 2; ERBB3, erb-b2 receptor tyrosine kinase 3; ERY, erythrocytes; ETV5, ets variant transcription factor 5; FABP7, fatty acid binding protein 7; FB, fibroblasts; FOXO4, forkhead box protein O4; GAP43, growth associated protein 43; GAS6, growth arrest-specific 6; GDNF, glial cell derived neurotrophic factor; GEM, Gel beads-in-emulsion; GFAP, glial fibrillary acidic protein; GPM6B, neuronal membrane glycoprotein M6-B; ICAM1, intercellular adhesion molecule 1; IF, immunofluorescence; IGFBP3, insulin-like growth factor-binding protein 3; IGFBP5, insulin-like growth factor-binding protein 5; IL1B, interleukin-1 beta; IL6, interleukin 6; ITGA4, integrin alpha 4; KC, keratinocytes; L1CAM, L1 cell adhesion molecule; LEC, lymphatic endothelial cells; LUM, lumican; MAC, macrophages; MAC-FB, macrophage-fibroblast intermediate cells; MAC-M1, M1-macrophages; MAC-M1/M2, cells with mixed M1/M2 macrophages phenotype; MAC-M2, M2-macrophages; MAG, myelin associated glycoprotein; MBP, myelin basic protein; MEL, melanocytes; MKI67, marker of proliferation Ki-67; MMP9, matrix metalloproteinase 9; MPZ, myelin protein zero; MRC1, macrophage mannose receptor; MSI1, musashi RNA binding protein 1; MSX1, msh homeobox 1; NCAM1, neural cell adhesion molecule 1; NES, nestin; NF1, neurofibroma type 1; NFpan, neurofilament protein; NGFR, nerve growth factor receptor; NR4A1, nuclear receptor 4A1; NR4A2, nuclear receptor 4A2; NRXN1, neuroligin 1; NT5E, 5'-nucleotidase ecto; OLIG1, oligodendrocyte transcription factor 1; PAX3, paired box gene 3; PDGFA, platelet derived growth factor alpha chain; PLP1, proteolipid protein 1; PMP22, peripheral myelin protein 22; POU3F1, pou class 3 homeobox 1; PRX, periaxin; PTN, pleiotrophin; PTPRZ1, protein tyrosine phosphatase receptor type Z1; SC, Schwann cells; SC-EC, Schwann cell-endothelial cell intermediate cells; SC-FB, Schwann cell-fibroblasts intermediate cells; SC-Keloid, keloidal Schwann cells; SC-Prolif, proliferating Schwann cells; SC-Promyel, promyelinating Schwann cells; scRNAseq, single-cell RNA sequencing; SC-Skin, mature Schwann cells from healthy skin; SCN7A, sodium voltage-gated channel alpha subunit 7; SELE, selectin-E; SHG, second harmonic generation; SMC/PC, smooth muscle cells and pericytes; SNAI1, snail family transcriptional repressor 1; SNAI2, snail family transcriptional repressor 2; SOX9, sry-box transcription factor 9; SOX10, sry-box transcription factor 10; SPARCL1, proliferation-inducing protein 33; TC, T-cells; TFAP2A, transcription factor ap-2 alpha; TGFBI, transforming growth factor beta-induced; TNC, tenascin c; TNF, TNF-alpha; TNFAIP6, TNF-alpha induced protein 6; TOP2A, DNA-Topoisomerase 2-alpha; TWIST1, twist

family bhlh transcription factor 1; TWIST2, twist family bhlh transcription factor 2; ZEB2, zinc finger e-box binding homeobox 2

¹These authors contributed equally to this work.

References

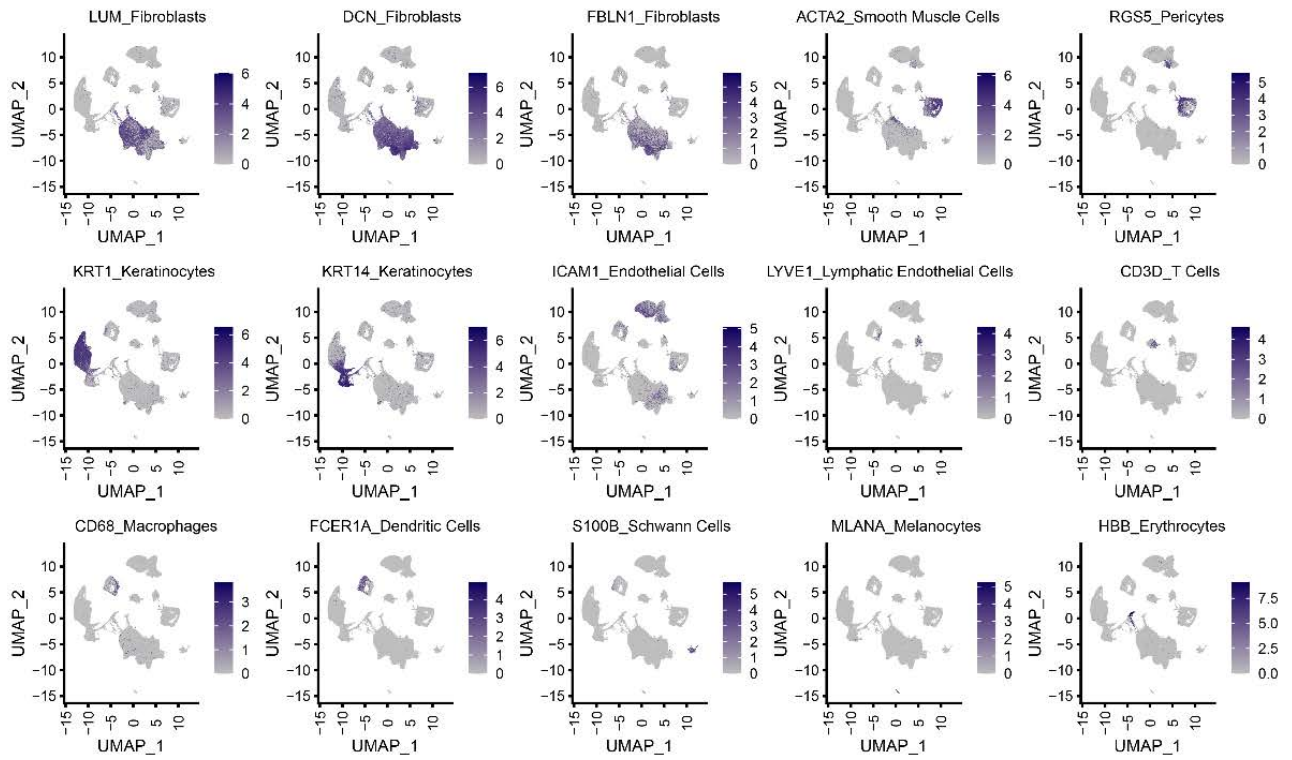
- [1] G.C. Limandjaja, F.B. Niessen, R.J. Scheper, S. Gibbs, The keloid disorder: heterogeneity, histopathology, mechanisms and models, *Front. Cell Dev. Biol.* 8 (2020) 360.
- [2] R.S. English, P.D. Shenefelt, Keloids and hypertrophic scars, *Dermatol. Surg.* 25 (8) (1999) 631–638.
- [3] J.C. Murray, Keloids and hypertrophic scars, *Clin. Dermatol.* 12 (1) (1994) 27–37.
- [4] S. Ud-Din, A. Bayat, New insights on keloids, hypertrophic scars, and striae, *Dermatol. Clin.* 32 (2) (2014) 193–209.
- [5] D.D. Balci, T. Inandi, C.A. Dogramaci, E. Celik, DLQI scores in patients with keloids and hypertrophic scars: a prospective case control study, *J. Dtsch. Dermatol. Ges.* 7 (8) (2009) 688–692.
- [6] S.M. Alhady, K. Sivanantharajah, Keloids in various races. A review of 175 cases, *Plast. Reconstr. Surg.* 44 (6) (1969) 564–566.
- [7] K.M. Ramakrishnan, K.P. Thomas, C.R. Sundararajan, Study of 1000 patients with keloids in South India, *Plast. Reconstr. Surg.* 53 (3) (1974) 276–280.
- [8] S.K. Kiprono, B.M. Chaula, J.E. Masenga, J.W. Muchunu, D.R. Mavura, M. Moehrle, Epidemiology of keloids in normally pigmented Africans and African people with albinism: population-based cross-sectional survey, *Br. J. Dermatol.* 173 (3) (2015) 852–854.
- [9] T.A. Mustoe, R.D. Cooter, M.H. Gold, F.D. Hobbs, A.A. Ramelet, P.G. Shakespeare, M. Stella, L. T éot, F.M. Wood, U.E. Ziegler, International clinical recommendations on scar management, *Plast. Reconstr. Surg.* 110 (2) (2002) 560–571.
- [10] I. Khansa, B. Harrison, J.E. Janis, Evidence-based scar management: how to improve results with technique and technology, *Plast. Reconstr. Surg.* 138 (2016) 165s–178s 3 Suppl.
- [11] C.M. Reinisch, E. Tschachler, The dimensions and characteristics of the subepidermal nerve plexus in human skin—terminal Schwann cells constitute a substantial cell population within the superficial dermis, *J. Dermatol. Sci.* 65 (3) (2012) 162–169.
- [12] M. Ashrafi, M. Baguneid, A. Bayat, The role of neuromediators and innervation in cutaneous wound healing, *Acta Derm. Venereol.* 96 (5) (2016) 587–594.
- [13] B. Hochman, F.X. Nahas, C.S. Sobral, V. Arias, R.F. Locali, Y. Juliano, L.M. Ferreira, Nerve fibres: a possible role in keloid pathogenesis, *Br. J. Dermatol.* 158 (3) (2008) 651–652.
- [14] T.M. Saffari, E. Bijlard, E.A.M. Van Bodegraven, M.A.M. Mureau, S.E.R. Hovius, F. Huygen, Sensory perception and nerve fibre innervation in patients with keloid scars: an investigative study, *Eur. J. Dermatol.* 28 (6) (2018) 828–829.
- [15] P.D. Drummond, L.F. Dawson, F.M. Wood, M.W. Fear, Up-regulation of $\alpha(1)$ -adrenoceptors in burn and keloid scars, *Burns* 44 (3) (2018) 582–588.
- [16] N.M. Shoukrey, K.F. Tabbara, Ultrastructural study of a corneal keloid, *Eye* 7 (1993) 379–387 (Lond)Pt 3.
- [17] E. Tschachler, C.M. Reinisch, C. Mayer, K. Paiha, H. Lassmann, W. Weninger, Sheet preparations expose the dermal nerve plexus of human skin and render the dermal nerve end organ accessible to extensive analysis, *J. Invest. Dermatol.* 122 (1) (2004) 177–182.
- [18] K.A. Nave, B.D. Trapp, Axon-glia signaling and the glial support of axon function, *Annu. Rev. Neurosci.* 31 (2008) 535–561.
- [19] D. Riethmacher, E. Sonnenberg-Riethmacher, V. Brinkmann, T. Yamaai, G.R. Lewin, C. Birchmeier, Severe neuropathies in mice with targeted mutations in the ErbB3 receptor, *Nature* 389 (6652) (1997) 725–730.
- [20] K.R. Jessen, R. Mirsky, The repair Schwann cell and its function in regenerating nerves, *J. Physiol.* 594 (13) (2016) 3521–3531.
- [21] P.J. Arthur-Farraj, M. Latouche, D.K. Wilton, S. Quintes, E. Chabrol, A. Banerjee, A. Woodhoo, B. Jenkins, M. Rahman, M. Turmaine, G.K. Wicher, R. Mitter, L. Greensmith, A. Behrens, G. Raivich, R. Mirsky, K.R. Jessen, c-Jun reprograms Schwann cells of injured nerves to generate a repair cell essential for regeneration, *Neuron* 75 (4) (2012) 633–647.
- [22] K.R. Jessen, R. Mirsky, P. Arthur-Farraj, The Role of cell plasticity in tissue repair: adaptive cellular reprogramming, *Dev. Cell* 34 (6) (2015) 613–620.
- [23] K.R. Jessen, R. Mirsky, The success and failure of the schwann cell response to nerve injury, *Front. Cell Neurosci.* 13 (2019) 33.
- [24] J.A. Gomez-Sanchez, K.S. Pilch, M. van der Lans, S.V. Fazal, C. Benito, L.J. Wagstaff, R. Mirsky, K.R. Jessen, After nerve injury, lineage tracing shows that myelin and remak Schwann cells elongate extensively and branch to form repair schwann cells, which shorten radically on remyelination, *J. Neurosci.* 37 (37) (2017) 9086–9099.
- [25] G. Stoll, H.W. Müller, Nerve injury, axonal degeneration and neural regeneration: basic insights, *Brain Pathol.* 9 (2) (1999) 313–325.
- [26] G.K. Tofaris, P.H. Patterson, K.R. Jessen, R. Mirsky, Deregulated Schwann cells attract macrophages by secretion of leukemia inhibitory factor (LIF) and monocyte chemoattractant protein-1 in a process regulated by interleukin-6 and LIF, *J. Neurosci.* 22 (15) (2002) 6696–6703.
- [27] J.A. Gomez-Sanchez, L. Carty, M. Iruarizaga-Lejarreta, M. Palomo-Irigoyen, M. Varela-Rey, M. Griffith, J. Hantke, N. Macias-Camara, M. Azkargorta, I. Aurrekoetxea, V.G. De Juan, H.B. Jefferies, P. Aspichueta, F. Elortza, A.M. Aransay, M.L. Martínez-Chantar, F. Baas, J.M. Mato, R. Mirsky, A. Woodhoo, K.R. Jessen, Schwann cell autophagy, myelinophagy, initiates myelin clearance from injured nerves, *J. Cell Biol.* 210 (1) (2015) 153–168.
- [28] S.Y. Jang, Y.K. Shin, S.Y. Park, J.Y. Park, H.J. Lee, Y.H. Yoo, J.K. Kim, H.T. Park, Autophagic myelin destruction by Schwann cells during Wallerian degeneration and segmental demyelination, *Glia* 64 (5) (2016) 730–742.
- [29] N. Yoshida, N. Edanami, N. Ohkura, T. Maekawa, N. Takahashi, A. Tohma, K. Izumi, T. Maeda, A. Hosoya, H. Nakamura, K. Tabeta, Y. Noiri, K. Yoshida, M2 phenotype macrophages Colocalize with Schwann cells in human dental pulp, *J. Dent. Res.* 99 (3) (2020) 329–338.
- [30] T. Lucas, A. Waisman, R. Ranjan, J. Roes, T. Krieg, W. Müller, A. Roers, S.A. Eming, Differential roles of macrophages in diverse phases of skin repair, *J. Immunol.* 184 (7) (2010) 3964–3977.
- [31] Z. Zhu, J. Ding, Z. Ma, T. Iwashina, E.E. Tredget, Systemic depletion of macrophages in the subacute phase of wound

- healing reduces hypertrophic scar formation, *Wound Repair Regen.* 24 (4) (2016) 644–656.
- [32] R. Mirza, L.A. DiPietro, T.J. Koh, Selective and specific macrophage ablation is detrimental to wound healing in mice, *Am. J. Pathol.* 175 (6) (2009) 2454–2462.
- [33] R. Bagabir, R.J. Byers, I.H. Chaudhry, W. Müller, R. Paus, A. Bayat, Site-specific immunophenotyping of keloid disease demonstrates immune upregulation and the presence of lymphoid aggregates, *Br. J. Dermatol.* 167 (5) (2012) 1053–1066.
- [34] D.E. Boyce, J. Ciampolini, F. Ruge, M.S. Murison, K.G. Harding, Inflammatory-cell subpopulations in keloid scars, *Br. J. Plast. Surg.* 54 (6) (2001) 511–516.
- [35] M.P. Clements, E. Byrne, L.F. Camarillo Guerrero, A.L. Cattin, L. Zakka, A. Ashraf, J.J. Burden, S. Khadayat, A.C. Lloyd, S. Marguerat, S. Parrinello, The wound microenvironment reprograms schwann cells to invasive mesenchymal-like cells to drive peripheral nerve regeneration, *Neuron* 96 (1) (2017) 98–114 e7.
- [36] V. Parfejevs, J. Debbache, O. Shakhova, S.M. Schaefer, M. Glausch, M. Wegner, U. Suter, U. Riekstina, S. Werner, L. Sommer, Injury-activated glial cells promote wound healing of the adult skin in mice, *Nat. Commun.* 9 (1) (2018) 236.
- [37] T. Tabib, C. Morse, T. Wang, W. Chen, R. Lafyatis, SFRP2/DPP4 and FMO1/LSP1 define major fibroblast populations in human skin, *J. Invest. Dermatol.* 138 (4) (2018) 802–810.
- [38] X. Liu, W. Chen, Q. Zeng, B. Ma, Z. Li, T. Meng, J. Chen, N. Yu, Z. Zhou, X. Long, Single-cell RNA-seq reveals lineage-specific regulatory changes of fibroblasts and vascular endothelial cells in keloids, *J. Invest. Dermatol.* (2021).
- [39] P. Bargagna-Mohan, G. Schultz, B. Rheaume, E.F. Trakhtenberg, P. Robson, S. Pal-Ghosh, M.A. Stepp, K.S. Given, W.B. Macklin, R. Mohan, Corneal nonmyelinating Schwann cells illuminated by single-cell transcriptomics and visualized by protein biomarkers, *J. Neurosci. Res.* 99 (3) (2021) 731–749.
- [40] D. Gerber, J.A. Pereira, J. Gerber, G. Tan, S. Dimitrieva, E. Yángñez, U. Suter, Transcriptional profiling of mouse peripheral nerves to the single-cell level to build a sciatic nerve Atlas (SNAT), *Elife* 10 (2021).
- [41] K.R. Jessen, R. Mirsky, The origin and development of glial cells in peripheral nerves, *Nat. Rev. Neurosci.* 6 (9) (2005) 671–682.
- [42] R. Mirsky, A. Woodhoo, D.B. Parkinson, P. Arthur-Farraj, A. Bhaskaran, K.R. Jessen, Novel signals controlling embryonic Schwann cell development, myelination and dedifferentiation, *J. Peripher. Nerv. Syst.* 13 (2) (2008) 122–135.
- [43] M. Finsch, S. Schreiner, T. Kichko, P. Reeh, E.R. Tamm, M.R. Bösl, D. Meijer, M. Wegner, Sox10 is required for Schwann cell identity and progression beyond the immature Schwann cell stage, *J. Cell Biol.* 189 (4) (2010) 701–712.
- [44] S. Britsch, D.E. Goerich, D. Riethmacher, R.I. Peirano, M. Rossner, K.A. Nave, C. Birchmeier, M. Wegner, The transcription factor Sox10 is a key regulator of peripheral glial development, *Genes Dev.* 15 (1) (2001) 66–78.
- [45] T. Weiss, S. Taschner-Mandl, A. Bileck, A. Slany, F. Kromp, F. Rifatbegovic, C. Frech, R. Windhager, H. Kitzinger, C.H. Tzou, P.F. Ambros, C. Gerner, I.M. Ambros, Proteomics and transcriptomics of peripheral nerve tissue and cells unravel new aspects of the human Schwann cell repair phenotype, *Glia* 64 (12) (2016) 2133–2153.
- [46] S.D. Ackerman, C. Garcia, X. Piao, D.H. Gutmann, K.R. Monk, The adhesion GPCR Gpr56 regulates oligodendrocyte development via interactions with Gα12/13 and RhoA, *Nat. Commun.* 6 (2015) 6122.
- [47] J.Z. Barlow, G.W. Huntley, Developmentally regulated expression of Thy-1 in structures of the mouse sensory-motor system, *J. Comp. Neurol.* 421 (2) (2000) 215–233.
- [48] S. Quintes, B.G. Brinkmann, M. Ebert, F. Frébourg, T. Kungl, F.A. Arlt, V. Tarabykin, D. Huylebroeck, D. Meijer, U. Suter, M. Wegner, M.W. Sereda, K.A. Nave, Zeb2 is essential for Schwann cell differentiation, myelination and nerve repair, *Nat. Neurosci.* 19 (8) (2016) 1050–1059.
- [49] C. Salim, Y.V. Boxberg, J. Alterio, S. Féréol, F. Nothias, The giant protein AHNAK involved in morphogenesis and laminin substrate adhesion of myelinating Schwann cells, *Glia* 57 (5) (2009) 535–549.
- [50] D.D. Mikol, S.S. Scherer, S.J. Duckett, H.L. Hong, E.L. Feldman, Schwann cell caveolin-1 expression increases during myelination and decreases after axotomy, *Glia* 38 (3) (2002) 191–199.
- [51] T. Weiss, S. Taschner-Mandl, L. Janker, A. Bileck, F. Rifatbegovic, F. Kromp, H. Sorger, M.O. Kauer, C. Frech, R. Windhager, C. Gerner, P.F. Ambros, I.M. Ambros, Schwann cell plasticity regulates neuroblastic tumor cell differentiation via epidermal growth factor-like protein 8, *Nat. Commun.* 12 (1) (2021) 1624.
- [52] M.L. Bang, A. Vainshtein, H.J. Yang, Y. Eshed-Eisenbach, J. Devaux, H.B. Werner, E. Peles, Glial M6B stabilizes the axonal membrane at peripheral nodes of Ranvier, *Glia* 66 (4) (2018) 801–812.
- [53] S.A. Banerjee, P.H. Patterson, Schwann cell CD9 expression is regulated by axons, *Mol. Cell. Neurosci.* 6 (5) (1995) 462–473.
- [54] J. Schira, A. Heinen, G. Poschmann, B. Ziegler, H.P. Hartung, K. Stühler, P. Köry, Secretome analysis of nerve repair mediating Schwann cells reveals Smad-dependent trophism, *FASEB J.* 33 (4) (2019) 4703–4715.
- [55] M. Ranjan, L.D. Hudson, Regulation of tyrosine phosphorylation and protein tyrosine phosphatases during oligodendrocyte differentiation, *Mol. Cell. Neurosci.* 7 (5) (1996) 404–418.
- [56] Z. Zhou, N. Zhang, P. Shi, J. Xie, Mechanism of miR-148b inhibiting cell proliferation and migration of Schwann cells by regulating CALR, *Artif. Cells Nanomed. Biotechnol.* 47 (1) (2019) 1978–1983.
- [57] Z. Zhang, B. Yu, Y. Gu, S. Zhou, T. Qian, Y. Wang, G. Ding, F. Ding, X. Gu, Fibroblast-derived tenascin-C promotes Schwann cell migration through β1-integrin dependent pathway during peripheral nerve regeneration, *Glia* 64 (3) (2016) 374–385.
- [58] S.K. Guo, M.F. Shen, H.W. Yao, Y.S. Liu, Enhanced expression of TGFβ1 promotes the proliferation and migration of glioma cells, *Cell. Physiol. Biochem.* 49 (3) (2018) 1097–1109.
- [59] A. Naba, K.R. Clauser, H. Ding, C.A. Whittaker, S.A. Carr, R.O. Hynes, The extracellular matrix: tools and insights for the "omics" era, *Matrix Biol.* 49 (2016) 10–24.
- [60] H. Mazuelas, M. Carrión, E. Serra, Modeling tumors of the peripheral nervous system associated with neurofibromatosis type 1: reprogramming plexiform neurofibroma cells, *Stem Cell Res.* 49 (2020) 102068.
- [61] J.P. Brosseau, A.A. Sathe, Y. Wang, T. Nguyen, D.A. Glass, C. Xing, L.Q. Le, Human cutaneous neurofibroma matrisome revealed by single-cell RNA sequencing, *Acta Neuropathol. Commun.* 9 (1) (2021) 11.
- [62] S.J. Getting, D.J. Mahoney, T. Cao, M.S. Rugg, E. Fries, C.M. Milner, M. Perretti, A.J. Day, The link module from human TSG-6 inhibits neutrophil migration in a hyaluronan- and inter-alpha-inhibitor-independent manner, *J. Biol. Chem.* 277 (52) (2002) 51068–51076.

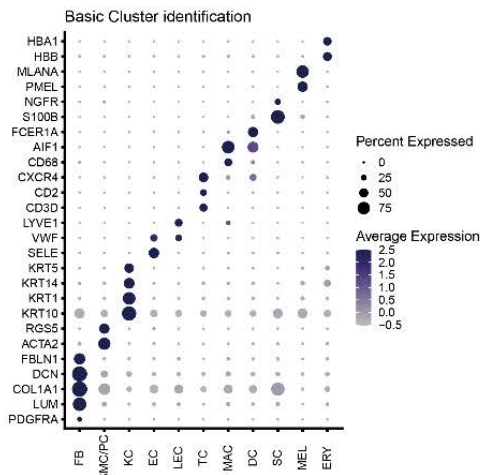
- [63] Q.M. Lin, S. Zhao, L.L. Zhou, X.S. Fang, Y. Fu, Z.T. Huang, Mesenchymal stem cells transplantation suppresses inflammatory responses in global cerebral ischemia: contribution of TNF- α -induced protein 6, *Acta Pharmacol. Sin.* 34 (6) (2013) 784–792.
- [64] G. Nagyeri, M. Radacs, S. Ghassemi-Nejad, B. Tryniszewska, K. Olasz, G. Hutás, Z. Gyorfy, V.C. Hascall, T.T. Glant, K. Mikecz, TSG-6 protein, a negative regulator of inflammatory arthritis, forms a ternary complex with murine mast cell tryptases and heparin, *J. Biol. Chem.* 286 (26) (2011) 23559–23569.
- [65] Y.M. Wan, H.M. Wu, Y.H. Li, Z.Y. Xu, J.H. Yang, C. Liu, Y.F. He, M.J. Wang, X.N. Wu, Y. Zhang, TSG-6 inhibits oxidative stress and induces M2 polarization of hepatic macrophages in mice with alcoholic hepatitis via suppression of STAT3 activation, *Front. Pharmacol.* 11 (2020) 10.
- [66] M. Mittal, C. Tirupathi, S. Nepal, Y.Y. Zhao, D. Grzych, D. Soni, D.J. Prockop, A.B. Malik, TNF- α -stimulated gene-6 (TSG6) activates macrophage phenotype transition to prevent inflammatory lung injury, *Proc. Natl. Acad. Sci. USA.* 113 (50) (2016) E8151–E8158.
- [67] P.C. Chen, H.C. Cheng, J. Wang, S.W. Wang, H.C. Tai, C.W. Lin, C.H. Tang, Prostate cancer-derived CCN3 induces M2 macrophage infiltration and contributes to angiogenesis in prostate cancer microenvironment, *Oncotarget* 5 (6) (2014) 1595–1608.
- [68] E. Seki, S. de Minicis, S. Inokuchi, K. Taura, K. Miyai, N. van Rooijen, R.F. Schwabe, D.A. Brenner, CCR2 promotes hepatic fibrosis in mice, *Hepatology* 50 (1) (2009) 185–197.
- [69] K.R. Karlmark, R. Weiskirchen, H.W. Zimmermann, N. Gassler, F. Ginhoux, C. Weber, M. Merad, T. Luedde, C. Trautwein, F. Tacke, Hepatic recruitment of the inflammatory Gr^{1b} monocyte subset upon liver injury promotes hepatic fibrosis, *Hepatology* 50 (1) (2009) 261–274.
- [70] S.C. Robinson, K.A. Scott, F.R. Balkwill, Chemokine stimulation of monocyte matrix metalloproteinase-9 requires endogenous TNF- α , *Eur. J. Immunol.* 32 (2) (2002) 404–412.
- [71] J.A. Stratton, A. Holmes, N.L. Rosin, S. Sinha, M. Vohra, N.E. Burma, T. Trang, R. Midha, J. Biernaskie, Macrophages regulate schwann cell maturation after nerve injury, *Cell Rep.* 24 (10) (2018) 2561–2572 e6.
- [72] H. Yasuoka, D.M. Jukic, Z. Zhou, A.M. Choi, C.A. Feghali-Bostwick, Insulin-like growth factor binding protein 5 induces skin fibrosis: a novel murine model for dermal fibrosis, *Arthritis Rheum.* 54 (9) (2006) 3001–3010.
- [73] H. Yasuoka, Z. Zhou, J.M. Pilewski, T.D. Oury, A.M. Choi, C.A. Feghali-Bostwick, Insulin-like growth factor-binding protein-5 induces pulmonary fibrosis and triggers mononuclear cellular infiltration, *Am. J. Pathol.* 169 (5) (2006) 1633–1642.
- [74] H. Yasuoka, Y. Yamaguchi, C.A. Feghali-Bostwick, The profibrotic factor IGFBP-5 induces lung fibroblast and mononuclear cell migration, *Am. J. Respir. Cell Mol. Biol.* 41 (2) (2009) 179–188.
- [75] H.K. Min, H. Maruyama, B.K. Jang, M. Shimada, F. Mirshahi, S. Ren, Y. Oh, P. Puri, A.J. Sanyal, Suppression of IGF binding protein-3 by palmitate promotes hepatic inflammatory responses, *FASEB J.* 30 (12) (2016) 4071–4082.
- [76] C.M. Reinisch, H. Traxler, S. Piringer, S. Tangl, A. Nader, E. Tschachler, Rarefaction of the peripheral nerve network in diabetic patients is associated with a pronounced reduction of terminal Schwann cells, *Diabetes Care* 31 (6) (2008) 1219–1221.
- [77] K. Choi, K. Komurov, J.S. Fletcher, E. Jousma, J.A. Cancelas, J. Wu, N. Ratner, An inflammatory gene signature distinguishes neurofibroma Schwann cells and macrophages from cells in the normal peripheral nervous system, *Sci. Rep.* 7 (2017) 43315.
- [78] S.L. Carroll, N. Ratner, How does the Schwann cell lineage form tumors in NF1? *Glia* 56 (14) (2008) 1590–1605.
- [79] N. Haider, L. Boscá, H.R. Zandbergen, J.C. Kovacic, N. Narula, S. González-Ramos, M. Fernández-Velasco, S. Agrawal, M. Paz-García, S. Gupta, K. DeLeon-Pennell, V. Fuster, B. Ibanez, J. Narula, Transition of macrophages to fibroblast-like cells in healing myocardial infarction, *J. Am. Coll. Cardiol.* 74 (25) (2019) 3124–3135.
- [80] J.P. Thiery, H. Acloque, R.Y. Huang, M.A. Nieto, Epithelial-mesenchymal transitions in development and disease, *Cell* 139 (5) (2009) 871–890.
- [81] Y. Kim, A.G. Remacle, A.V. Chernov, H. Liu, I. Shubayev, C. Lai, J. Dolkas, S.A. Shiryayev, V.S. Golubkov, A.P. Mizisin, A.Y. Strongin, V.I. Shubayev, The MMP-9/TIMP-1 axis controls the status of differentiation and function of myelin-forming Schwann cells in nerve regeneration, *PLoS One* 7 (3) (2012) e33664.
- [82] Y. Hao, S. Hao, E. Andersen-Nissen, W.M. Mauck, S. Zheng, A. Butler, M.J. Lee, A.J. Wilk, C. Darby, M. Zager, P. Hoffman, M. Stoeckius, E. Papalexi, E.P. Mimitou, J. Jain, A. Srivastava, T. Stuart, L.M. Fleming, B. Yeung, A.J. Rogers, J.M. McElrath, C.A. Blish, R. Gottardo, P. Smibert, R. Satija, Integrated analysis of multimodal single-cell data, *Cell* (2021).
- [83] C. Ahlmann-Eltze, W. Huber, glmGamPoi: fitting Gamma-Poisson generalized linear models on single cell count data, *Bioinformatics* 36 (24) (2021) 5701–5702.
- [84] C. Hafemeister, R. Satija, Normalization and variance stabilization of single-cell RNA-seq data using regularized negative binomial regression, *Genome Biol.* 20 (1) (2019) 296.
- [85] C. Trapnell, D. Cacchiarelli, J. Grimsby, P. Pokharel, S. Li, M. Morse, N.J. Lennon, K.J. Livak, T.S. Mikkelsen, J.L. Rinn, The dynamics and regulators of cell fate decisions are revealed by pseudotemporal ordering of single cells, *Nat. Biotechnol.* 32 (4) (2014) 381–386.
- [86] X. Qiu, Q. Mao, Y. Tang, L. Wang, R. Chawlia, H.A. Pliner, C. Trapnell, Reversed graph embedding resolves complex single-cell trajectories, *Nat. Methods* 14 (10) (2017) 979–982.
- [87] J. Cao, M. Spielmann, X. Qiu, X. Huang, D.M. Ibrahim, A.J. Hill, F. Zhang, S. Mundlos, L. Christiansen, F.J. Steemers, C. Trapnell, J. Shendure, The single-cell transcriptional landscape of mammalian organogenesis, *Nature* 566 (7745) (2019) 496–502.
- [88] V.A. Traag, L. Waltman, N.J. van Eck, From Louvain to Leiden: guaranteeing well-connected communities, *Sci. Rep.* 9 (1) (2019) 5233.
- [89] J.H. Levine, E.F. Simonds, S.C. Bendall, K.L. Davis, A.D. Amir el, M.D. Tadmor, O. Litvin, H.G. Fienberg, A. Jager, E.R. Zunder, R. Finck, A.L. Gedman, I. Radtke, J.R. Downing, D. Pe'er, G.P. Nolan, Data-driven phenotypic dissection of AML reveals progenitor-like cells that correlate with prognosis, *Cell* 162 (1) (2015) 184–197.
- [90] Y. Zhou, B. Zhou, L. Pache, M. Chang, A.H. Khodabakhshi, O. Tanaseichuk, C. Benner, S.K. Chanda, Metascape provides a biologist-oriented resource for the analysis of systems-level datasets, *Nat. Commun.* 10 (1) (2019) 1523.
- [91] J. Schindelin, I. Arganda-Carreras, E. Frise, V. Kaynig, M. Longair, T. Pietzsch, S. Preibisch, C. Rueden, S. Saalfeld, B. Schmid, J.Y. Tinevez, D.J. White, V. Hartenstein, K. Eliceiri, P. Tomancak, A. Cardona, Fiji: an open-source platform for biological-image analysis, *Nat. Methods* 9 (7) (2012) 676–682.

Supplementary Figure 1

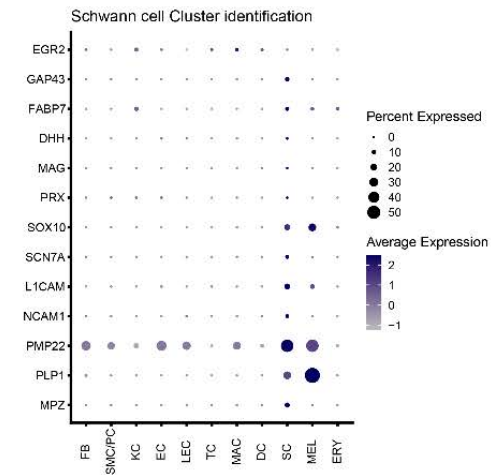
(A)



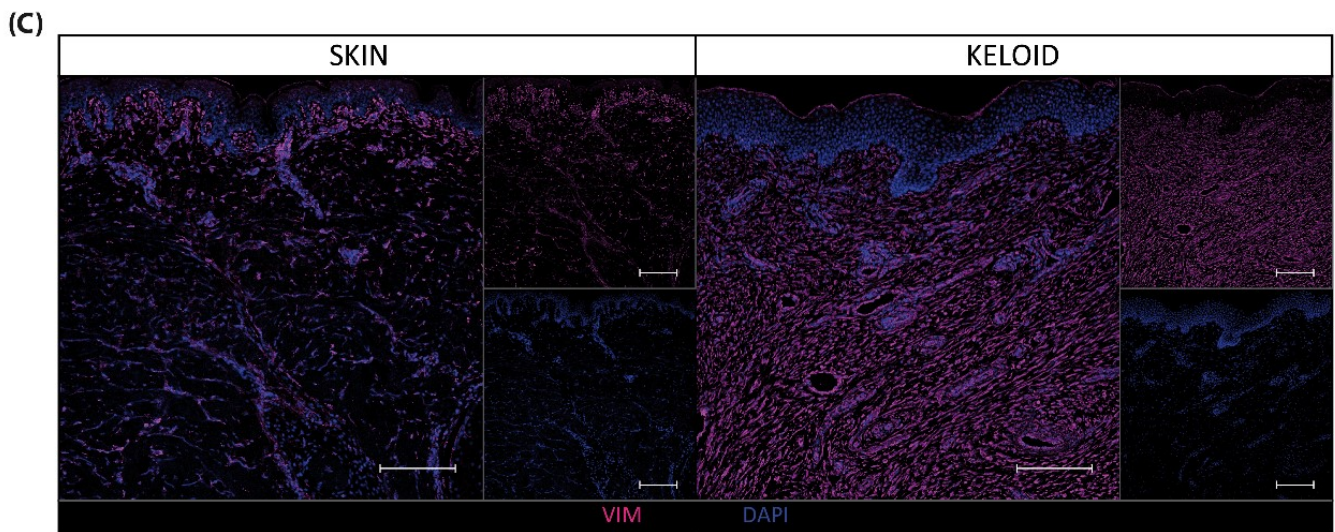
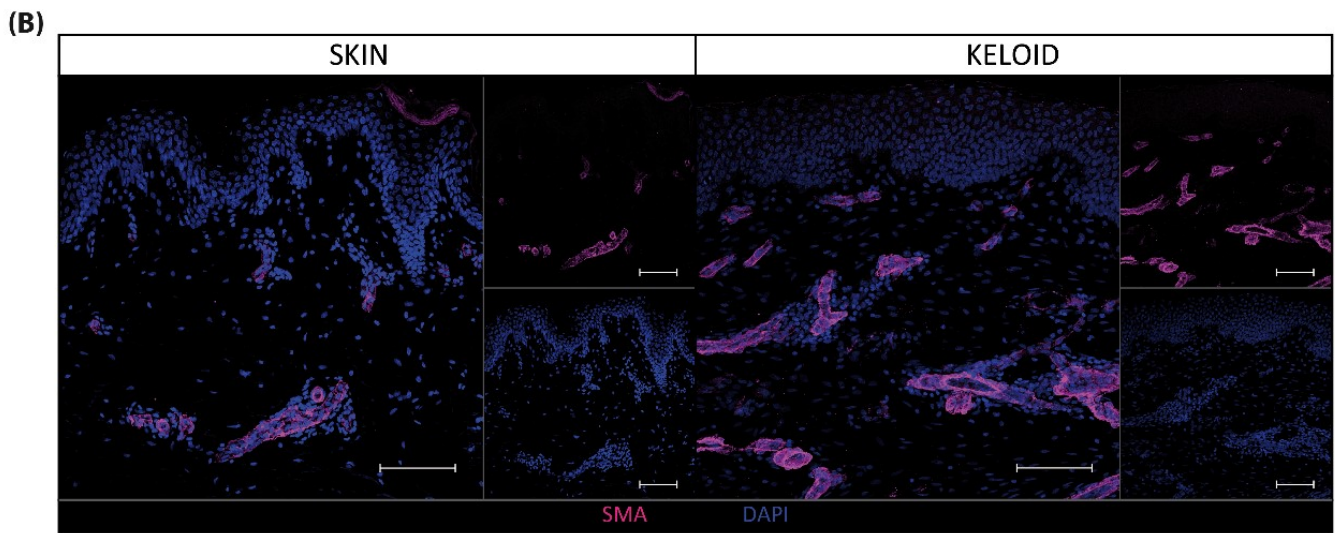
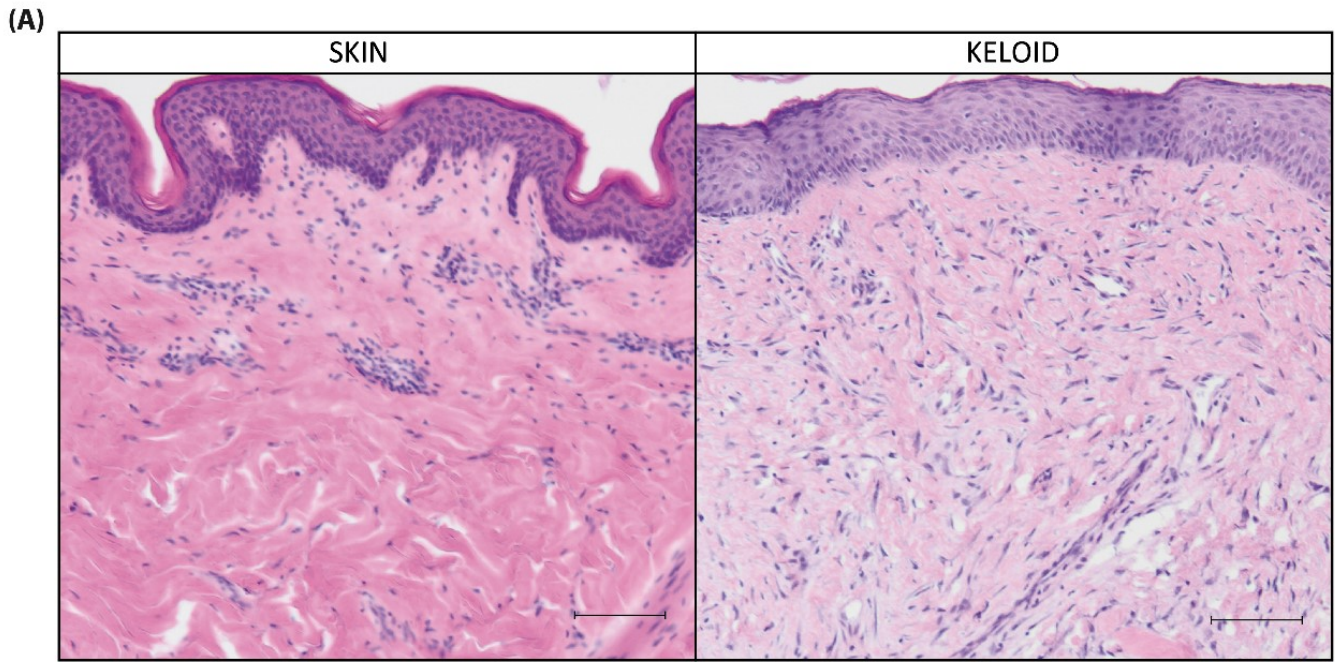
(B)



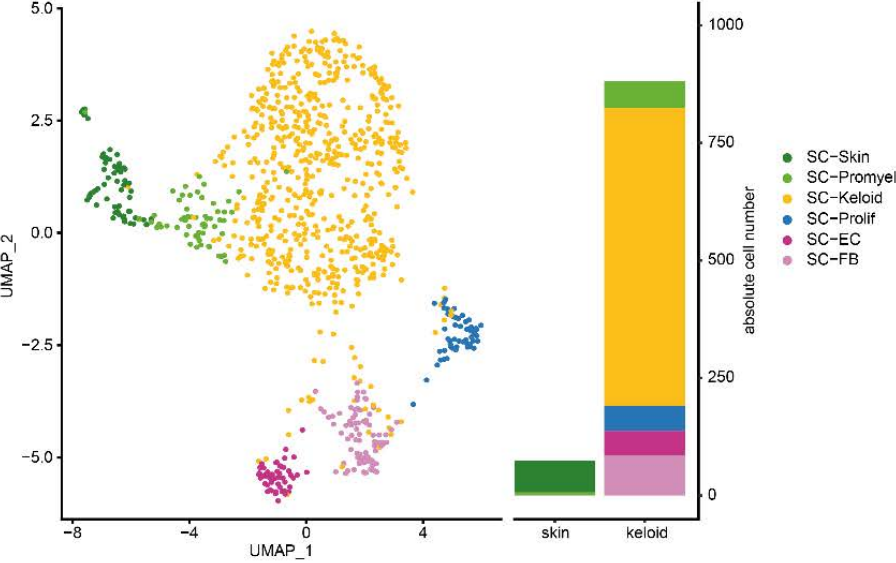
(C)



Supplementary Figure 2

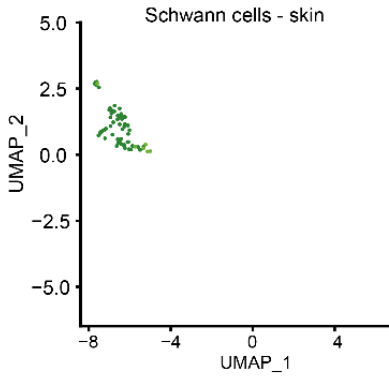


Supplementary Figure 3

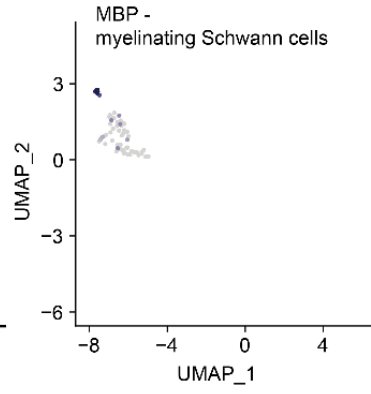


Supplementary Figure 4

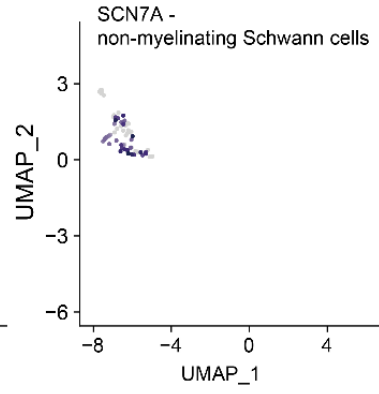
(A)



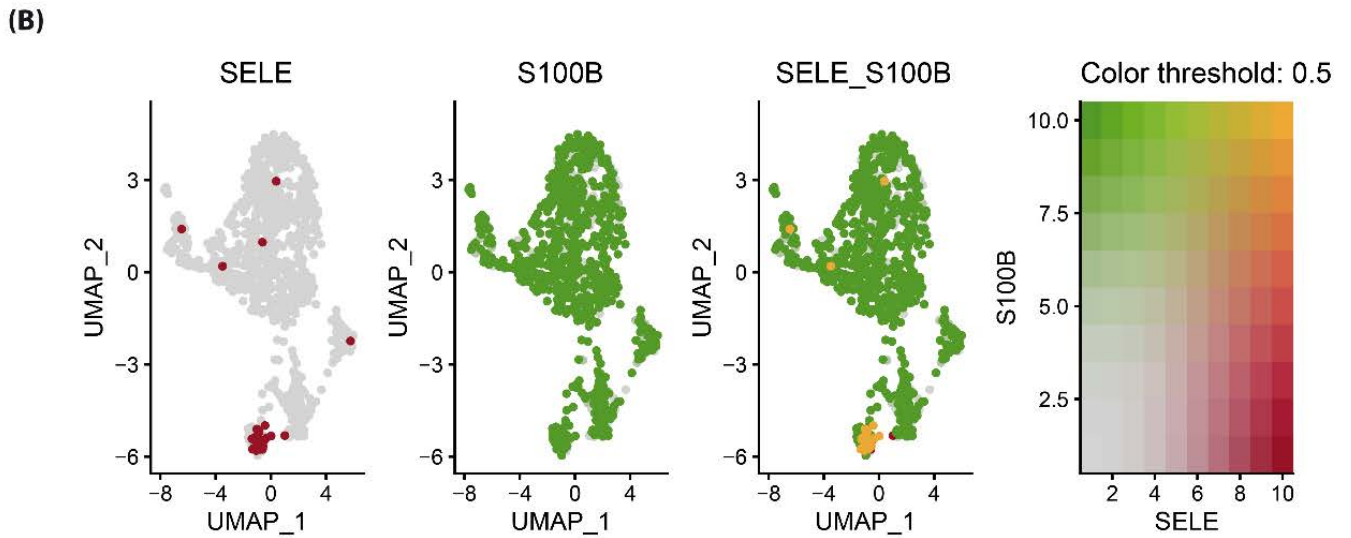
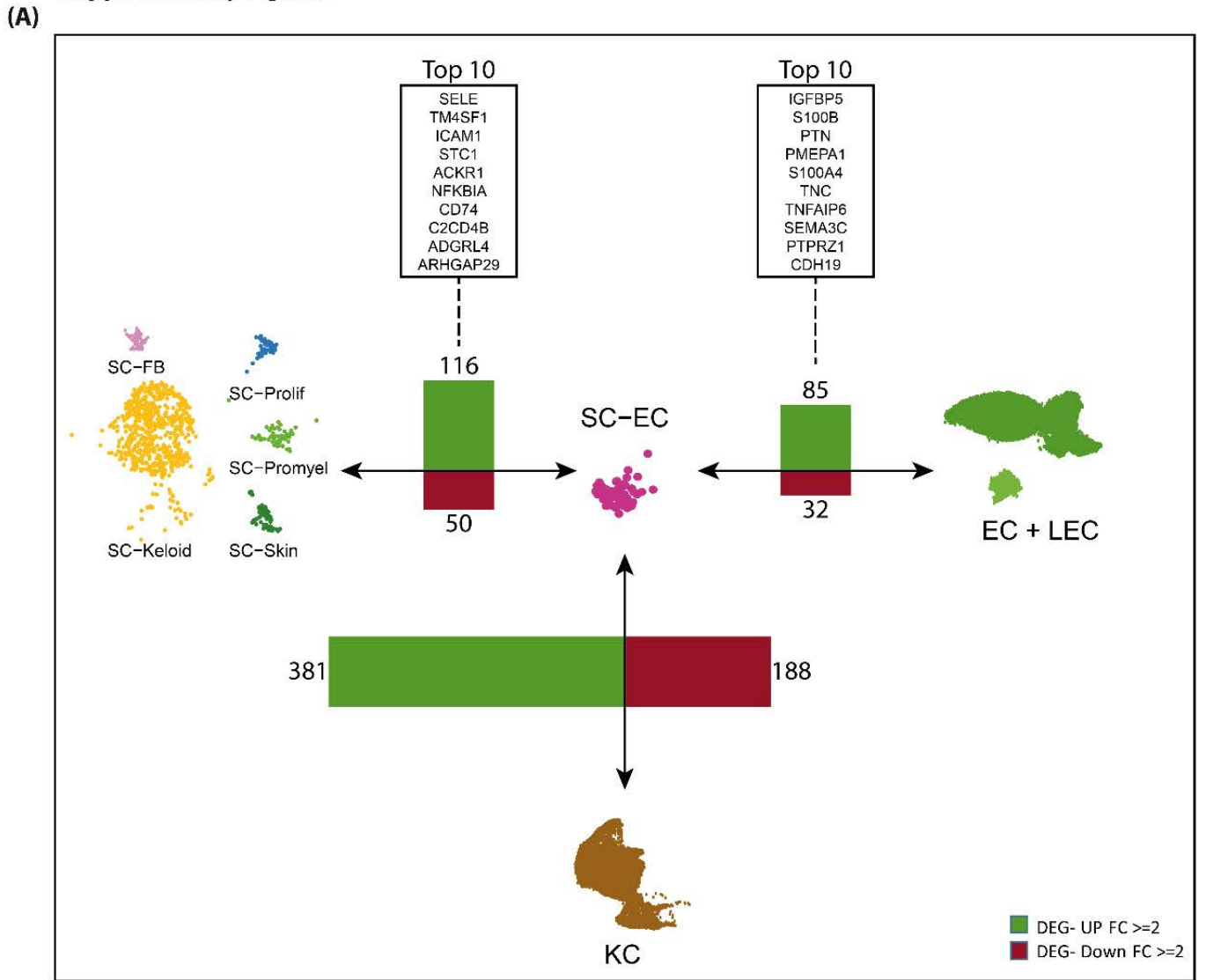
(B)



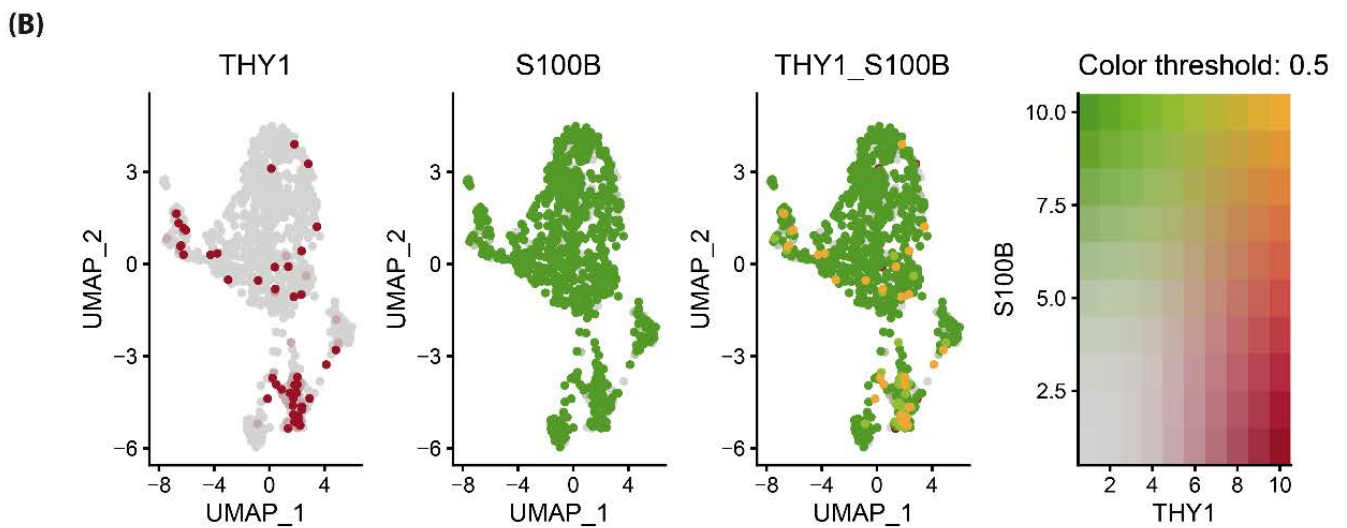
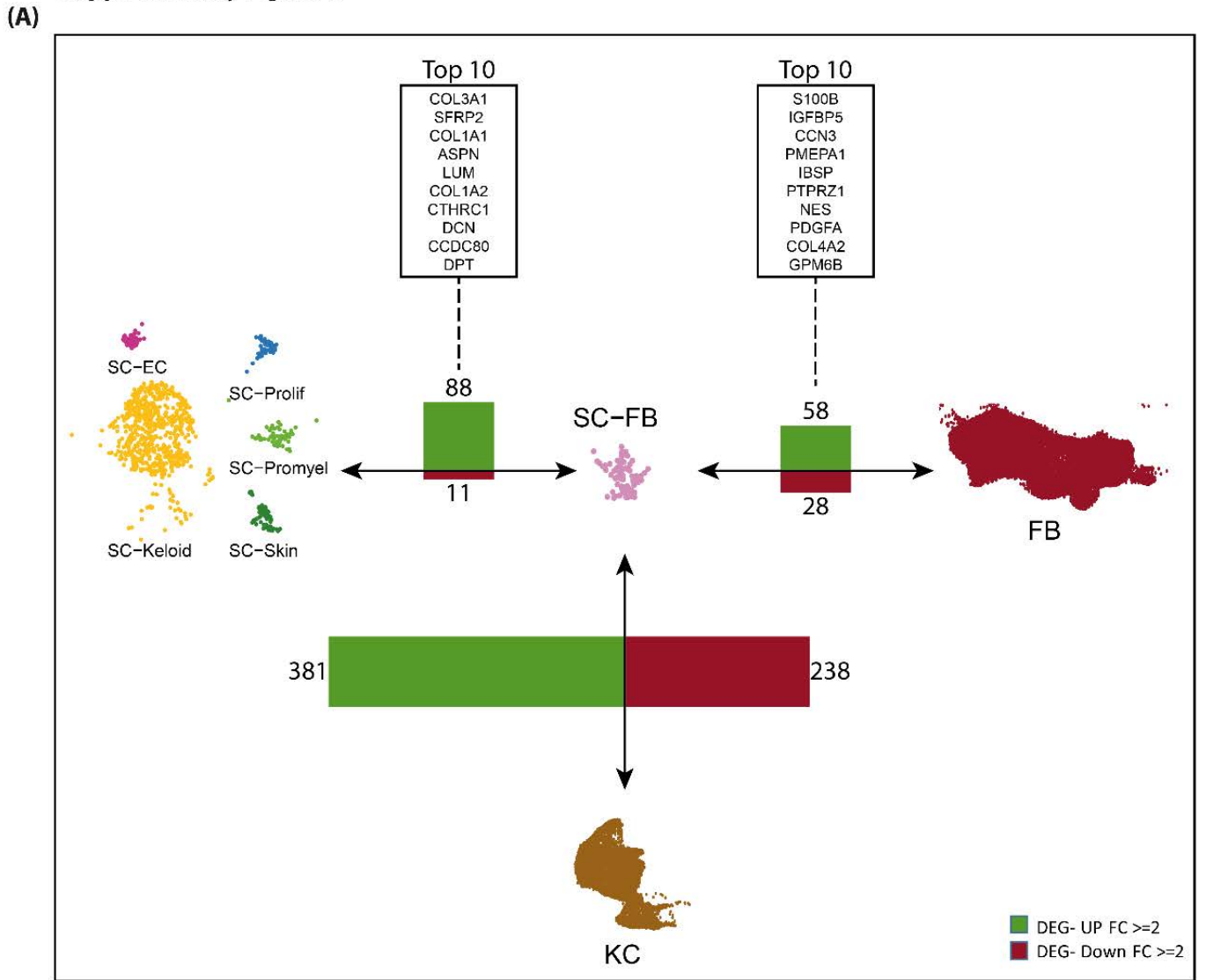
(C)



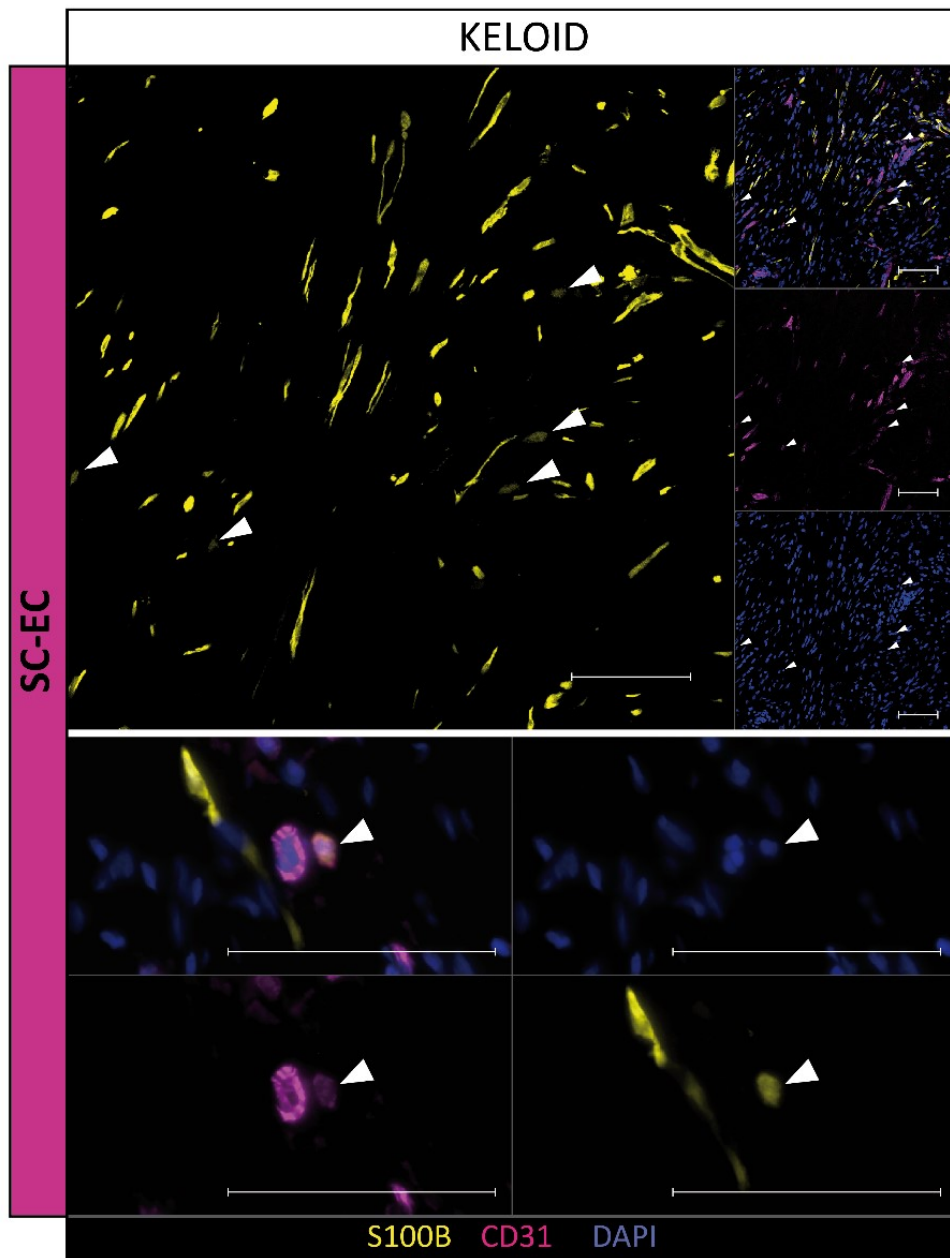
Supplementary Figure 5



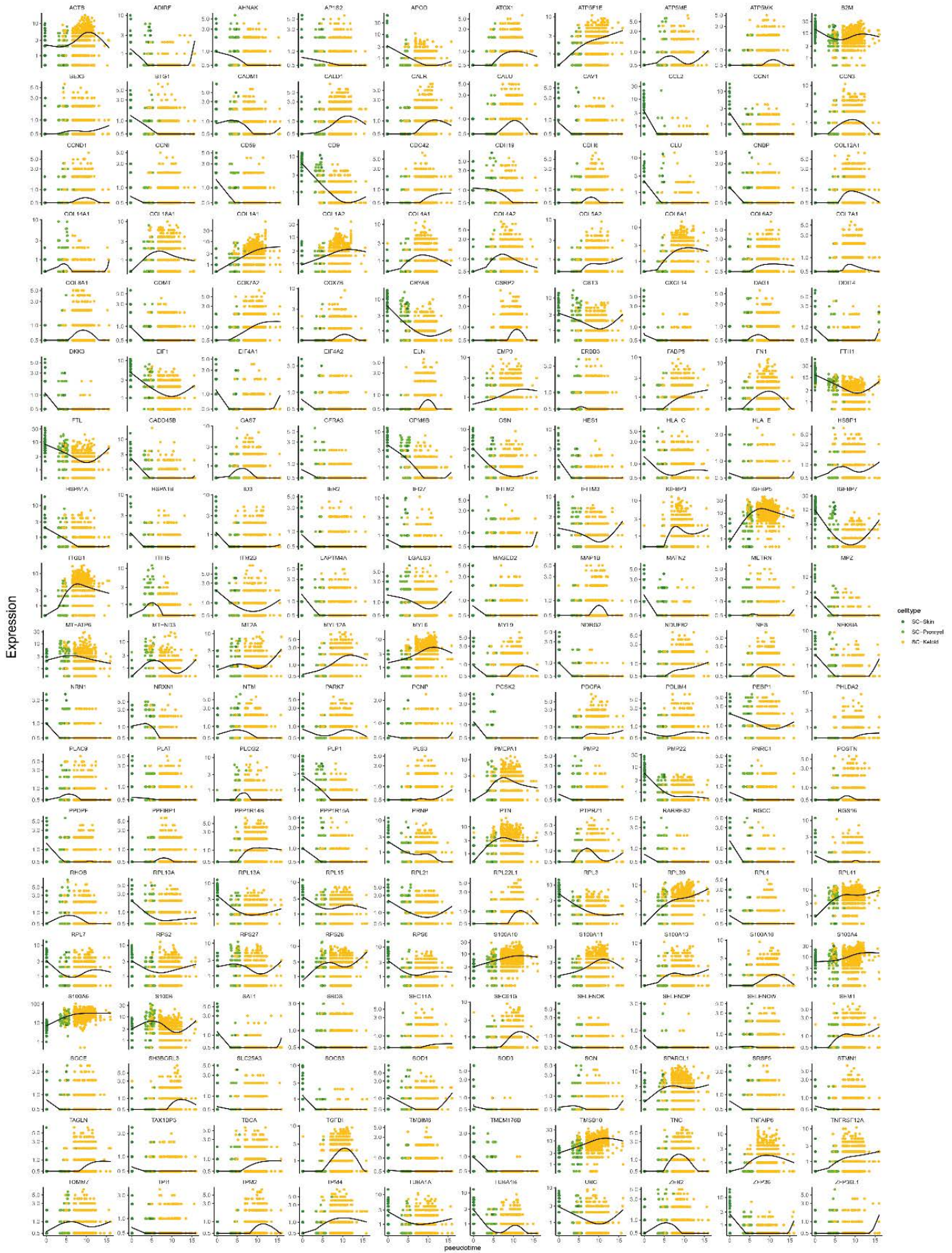
Supplementary Figure 6



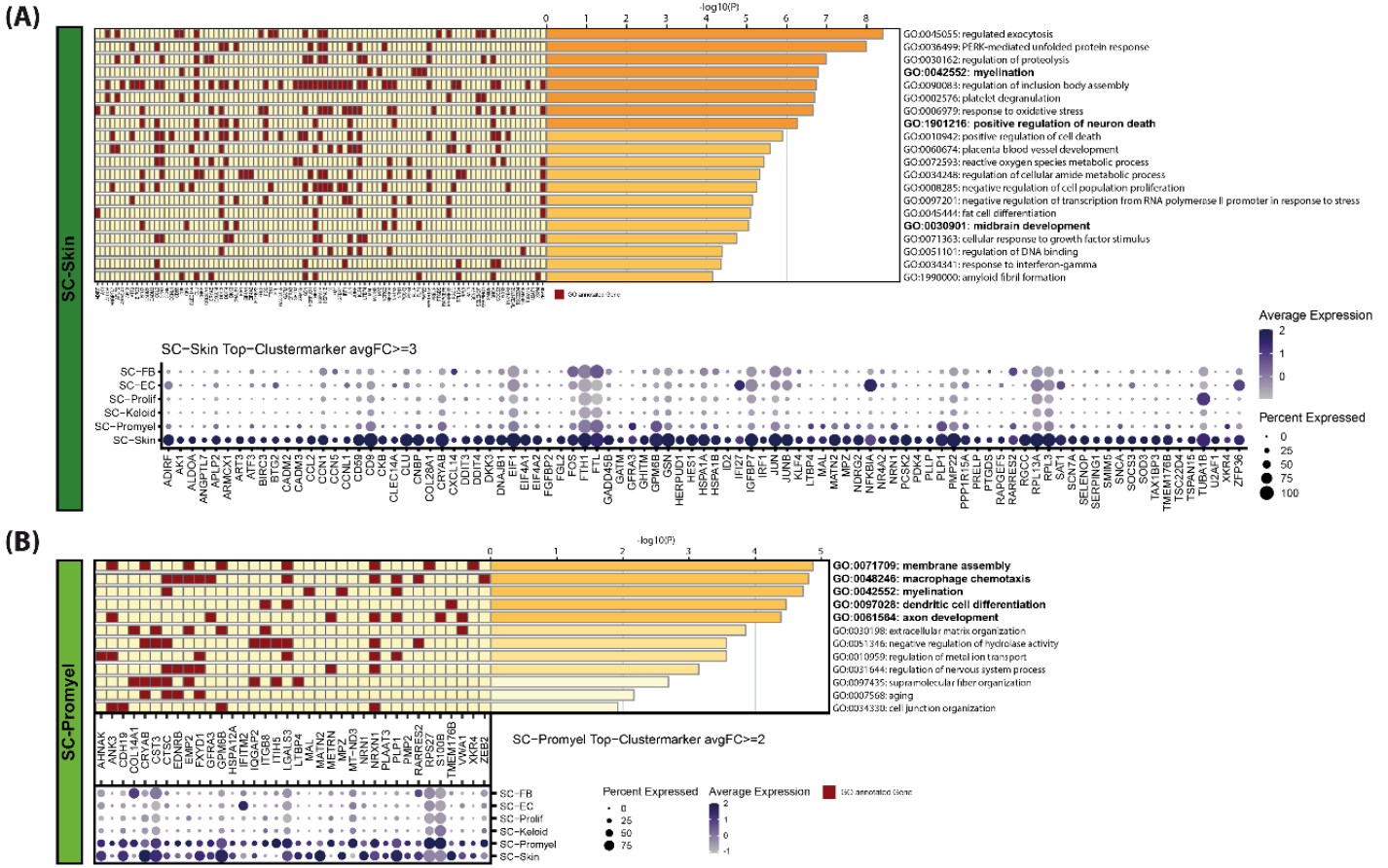
Supplementary Figure 7



Supplementary Figure 8

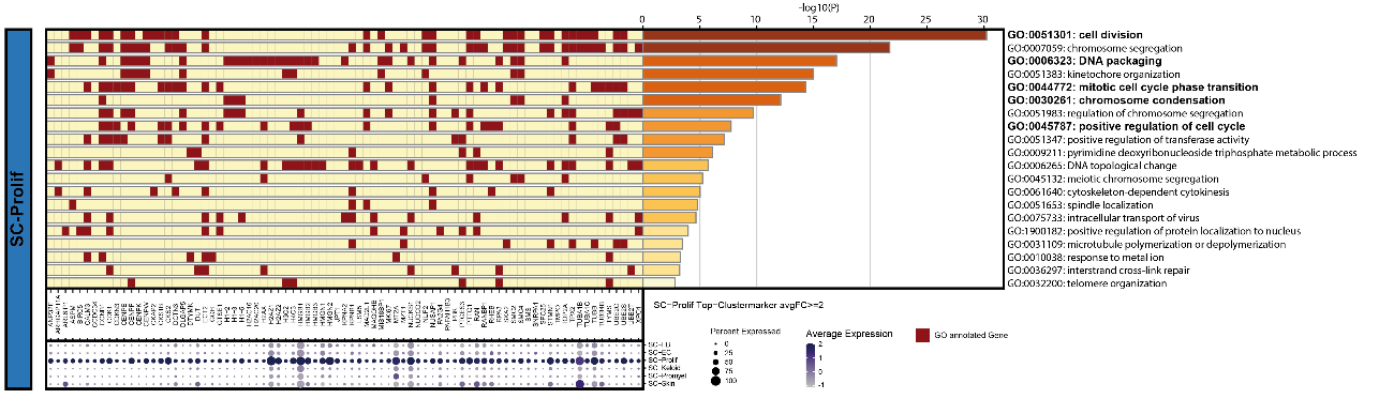


Supplementary Figure 9

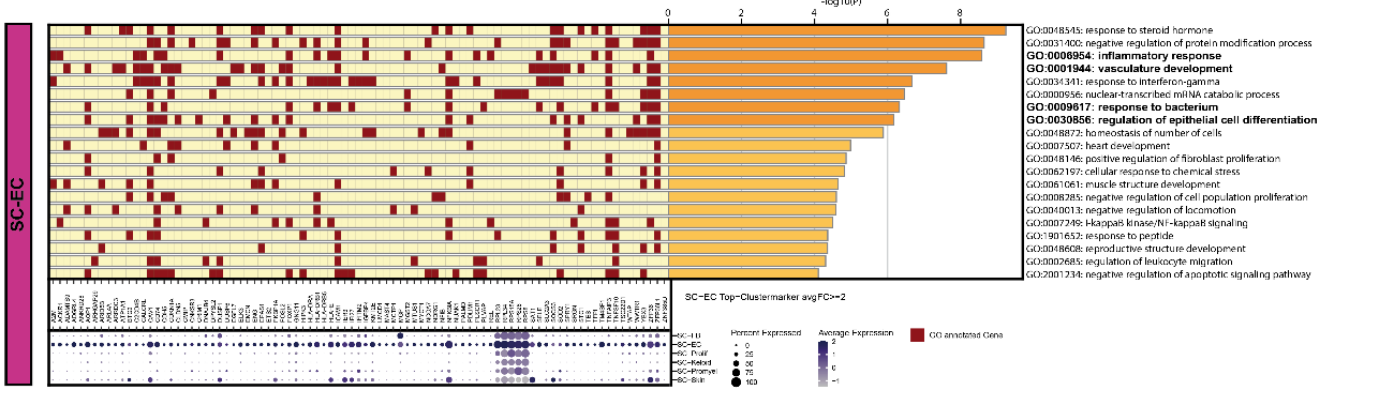


Supplementary Figure 10

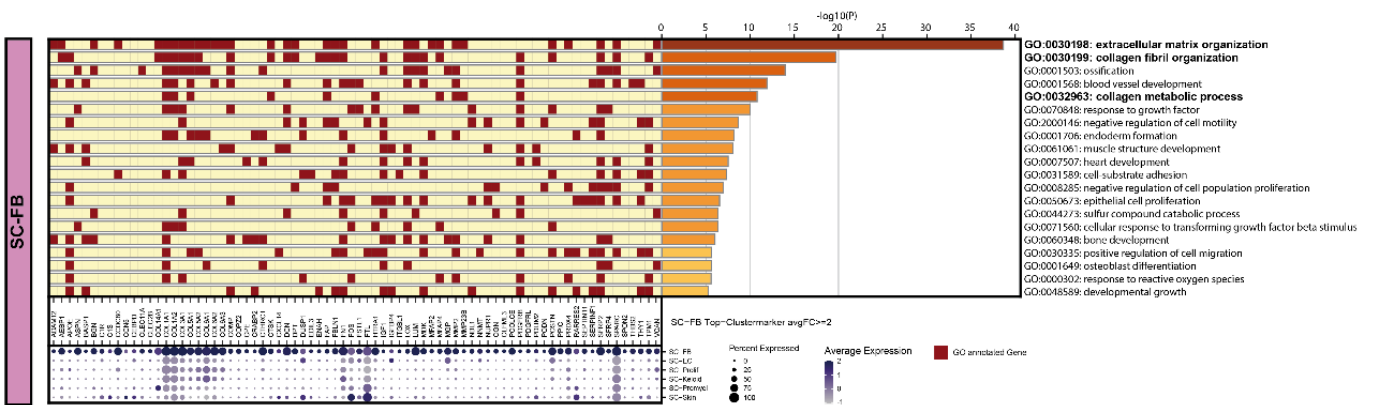
(A)



(B)

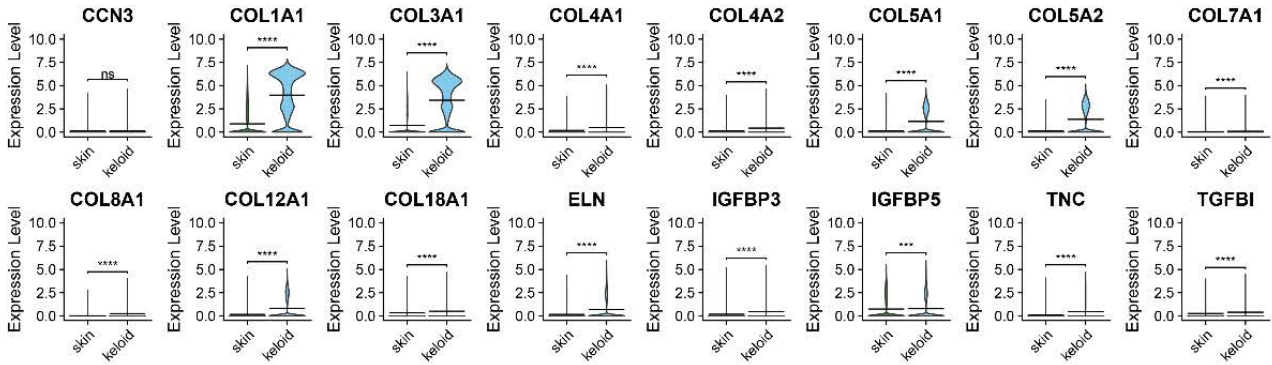


(C)

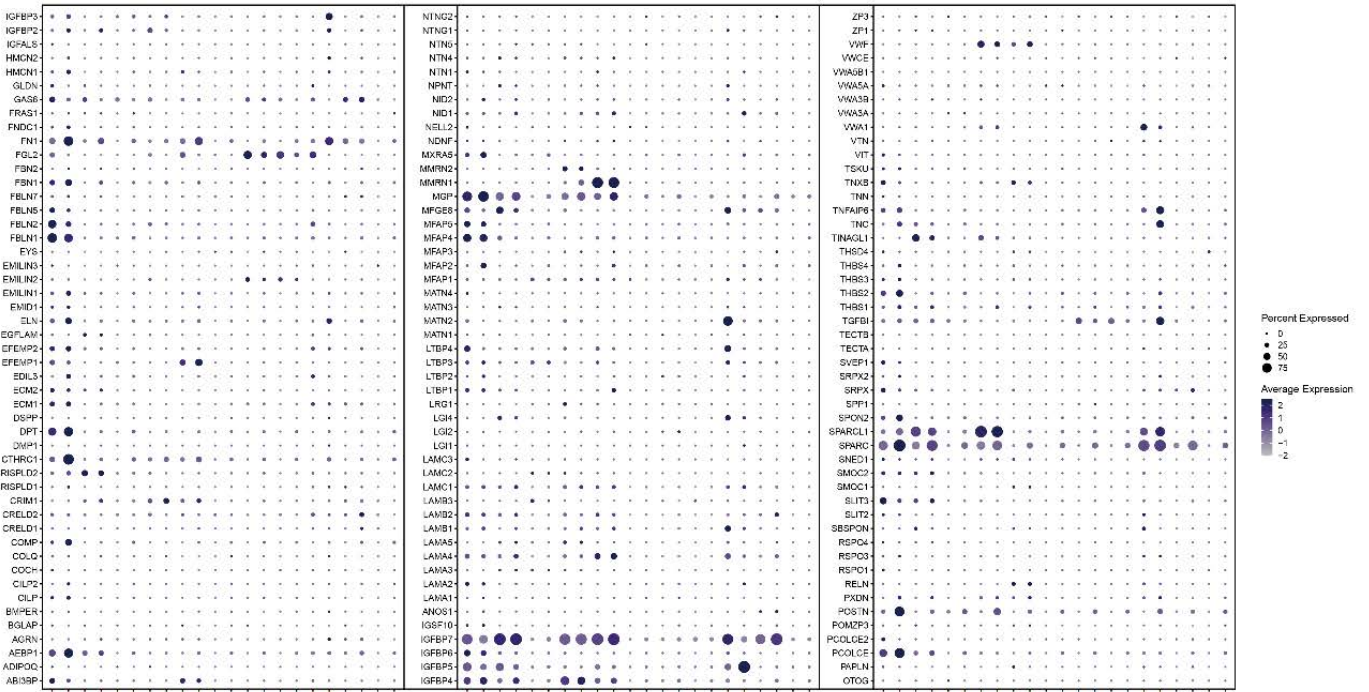


Supplementary Figure 11

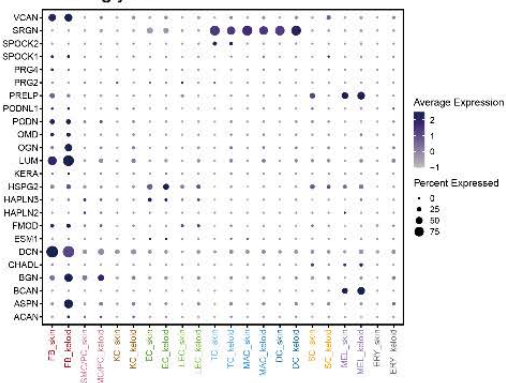
(A) Matrix-associated gene expression_all cells



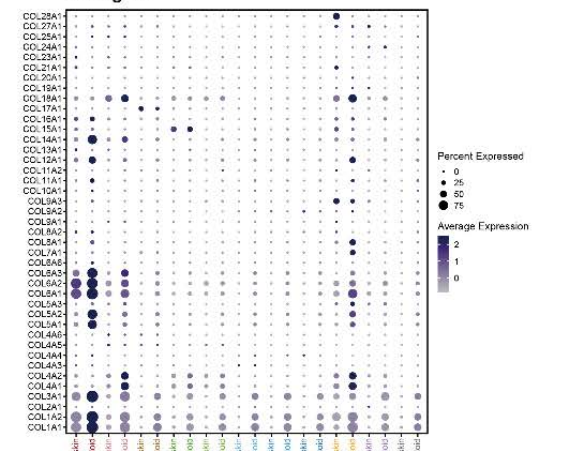
(B) ECM_Glycoproteins



(C) Proteoglycans

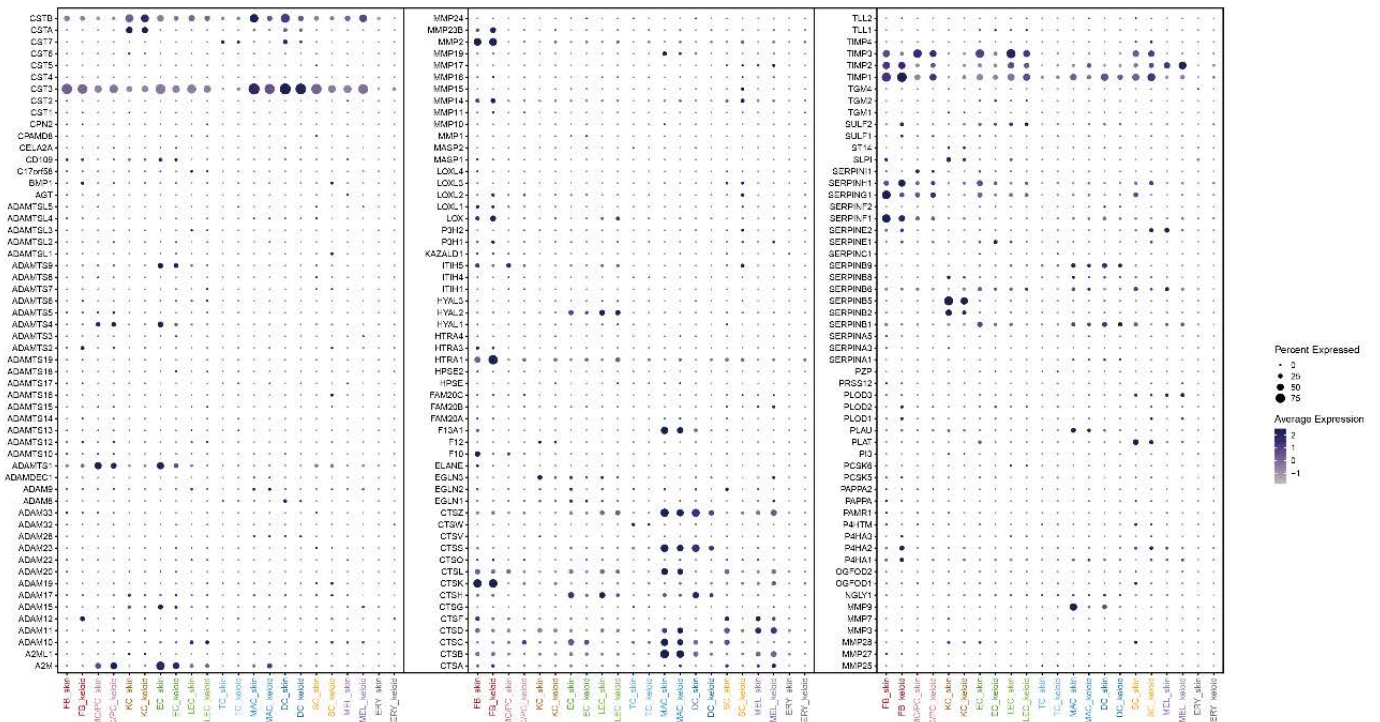


(D) Collagens

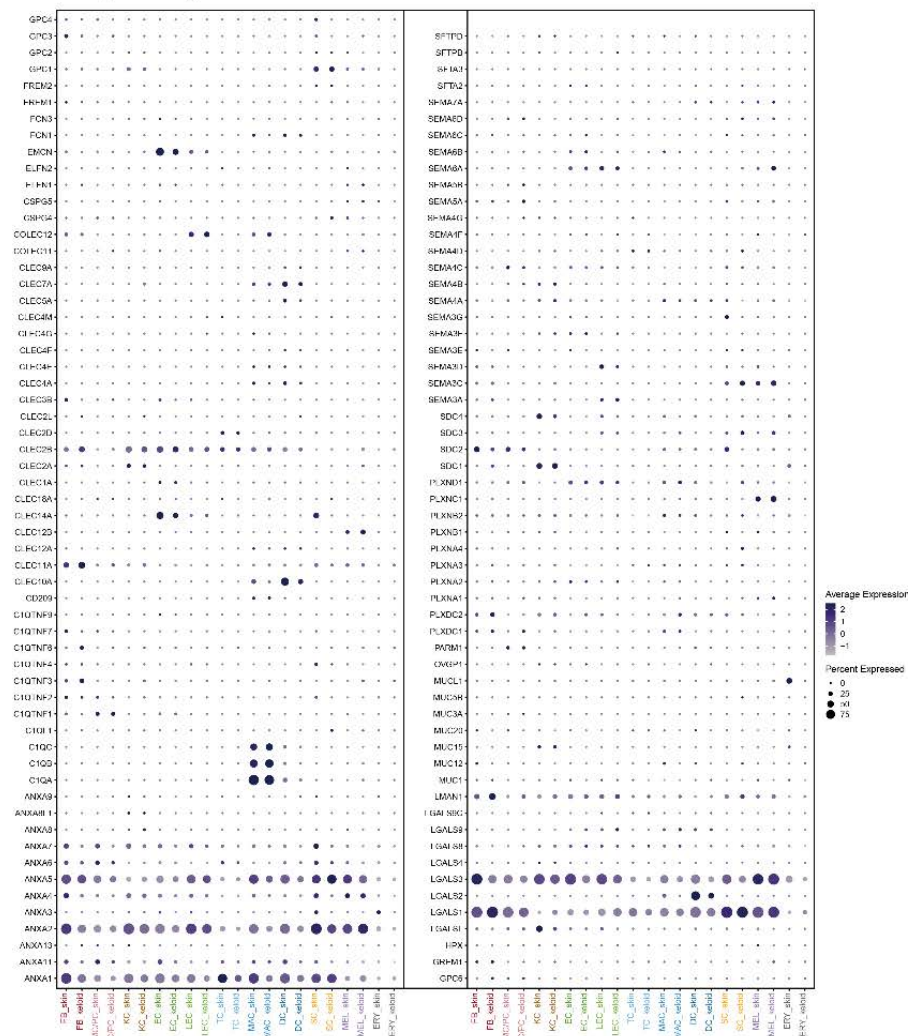


Supplementary Figure 12

(A) ECM_Regulators

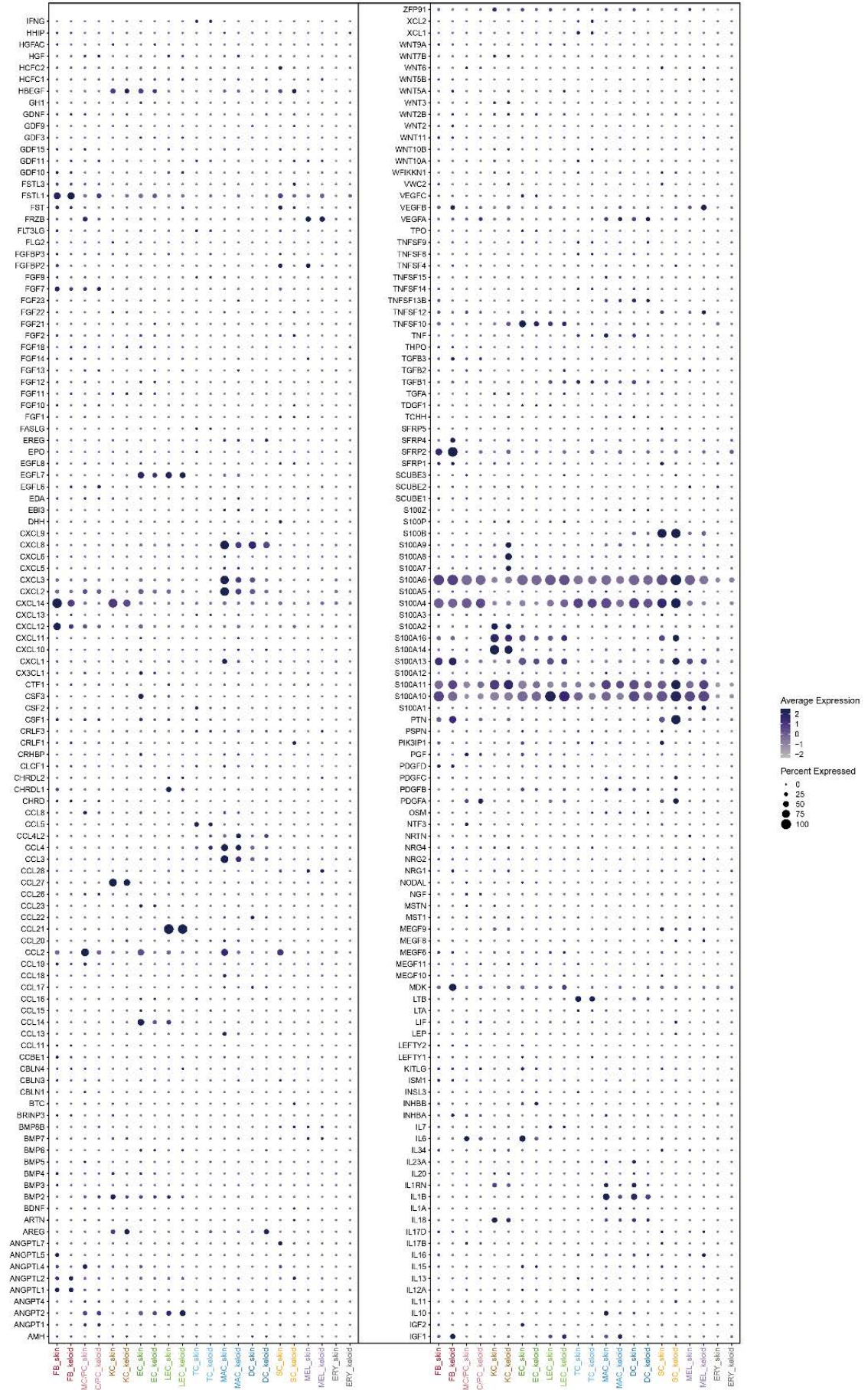


(B) ECM_affiliated_Proteins



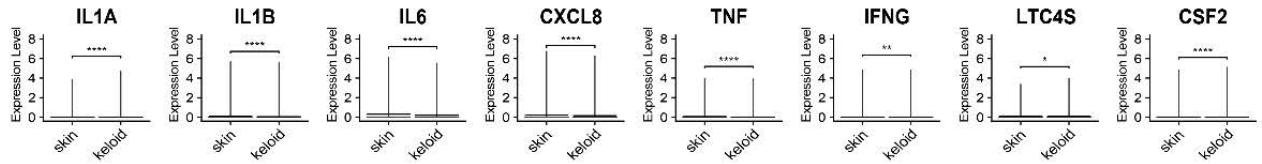
Supplementary Figure 13

Secreted_Factors

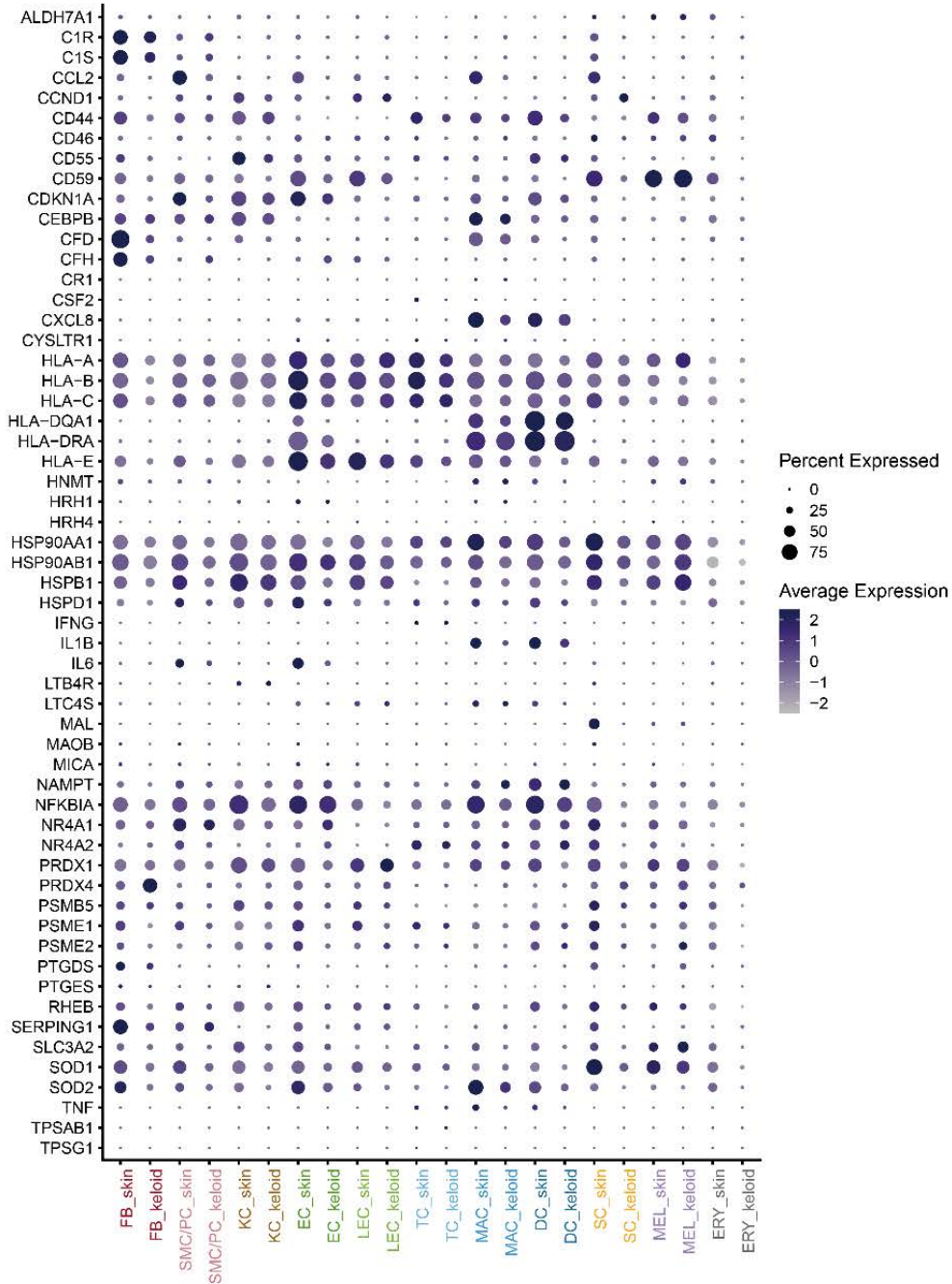


Supplementary Figure 14

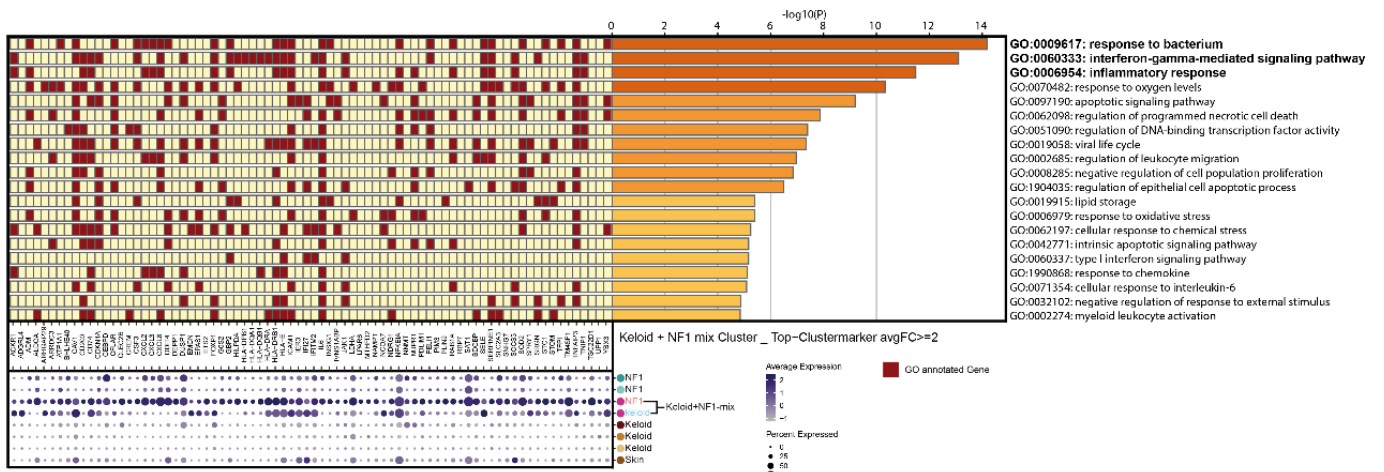
(A) Inflammation-associated gene expression_all cells



(B) Immunology-associated genes in cells of skin and keloid

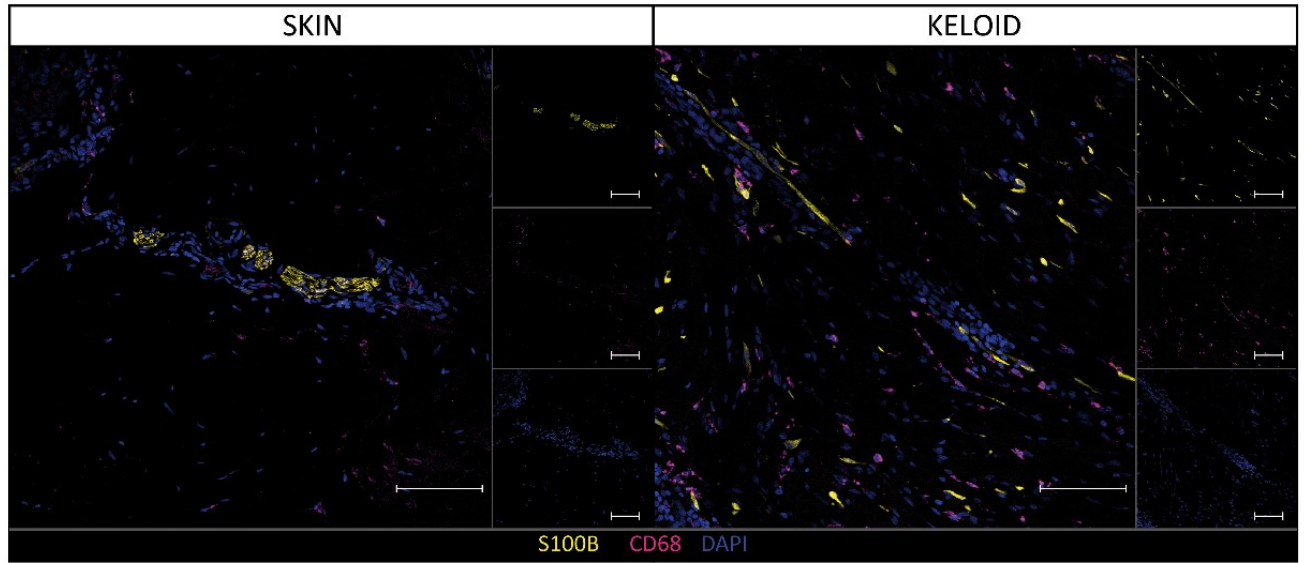


Supplementary Figure 15

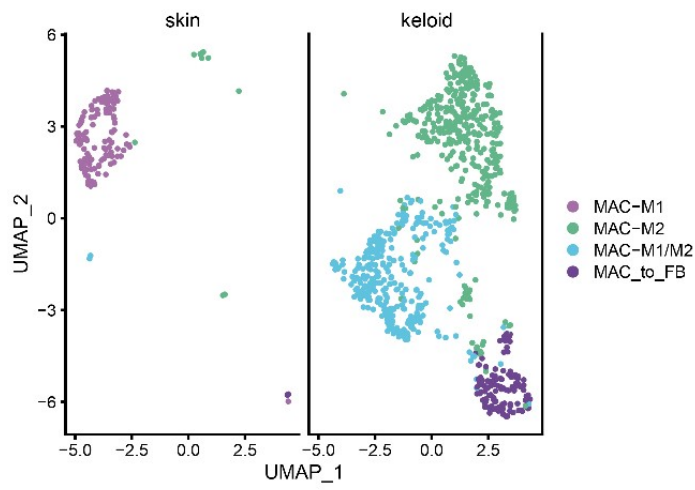


Supplementary Figure 16

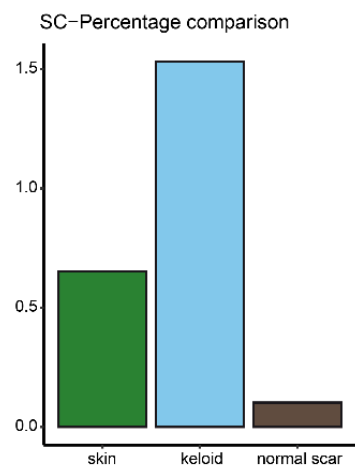
(A)



(B)

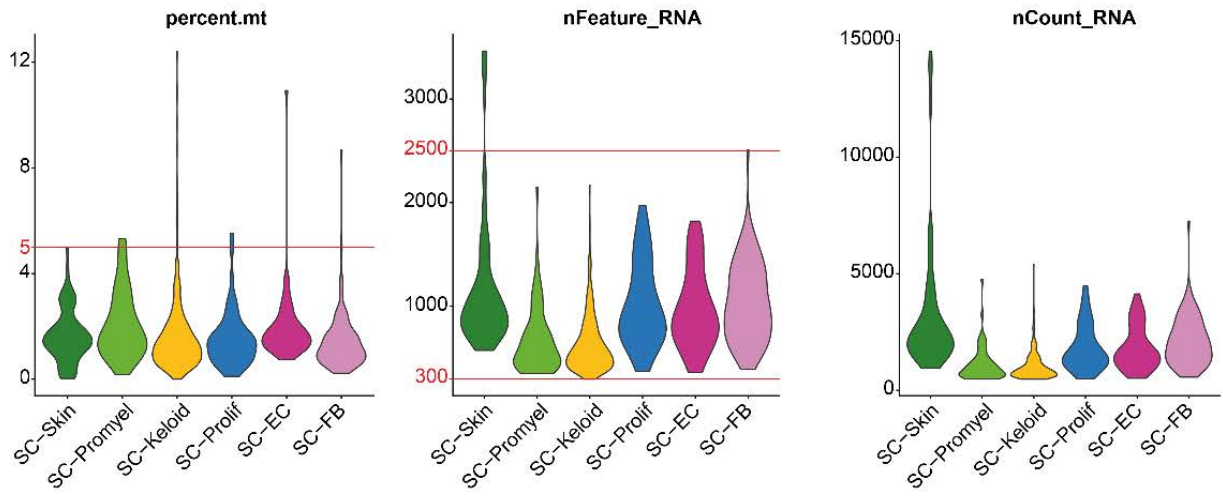


Supplementary Figure 17



Supplementary Figure 18

(A)



Supplementary Table 1 – donor information

Type	ID	Site	Age	Sex	Race	Source
normal skin	skin_1	Forearm	63	Male	Caucasian	Tabib ¹
normal skin	skin_2	Forearm	54	Male	Caucasian	Tabib ¹
normal skin	skin_3	Forearm	66	Female	Caucasian	Tabib ¹
normal skin	skin_4	Forearm	23	Female	Asian	Tabib ¹
normal skin	skin_5	Forearm	62	Female	Caucasian	Tabib ¹
normal skin	skin_6	Forearm	24	Male	Caucasian	Tabib ¹
normal skin	skin_7	Abdomen	33	Male	Caucasian	Direder
Keloid	keloid_1	Sternum	36	Female	Caucasian	Direder
Keloid	keloid_2	Earlobe	60	Female	African	Direder
Keloid	keloid_3L	Earlobe - left	34	Male	Caucasian	Direder
Keloid	keloid_3R	Earlobe - right	34	Male	Caucasian	Direder
normal scar	scar1	Abdomen	26	Female	Caucasian	Direder
normal scar	scar2	Abdomen	43	Female	Caucasian	Direder
normal scar	scar3	Abdomen	60	Male	Caucasian	Direder

Supplementary Table 1. donor information.

¹Tabib, T., Morse, C., Wang, T., Chen, W. & Lafyatis, R. SFRP2/DPP4 and FMO1/LSP1 Define Major Fibroblast Populations in Human Skin. *J Invest Dermatol* 138, 802-810, doi:10.1016/j.jid.2017.09.045 (2018).

Supplementary Table 2 - marker genes information

celltype	abbreviation	marker gene
Fibroblast	FB	PDGFRA ¹ , LUM ² , COL1A1 ^{3,4} , DCN ¹ , FBLN1 ⁵
Smooth muscle cell or pericyte	SMC/PC	ACTA2 ^{2,4} , RGS5 ^{2,4,5}
Keratinocyte	KC	KRT10 ⁶ , KRT1 ^{2,6} , KRT14 ^{2,6} , KRT5 ⁶
Endothelial cell	EC	SELE ² , VWF ⁵
Lymphatic Endothelial cell	LEC	VWF ⁵ , LYVE1 ^{2,4}
T-cell	TC	CD3D ^{4,7} , CD2 ⁵ , CXCR4 ⁸
Macrophage	MAC	CD68 ⁴ , AIF1 ²
Dendritic cell	DC	AIF1 ² , FCER1A ^{7,9}
Schwann cell	SC	S100B ⁴ , NGFR ^{4,5}
Melanocyte	MEL	PMEL ^{2,5} , MLANA ⁵
Erythrocyte	ERY	HBB ⁷ , HBA1 ⁷

Supplementary Table 2. marker genes information.

¹Muhl, L. et al. Single-cell analysis uncovers fibroblast heterogeneity and criteria for fibroblast and mural cell identification and discrimination. *Nat Commun* 11, 3953, doi:10.1038/s41467-020-17740-1 (2020).

²Vorstandlechner, V. et al. Deciphering the functional heterogeneity of skin fibroblasts using single-cell RNA sequencing. *Faseb j* 34, 3677-3692, doi:10.1096/fj.201902001RR (2020).

³Tabib, T., Morse, C., Wang, T., Chen, W. & Lafyatis, R. SFRP2/DPP4 and FMO1/LSP1 Define Major Fibroblast Populations in Human Skin. *J Invest Dermatol* 138, 802-810, doi:10.1016/j.jid.2017.09.045 (2018).

⁴Wolbert, J. et al. Redefining the heterogeneity of peripheral nerve cells in health and autoimmunity. *Proc Natl Acad Sci U S A* 117, 9466-9476, doi:10.1073/pnas.1912139117 (2020).

⁵Voigt, A. P. et al. Single-cell transcriptomics of the human retinal pigment epithelium and choroid in health and macular degeneration. *Proc Natl Acad Sci U S A* 116, 24100-24107, doi:10.1073/pnas.1914143116 (2019).

⁶Finnegan, A. et al. Single-Cell Transcriptomics Reveals Spatial and Temporal Turnover of Keratinocyte Differentiation Regulators. *Front Genet* 10, 775, doi:10.3389/fgene.2019.00775 (2019).

⁷Saichi, M. et al. Single-cell RNA sequencing of blood antigen-presenting cells in severe COVID-19 reveals multi-process defects in antiviral immunity. *Nat Cell Biol* 23, 538-551, doi:10.1038/s41556-021-00681-2 (2021).

⁸Elsner, R. A., Ernst, D. N. & Baumgarth, N. Single and coexpression of CXCR4 and CXCR5 identifies CD4 T helper cells in distinct lymph node niches during influenza virus infection. *J Virol* 86, 7146-7157, doi:10.1128/jvi.06904-11 (2012).

⁹Villani, A. C. et al. Single-cell RNA-seq reveals new types of human blood dendritic cells, monocytes, and progenitors. *Science* 356, doi:10.1126/science.aah4573 (2017).

Supplementary Table 3 – antibody information

1 st Antibodies					
Antigen	Species	catalog No	company	dilution	comment
S100	rabbit	#Z0311	DAKO	ready to use	4 hr, RT
NGFR	mouse	#sc-13577	SantaCruz	1:100	o.n., 4°C
NGFR	rabbit	#8238	CellSignaling	1:300	4 hr, RT
SOX10	mouse	#sc-365692	SantaCruz	1:33	o.n., 4°C
Nestin	mouse	#MAB5326	Millipore	1:200	o.n., 4°C
Ki67	rabbit	#NB500-170	Novus	1:50	o.n., 4°C
MBP	mouse	#ab62631	Abcam	1:300	o.n., 4°C
CD31	mouse	#M0823	DAKO	1:20	4 hr, RT
IGFBP-5	goat	#AF875-SP	R&D	1:50	o.n., 4°C
JUN	rabbit	#9165S	CellSignaling	1:300	4 hr, RT
CD90	mouse	# 550402	BD Pharmingen	1:50	4 hr, RT
PGP9.5	mouse	#7863-1004	BioRad	1:250	o.n., 4°C
vimentin	chicken	#AB5733	Merck Millipore	1:300	4 hr, RT
SMA	rabbit	#14395-I-AP	Proteintech	1:200	4 hr, RT
NFpan	mouse	#M0762	DAKO	1:100	o.n., 4°C
CD68	mouse	#333809	BioLegend	1:50	o.n., 4°C
2 nd Antibodies					
Antigen	Species	catalog No	company	dilution	comment
α ch DL650	goat	#SA5-10073	Invitrogen	1:400	1 hr, RT
α rb AF488	goat	#A32731	Invitrogen	1:600	1 hr, RT
α ch AF488	goat	#A-11039	Invitrogen	1:400	1 hr, RT
α rb AF594	goat	#A11012	Invitrogen	1:400	1 hr, RT
α ms AF594	donkey	#A21203	Invitrogen	1:400	1 hr, RT
α g AF546	donkey	#A11056	Invitrogen	1:400	1 hr, RT
α rb AF647	goat	#A32733	Invitrogen	1:400	2 hr RT

2.2 Interlude

In the first study, we explored the keloidal Schwann cells with their pro-fibrotic expression pattern in keloids.

In the second study of this thesis, we verified the tissue specificity of keloidal Schwann cells in independent datasets of healthy skin, normal scars, keloids and skin adjacent to keloids generated by four independent research groups. Furthermore, we aimed to allocate the keloidal Schwann cells in the lineage development of so far described Schwann cell subtypes.

The transcriptional profile of keloidal Schwann cells

Martin Direder^{1,2}, Matthias Wielscher³, Tamara Weiss⁴, Maria Laggner^{1,2}, Dragan Copic^{1,2}, Katharina Klas^{1,2}, Daniel Bormann^{1,2}, Vera Vorstandlechner⁴, Erwin Tschachler³, Hendrik Jan Ankersmit^{1,2} and Michael Mildner³✉

© The Author(s) 2022

Recently, a specific Schwann cell type with profibrotic and tissue regenerative properties that contributes to keloid formation has been identified. In the present study, we reanalyzed published single-cell RNA sequencing (scRNA-seq) studies of keloids, healthy skin, and normal scars to reliably determine the specific gene expression profile of keloid-specific Schwann cell types in more detail. We were able to confirm the presence of the repair-like, profibrotic Schwann cell type in the datasets of all three studies and identified a specific gene-set for these Schwann cells. In contrast to keloids, in normal scars, the number of Schwann cells was not increased, nor was their gene expression profile distinctly different from that of Schwann cells of normal skin. In addition, our bioinformatics analysis provided evidence for a role of transcription factors of the AP1, STAT, and KLF families, and members of the IER genes in the dedifferentiation process of keloidal Schwann cells. Together, our analysis strengthens the role of the profibrotic Schwann cell type in the formation of keloids. Knowledge of the exact gene expression profile of these Schwann cells will facilitate their identification in other organs and diseases.

Experimental & Molecular Medicine <https://doi.org/10.1038/s12276-022-00874-1>

INTRODUCTION

Schwann cells are glial cells of the peripheral nervous system and ensure proper nerve development and integrity¹. After peripheral nerve injury, mature Schwann cells undergo transcriptional reprogramming that involves dedifferentiation into an immature cell state and the acquisition of repair-specific functions^{2,3}. These repair Schwann cells are essential to orchestrate nerve regeneration by attracting immune cells to the site of injury, phagocytosis of myelin debris, secretion of neurotrophic and neuritogenic factors and formation of regeneration tracks (Bungner bands) to stimulate and guide regrowing axons⁴. Dedifferentiation into repair Schwann cells has been shown to involve the expression and activation of a variety of specific factors⁵, including JUN, STAT3, BDNF, ARTN, IGFBP2 and GDNF⁵. In particular, OLIG1 and SHH have been suggested as specific markers for Schwann cell repair⁴.

In healthy skin, Schwann cells persist in myelinating and nonmyelinating states¹. Recently, Parfejevs et al. provided evidence that Schwann cells contribute not only to the regeneration of the nerve but also to dermal wound healing by proliferating and emanating from the disrupted nerve. These skin-derived repair Schwann cells populate the damaged area, where they support the differentiation of fibroblasts into myofibroblasts and promote wound contraction and closure as well as re-epithelization⁶. After the completion of neuronal regeneration and wound healing, skin repair Schwann cells redifferentiate into their adult state and ensheath the restored axons⁷. Ideally, the entire healing process results in an asymptomatic, fine-lined, flat scar.

Abnormal scars, such as hypertrophic scars or keloids, can result in serious health problems, including movement restrictions,

persistent itch, and pain^{8–11}. Keloids represent a special type of scar characterized by tumor-like continuous growth beyond the margins of the original wound⁸. They exclusively develop in humans, and the lack of adequate model systems complicates basic research into their pathogenesis^{12,13}. Therefore, despite several decades of research, the exact mechanistic events driving keloid formation remain largely unclear¹⁴.

The recent development of single-cell RNA sequencing (scRNA-seq) enables a completely new approach to decode disease pathomechanisms. To date, three research groups have applied scRNA-seq to study keloid tissue at the cellular and transcriptional levels. Liu et al. compared the center of keloids with adjacent skin. These researchers identified various dysregulated genes and pathways in keloidal fibroblasts and endothelial cells and revealed TWIST1 as an important factor in keloidal fibrogenesis¹⁵. Deng et al. applied scRNA-seq to compare keloids with normal scars¹⁶. This group subdivided keloidal fibroblasts into four major groups and identified an increase in extracellular matrix (ECM)-producing mesenchymal fibroblasts in keloid tissue. Whereas these studies focused on fibroblasts and endothelial cells, a recent study by our group demonstrated that keloids contain an increased number of phenotypically distinct Schwann cells¹⁷. The vast majority of these keloidal Schwann cells displayed a cellular state comparable to that described for Schwann cells in regenerating nerves¹⁷. Our additional finding that these Schwann cells expressed multiple genes associated with matrix formation makes them highly plausible candidates for playing a crucial role in the development of keloids¹⁷.

Owing to donor variabilities, differences in sample preparation and data processing, scRNA-seq studies are not always

¹Laboratory for Cardiac and Thoracic Diagnosis, Regeneration and Applied Immunology, Department of Thoracic Surgery, Medical University of Vienna, Vienna, Austria.

²Aposcience AG (FN 308089y), Dresdner Straße 87/A21, Vienna, Austria. ³Department of Dermatology, Medical University of Vienna, Vienna, Austria. ⁴Department of Plastic, Reconstructive, and Aesthetic Surgery, Medical University of Vienna, Vienna, Austria. ✉email: michael.mildner@meduniwien.ac.at

Received: 15 March 2022 Revised: 7 July 2022 Accepted: 8 August 2022

Published online: 04 November 2022

straightforwardly comparable^{18–21}. For more consistent data, individual datasets from different laboratories should be re-evaluated in a combined analysis, as previously shown for skin fibroblast populations²². This study clearly demonstrated that, despite differences in the experimental procedures, major similarities among all fibroblast populations are conserved across the scRNA-seq datasets published by the different laboratories. Studies on the comparability of smaller cell clusters, such as Schwann cells, in scRNA-seq datasets are thus far not available.

Here, we performed a comparative analysis of Schwann cells in different scRNA-seq datasets of healthy skin, normal scars, keloids, and keloid-adjacent skin from four independent research groups to elucidate the gene-set most reliably identifying the keloidal Schwann cell population. In addition, we compared two distinct bioinformatics approaches for the analysis of numerous different scRNA-seq datasets, revealing significant variations in the two calculation methods. Our study shows that the presence of the previously described repair-like, profibrotic Schwann cells in keloids is indeed conserved across different scRNA-seq datasets and provides a specific expression pattern for keloidal Schwann cells. Thus far, unrecognized cells might represent a novel, potential target for keloid treatment.

MATERIALS AND METHODS

Data acquisition

In this study, scRNA-seq datasets of 6 healthy skin, 6 normal scar, 11 keloid and 4 keloid-adjacent skin samples were analyzed (Fig. 1a). ScRNA-seq data of normal scars and keloids have already been generated by Direder et al. and were deposited in NCBI's Gene Expression Omnibus (GSE181316)¹⁷. Skin data published by Tabib et al. (2018) were downloaded from https://dom.pitt.edu/wp-content/uploads/2018/10/Skin_6Control_rawUMI.zip and https://dom.pitt.edu/wp-content/uploads/2018/10/Skin_6Control_Metadata.zip¹⁸. ScRNA-seq data of keloids and normal scars generated by Deng et al. were downloaded from the Gene Expression Omnibus database (dataset GSE163973)¹⁶. Transcriptomic data from Liu et al. were downloaded from the Genome Sequencing Archive (BioProject PRJCA003143)⁵. Count tables were obtained from the original fastq read files applying the Cell Ranger pipeline (10X Genomics Cell Ranger 3.0.2, Pleasanton, CA, USA)²³.

Data processing

Computational analyses were performed utilizing R and R Studio (version 4.0.3, The R Foundation, Vienna, Austria). All features of the included datasets were screened, and doublets were removed. The feature designation was harmonized, and only features detected in all datasets were included in subsequent analyses. Datasets were transformed into a Seurat object using Seurat (Seurat v4.0.1, Satija Lab)⁴. Scran normalization in combination with the glmGamPoi package and removal of the mitochondrial mapping percentage were applied to preprocess the data^{25,26}. Erythrocytes were excluded by removing cells with a hemoglobin subunit beta (HBB) expression >5. For this study, the included datasets were combined all together and individually by source and tissue type (Fig. 1b). All dataset combinations were processed according to the Seurat Vignette. Principal component analysis (PCA), uniform manifold approximation (UMAP) and projection dimensionality reduction were applied according to the Seurat protocol. Clusters were identified as cell types according to their expression of well-established marker genes¹⁷. Schwann cell clusters were subsetted, and data were preprocessed and calculated in the same way as described above. The commands "RunUMAP" and "FindNeighbors" were performed on 30 dimensions, and "FindClusters" was applied with a resolution of "0.3". Subset clusters expressing marker genes typical for melanocytes were removed. Schwann cells were characterized by the expression of established marker genes^{17,27}. Differentially expressed genes were defined as genes displaying an average fold change >2. The SC-Keloid-specific gene expression pattern was identified by examination of SC-Keloid against all myelinating and nonmyelinating Schwann cells of all dataset combinations (Supplementary Tables 1–5). From these lists, the top 100 upregulated genes were compared, and only genes included in all gene lists were selected as members of the SC-Keloid gene expression pattern. Genes without a clear demarcation from the myelinating and nonmyelinating Schwann cells were excluded. Gene Ontology (GO) enrichment analysis was performed

using Metascape with 0.05 as the p-value cutoff and 2 as the minimum enrichment score²⁸. Only corresponding GO terms with "Summary" Group ID are shown. For pseudotime analysis, the Schwann cell clusters from all single calculated datasets were combined and preprocessed in the same way. As normal scar datasets from both sources revealed no Schwann cell cluster, these datasets were excluded from the pseudotime analysis. The commands "RunUMAP" and "FindNeighbors" were performed on 18 dimensions, and "FindClusters" was applied with a resolution of 0.5. Monocle3 (Monocle3, v.0.2.3.0, Trapnell Lab, Seattle, Washington, USA) was used to create the pseudotime trajectory^{29–33}. The principal graph was not pruned, and a total of 7 centers were determined. The generated Metascape lists were matched, and only $-\log_{10}(p)$ values of terms identified in all lists were pictured together with their arithmetic mean. For identification of upregulated genes specific for the branching point in the combined Schwann cell object, the command "FindMarkers" was executed, comparing the newly identified Seurat cluster located at the branching point against all remaining Schwann cells. Potential interactions of Schwann cells at the branching point or of Schwann cell subtypes in keloids and healthy skin were analyzed using CellChat³⁴.

Sequencing data juxtaposition to the gene expression profile of peripheral nerve regeneration

The human homologs of the gene list published by Bosse et al.⁵ were identified using the GenBank accession number and the website UniProt (<https://www.uniprot.org/>, accessed on 2021-10-18). Relative expression levels were identified using the command "FindMarkers" with SC-Keloid as ident.1 and the myelinating and nonmyelinating cluster as the opposite ident. A min.pct of 0.01 and a logfc.threshold of 0.01 was set. Expression changes <0.01 were set as 0. Significantly regulated genes published by Bosse et al. were identified in our list of differentially expressed genes, and expression levels were colored corresponding to the color code by Bosse et al.

Collagen alignment examination

Hematoxylin and eosin staining of healthy skin, normal scar, and keloid samples was imaged. Alignment of collagen bundles was determined by applying Curvalign V4.0 Beta (MATLAB software, Cleve Moler, MathWorks, Natick, Massachusetts, USA). Collagen color, contrast and brightness were edited by Adobe Photoshop CS6 (Adobe, Inc., San Jose, CA, USA). The region of interest (ROI) was defined by size (256 height, 256 width), and four ROIs per condition were analyzed. The coefficient of alignment was statistically evaluated.

Immunofluorescence

Tissue samples were fixed in neutral buffered 4.5% formaldehyde (SAV Liquid Production GmbH, Flintsbach am Inn, Germany) at 4 °C overnight, followed by a washing step with phosphate-buffered saline (PBS) overnight. Dehydration was performed by sequential incubations with 10%, 25%, and 42% sucrose for 24 h each. Tissues were embedded in optimal cutting temperature compound (OCT compound, TissueTek, Sakura, Alphen aan den Rijn, The Netherlands) and stored at -80°C . Samples were cut into 10 μm -thick sections and dried for 30 min at room temperature. Slides were blocked and permeabilized for 15 min with 1% BSA, 5% goat serum (DAKO, Glostrup, Denmark), and 0.3% Triton-X (Sigma Aldrich, St. Louis, MO, USA) in 1x PBS. Sections were incubated with primary antibody solution overnight at 4 °C followed by three washing steps with 1x PBS for 5 min each (Supplementary Table 6). Sections were incubated with secondary antibodies and 50 $\mu\text{g}/\text{ml}$ 4,6-diamidino-2-phenylindole (DAPI, Thermo Fisher Scientific, Waltham, MA, USA) in 1x PBS for 50 min at room temperature. After three washing steps, sections were covered using mounting medium and stored at 4 °C. Images were acquired using a confocal laser scanning microscope (TCS SP8X, Leica, Wetzlar, Germany) equipped with a 10x (0.3 HCPL FluoTar), a 20x (0.75 HC-Plan-Apochromat, Multimmersion), a 20x (0.75 HC-Plan-Apochromat) and a 63x (1.3 HC-Plan-Apochromat, Glycerol) objective using the Leica application suite X version 1.8.1.13759 or LAS AF Lite software (both Leica). Final images constitute a maximum projection of total z-stacks.

Statistics

Statistical evaluation was performed using GraphPad Prism 8 software (GraphPad Software Inc., La Jolla, CA, USA). The Shapiro-Wilk test was used to test for normal distribution. One-way ANOVA with Tukey's post-hoc test was used to compare three and more groups. p-values are marked with asterisks: * $p < 0.05$, ** $p < 0.01$, *** $p < 0.001$, **** $p < 0.0001$.

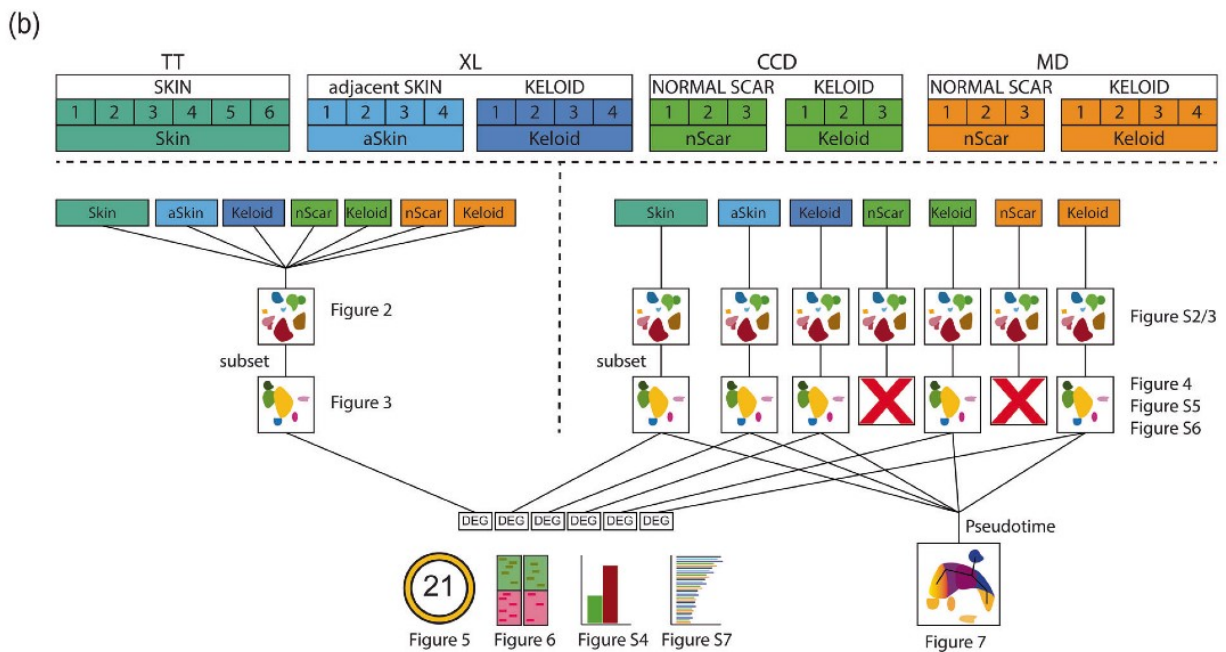
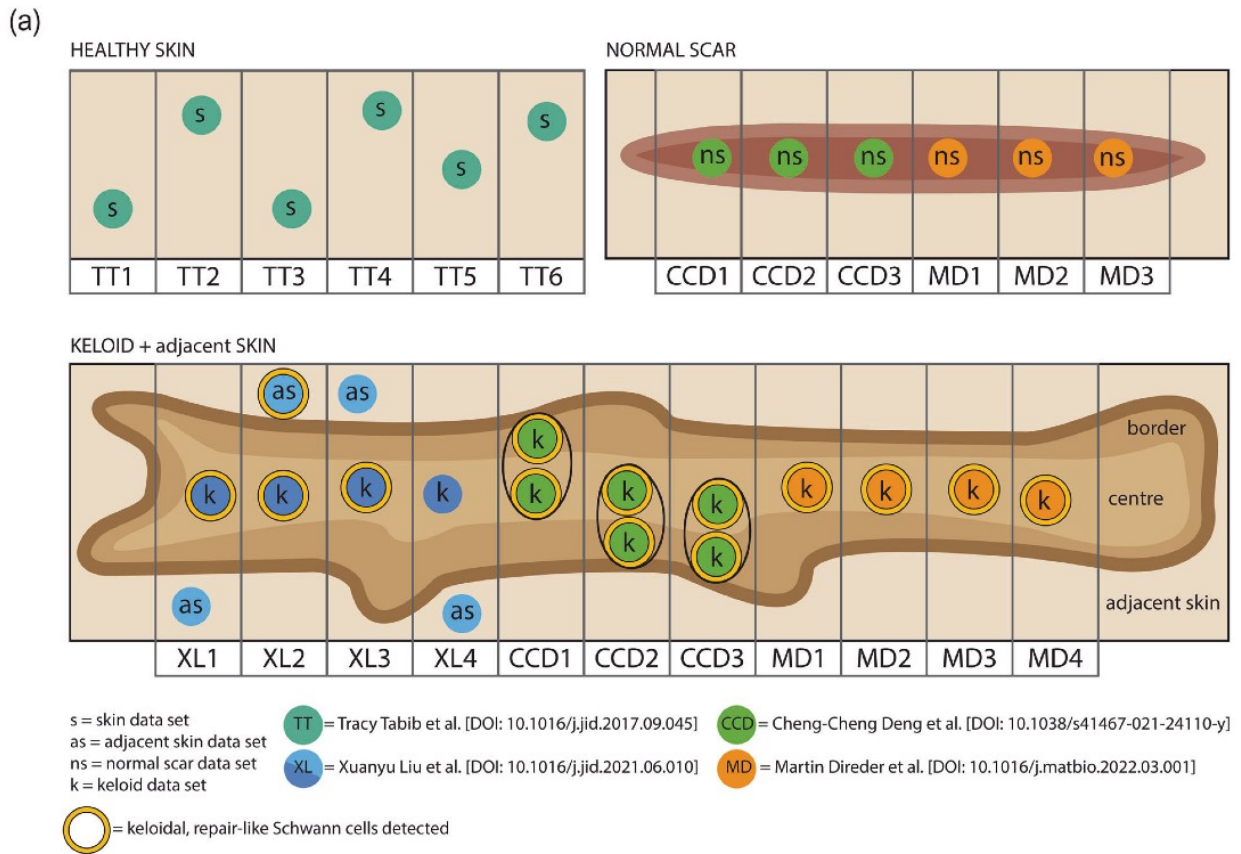


Fig. 1 Graphical scheme of the included datasets and bioinformatics method overview. a Schematic illustration of the regional sampling point of every dataset. b Synoptical chart of all dataset combinations included in this study with links for each respective figure. Skin (s), adjacent skin (as/aSkin), normal scar (ns/nScar), keloid (k); data source: Tracy Tabib et al., 2018 (TT)¹⁸; Xuanyu Liu et al., 2021 (XL)¹⁵; Cheng-Cheng Deng et al., 2021 (CCD)¹⁶; Martin Direder et al., 2022 (MD)¹⁷; DEG differentially expressed gene.

RESULTS

Combined integration of all scRNA-seq datasets identifies significant differences in the cellular composition of normal skin, normal scars, and keloids
 Histological examination of normal skin samples, normal scars and keloids showed increased dermal cell numbers and abnormalities

of the ECM in both types of scars, including increased linearity of collagen bundles (Fig. 2a and Supplementary Fig. 1)³⁵. To determine how cell populations differ among healthy skin, skin adjacent to keloids, normal scars and keloids, we performed a combined integration of individual scRNA-seq datasets¹⁵⁻¹⁸. In total, datasets of six normal skin samples, four skin samples

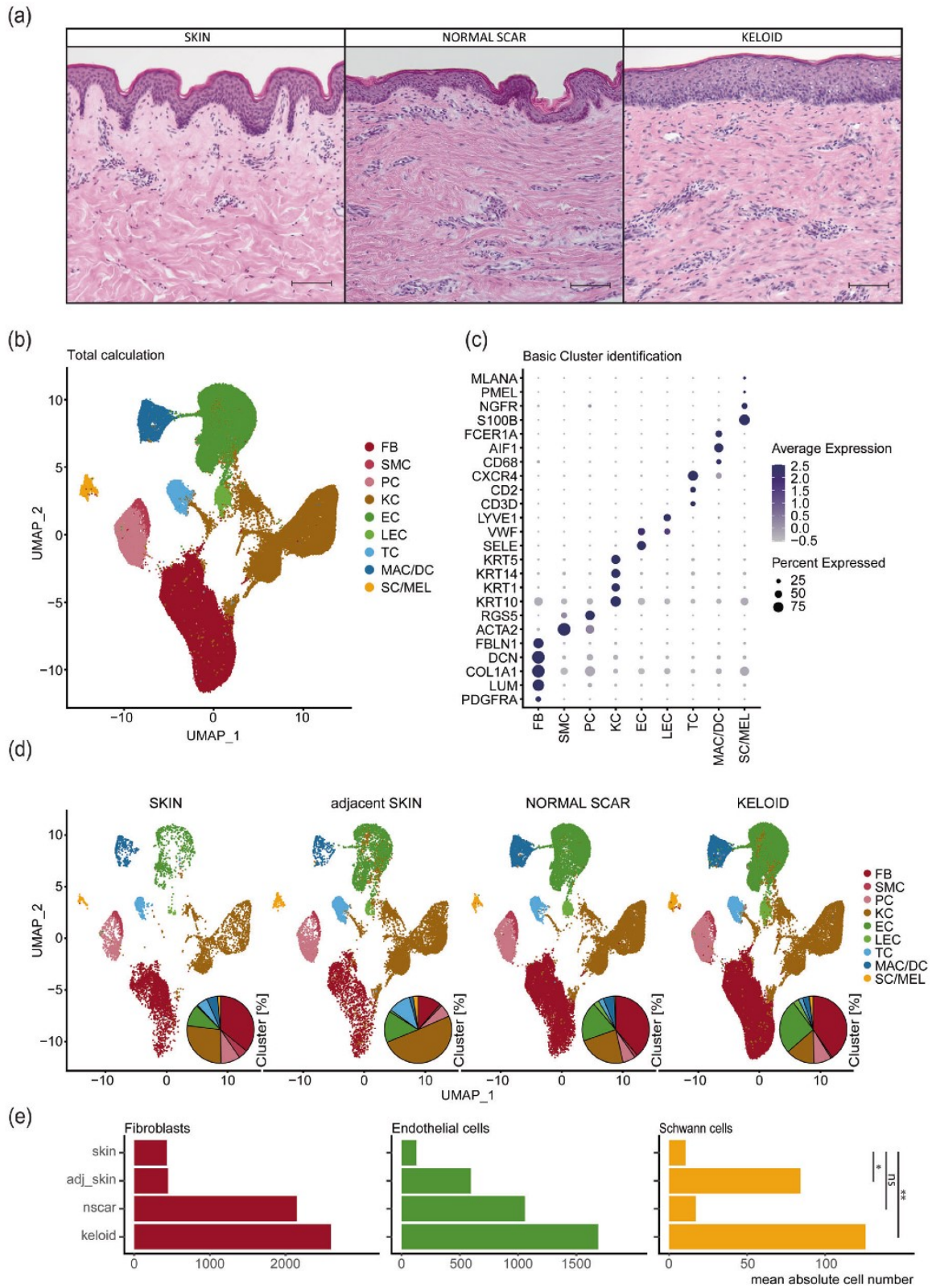


Fig. 2 Cellular composition of skin, normal scars, keloids, and keloid-adjacent skin. a Hematoxylin-eosin staining of skin, normal scar, and keloid. Scale bars: 250 μ m. b UMAP plot after integration of all datasets. Cluster identifications of fibroblasts (FB), smooth muscle cells (SMC), pericytes (PC), keratinocytes (KC), endothelial cells (EC), lymphatic endothelial cells (LEC), T cells (TC), macrophages and dendritic cells (MAC / DC), Schwann cells and melanocytes (SC/MEL). c Dot plots showing well-known marker genes to characterize clusters: PDGFRA, LUM, COL1A1, DCN, FBN1 for FB, ACTA2, RGS5 for SMC and PC, KRT10, KRT1, KRT14, KRT5 for KC, SELE, VWF for EC, LYVE1 for LEC, CD3D, CD2, CXCR4 for TC, CD68, AIF1 for MAC, FCER1A for DC, S100B, NGFR for SC, PMEL, MLANA for MEL; Dot size symbolizes percentage of cells expressing the gene, color gradient represents average gene expression. d Split UMAP plots show the cellular composition within each tissue. Pie plots depict the relative amounts of each cell type within a tissue. e Bar plots depict arithmetic means of the absolute numbers of FB, EC, and SC within each condition. Asterisks represent p-values: * $p < 0.05$, ** $p < 0.01$, *** $p < 0.001$, ns: not significant.

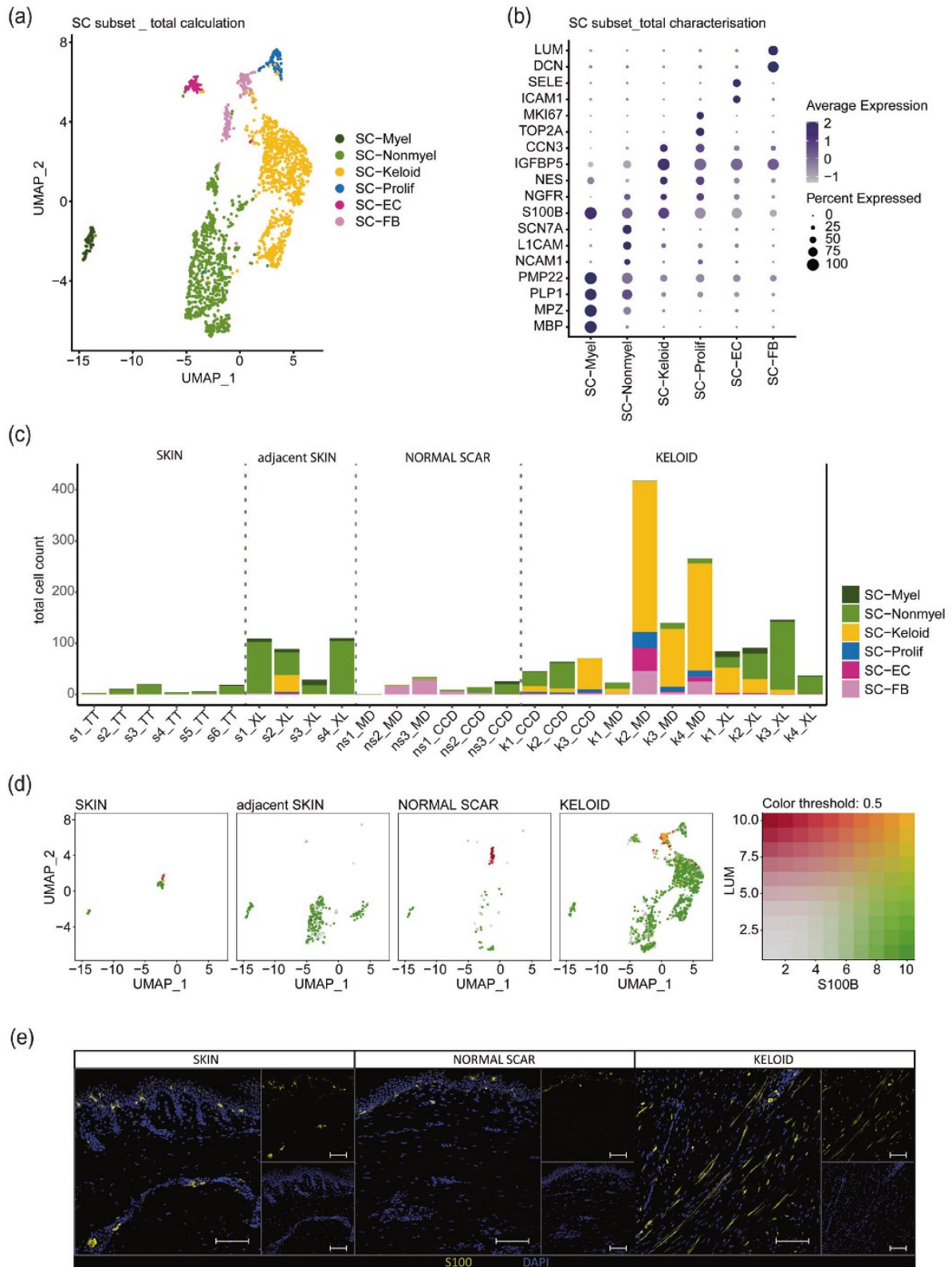
Table 1. Donor information.

Tissue	Source	Paper ID	Original ID	Site	Age	Sex	Race
Normal skin	TT ¹⁸	TT1_s	SC18control	Forearm	63	Male	Caucasian
Normal skin	TT ¹⁸	TT2_s	SC1control	Forearm	54	Male	Caucasian
Normal skin	TT ¹⁸	TT3_s	SC32control	Forearm	66	Female	Caucasian
Normal skin	TT ¹⁸	TT4_s	SC33control	Forearm	23	Female	Asian
Normal skin	TT ¹⁸	TT5_s	SC34control	Forearm	62	Female	Caucasian
Normal skin	TT ¹⁸	TT6_s	SC4control	Forearm	24	Male	Caucasian
Adjacent skin	XL ¹⁵	XL1_s	K007CTRL	Chest	28	Female	Chinese
Adjacent skin	XL ¹⁵	XL2_s	K009CTRL	Chest	32	Female	Chinese
Adjacent skin	XL ¹⁵	XL3_s	K013CTRL	Chest	26	Female	Chinese
Adjacent skin	XL ¹⁵	XL4_s	K012CTRL	Chest	26	Female	Chinese
Normal scar	CCD ¹⁶	CCD1_ns	human_normal_scar_sample1	Back	39	Male	Han nationality
Normal scar	CCD ¹⁶	CCD2_ns	human_normal_scar_sample2	Chest	28	Male	Han nationality
Normal scar	CCD ¹⁶	CCD3_ns	human_normal_scar_sample3	Chest	26	Female	Han nationality
Normal scar	MD ¹⁷	MD1_ns	scar1	Abdomen	26	Female	Caucasian
Normal scar	MD ¹⁷	MD2_ns	scar2	Abdomen	43	Female	Caucasian
Normal scar	MD ¹⁷	MD3_ns	scar3	Abdomen	60	Male	Caucasian
Keloid	XL ¹⁵	XL1_k	K007CASE	Chest	28	Female	Chinese
Keloid	XL ¹⁵	XL2_k	K009CASE	Chest	32	Female	Chinese
Keloid	XL ¹⁵	XL3_k	K013CASE	Chest	26	Female	Chinese
Keloid	XL ¹⁵	XL4_k	K012CASE	Chest	26	Female	Chinese
Keloid	CCD ¹⁶	CCD1_k	human_keloid_sample1	Back	20	Male	Han nationality
Keloid	CCD ¹⁶	CCD2_k	human_keloid_sample2	Chest	23	Male	Han nationality
Keloid	CCD ¹⁶	CCD3_k	human_keloid_sample3	Chest	34	Female	Han nationality
Keloid	MD ¹⁷	MD1_k	keloid_1	Chest	36	Female	Caucasian
Keloid	MD ¹⁷	MD2_k	keloid_2	Earlobe	60	Female	African
Keloid	MD ¹⁷	MD3_k	keloid_3 L	Earlobe—left	34	Male	Caucasian
Keloid	MD ¹⁷	MD4_k	keloid_3R	Earlobe—right	34	Male	Caucasian

adjacent to keloids, six normal scars and eleven keloids were included. Demographic data on the samples and methodological differences in sample preparation are shown in Table 1 and Supplementary Table 7, respectively. Combined bioinformatics analysis of the datasets revealed several main cell clusters (Fig. 2b), which were further characterized by marker gene expression (Fig. 2c). The clusters were identified as fibroblasts (FB), smooth muscle cells (SMC), pericytes (PC), keratinocytes (KC), endothelial cells (EC), lymphatic endothelial cells (LEC), T cells (TC), macrophages (MAC), dendritic cells (DC), Schwann cells (SC) and melanocytes (MEL) (Fig. 2b, c). Interestingly, macrophages and dendritic cells as well as Schwann cells and melanocytes clustered together (Fig. 2b). Split analysis revealed similar cell clusters but different cell numbers in each condition (Fig. 2d). While the cell numbers of fibroblasts and endothelial cells were increased in normal scars and keloids, increased numbers of Schwann cells were only detectable in keloids, indicating a specific role of Schwann cells in the pathogenesis of keloids (Fig. 2e).

Keloidal Schwann cells are conserved in different scRNA-seq datasets

As the main goals of our study were the in-depth analysis of Schwann cells in the different scar types and their comparability across different single-cell datasets, we next recalculated the combined integrated Schwann cell cluster, removed all melanocytes and performed subclustering (Fig. 3). The different Schwann cell subclusters (Fig. 3a) were identified using well-established Schwann cell markers (Fig. 3b)^{17,27}. This analysis identified myelinating Schwann cells (SC-Myel), nonmyelinating Schwann cells (SC-Nonmyel), proliferating Schwann cells (SC-Prolif), Schwann cells additionally expressing genes typical for endothelial cells (SC-EC) or fibroblasts (SC-FB) and the previously described repair-like, profibrotic keloidal Schwann cells (SC-Keloid) (Fig. 3a, b). We next separated each dataset and detected only a few Schwann cells in normal skin (Fig. 3c). In contrast, the number of Schwann cells was markedly increased in keloids (Fig. 3c). Interestingly, we also found an increased number of Schwann



cells in skin adjacent to keloids but not in normal scars (Fig. 3c). Schwann cells of normal skin were identified as either myelinating or nonmyelinating Schwann cells. In contrast, we found a high plasticity of Schwann cells in keloids, with a high number of cells displaying a profibrotic phenotype. These keloidal Schwann cells were also detected in one skin sample adjacent to keloids (Fig. 3c).

Of note, a substantial number of cells in the Schwann cell cluster present in normal scars did not express the Schwann cell marker gene *S100B* but expressed genes typical for fibroblasts, such as *LUM*, suggesting incorrect cluster assignment of some fibroblasts in the combined integration (Fig. 3d, single red dots in normal scar). In contrast, some keloids contained Schwann cells coexpressing

Fig. 3 Schwann cell subset detects pro-fibrotic Schwann cells in datasets from all sources. **a** UMAP plot of the Schwann cell subset (SC subset) after melanocyte removal. **b** Dot plot identifying the Schwann cell subcluster by expression of marker genes: MBP, MPZ, PLP1, PMP22 for myelinating Schwann cells (SC-Myel); NCAM1, L1CAM, SCN7A for nonmyelinating Schwann cells (SC-Nonmyel); S100B, NGFR as general Schwann cell marker; NES, IGFBP5, CCN3 for keloidal Schwann cells (SC-Keloid); TOP2A, MKI67 for proliferating Schwann cells (SC-Prolif), DCN, LUM for cells expressing Schwann cell-specific and fibroblast-specific genes (SC-FB), ICAM1, SELE for cells expressing Schwann cell-specific and endothelial cell-specific genes (SC-EC). **c** Bar plots depicting the absolute number of distinct Schwann cell subtypes within each dataset: skin (s), normal scar (ns), keloid (k); data source: Tracy Tabib et al., 2018 (TT)¹⁸; Xuanyu Liu et al., 2021 (XL)¹⁵; Cheng-Cheng Deng et al., 2021 (CCD)¹⁶; Martin Direder et al., 2021 (MD)¹⁷; **d** Feature blends show the expression of S100B (green), LUM (red) and double expression of both genes (yellow) in the SC subset split by tissue. **e** Immunofluorescence staining of S100-positive SCs in the dermal layer of a keloid; Scale bar: 100 μ m.

fibroblast markers and S100B (Fig. 3d, double positive, yellow dots in keloids). To confirm our transcriptomic data, we performed S100 immunostaining of normal skin, normal scars and keloids (Fig. 3e). As suggested by our scRNA-seq data, we found a markedly increased number of Schwann cells in keloids. These cells were spindle-shaped with long extensions on both ends (Fig. 3e), a morphology previously described for repair Schwann cells^{7,17,36}.

To overcome possible calculation errors of combined integration, we also integrated the datasets of each study individually. In line with our previous calculation approach, we found increased numbers of Schwann cells in keloids (Supplementary Figs. 2 and 3). Interestingly, we were not able to identify a Schwann cell cluster in normal scars by separate integration of the datasets (Supplementary Fig. 2). Therefore, only healthy skin, adjacent skin and the three keloid datasets were included for further analysis. All main clusters and subclusters were calculated using the same R-protocol with corresponding identical parameters. Subset analysis uncovered up to five clusters of Schwann cell subtypes in the individual conditions (Fig. 4a). Similar to the combined calculation, individual integration of each dataset also identified the presence of profibrotic Schwann cells in almost all keloids and in one skin sample adjacent to a keloid (Fig. 4a, b). In contrast to the combined integration, we detected a high number of S100B-negative cells that were lumican-positive in the single integrated skin samples (Fig. 4c, single-positive red dots). Together, our data indicate that profibrotic Schwann cells are robustly detectable in keloids regardless of the calculation method. Problems with incorrectly assigned fibroblasts were found in both calculation methods and mainly affected very small Schwann cell clusters present in normal skin or normal scars (Fig. 4d).

Characterization of a gene-set specific for keloidal, pro-fibrotic Schwann cells

We next analyzed all differentially expressed genes by comparing one Schwann cell cluster with all other Schwann cells within each dataset. More genes were downregulated in the SC-Keloid cluster in keloids than adjacent skin (Supplementary Fig. 4 and Supplementary Tables 1–5). Evaluation of the top differentially expressed genes between profibrotic Schwann cells and myelinating/nonmyelinating Schwann cells revealed a set of 21 genes that were characteristic of profibrotic Schwann cells in keloids (Fig. 5a, b). Comparison of the mean expression values of these genes in the individual datasets confirmed the highly specific expression pattern of keloidal Schwann cells (Fig. 5a). Interestingly, the expression of most of these genes was comparable between some of the keloid-specific Schwann cell clusters (SC-Prolif, SC-EC, and SC-FB) and the profibrotic Schwann cells (SC-Keloid), indicating that although SC-Prolif, SC-EC and SC-FB cluster separately and show some additional characteristics, they also share most of the features of keloidal profibrotic Schwann cells (Supplementary Fig. 5). In our previous work, we discovered a contribution of Schwann cells to ECM formation in keloids¹⁷. We therefore analyzed the expression of matrix proteins in all Schwann cells of the different datasets and found that most collagen genes were significantly increased in keloidal Schwann cells in all datasets (Supplementary Fig. 6). Furthermore, GO-term analysis of keloidal Schwann cells in all datasets confirmed a strong association of these cells with ECM

organization and wound healing (Supplementary Fig. 7). Interestingly, some collagens and other factors of the ECM were also found among the SC-Keloid-specific genes (Fig. 5b). Together with the previously shown NES protein expression¹⁷, we further confirmed ELN, IGFBP5 and CCN3 protein expression in keloidal Schwann cells (Fig. 5c–e).

Keloidal Schwann cells show similarities with repair Schwann cells in damaged peripheral nerves. Bosse et al. were the first to describe a specific panel of genes regulated in nerve-associated cells upon damage to peripheral nerves⁵. This set of genes was associated with the formation of repair Schwann cells and their function to promote regeneration of the peripheral nerve³⁶. To investigate similarities of repair Schwann cells, present in the injured nerve, and keloidal Schwann cells, we compared the gene list of Bosse et al. with our dataset and detected 40 genes that were similarly regulated in both datasets (Fig. 6). For example, ACTB, GPC1, MYH9, S100A4, TGFBI, ATP1A2, MAL, MPZ, NFKBIA, PLLP, PLP1, and SCN7A showed comparable regulation (Fig. 6a and Supplementary Table 8). GO-term analysis of the corresponding regulated genes revealed a typical regulation of cellular processes associated with repair Schwann cells, including regulation of cell adhesion and division, generation of precursor metabolites and energy and down-regulation of myelination (Fig. 6b, c). These data suggest that a part of the repair Schwann cell gene-set identified by Bosse et al. is conserved in keloidal Schwann cells.

Pseudotime trajectory analysis identifies candidate factors decisive for keloidal, pro-fibrotic Schwann cell development. To further identify novel signaling molecules involved in the development of keloidal profibrotic Schwann cells, we performed pseudotime trajectory analysis. Therefore, we reintegrated all individually identified Schwann cell clusters from each study (Fig. 7a). A UMAP, colored by the previously defined Schwann cell subtypes, showed a clear demarcation of the different Schwann cell populations (Fig. 7b). Pseudotime trajectory calculation suggested that myelinating and nonmyelinating Schwann cells dedifferentiate toward one common branching point and then further into profibrotic Schwann cells (Fig. 7c). Since JUN, STAT3, ARTN, BDNF, GDNF, SHH, and OLIG1 are known decisive factors for the development of repair Schwann cells upon neural damage⁴, we next plotted their expression on the pseudotime trajectory. The transcription factors JUN and STAT3 were highly expressed, specifically in cells at the branching point, confirming their role in the dedifferentiation process of repair Schwann cells (Fig. 7d, e). Of note, other described factors involved in the repair of Schwann cell development in peripheral nerves (ARTN, BDNF, GDNF, SHH, OLIG1 and IGFBP2) were not or only weakly expressed in keloidal Schwann cells (Supplementary Fig. 8a). In addition, our analysis identified several specific groups of transcription factors significantly enriched at the branching point, such as members of the AP-1 family (Fig. 7f and Supplementary Fig. 8b), Kruppel-like factors (KLF) (Fig. 7g and Supplementary Fig. 8c) and immediate early response genes (IER) (Supplementary Fig. 8d), as well as some other transcription factors (EGR1, ATF3, HES1, ZFP36) (Fig. 7h

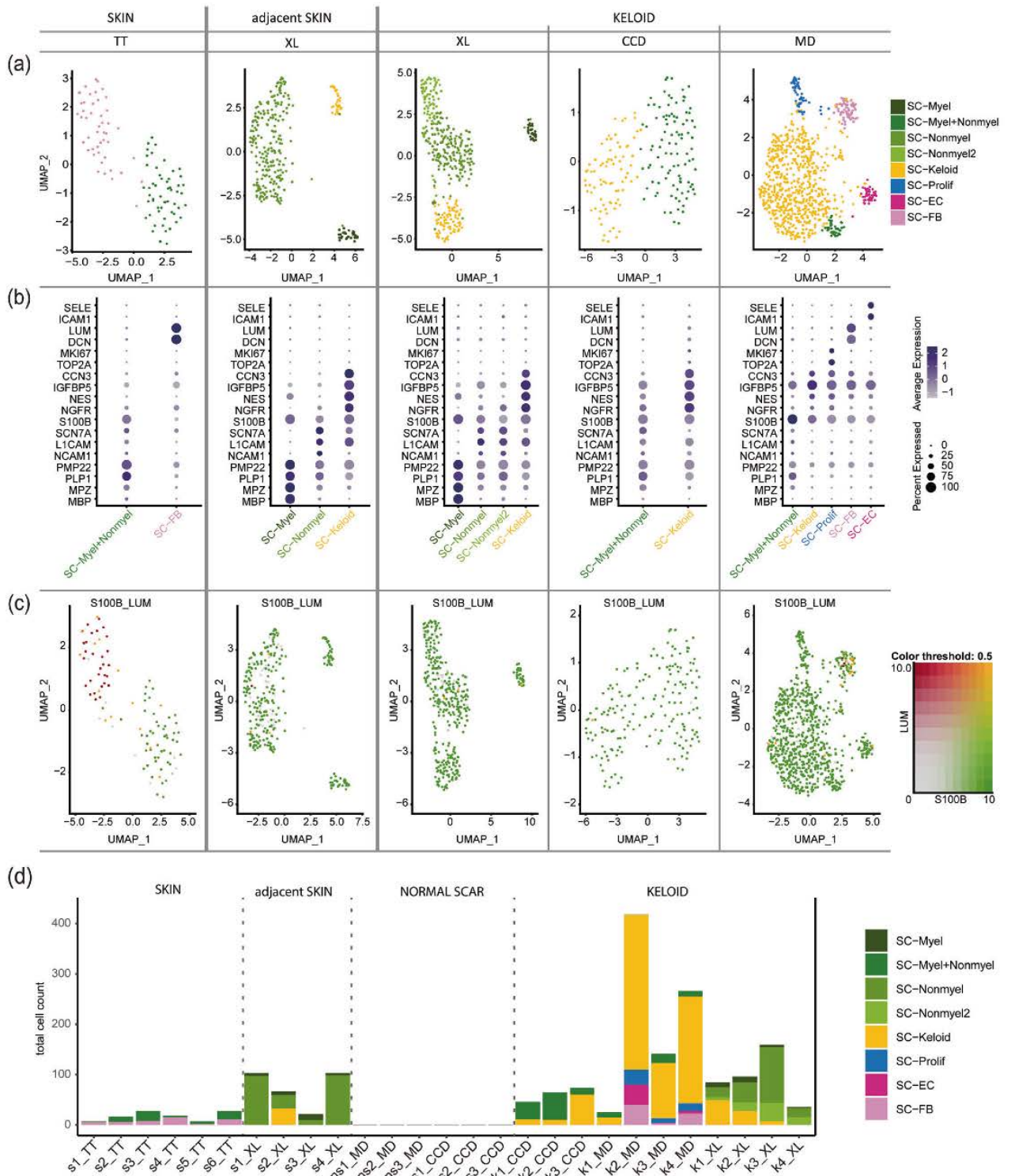
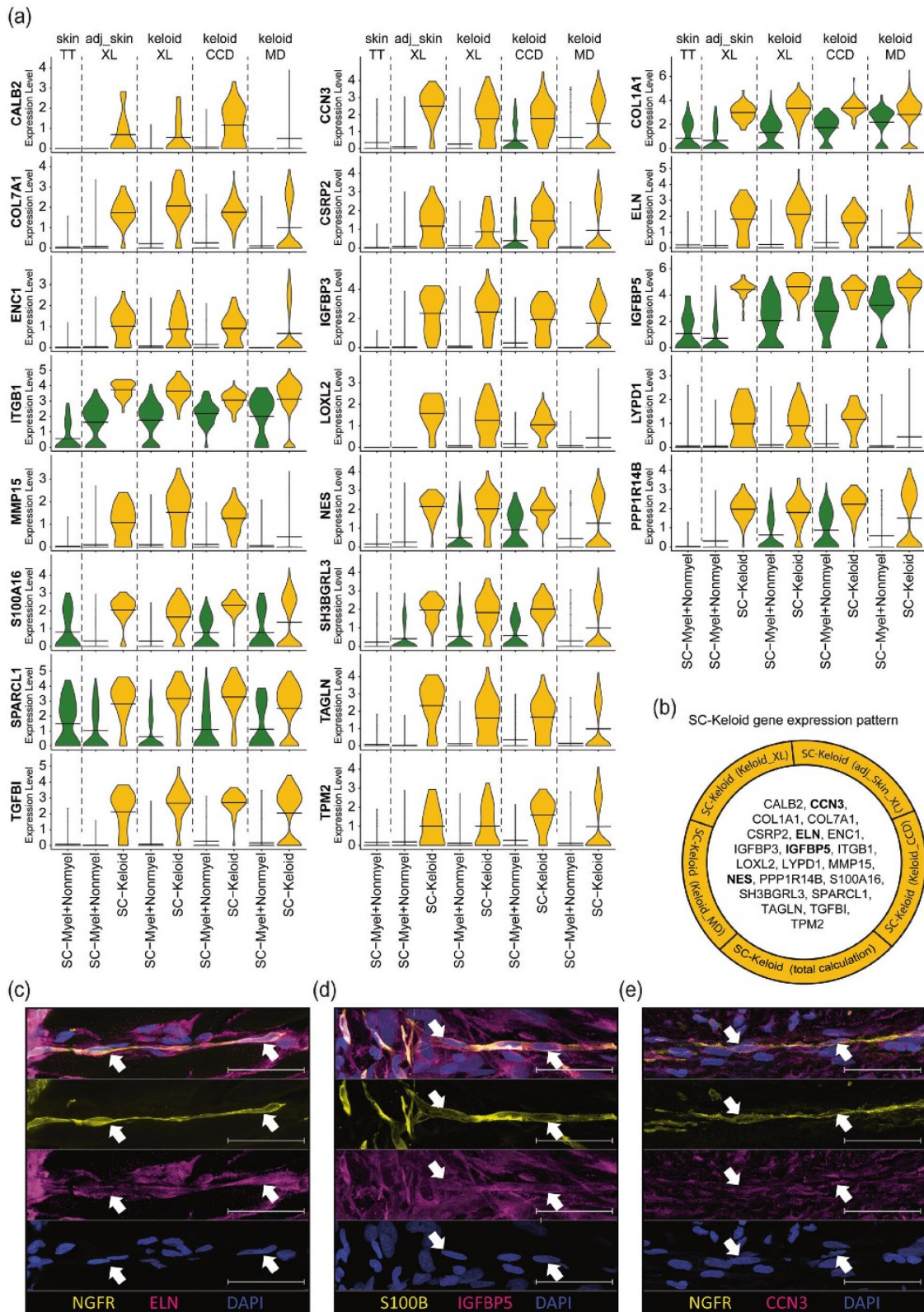


Fig. 4 Tissue- and source-specific dataset evaluation confirms keloidal profibrotic Schwann cells. **a** UMAP plots depict subsets of identified Schwann cell clusters. Data sources: Tracy Tabib et al., 2018 (TT)¹⁸; Xuanyu Liu et al., 2021 (XL)¹⁵; Cheng-Cheng Deng et al., 2021 (CCD)¹⁶; Martin Direder et al., 2021 (MD)¹⁷; **b** Dot plots of well-known marker genes to characterize Schwann cell subtypes. MBP, MPZ, PLP1, and PMP22 for myelinating Schwann cells (SC-Myel); NCAM1, L1CAM, and SCN7A for nonmyelinating Schwann cells (SC-Nonmyel, SC-Nonmyel2); S100B and NGFR as general Schwann cell markers; NES, IGFBP5, CCN3 for keloidal Schwann cells (SC-Keloid); TOP2A and MKI67 for proliferating Schwann cells (SC-Prolif); DCN and LUM for cells expressing Schwann cell and fibroblast-specific genes (SC-FB); ICAM1 and SELE for cells expressing Schwann cell and endothelial cell-specific genes (SC-EC); mixed myelinating and nonmyelinating Schwann cell cluster (SC-Myel + Nonmyel); Color codes indicate average gene expression levels; Dot sizes visualize relative amounts of positive cells. **c** Feature blends reveal cells positive for S100B (green) and LUM (red) and double-positive cells (yellow). **d** Bar plots show the absolute cell count of distinct Schwann cell clusters in each included dataset. skin (s), normal scar (ns), keloid (k); data source: Tracy Tabib et al., 2018 (TT)¹⁸; Xuanyu Liu et al., 2021 (XL)¹⁵; Cheng-Cheng Deng et al., 2021 (CCD)¹⁶; Martin Direder et al., 2021 (MD)¹⁷.



and Supplementary Fig. 8e), suggesting an involvement in keloidal repair-like, profibrotic Schwann cell development. Immunofluorescence staining confirmed the presence of nuclear JUN, STAT3, JUNB, KLF4 and EGR1 proteins in NGFR⁺ keloidal Schwann cells in situ (Fig. 7i–m).

To investigate cell–cell communication processes possibly involved in the dedifferentiation process of keloidal Schwann cells, we next performed CellChat analysis. Therefore, we calculated interactions between Schwann cells located at the branching point and all other cell types present in the tissue

Fig. 5 Individual dataset combinations reveal the gene expression pattern of keloidal profibrotic Schwann cells. a Violin plots of corresponding, meaningful genes detected in all individual top 100 gene lists comparing keloidal Schwann cells (SC-Keloid) with mature Schwann cells (myelinating and nonmyelinating Schwann cells). Data sources: Tracy Tabib et al., 2018 (TT)¹⁸; Xuanyu Liu et al., 2021 (XL)¹⁵; Cheng-Cheng Deng et al., 2021 (CCD)¹⁶; Martin Direder et al., 2021 (MD)¹⁷; adjacent skin (adj_skin); Crossbeams show mean expression values; maximum expression is depicted by vertical lines; frequency of cells with the respective expression level is shown by violin width; myelinating Schwann cells (SC-Myel); nonmyelinating Schwann cells (SC-Nonmyel, SC-Nonmyel2), myelination and nonmyelinating Schwann cell mixed cluster (SC-Myel + Nonmyel); keloidal Schwann cells (SC-Keloid); proliferating Schwann cells (SC-Prolif), cells expressing Schwann cell and endothelial cell-specific genes (SC-EC); cells expressing Schwann cell and fibroblast-specific genes (SC-FB). b List of all members from the SC-Keloid gene expression pattern. mRNAs in bold have been verified at the protein level. c–e Immunofluorescence staining of keloidal Schwann cells visualized by S100B or NGFR (yellow) in combination with ELN, IGFBP5 or CCN3. Arrowheads indicate double-positive Schwann cells. Nuclei were stained with DAPI (blue). Scale bars: 50 μ m.

(Supplementary Fig. 9a). Our analysis revealed a strong impact of fibroblasts on keloidal Schwann cells, suggesting the involvement of fibroblasts in the dedifferentiation process (Supplementary Fig. 9b). Furthermore, keratinocytes and smooth muscle cells/pericytes seemed to be influenced by keloidal Schwann cells (Supplementary Fig. 9b). Interestingly, such strong cell–cell interactions were not observed in healthy skin (Supplementary Fig. 10a–d). More detailed analysis of these cell–cell interactions in keloids mainly identified interactions with components of the ECM, including collagens and laminin subunits (Supplementary Fig. 9c). Similar cell–cell interactions were observed between the different subsets of keloidal Schwann cells and all other cell types present in keloids (Supplementary Fig. 11a–f). Together, these data suggest that the keloidal microenvironment contributes to the formation of keloidal repair Schwann cells.

DISCUSSION

Recently, we identified an important role of Schwann cells in the pathogenesis of keloids¹⁷. Using scRNA-seq, we were able to demonstrate that a high number of Schwann cells are present in keloids and that these cells significantly contribute to the overproduction of the extracellular matrix¹⁷. Interestingly, these Schwann cells were not associated with axons and showed a nonclassical repair-like phenotype. However, their exact transcriptional profile and marker genes unambiguously determining this keloidal Schwann cell type have not yet been described. Although scRNA-seq represents a powerful tool for studying gene expression in organs and tissues at a single-cell resolution, the comparability of different scRNA-seq datasets and generation of reproducible data are still challenging. Donor variabilities, differences in the tissue dissociation procedure and differences in bioinformatics processing of the data are the main reasons for heterogeneous results^{37–39}. Such methodological differences could significantly affect absolute cell numbers and gene expression patterns. As Schwann cell numbers are already strongly dependent on the body site⁴⁰ and certain diseases further influence the number and expression profile of Schwann cells in the skin^{17,41}, a combined evaluation of several datasets was essential to decipher the transcriptional profile of the newly identified keloidal Schwann cell type.

To date, several studies have underlined the impact of the tissue dissociation procedure on gene expression^{37–39}. The commercially available whole-skin dissociation kit is the most commonly used skin dissociation method for scRNA-seq experiments^{22,42} and was used in 3 of the 4 studies analyzed (Supplementary Table 7). In only one study, keloids were digested with dispase II and collagenase IV for two hours. Interestingly, this dataset contained significantly fewer Schwann cells, suggesting that the use of the whole-skin dissociation kit yields more reliable data representing all cell types present in the tissue of interest. In the other three studies, the tissue was digested for different time periods. Of note, keloid samples generated by an overnight dissociation step showed significantly more myelinating Schwann cells compared to the studies using a shorter dissociation time (up

to 2.5 h), indicating that the dissociation of Schwann cells attached to axons is difficult and can be improved by a longer digestion period. This finding is in line with established isolation methods of Schwann cells from human peripheral nerves that include an overnight dissociation step^{3,43}. Furthermore, in a recent publication describing a method for the isolation of Schwann cells from healthy skin, the authors discussed preculturing steps to disintegrate the nerve for more efficient Schwann cell isolation⁴⁴. Nevertheless, given the high plasticity of Schwann cells² and unwanted effects of long-lasting isolation protocols on the transcriptome, short-term isolation protocols are preferable. In contrast to myelinating and nonmyelinating Schwann cells, we found considerable numbers of keloidal profibrotic Schwann cells in all datasets, indicating that Schwann cells that are not associated with an axon can be easily isolated from the tissue.

To compare the phenotype of keloidal Schwann cells with those of normal scars, we also included scRNA-seq data from normal scars in our analyses. Interestingly, only after a comprehensive computation of all datasets together we were able to identify a few Schwann cells in normal scars. The lack of Schwann cells in normal scars is in line with a recent publication reporting an important role of Schwann cells during wound healing in mice⁵. Parfejevs et al. showed that murine Schwann cells dedifferentiate and re-enter the cell cycle after wounding and promote wound healing by releasing paracrine factors, thereby inducing myfibroblast differentiation⁵. Importantly, these Schwann cells completely disappeared from the wounded area after successful completion of wound healing⁴⁵. Whether these Schwann cells convert into other cells, such as fibroblasts, or migrate back to an axon remains to be elucidated. The low numbers of Schwann cells detected in normal human scars suggest that such a mechanism might also be apparent in human wound healing and that the development of keloids might be associated with defects in removing these Schwann cells after wound healing. However, further studies are necessary to fully elucidate the impact of Schwann cells on human wound healing.

The adjacent skin around keloids has been reported to exhibit features typical of keloids¹⁴. Strikingly, our bioinformatics analysis also uncovered keloidal profibrotic Schwann cells in one dataset of keloid-adjacent skin. This finding supports our assumption that the persistence of keloidal Schwann cells in the dermis contributes to disease progression. Two scenarios by which these Schwann cells might affect keloid progression appear reasonable. First, keloidal Schwann cells spread into the surrounding healthy skin, generating a milieu that favors the growth of keloids. Second, the continuously growing keloids might affect nerves in the surrounding healthy skin and trigger dedifferentiation of Schwann cells, which in turn further contributes to ECM overproduction, as reported previously¹⁷. Our transcriptomic data and bioinformatics analyses have built a good basis for further studies addressing these open questions in more sophisticated *in vivo* studies.

Injury of peripheral nerves causes dedifferentiation of both types of mature Schwann cells (myelinating and nonmyelinating) into repair Schwann cells^{46–48}. Our pseudotime trajectory calculations suggest that myelinating and nonmyelinating Schwann cells

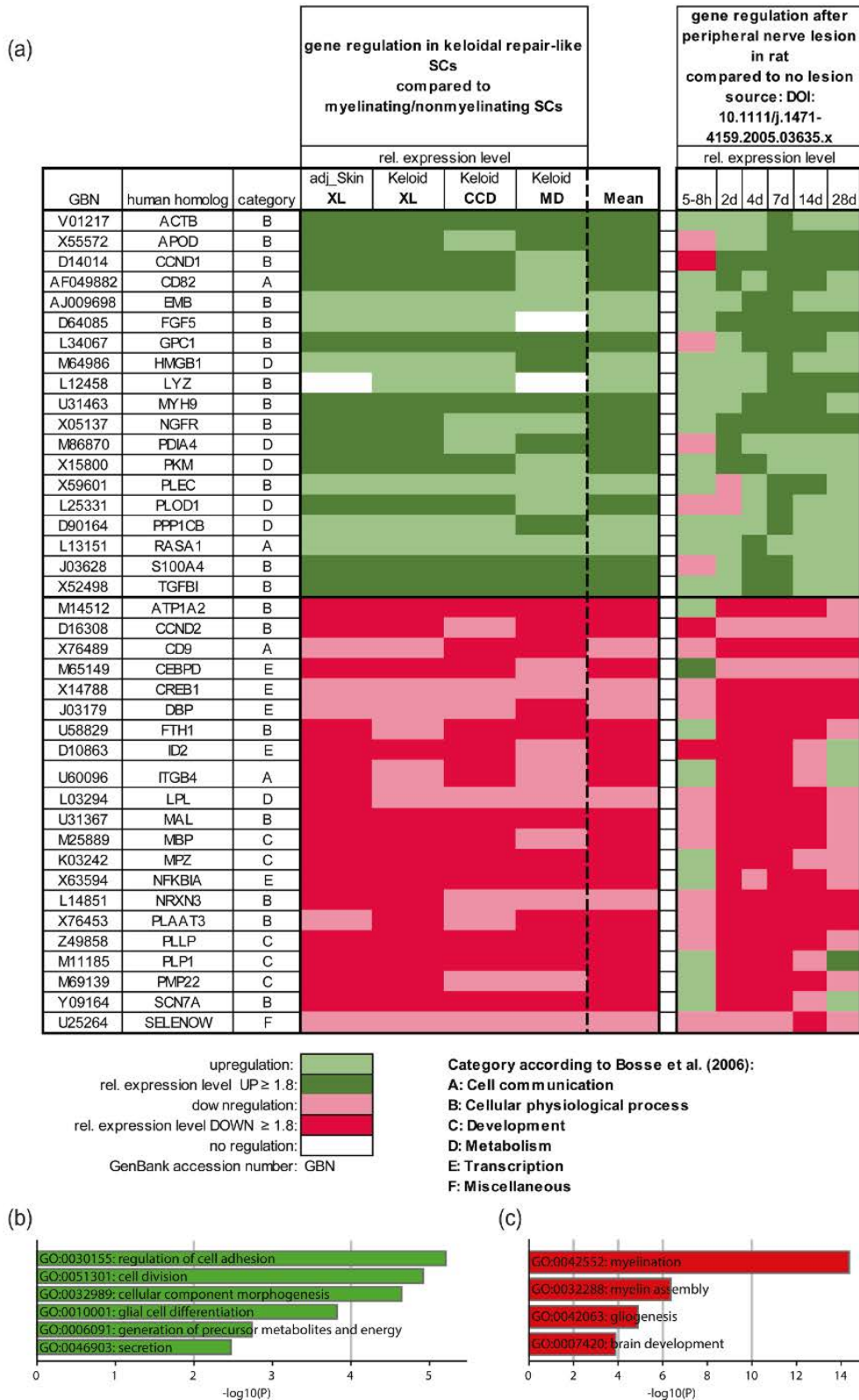


Fig. 6 Gene regulation of keloidal Schwann cells partially matches gene regulation upon neural damage. a Heatmap of genetic conformities between keloidal Schwann cells and activated nerve-associated cells upon neuronal damage. Genes were sorted alphabetically and categorized according to the source list of Bosse et al. (2006)³. GO-term enrichment of the corresponding b up- and c downregulated genes. The bar length depicts the statistical significance of the annotated term.

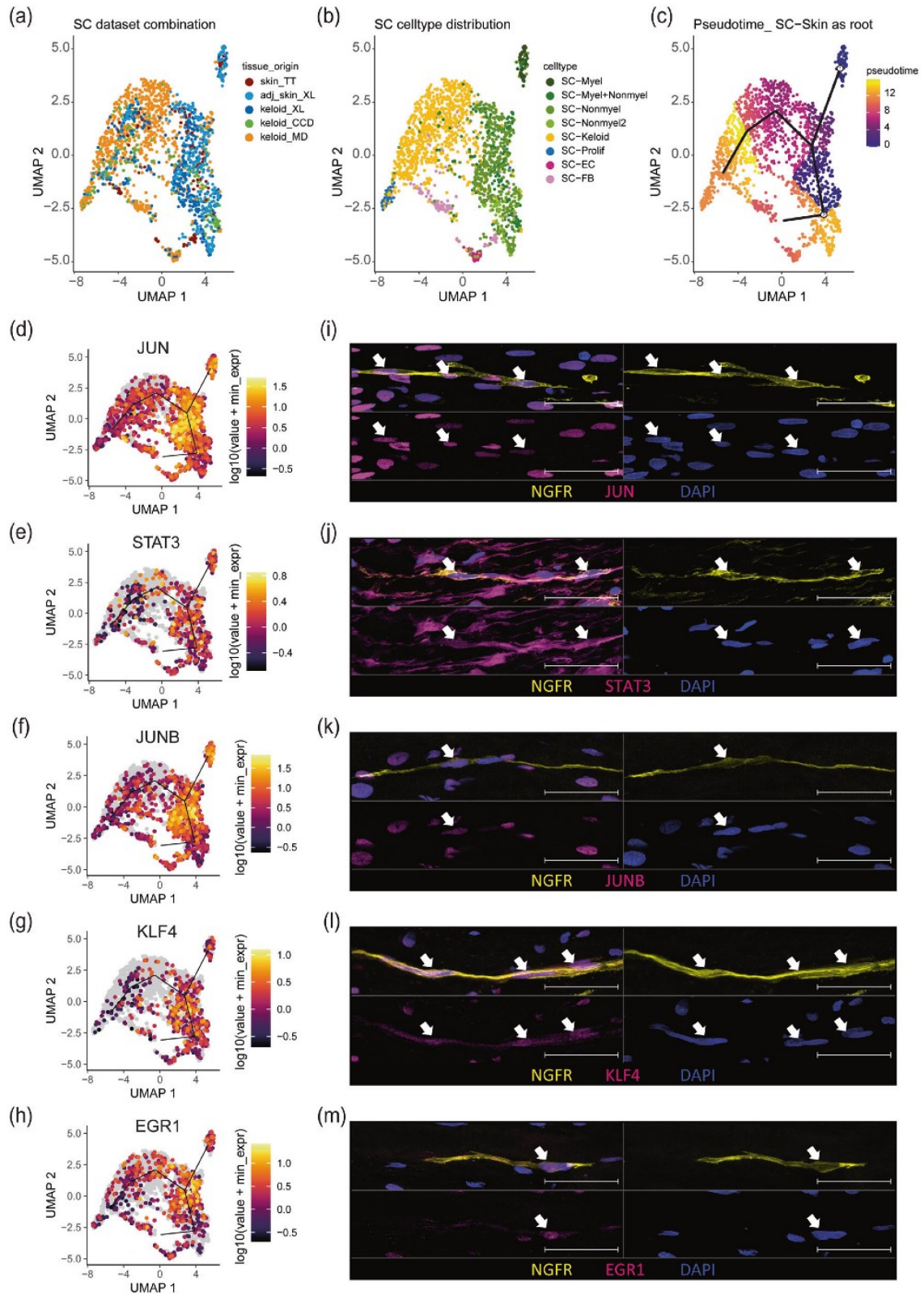


Fig. 7 Pseudotime analysis uncovers pivotal genes in the dedifferentiation track of Schwann cells. UMAP plots combining Schwann cells detected in all individual computations colored by tissue source (a) and cell type (b) and pseudotime trajectory with principal graph (c, myelinating and nonmyelinating Schwann cell as root). d–h Feature plots of JUN, STAT3, JUNB, KLF4, and EGR1. i–m Immunofluorescence staining of keloidal Schwann cells visualized by NGFR in combination with JUN, STAT3, JUNB, KLF4, or EGR1. Nuclei were stained with DAPI (blue). Arrowheads indicate double-positive Schwann cells. Scale bars: 50 μm .

of the skin dedifferentiate into profibrotic, repair-like Schwann cells in keloids. Interestingly, many of the marker genes specifically expressed by bona fide repair Schwann cells (STAT3, ARTN, BDNF, GDNF, SHH, OLIG1 and IGFBP2) were not or only weakly detected in keloidal Schwann cells. However, c-Jun, a key factor for guiding dedifferentiation and enabling proper function of repair Schwann cells^{4,47,49–52}, was also strongly expressed in keloidal Schwann cells, especially at the branching point of the pseudotime trajectory. However, in fully dedifferentiated keloidal Schwann cells, c-Jun expression levels were again decreased. Interestingly, our analyses revealed that several other transcription factors, including other AP-1 members (JUNB, JUND, FOS, FOSB, members of the Kruppel-like factor family (KLF2, KLF4, KLF6, KLF10) and members of the immediate early response gene family (IRE2, IRE3, IER5, IER5L), were similarly regulated, suggesting that these transcription factors might also play an important role in the dedifferentiation process of skin Schwann cells. Whereas the function of most of these factors in Schwann cells needs further in-depth investigation, several members of the KLF family have already been reported to be crucial for Schwann cell differentiation^{53–57}. In particular, the high expression of KLF4 suggests that keloidal Schwann cells indeed underwent a dedifferentiation process. The reason for the lack of bona fide repair Schwann cell markers in keloidal Schwann cells is currently not known. As c-Jun is the major regulator of most of these marker genes⁴, its downregulation might be responsible for this observation. Although c-Jun activation is important for the induction of repair Schwann cell development after neural damage, chronic denervation was shown to strongly reduce c-Jun levels in Schwann cells⁴. We therefore hypothesize that due to the prolonged axon-free occurrence of Schwann cells in keloids, their expression pattern changes significantly. Whether these keloidal Schwann cells, despite the loss of expression of several repair marker genes, still represent functional repair Schwann cells has to be determined in future experiments. However, the comparison of our dataset with a dataset of an acute nerve lesion⁵ revealed that a high number of genes characteristic of repair Schwann cells were similarly regulated in both Schwann cell types, suggesting that at least some parts of the repair Schwann cell function are still conserved in keloidal Schwann cells.

Our cell–cell interaction analysis suggests the involvement of fibroblasts in the conversion of myelinated and nonmyelinated Schwann cells into keloid-specific profibrotic Schwann cells, as a high communication probability has been detected for collagen-integrin and midkine-integrin interactions. Interestingly, these receptor–ligand interactions have already been reported to be involved in cellular development, reprogramming, survival and proliferation, which is consistent with our analysis^{8,59}. Furthermore, our analyses suggest that keloidal Schwann cells affect keratinocytes and smooth muscle cells/pericytes, especially by PTN–NCL interactions. Such interactions have been previously shown to be involved in tumorigenesis and cell migration, suggesting their involvement in the tumor-like growth of keloids⁶⁰. Intriguingly, only minor interactions of Schwann cells with macrophages were detected in our analysis. This result is in stark contrast to our previous findings, where we described an important crosstalk of keloidal Schwann cells and macrophages, thereby contributing to the infinite growth of keloids¹⁷. As bioinformatics analyses always entail a certain risk of overlooking or overinterpreting biologic processes, further studies are needed to fully understand the whole communication network of Schwann cells in keloids and their contribution to keloid formation or progression.

As we have previously shown that keloidal Schwann cells significantly contribute to ECM formation¹⁷, it is conceivable that keloidal Schwann cells acquire profibrotic properties. This hypothesis is supported by the identified gene-set that contains several profibrotic genes (COL1A1, COL7A1, ELN, IGFBP3, IGFBP5, ITGB1, LOXL2, MMP15, S100A16, SPARCL1, TAGLN, TGFBI, TPM2) the

identification of this specific gene-set enables further investigations of the contribution of Schwann cells to fibrosis in other fibrotic disorders, such as liver cirrhosis, idiopathic pulmonary fibrosis or renal fibrosis. Considering the current literature and our new data, we hypothesize that there are at least two types of repair(-like) Schwann cells. One type occurs temporarily after acute injury to functionally regenerate a disrupted nerve, and another type persists after complete tissue regeneration in keloids for a long time period, thereby acquiring profibrotic properties^{4,6}. Why this Schwann cell type is not removed after wound healing is currently not known and matter of ongoing experiments.

In conclusion, we confirmed the presence of a repair-like, profibrotic Schwann cell type in keloids from three independent scRNA-seq datasets and identified a conserved expression pattern of twenty-one genes that specifically characterizes this Schwann cell type. This special repair-like, profibrotic Schwann cell type present in keloids exhibits distinct genetic differences compared to classical repair Schwann cells but presumably arises from a common initial injury event. Our study has built the foundation for further studies to investigate the frequency of these cells and the contribution to fibrotic processes in other organs. With respect to the described bioinformatics analyses, our study provides a practical strategy to reliably analyze even small cell clusters and obviate incorrect cluster assignment.

DATA AVAILABILITY

All scRNA-seq data are publicly accessible in NCBI's Gene Expression Omnibus (GSE181316, GSE163973), at the Genome Sequencing Archive (BioProject PRJCA003143) and under the following links: https://dom.pitt.edu/wp-content/uploads/2018/10/Skin_6Control_rawUMI.zip https://dom.pitt.edu/wp-content/uploads/2018/10/Skin_6Control_Metadata.zip The source codes for generating the data are accessible under the following link: https://github.com/Mwielscher/scRNAseq/tree/main/keloidal_Schwann

REFERENCES

- Bhatheja, K. & Field, J. Schwann cells: origins and role in axonal maintenance and regeneration. *Int. J. Biochem. Cell Biol.* 38, 1995–1999 (2006).
- Jessen, K. R., Mirsky, R. & Arthur-Farraj, P. The role of cell plasticity in tissue repair: adaptive cellular reprogramming. *Dev. Cell.* 34, 613–620 (2015).
- Weiss, T. et al. Proteomics and transcriptomics of peripheral nerve tissue and cells unravel new aspects of the human Schwann cell repair phenotype. *Glia* 64, 2133–2153 (2016).
- Jessen, K. R. & Mirsky, R. The success and failure of the schwann cell response to nerve injury. *Front. Cell. Neurosci.* 13, 33 (2019).
- Bosse, F., Hasenpusch-Theil, K., Kürty, P. & Müller, H. W. Gene expression profiling reveals that peripheral nerve regeneration is a consequence of both novel injury-dependent and reactivated developmental processes. *J. Neurochem.* 96, 1441–1457 (2006).
- Parfejevs, V. et al. Injury-activated glial cells promote wound healing of the adult skin in mice. *Nat. Commun.* 9, 236 (2018).
- Gomez-Sanchez, J. A. et al. After nerve injury, lineage tracing shows that myelin and remak schwann cells elongate extensively and branch to form repair schwann cells, which shorten radically on remyelination. *J. Neurosci.* 37, 9086–9099 (2017).
- Murray, J. C. Keloids and hypertrophic scars. *Clin. Dermatol.* 12, 27–37 (1994).
- Ud-Din, S. & Bayat, A. New insights on keloids, hypertrophic scars, and striae. *Dermatol. Clin.* 32, 193–209 (2014).
- Balci, D. D., Inandi, T., Dogramaci, C. A. & Celik, E. DLQI scores in patients with keloids and hypertrophic scars: a prospective case control study. *J. Dtsch. Dermatol. Ges.* 7, 688–692 (2009).
- Alhady, S. M. & Sivanantharajah, K. Keloids in various races. A review of 175 cases. *Plast. Reconstr. Surg.* 44, 564–566 (1969).
- Tuan, T. L. & Nichter, L. S. The molecular basis of keloid and hypertrophic scar formation. *Mol. Med. Today* 4, 19–24 (1998).
- Yang, G. P., Lim, I. J., Phan, T. T., Lorenz, H. P. & Longaker, M. T. From scarless fetal wounds to keloids: molecular studies in wound healing. *Wound Repair Regen.* 11, 411–418 (2003).
- Limandjaja, G. C., Niessen, F. B., Scheper, R. J. & Gibbs, S. The keloid disorder: heterogeneity, histopathology, mechanisms and models. *Front. Cell. Dev. Biol.* 8, 360 (2020).

15. Liu, X. et al. Single-cell RNA-seq reveals lineage-specific regulatory changes of fibroblasts and vascular endothelial cells in keloids. *J. Invest. Dermatol.* **142**, 124–135.e11 (2021).
16. Deng, C. C. et al. Single-cell RNA-seq reveals fibroblast heterogeneity and increased mesenchymal fibroblasts in human fibrotic skin diseases. *Nat. Commun.* **12**, 3709 (2021).
17. Direder, M. et al. Schwann cells contribute to keloid formation. *Matrix Biol.* **108**, 55–76 (2022).
18. Tabib, T., Morse, C., Wang, T., Chen, W. & Lafyatis, R. SFRP2/DPP4 and FMO1/LSP1 define major fibroblast populations in human skin. *J. Invest. Dermatol.* **138**, 802–810 (2018).
19. Vorstandlechner, V. et al. Deciphering the functional heterogeneity of skin fibroblasts using single-cell RNA sequencing. *Faseb J.* **34**, 3677–3692 (2020).
20. Solé-Boldo, L. et al. Single-cell transcriptomes of the human skin reveal age-related loss of fibroblast priming. *Commun. Biol.* **3**, 188 (2020).
21. He, H. et al. Single-cell transcriptome analysis of human skin identifies novel fibroblast subpopulation and enrichment of immune subsets in atopic dermatitis. *J. Allergy Clin. Immunol.* **145**, 1615–1628 (2020).
22. Ascensión, A. M., Fuertes-Álvarez, S., Ibañez-Solé, O., Izeta, A. & Araúzo-Bravo, M. J. Human dermal fibroblast subpopulations are conserved across single-cell RNA sequencing studies. *J. Invest. Dermatol.* **141**, 1735–1744.e1735 (2021).
23. Zheng, G. X. Y. et al. Massively parallel digital transcriptional profiling of single cells. *Nat. Commun.* **8**, 14049 (2017).
24. Hao, Y. et al. Integrated analysis of multimodal single-cell data. *Cell* **184**, 3573–3587.e29 (2021).
25. Ahlmann-Eltze, C. & Huber, W. glmGamPoi: fitting Gamma-Poisson generalized linear models on single cell count data. *Bioinformatics* **36**, 5701–5702 (2021).
26. Hafemeister, C. & Satija, R. Normalization and variance stabilization of single-cell RNA-seq data using regularized negative binomial regression. *Genome Biol.* **20**, 296 (2019).
27. Bargagna-Mohan, P. et al. Corneal nonmyelinating Schwann cells illuminated by single-cell transcriptomics and visualized by protein biomarkers. *J. Neurosci. Res.* **99**, 731–749 (2021).
28. Zhou, Y. et al. Metascape provides a biologist-oriented resource for the analysis of systems-level datasets. *Nat. Commun.* **10**, 1523 (2019).
29. Trapnell, C. et al. The dynamics and regulators of cell fate decisions are revealed by pseudotemporal ordering of single cells. *Nat. Biotechnol.* **32**, 381–386 (2014).
30. Qiu, X. et al. Reversed graph embedding resolves complex single-cell trajectories. *Nat. Methods* **14**, 979–982 (2017).
31. Cao, J. et al. The single-cell transcriptional landscape of mammalian organogenesis. *Nature* **566**, 496–502 (2019).
32. Traag, V. A., Waltman, L. & van Eck, N. J. From Louvain to Leiden: guaranteeing well-connected communities. *Sci. Rep.* **9**, 5233 (2019).
33. Levine, J. H. et al. Data-driven phenotypic dissection of AML reveals progenitor-like cells that correlate with prognosis. *Cell* **162**, 184–197 (2015).
34. Jin, S. et al. Inference and analysis of cell-cell communication using CellChat. *Nat. Commun.* **12**, 1088 (2021).
35. Xue, M. & Jackson, C. J. Extracellular matrix reorganization during wound healing and its impact on abnormal scarring. *Adv. Wound Care.* **4**, 119–136 (2015).
36. Jessen, K. R. & Mirsky, R. The repair Schwann cell and its function in regenerating nerves. *J. Physiol.* **594**, 3521–3531 (2016).
37. van den Brink, S. C. et al. Single-cell sequencing reveals dissociation-induced gene expression in tissue subpopulations. *Nat. Methods* **14**, 935–936 (2017).
38. Denisenko, E. et al. Systematic assessment of tissue dissociation and storage biases in single-cell and single-nucleus RNA-seq workflows. *Genome Biol.* **21**, 130 (2020).
39. Fadl, B. R. et al. An optimized protocol for retina single-cell RNA sequencing. *Mol. Vis.* **26**, 705–717 (2020).
40. Reinisch, C. M. & Tschachler, E. The dimensions and characteristics of the sub-epidermal nerve plexus in human skin-terminal Schwann cells constitute a substantial cell population within the superficial dermis. *J. Dermatol. Sci.* **65**, 162–169 (2012).
41. Reinisch, C. M. et al. Rarefaction of the peripheral nerve network in diabetic patients is associated with a pronounced reduction of terminal Schwann cells. *Diabetes Care* **31**, 1219–1221 (2008).
42. Vorstandlechner, V. et al. The serine proteases dipeptidyl-peptidase 4 and urokinase are key molecules in human and mouse scar formation. *Nat. Commun.* **12**, 6242 (2021).
43. Weiss, T., Taschner-Mandl, S., Ambros, P. F. & Ambros, I. M. Detailed protocols for the isolation, culture, enrichment and immunostaining of primary human Schwann Cells. *Methods Mol. Biol.* **1739**, 67–86 (2018).
44. Andersen, N. D., Srinivas, S., Piñero, G. & Monje, P. V. A rapid and versatile method for the isolation, purification and cryogenic storage of Schwann cells from adult rodent nerves. *Sci. Rep.* **6**, 31781 (2016).
45. Silva, W. N. et al. Role of Schwann cells in cutaneous wound healing. *Wound Repair Regen.* **26**, 392–397 (2018).
46. Nagarajan, R., Le, N., Mahoney, H., Araki, T. & Milbrandt, J. Deciphering peripheral nerve myelination by using Schwann cell expression profiling. *Proc. Natl Acad. Sci. U.S.A.* **99**, 8998–9003 (2002).
47. Arthur-Farraj, P. J. et al. c-Jun reprograms Schwann cells of injured nerves to generate a repair cell essential for regeneration. *Neuron* **75**, 633–647 (2012).
48. Barrette, B., Calvo, E., Vallières, N. & Lacroix, S. Transcriptional profiling of the injured sciatic nerve of mice carrying the *Wld(S)* mutant gene: identification of genes involved in neuroprotection, neuroinflammation, and nerve regeneration. *Brain Behav. Immun.* **24**, 1254–1267 (2010).
49. De Felipe, C. & Hunt, S. P. The differential control of c-jun expression in regenerating sensory neurons and their associated glial cells. *J. Neurosci.* **14**, 2911–2923 (1994).
50. Shy, M. E., Shi, Y., Wrabetz, L., Kamholz, J. & Scherer, S. S. Axon-Schwann cell interactions regulate the expression of c-jun in Schwann cells. *J. Neurosci. Res.* **43**, 511–525 (1996).
51. Parkinson, D. B. et al. Krox-20 inhibits Jun-NH2-terminal kinase/c-Jun to control Schwann cell proliferation and death. *J. Cell Biol.* **164**, 385–394 (2004).
52. Parkinson, D. B. et al. c-Jun is a negative regulator of myelination. *J. Cell Biol.* **181**, 625–637 (2008).
53. Fogarty, E. A., Kitzman, J. O. & Antonellis, A. SOX10-regulated promoter use defines isoform-specific gene expression in Schwann cells. *BMC Genomics* **21**, 549 (2020).
54. Widera, D. et al. Schwann cells can be reprogrammed to multipotency by culture. *Stem Cells Dev.* **20**, 2053–2064 (2011).
55. Gui, T. et al. Krüppel-like factor 6 rendered rat Schwann cell more sensitive to apoptosis via upregulating FAS expression. *PLoS ONE* **8**, e82449 (2013).
56. Li, M., Banton, M. C., Min, Q., Parkinson, D. B. & Dun, X. Meta-analysis reveals transcription factor upregulation in cells of injured mouse sciatic nerve. *Front. Cell. Neurosci.* **15**, 688243 (2021).
57. Wang, Y. et al. KLF7-transfected Schwann cell graft transplantation promotes sciatic nerve regeneration. *Neuroscience* **340**, 319–332 (2017).
58. Mizuno, M., Fujisawa, R. & Kuboki, Y. Type I collagen-induced osteoblastic differentiation of bone-marrow cells mediated by collagen- α 2 β 1 integrin interaction. *J. Cell. Physiol.* **184**, 207–213 (2000).
59. Campbell, W. A. et al. Midkine is neuroprotective and influences glial reactivity and the formation of Müller glia-derived progenitor cells in chick and mouse retinas. *Glia* **69**, 1515–1539 (2021).
60. Koutsoumpa, M. et al. Interplay between α v β 3 integrin and nucleolin regulates human endothelial and glioma cell migration. *J. Biol. Chem.* **288**, 343–354 (2013).

ACKNOWLEDGEMENTS

The authors would like to thank HP Haselsteiner and the CRISCAR Familienstiftung for their ongoing support of the Medical University/Aposcience AG public private partnership aiming at augmenting basic and translational clinical research in Austria/Europe. We acknowledge the core facilities of the Medical University of Vienna, a member of Vienna Life Science Instruments. The study was funded by the FFG Grant “APOSEC” (852748 and 862068; 2015–2019), the Vienna Business Agency “APOSEC to clinic” (ID 2343727, 2018–2020) and by the Aposcience AG under the direction of group leader HJA. MM was funded by the Sparkling Science Program of the Austrian Federal Ministry of Education, Science and Research (SPA06/055).

AUTHOR CONTRIBUTIONS

Conceptualization, M.D., T.W. and M.M.; methodology, M.D., M.W., D.C. and M.M.; software, M.D., M.W., D.C. and K.K.; validation, M.D. and M.M.; formal analysis, M.D.; investigation, M.D. and D.C.; resources, H.J.A. and M.M.; data curation, M.D.; writing original draft preparation, M.D., M.L. and M.M.; writing, review and editing, M.D., M.W., T.W., M.L., K.K., D.B., V.V. and M.M.; visualization, M.D.; supervision, M.M.; project administration, M.D. and M.M.; funding acquisition, M.M. and H.J.A. All authors have read and agreed to the final version of the manuscript.

COMPETING INTERESTS

The authors declare no competing interests.

ETHICS APPROVAL AND CONSENT TO PARTICIPATE

The study was conducted according to the guidelines of the Declaration of Helsinki. The use of resected skin and keloids was approved by the ethics committee of the Medical University of Vienna (votes 217/2010 and 1190/2020). Written informed consent was obtained from all donors.


ADDITIONAL INFORMATION

Supplementary information The online version contains supplementary material available at <https://doi.org/10.1038/s12276-022-00874-1>

Correspondence and requests for materials should be addressed to Michael Mildner.

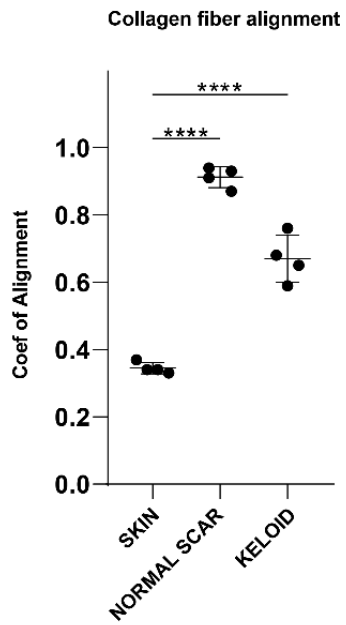
Reprints and permission information is available at <http://www.nature.com/reprints>

Publisher's note Springer Nature remains neutral with regard to jurisdictional claims in published maps and institutional affiliations.

 Open Access This article is licensed under a Creative Commons Attribution 4.0 International License, which permits use, sharing, adaptation, distribution and reproduction in any medium or format, as long as you give appropriate credit to the original author(s) and the source, provide a link to the Creative Commons license, and indicate if changes were made. The images or other third party material in this article are included in the article's Creative Commons license, unless indicated otherwise in a credit line to the material. If material is not included in the article's Creative Commons license and your intended use is not permitted by statutory regulation or exceeds the permitted use, you will need to obtain permission directly from the copyright holder. To view a copy of this license, visit <http://creativecommons.org/licenses/by/4.0/>.

© The Author(s) 2022

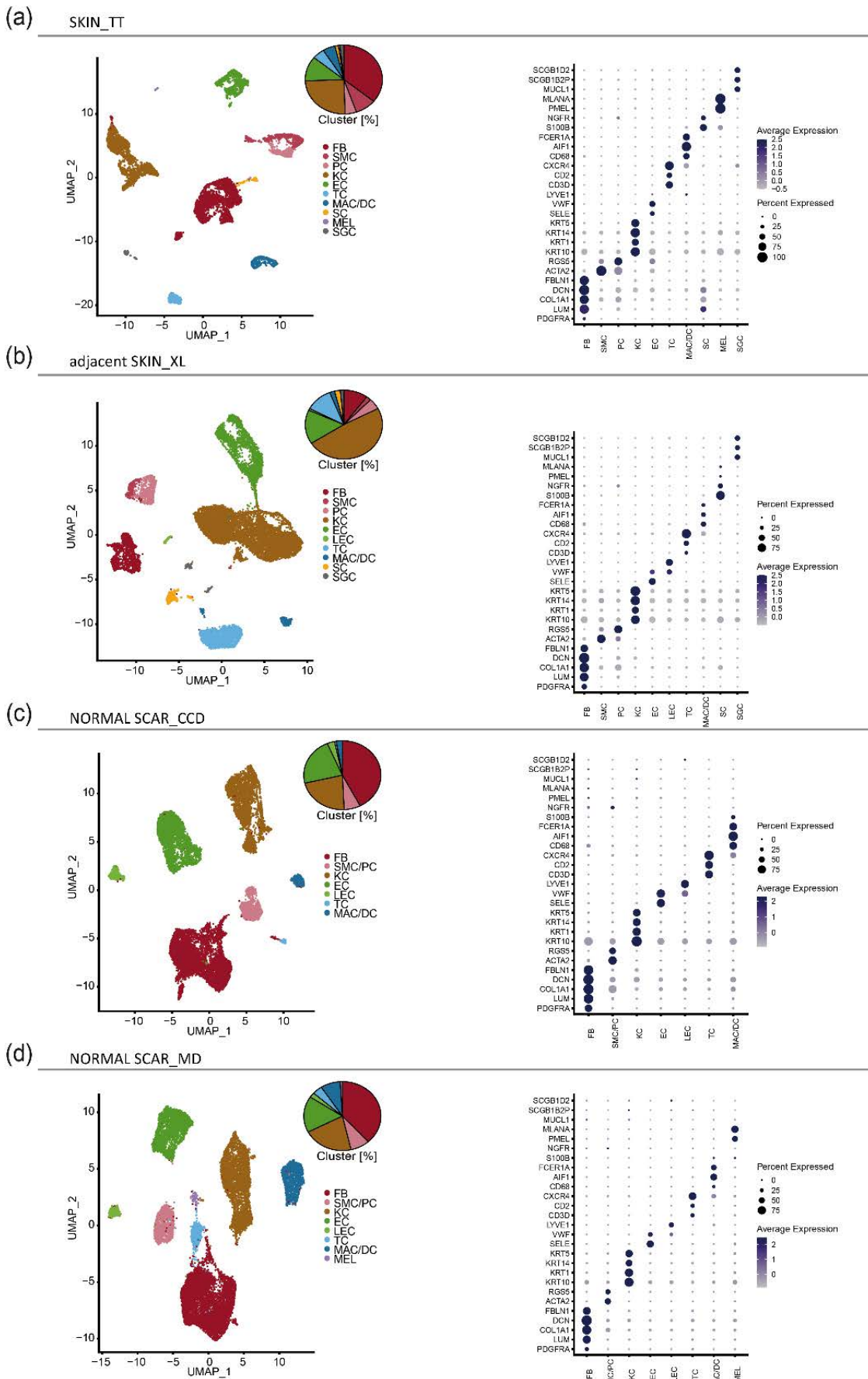
Supplementary Fig. 1



Supplementary Fig. 1: Collagen alignment in skin, normal scar and keloid

Evaluation of the alignment coefficient of healthy skin, normal scar and keloid tissue. Maximum and minimum value with <1.5 interquartile range is shown by whiskers. The middle line represents the mean. Normally distributed data were compared by one-way ANOVA with Tukey post hoc test. **** $p < 0.0001$.

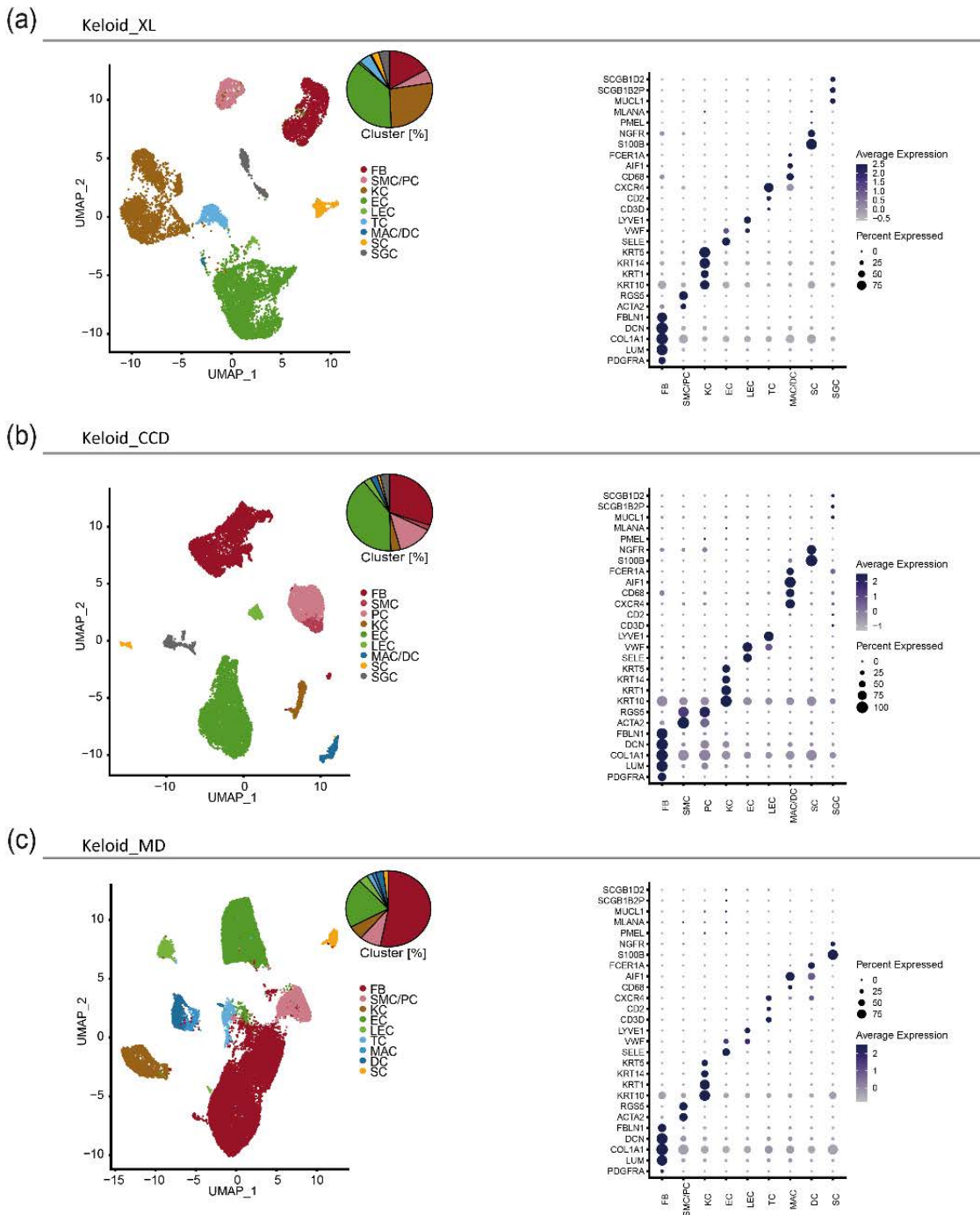
Supplementary Fig. 2



Supplementary Fig. 2: Individual dataset integration unravels cluster consistency

UMAP-Plots and Dot plots individual integrations of datasets from distinct conditions and sources: SKIN_TT, n=6 (a); adjacent SKIN_XL, n=4 (b); NORMAL SCAR_CCD, n=3 (c); NORMAL SCAR_MD, n=3 (d); cluster classification as fibroblasts (FB), smooth muscle cells (SMC), pericytes (PC), smooth muscle cells and pericytes (SMC/PC), keratinocytes (KC), endothelial cells (EC), lymphatic endothelial cells (LEC), T-cells (TC), macrophages (MAC), dendritic cells (DC), macrophages and dendritic cells (MAC/DC), Schwann cells (SC), melanocytes (MEL), erythrocytes (ERY) and sweat gland cells (SGC); Pie plots show cluster composition within each dataset combination. Dot plots showing well-known marker genes to characterise clusters: *PDGFRA*, *LUM*, *COL1A1*, *DCN*, *FBLN1* for FB; *ACTA2*, *RGS5* for SMC and PC; *KRT10*, *KRT1*, *KRT14*, *KRT5* for KC; *SELE*, *VWF* for EC; *LYVE1* for LEC; *CD3D*, *CD2*, *CXCR4* for TC; *CD68*, *AIF1* for MAC; *FCER1A* for DC; *S100B*, *NGFR* for SC; *PMEL*, *MLANA* for MEL; Dot size symbolizes percentage of cells expressing the gene, colour gradient shows level of average gene expression.

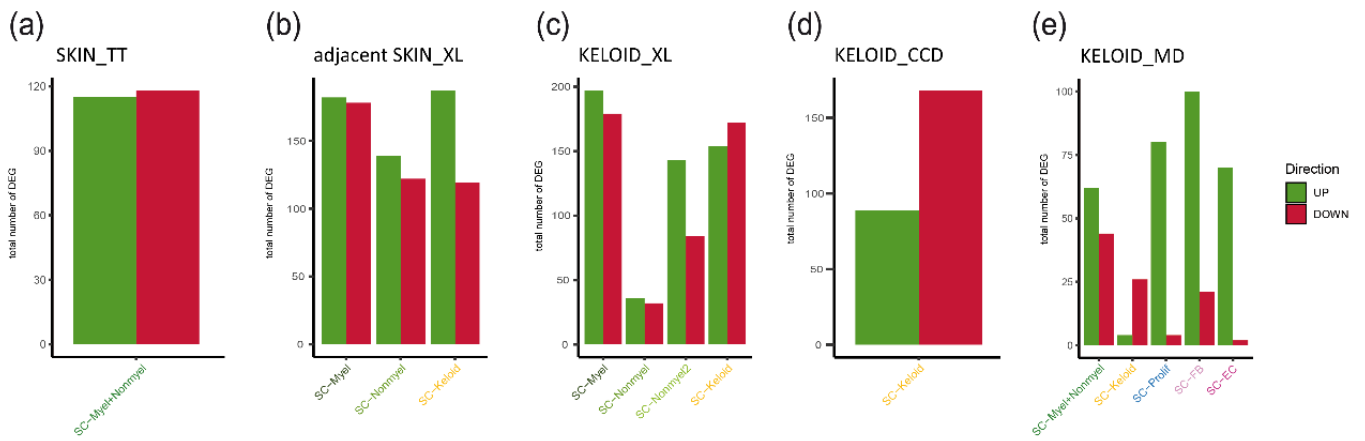
Supplementary Fig. 3



Supplementary Fig. 3: Individual dataset integration unravels cluster consistency

UMAP-plots and DotPlots individual integrations of datasets from distinct conditions and sources: KELOID_XL, n=4 (a); KELOID_CCD, n=3 (b); KELOID_MD, n=4 (c); cluster classification as fibroblasts (FB), smooth muscle cells (SMC), pericytes (PC), smooth muscle cells and pericytes (SMC/PC), keratinocytes (KC), endothelial cells (EC), lymphatic endothelial cells (LEC), T-cells (TC), macrophages (MAC), dendritic cells (DC), macrophages and dendritic cells (MAC/DC), Schwann cells (SC), melanocytes (MEL), erythrocytes (ERY) and sweat gland cells (SGC); Pie plots show cluster composition within each dataset combination. Dot plots showing well-known marker genes to characterise clusters: *PDGFRA*, *LUM*, *COL1A1*, *DCN*, *FBLN1* for FB; *ACTA2*, *RGSS5* for SMC and PC; *KRT10*, *KRT1*, *KRT14*, *KRT5* for KC; *SELE*, *VWF* for EC; *LYVE1* for LEC; *CD3D*, *CD2*, *CXCR4* for TC; *CD68*, *AIF1* for MAC; *FCER1A* for DC; *S100B*, *NGFR* for SC; *PMEL*, *MLANA* for MEL; Dot size symbolizes percentage of cells expressing the gene, colour gradient shows level of average gene expression.

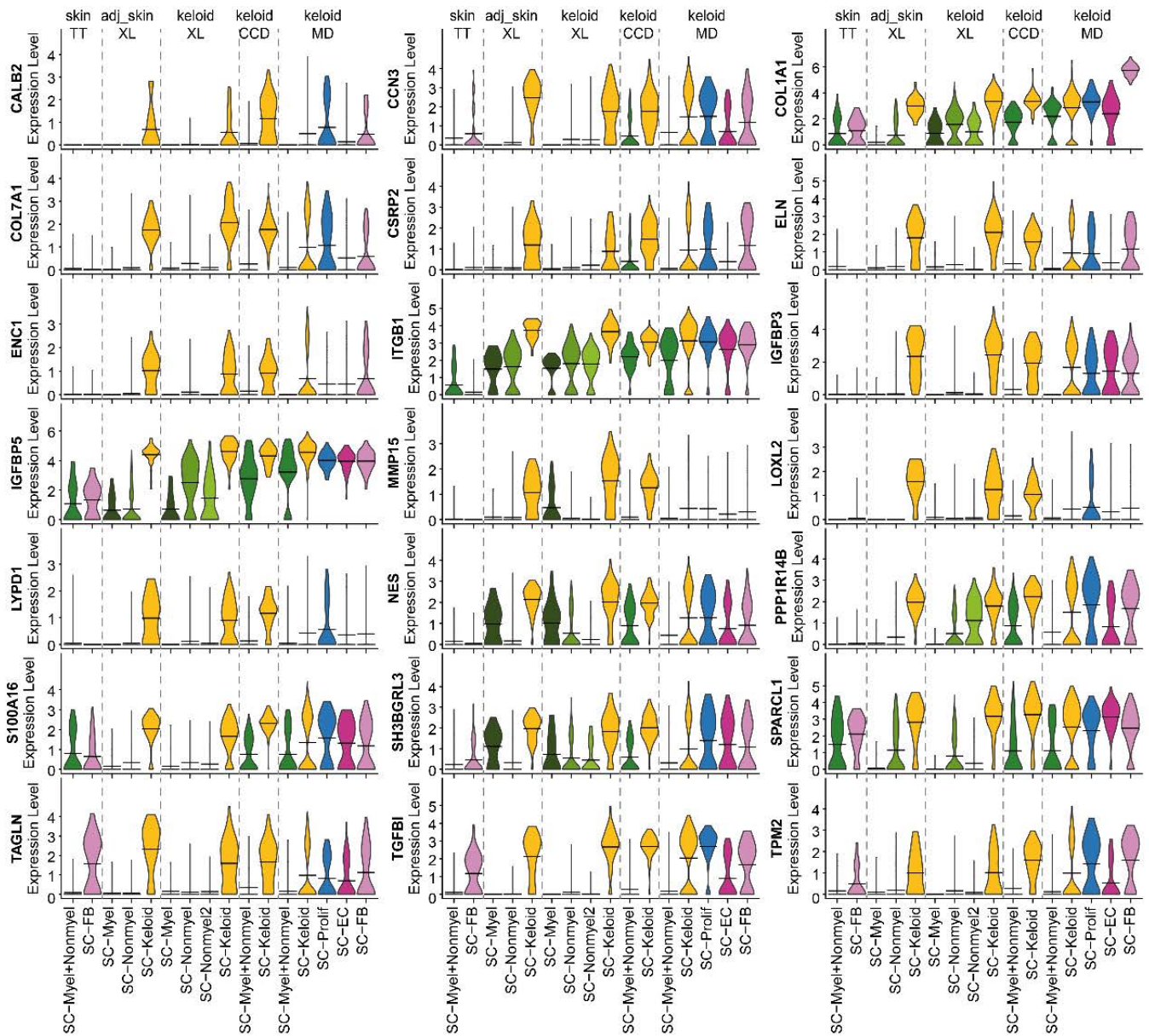
Supplementary Fig. 4



Supplementary Fig. 4: Total number of differentially expressed genes in each individual computation

Bar plots show the total number of differentially expressed genes (fold change ≥ 2) between all Schwann cell cluster of SKIN_TT (a); adjacent SKIN_XL (b); KELOID_XL (c); KELOID_CCD (d); KELOID_MD (e); green= UP regulation, red= DOWN regulation

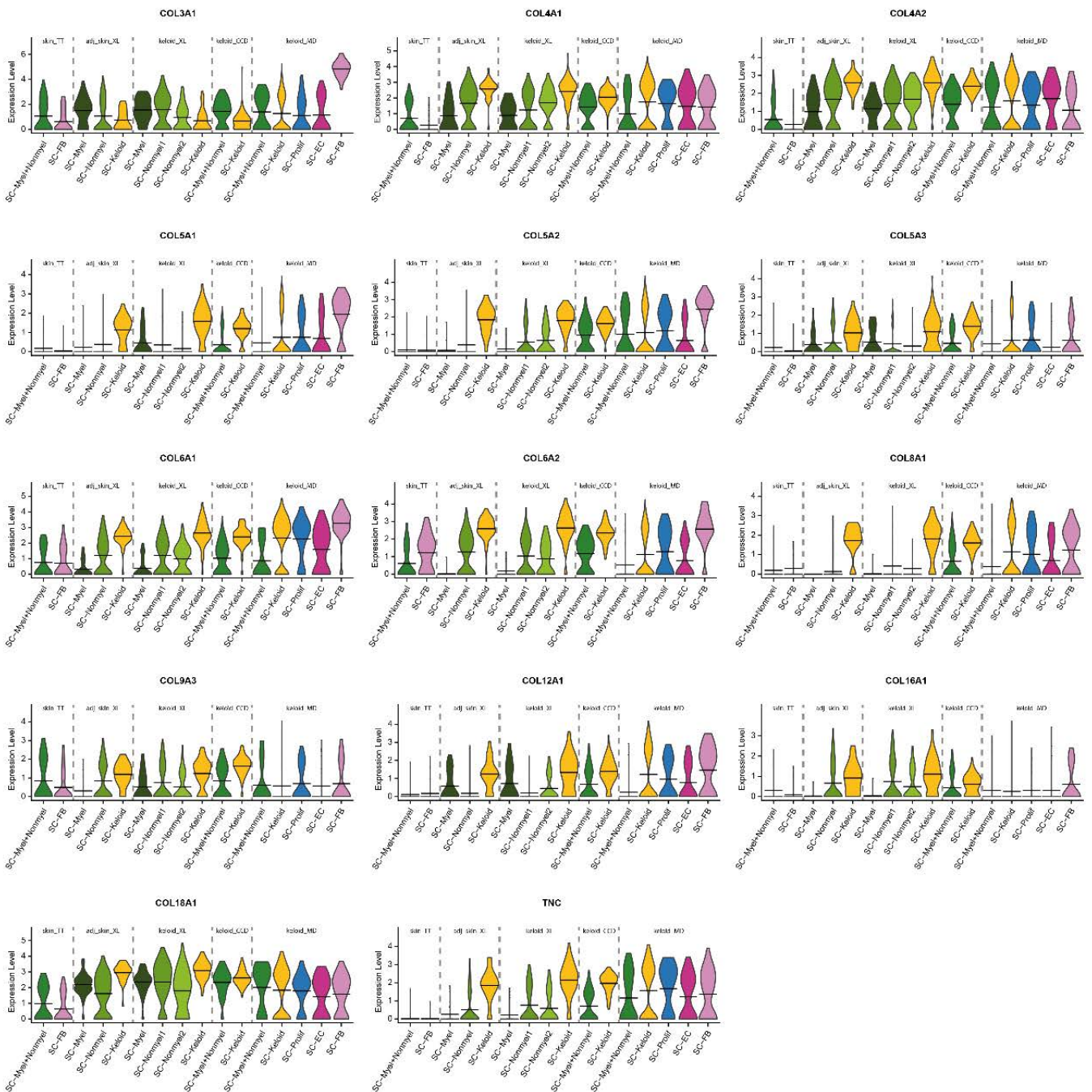
Supplementary Fig. 5



Supplementary Fig. 5: SC-Keloid pattern gene expression in all Schwann cell subtypes

Violin plots show the expression of the identified SC-Keloid expression pattern in all Schwann cell subtypes. Crossbeams mark the mean expression, vertical lines show maximum expression, violin width symbolizes frequency of cells on a distinct expression level.

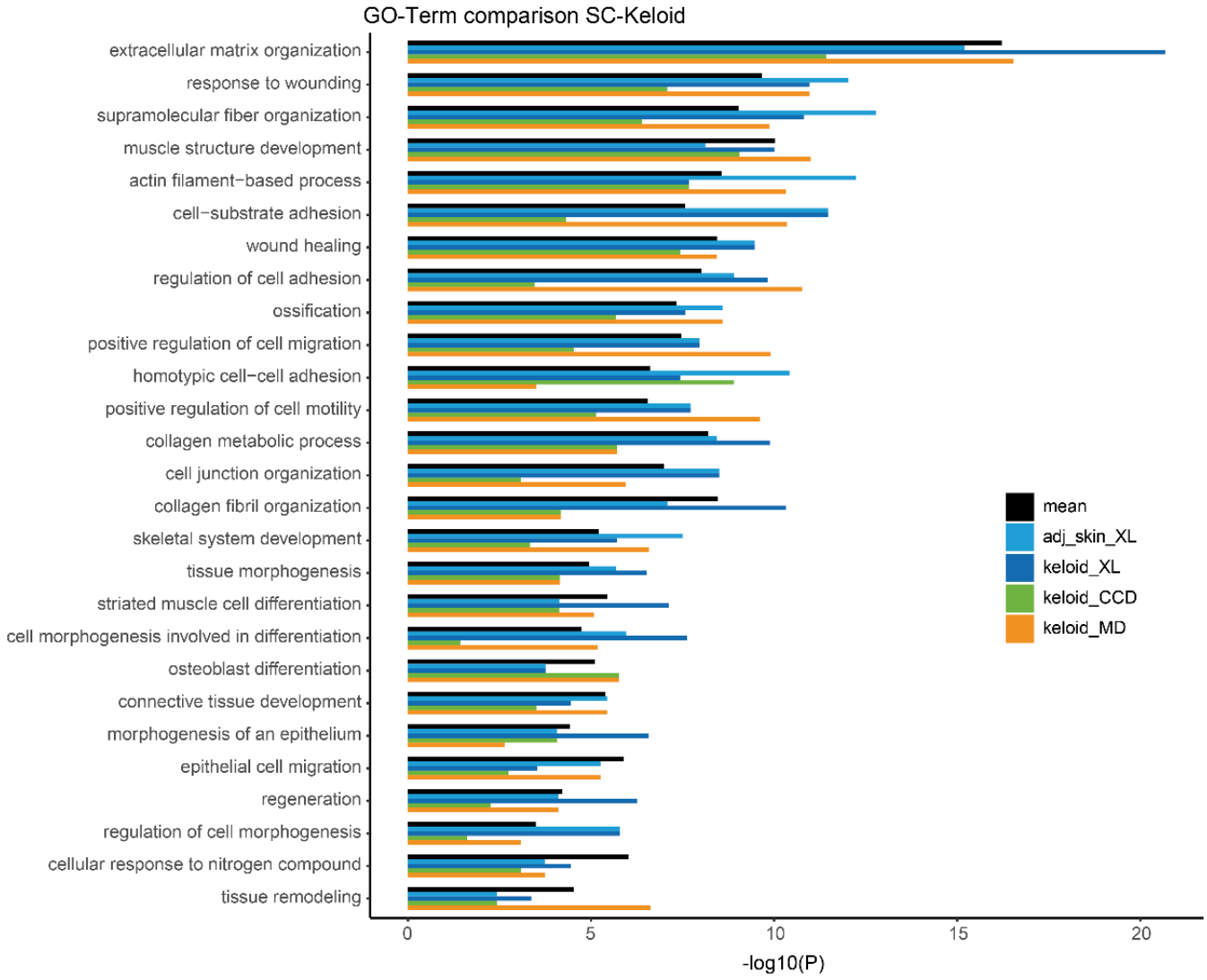
Supplementary Fig. 6



Supplementary Fig. 6: Extracellular matrix associated gene expression in SC-Keloid of distinct sources

Violin plots show the expression of several genes associated with matrix formation in all Schwann cell subtypes. Crossbeams mark the mean expression, vertical lines show maximum expression, violin width symbolizes frequency of cells on a distinct expression level.

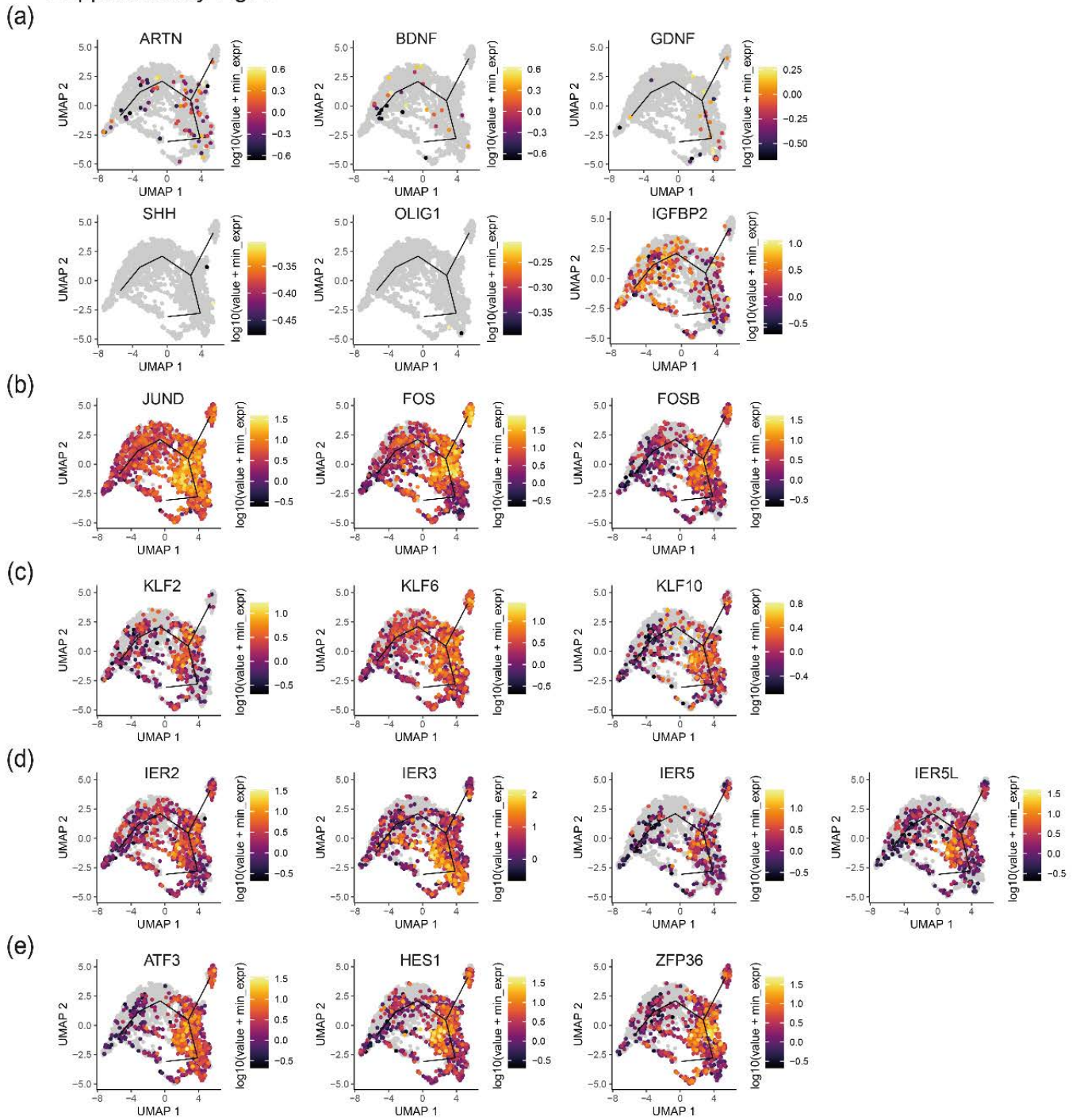
Supplementary Fig. 7



Supplementary Fig. 7: Corresponding GO-Terms encourage reported functions of keloidal Schwann cells

Enrichment analysis of top 100 upregulated genes resulted by data confrontation of SC-Keloid with myelination and nonmyelinating Schwann cells. Bar length shows statistical significance; mean value is depicted in black.

Supplementary Fig. 8

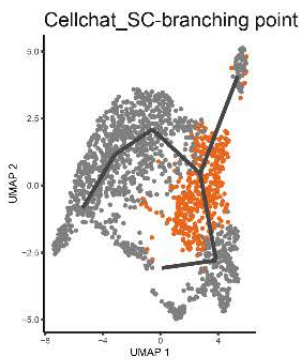


Supplementary Fig. 8: Pivotal gene groups potentially involved in the Schwann cell dedifferentiation process

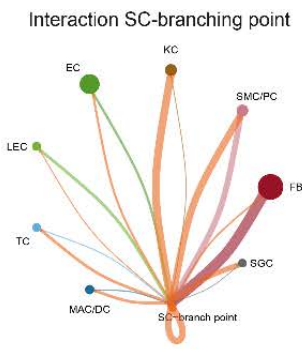
(a) Feature Plots with pseudotime track of *BDNF*, *GDNF*, *ARTN*, *SHH*, *OLIG1* and *IGFBP2*. (b) Feature Plots with UMAP Plot of combined Schwann cell clusters of all individual computations as basis showing activator protein 1 (AP-1) members *JUND*, *FOS* and *FOSB*. (c) Feature Plots of the kruppel-like factors (KLF) members *KLF2*, *KLF6* and *KLF10*. (d) Feature Plots of the immediate early response (IER) genes *IER2*, *IER3*, *IER5L* and *IER5*. (e) Feature Plots of *ATF3*, *HES1* and *ZFP36*.

Supplementary Fig. 9

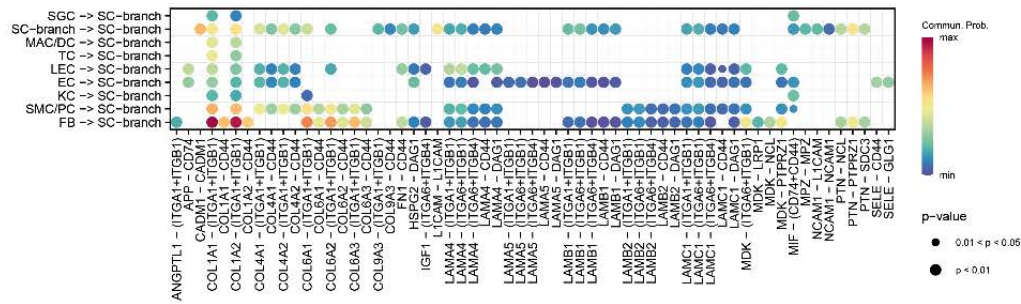
(a)



(b)



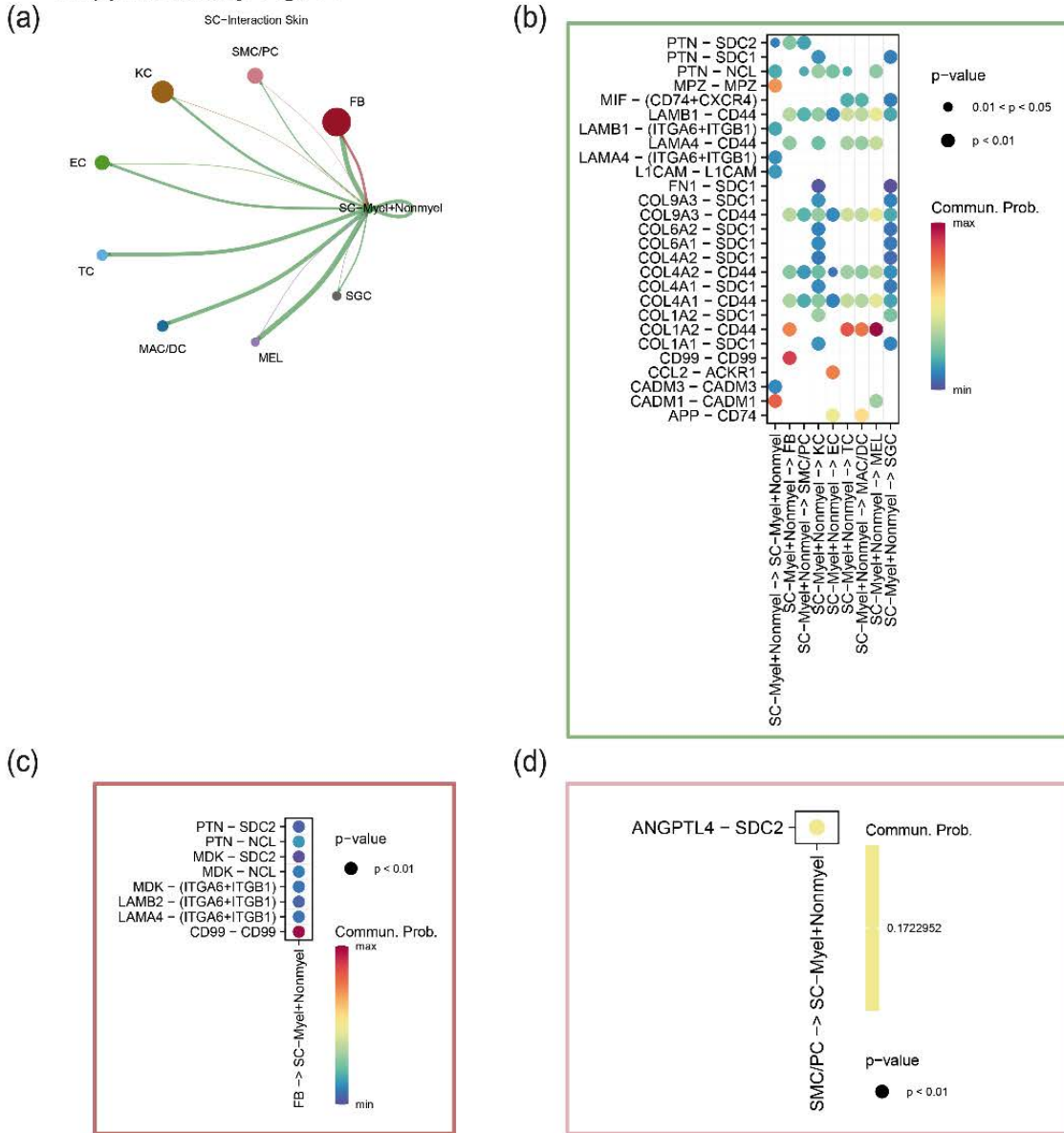
(c)



Supplementary Fig. 9: Potential impact of different cell types in the Schwann cell dedifferentiation process

(a) UMAP-Plot of combined Schwann cell clusters with determining cells at the branching point highlighted in orange. (b) Circle plot of detected interactions between the distinct keloidal cell types and the determining Schwann cells at the branching point; fibroblasts (FB), smooth muscle cells and pericytes (SMC/PC), keratinocytes (KC), endothelial cells (EC), lymphatic endothelial cells (LEC), T-cells (TC), macrophages and dendritic cells (MAC/DC), sweat gland cells (SGC); bows are coloured according to the signal-sending cell type; bow thickness symbolizes extent of detected interactions. (c) Dotplot shows all identified interactions of the distinct keloidal cell types with the pivotal Schwann cells at the branching point; dots symbolize a detected interaction, dot size shows p-value, dot colour depicts extent of the communication probability.

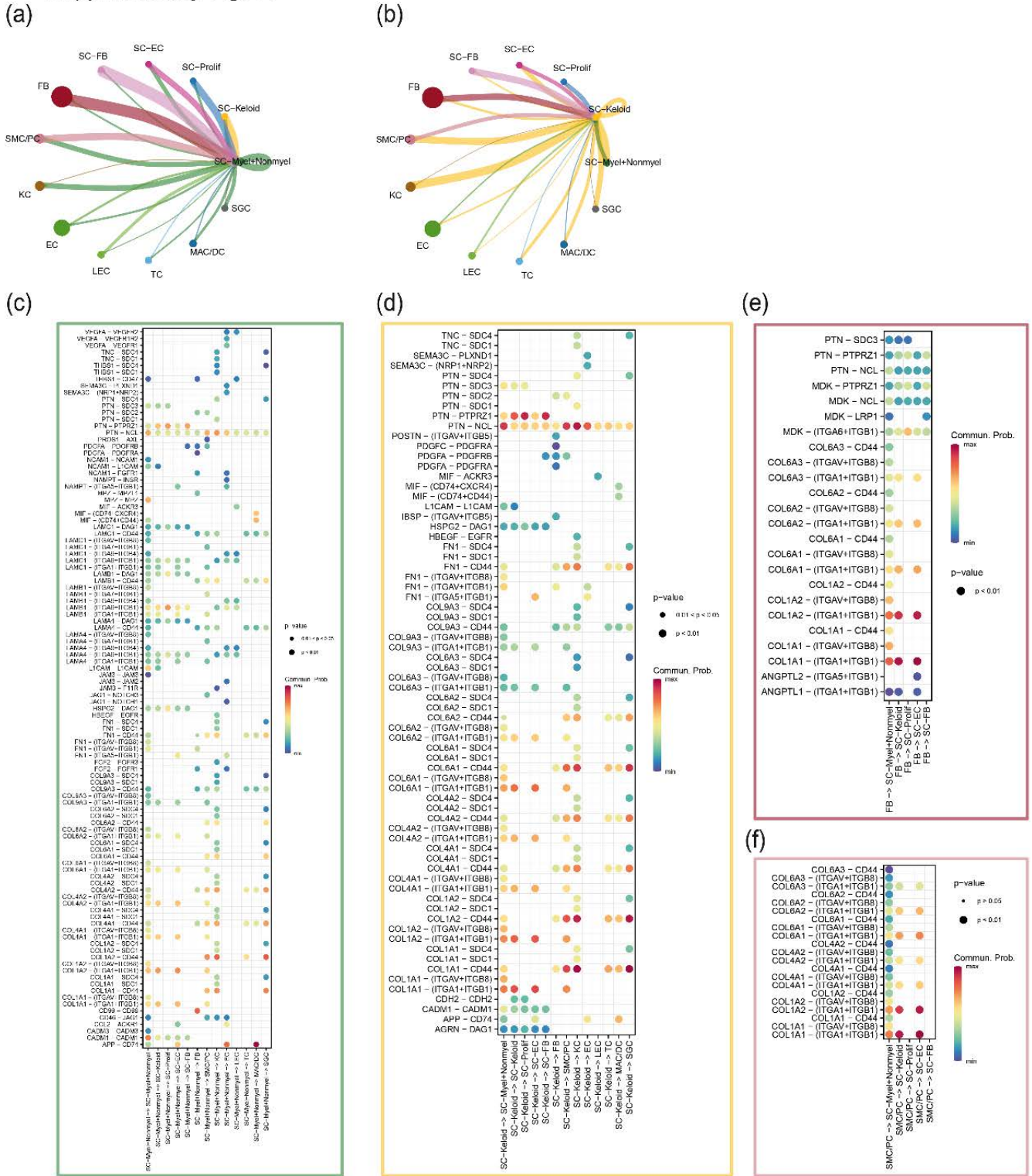
Supplementary Fig. 10



Supplementary Fig. 10: Potential Schwann cell interaction in healthy skin.

(a) Circle plot of the detected interactions in healthy skin between myelinating + nonmyelinating Schwann cells (SC-Myel+Nonmyel) and the remaining cell types [fibroblasts (FB), smooth muscle cells and pericytes (SMC/PC), keratinocytes (KC), endothelial cells (EC), T-cells (TC), macrophages and dendritic cells (MAC/DC), melanocytes (MEL), sweat gland cells (SGC)]; bows are coloured according to the signal-sending celltype; bow thickness symbolizes extent of detected interactions. Dotplots show all identified interactions with cells present in keloids sent by (b) SC-Myel+Nonmyel, (c) FB and (d) SMC/PC; dots symbolize a detected interaction, dotsize shows p-value, dot colour depicts extent of the communication probability.

Supplementary Fig. 11



Supplementary Fig. 11: Potential Schwann cell interaction in keloids .

Circle plots of detected interactions in keloids between (a) myelinating and nonmyelinating Schwann cells (SC-Myel+Nonmyel), (b) keloidal Schwann cells (SC-Keloid) and the remaining cell types; fibroblasts (FB), smooth muscle cells and pericytes (SMC/PC), keratinocytes (KC), endothelial cells (EC), lymphatic endothelial cells (LEC), T-cells (TC), macrophages and dendritic cells (MAC/DC), sweat gland cells (SGC), proliferating Schwann cells (SC-Prolif), Schwann cells expressing genes typical for endothelial cells (SC-EC) or fibroblasts (SC-FB); bows are coloured according to the signal-sending cell type; bow thickness symbolizes extent of detected interactions. Dotplots show all identified interactions with cells present in keloids sent by (c) SC-Myel+Nonmyel, (d) SC-Keloid, (e) FB and (f) SMC/PC; dots symbolize a detected interaction, dotsize shows p-value, dot colour depicts extent of the communication probability.

Supplementary Table 1

Differentially expressed genes_adjacent-skin-XL_ comparing SC-Keloid vs. (SC-Myel, SC-Nommyel)										
gene	p_val	avg_log2FC	pct.1	pct.2	p_val_adj	Foldchange_UP	Foldchange_DOWN	Ratio_pctl_pct2		
IGFBP5	3,75985E-24	4,172214618	1	0,32	7,93367E-20	18,02858943	0,055467457	3,125		
TAGLN	8,41937E-42	4,034051171	0,844	0,031	1,77657E-37	16,38213146	0,061042118	27,22580645		
IGFBP3	5,44115E-46	3,979903772	0,906	0,027	1,14814E-41	15,7786708	0,063376695	33,55555556		
TGFBI	7,82192E-48	3,809347934	0,812	0,008	1,6505E-43	14,01935367	0,071329965	101,5		
CCN3	2,74623E-40	3,553600279	0,938	0,059	5,79481E-36	11,74195135	0,08516472	15,89830508		
PMEPAL1	6,37599E-25	2,991178137	1	0,289	1,3454E-20	7,951230464	0,125766698	3,460207612		
ELN	9,39877E-25	2,744572089	0,812	0,105	1,98323E-20	6,701908962	0,149211218	7,733333333		
COL1A1	2,80222E-20	2,687854737	1	0,328	5,91296E-16	6,443545503	0,155194062	3,048780488		
LOXL2	1,24566E-57	2,566847202	0,906	0	2,62846E-53	5,925131621	0,168772622	#DIV/0!		
APOD	1,28159E-24	2,497995728	0,75	0,074	2,70428E-20	5,649000888	0,177022454	10,13513514		
ITGB1	1,17015E-18	2,47289199	1	0,715	2,46913E-14	5,551555232	0,180129704	1,398601399		
NES	1,65975E-27	2,445557305	0,969	0,16	3,50224E-23	5,447360344	0,183575151	6,05625		
COL7A1	3,6255E-41	2,436012037	0,938	0,051	7,65017E-37	5,411438076	0,184793762	18,39215686		
S100A16	2,91126E-22	2,328345725	0,906	0,207	6,14305E-18	5,022291356	0,199112303	4,376811594		
COL8A1	5,14801E-33	2,326828989	0,875	0,07	1,08628E-28	5,017014086	0,199321745	12,5		
PTN	7,39689E-16	2,298231868	0,969	0,422	1,56082E-11	4,918545907	0,203312121	2,296208531		
FN1	1,301E-16	2,268482516	0,969	0,348	2,74525E-12	4,818160713	0,207548079	2,784482759		
PDLIM7	4,71905E-37	2,256920578	0,875	0,055	9,95767E-33	4,779701683	0,209218078	15,90909091		
S100A13	1,8595E-21	2,221078711	0,938	0,207	3,92374E-17	4,662419158	0,214480931	4,531400966		
PCDH20	1,15617E-21	2,200924696	0,875	0,141	2,43964E-17	4,597739399	0,217498191	6,205673759		
TIMP4	2,68071E-35	2,195462089	0,75	0,027	5,65656E-31	4,580363477	0,2183323285	27,77777778		
PPP1R14B	1,23462E-23	2,120857034	0,969	0,191	2,60518E-19	4,349522521	0,229910294	5,073298429		
MYL6	1,03389E-17	2,011367588	1	0,715	2,18161E-13	4,031642142	0,248037887	1,398601399		
SH3BGR13	1,28347E-19	1,995802282	0,969	0,258	2,70824E-15	3,98837837	0,250728468	3,755813953		
PFN1	3,5014E-17	1,978006745	0,969	0,469	7,3883E-13	3,939484189	0,2538840339	2,066098081		
CSRP2	2,098E-25	1,97308897	0,719	0,059	4,42699E-21	3,926078368	0,254707091	12,18644068		
COL5A2	2,67889E-19	1,898472142	0,938	0,203	5,65273E-15	3,728181616	0,268227276	4,620689655		
TMSB10	1,17749E-15	1,88373001	1	0,91	2,48462E-11	3,690279297	0,270982199	1,098901099		
COL1A2	5,80342E-15	1,875042622	1	0,578	1,22458E-10	3,66812454	0,272618879	1,730103806		
SPARCL1	3,94377E-10	1,841613943	0,875	0,406	8,32175E-06	3,584107584	0,279009482	2,155172414		

In order to keep the number of pages of the doctoral thesis within limits, only the first page of this Supplementary Table is shown, the complete table can be viewed online in the supplements

Supplementary Table 2

Differentially expressed genes_keloid-XL_ comparing SC-Keloid vs. (SC-Myel, SC-Nonmyel, SC-Nonmyel2)										
gene	p_val	avg_log2FC	pct.1	pct.2	p_val_adj	Foldchange_UP	Foldchange_DOWN	Ratio_pct1_pct2		
TGFB1	1,62559E-63	4,114407312	0,939	0,049	3,43016E-59	17,32048367	0,0577735108	19,16326531		
IBSP	1,76098E-49	4,02492376	0,744	0,025	3,71584E-45	16,27881479	0,061429534	29,76		
IGFBP3	2,56146E-59	3,882741596	0,902	0,042	5,40493E-55	14,75100757	0,067791979	21,47619048		
SPARCL1	1,80626E-38	3,198701767	0,951	0,281	3,81138E-34	9,181321159	0,1089916787	3,384341637		
ELN	1,45092E-46	3,00729267	0,915	0,126	3,06158E-42	8,040541529	0,124369733	7,261904762		
TAGLN	2,86713E-39	2,872219187	0,768	0,088	6,04993E-35	7,321905671	0,136576466	8,727272727		
COL7A1	3,01719E-45	2,7498591	0,902	0,126	6,36657E-41	6,726514348	0,148665408	7,158730159		
MMP15	9,57764E-48	2,51027746	0,829	0,07	2,02098E-43	5,697296385	0,17552185	11,84285714		
COL1A1	1,86368E-30	2,492821807	0,988	0,656	3,93254E-26	5,628778225	0,177658447	1,506097561		
IGFBP5	6,04209E-33	2,463500531	1	0,702	1,27494E-28	5,515533849	0,181306112	1,424501425		
FN1	3,93038E-29	2,438870099	0,963	0,488	8,29349E-25	5,422169072	0,184428037	1,973360656		
CCN3	3,09733E-32	2,417916588	0,793	0,137	6,53567E-28	5,343987333	0,187126192	5,788321168		
ITGB1	4,92765E-35	2,248125	1	0,765	1,03978E-30	4,750650259	0,210497499	1,307189542		
PCDH20	1,48287E-30	2,235276058	0,841	0,193	3,12901E-26	4,708527835	0,212380607	4,357512953		
APOD	8,17119E-31	2,16544267	0,854	0,204	1,7242E-26	4,486040577	0,222913722	4,18627451		
COL6A2	8,30144E-29	2,148125105	0,951	0,502	1,75169E-24	4,432513745	0,225605617	1,894422311		
LOXL2	2,83567E-49	2,073879796	0,817	0,049	5,98355E-45	4,210173817	0,237519885	16,67346939		
NES	1,81968E-29	2,06620237	0,902	0,288	3,83971E-25	4,187828523	0,238787237	3,131944444		
COL8A1	6,91195E-32	2,01267362	0,866	0,214	1,45849E-27	4,035293531	0,247813447	4,046728972		
S100A16	4,14099E-31	2,004861574	0,829	0,2	8,73791E-27	4,013501882	0,249158971	4,145		
COL1A2	2,89243E-25	1,978320612	0,976	0,723	6,10332E-21	3,940341342	0,25378512	1,3499930844		
MYL9	4,53715E-27	1,956163331	0,927	0,354	9,57385E-23	3,880286913	0,257712902	2,618644068		
TNFAIP6	8,63425E-23	1,944135252	0,89	0,442	1,82191E-18	3,848070556	0,259870495	2,013574661		
TNC	6,21347E-25	1,943263571	0,927	0,365	1,3111E-20	3,845746242	0,260027557	2,539726027		
S100A6	4,10404E-33	1,939016777	1	0,954	8,65993E-29	3,834442343	0,260794116	1,048218029		
COL6A1	1,67035E-25	1,92907186	0,976	0,565	3,52461E-21	3,808101309	0,262598056	1,727433628		
PTN	1,35095E-27	1,900107448	1	0,596	2,85065E-23	3,732409936	0,267923411	1,677852349		
ACTB	7,55083E-25	1,893136081	1	0,853	1,5933E-20	3,714417753	0,269221199	1,172332943		
S100A11	4,39506E-23	1,873087428	0,976	0,695	9,27401E-19	3,663156728	0,272988593	1,404316547		
GPC1	3,17181E-29	1,850565564	0,927	0,298	6,69284E-25	3,606415357	0,277283646	3,110738255		

In order to keep the number of pages of the doctoral thesis within limits, only the first page of this Supplementary Table is shown, the complete table can be viewed online in the supplements

Supplementary Table 3

Differentially expressed genes_keloid-MD_ comparing SC-Keloid vs. (SC-Myel+Nonmyel)											
gene	p_val	avg_log2FC	pct.1	pct.2	p_val_adj	Foldchange_UP	Foldchange_DOWN	Ratio_pct1_pct2	#DIV/0!		
IGFBP3	2,22407E-10	3,826013826	0,558	0	4,69301E-06	14,1822431	0,070510708		#DIV/0!		
TGFBI	1,18949E-11	3,072015943	0,665	0,073	2,50995E-07	8,409476203	0,11891347		9,109589041		
IBSP	0,001347452	3,016370678	0,206	0	1	8,091295313	0,123589606		#DIV/0!		
TNFAIP6	1,65361E-08	2,530897305	0,616	0,146	0,000348929	5,77931019	0,173031031		4,219178082		
CSRP2	2,24514E-05	2,376098972	0,352	0,024	0,473747591	5,191311189	0,192629562		14,666666667		
ELN	1,98271E-05	2,361032928	0,354	0,024	0,418372299	5,137380489	0,19465173		14,75		
COL7A1	2,16879E-05	2,197332219	0,378	0,049	0,457635946	4,58630474	0,218040461		7,714285714		
ENC1	0,000142734	2,154935498	0,271	0	1	4,453487356	0,224543132		#DIV/0!		
TAGLN	0,000112532	2,154164283	0,364	0,073	1	4,451107312	0,224663197		4,98630137		
TPM2	4,75012E-05	2,150011461	0,367	0,049	1	4,438313146	0,225310826		7,489795918		
COL6A1	1,74493E-09	2,003241665	0,753	0,341	3,68197E-05	4,008997909	0,249438893		2,208211144		
COL12A1	1,39165E-05	1,989216882	0,451	0,098	0,293653107	3,970214301	0,251875573		4,602040816		
ABI2	0,000607262	1,924139098	0,26	0,024	1	3,79510315	0,263497449		10,833333333		
PHLDA2	0,000170642	1,912549396	0,332	0,049	1	3,764737816	0,265622747		6,775510204		
CALB2	0,001745422	1,823248491	0,198	0	1	3,53877121	0,282583965		#DIV/0!		
CYTOR	0,000955647	1,812957228	0,247	0,024	1	3,513617702	0,284606945		10,291666667		
RGS16	0,00545016	1,701067917	0,278	0,098	1	3,251415469	0,307558357		2,836734694		
MIR4435-2HG	0,003052658	1,631515263	0,18	0	1	3,09838251	0,322749046		#DIV/0!		
RPL22L1	0,000961423	1,622006838	0,381	0,146	1	3,078029029	0,324883226		2,609589041		
APOD	0,010631937	1,601735768	0,351	0,171	1	3,035082575	0,329480327		2,052631579		
CAV1	0,002760453	1,56530164	0,183	0	1	2,959393707	0,337907051		#DIV/0!		
PDGFC	0,004117545	1,55989176	0,171	0	1	2,948317226	0,339176528		#DIV/0!		
PEG10	0,012341638	1,558748519	0,199	0,049	1	2,945981803	0,33944541		4,06122449		
SPARCL1	9,37615E-07	1,55499519	0,751	0,366	0,019784609	2,938327469	0,340329664		2,051912568		
SCRG1	0,015608841	1,540000321	0,228	0,073	1	2,907945682	0,343885378		3,123287671		
RAPH1	0,006100788	1,533475566	0,158	0	1	2,894823856	0,345444162		#DIV/0!		
PPP1R14B	7,07426E-05	1,525258782	0,537	0,244	1	2,878383422	0,347417232		2,200819672		
MACF1	0,006009828	1,512488868	0,226	0,049	1	2,853018037	0,350506021		4,612244898		
SH3BGR13	0,001371387	1,509299061	0,376	0,146	1	2,846716966	0,351281849		2,575342466		
LRRFIP1	0,004775282	1,495976646	0,166	0	1	2,820550263	0,354540748		#DIV/0!		

In order to keep the number of pages of the doctoral thesis within limits, only the first page of this Supplementary Table is shown, the complete table can be viewed online in the supplements

Supplementary Table 4

Differentially expressed genes_keloid-CCD_ comparing SC-Keloid vs. (SC-Myel, SC-Nonmyel)										
gene	p_val	avg_log2FC	pct.1	pct.2	p_val_adj	Foldchange_UP	Foldchange_DOWN	Ratio_pct1_pct2		
TGFB1	3,3958E-29	3,029870367	0,975	0,14	7,16547E-25	8,167363097	0,122438538	6,964285714		
IGFBP3	6,21642E-20	2,225248255	0,875	0,15	1,31173E-15	4,675913543	0,213861952	5,833333333		
SPARCL1	5,90085E-17	2,144847772	0,95	0,46	1,24514E-12	4,422455947	0,226118702	2,065217391		
CALB2	2,05172E-20	2,118389279	0,725	0,05	4,32934E-16	4,342088945	0,230303896	14,5		
COL1A1	1,63999E-24	2,093393801	1	0,81	3,46053E-20	4,267507831	0,234328803	1,234567901		
COL7A1	6,3641E-26	2,067868872	0,988	0,16	1,34289E-21	4,192668807	0,238511565	6,175		
TAGLN	5,87919E-16	2,052665699	0,825	0,22	1,24057E-11	4,148718293	0,241038299	3,75		
TPM2	3,5852E-21	1,999061802	0,887	0,21	7,56513E-17	3,997399608	0,25016263	4,223809524		
CCN3	8,75885E-16	1,990677492	0,9	0,28	1,8482E-11	3,974235852	0,251620698	3,214285714		
SH3BGR13	1,45349E-21	1,86491222	0,975	0,39	3,06702E-17	3,642457705	0,274539907	2,5		
S100A16	3,44511E-25	1,835382546	0,988	0,48	7,26952E-21	3,568860221	0,280217207	2,058333333		
GAPDH	7,72324E-24	1,805821795	1	0,88	1,62968E-13	3,496282587	0,286018071	1,136363636		
MYL9	4,00764E-17	1,803266166	0,912	0,45	8,45653E-13	3,490094659	0,28652518	2,026666667		
MMP15	6,83522E-27	1,76026051	0,925	0,08	1,4423E-22	3,387592898	0,295194857	11,5625		
TUBB	4,19036E-15	1,691825785	0,925	0,52	8,84208E-11	3,230652965	0,309534949	1,778846154		
TMSB10	2,3336E-28	1,682307007	1	0,99	4,92412E-24	3,209407559	0,311583986	1,01010101		
ACTB	1,47582E-19	1,633679244	1	0,98	3,11414E-15	3,103033439	0,322265299	1,020408163		
ACTG1	1,97276E-22	1,573185619	1	0,99	4,16273E-18	2,975610346	0,336065507	1,01010101		
LYPD1	2,83443E-23	1,563763486	0,875	0,12	5,98092E-19	2,956240181	0,338267508	7,291666667		
MYL6	2,71876E-24	1,557423071	1	0,96	5,73685E-20	2,943276483	0,339757412	1,041666667		
DYNLT1	1,34649E-23	1,557257959	0,95	0,22	2,84123E-19	2,942939654	0,339796298	4,318181818		
ELN	3,06905E-18	1,547271244	0,887	0,2	6,476E-14	2,922638197	0,342156618	4,435		
COL6A1	3,31601E-18	1,540858142	0,975	0,59	6,99711E-14	2,909675248	0,343680966	1,652542373		
PFN1	5,70664E-20	1,52880683	0,988	0,71	1,20416E-15	2,885470996	0,346563872	1,391549296		
PPP1R14B	1,41925E-18	1,522643659	0,988	0,5	2,99477E-14	2,873170601	0,348047554	1,976		
TNC	8,27834E-20	1,502706938	1	0,48	1,74681E-15	2,833739103	0,352890638	2,083333333		
CSRP2	1,6932E-14	1,49962749	0,863	0,27	3,57281E-10	2,827696907	0,353644691	3,196296296		
LGALS1	6,26133E-22	1,470354423	1	1	1,3212E-17	2,770899573	0,360893628	1		
PKM	2,16474E-16	1,453166298	0,925	0,46	4,56782E-12	2,738083224	0,365218994	2,010869565		
PDLIM7	2,77723E-19	1,450864861	0,963	0,31	5,86023E-15	2,73371882	0,365802069	3,106451613		

In order to keep the number of pages of the doctoral thesis within limits, only the first page of this Supplementary Table is shown, the complete table can be viewed online in the supplements

Supplementary Table 5

Differentially expressed genes_total calculation_ comparing SC-Keloid vs. (SC-Myel, SC-Nonmyel)										
gene	p_val	avg_log2FC	pct.1	pct.2	p_val_adj	Foldchange_UP	Foldchange_DOWN	Ratio_pct1_pct2		
TGFB1	5,4254E-157	3,9142699	0,689	0,031	1,1448E-152	15,07692072	0,066326541	22,22580645		
IGFBP3	2,1896E-125	3,623292358	0,596	0,028	4,6202E-121	12,32309178	0,081148466	21,28571429		
IBSP	7,03777E-47	3,041607221	0,256	0,005	1,48504E-42	8,234078603	0,121446497	51,2		
IGFBP5	8,3086E-213	2,938763044	0,986	0,569	1,7532E-208	7,667536046	0,130419993	1,732864675		
COL1A1	2,2691E-135	2,504172227	0,858	0,505	4,788E-131	5,673237367	0,176266201	1,699009901		
CCN3	3,72269E-82	2,458134656	0,568	0,129	7,85525E-78	5,495057797	0,181981707	4,403100775		
TAGLN	3,88557E-60	2,38256811	0,428	0,08	8,19895E-56	5,214641635	0,191767732	5,35		
COL7A1	4,3247E-77	2,35507468	0,482	0,071	9,12554E-73	5,116207155	0,195457293	6,788732394		
ELN	3,6153E-57	2,230519265	0,447	0,11	7,62865E-53	4,693028642	0,213082015	4,063663664		
ATOX1	7,35647E-70	2,21901903	0,567	0,193	1,55229E-65	4,655767549	0,214787356	2,937823834		
SPARCL1	2,04561E-89	2,217783107	0,757	0,365	4,31644E-85	4,651780771	0,214971438	2,073972603		
S100A4	2,2655E-101	2,20859288	0,896	0,665	4,78052E-97	4,622134648	0,216350253	1,347368421		
S100A6	1,1638E-225	2,182991865	0,999	0,974	2,4558E-221	4,540942804	0,220218585	1,025667351		
PTN	2,1761E-126	2,126556702	0,874	0,56	4,5918E-122	4,366740206	0,229003777	1,560714286		
TPM2	2,07177E-49	2,103962793	0,414	0,106	4,37165E-45	4,298885823	0,232618413	3,905660377		
ITGB1	3,6323E-133	2,100228278	0,891	0,73	7,6646E-129	4,287772252	0,233221342	1,220547945		
PPP1R14B	5,36656E-67	2,099050849	0,61	0,275	1,1324E-62	4,284274294	0,233411759	2,218181818		
MYL6	1,24E-144	2,097600275	0,905	0,78	2,6165E-140	4,279968786	0,233646564	1,16025641		
CSR2	1,18306E-50	2,087842339	0,399	0,088	2,49638E-46	4,2511181	0,235232232	4,534090909		
S100A13	4,91823E-64	2,069656286	0,622	0,313	1,0378E-59	4,197866498	0,238216246	1,987220447		
LSM7	1,42662E-63	2,043179313	0,607	0,28	3,01031E-59	4,121528048	0,242628459	2,167857143		
FABP5	1,3676E-55	2,018973627	0,542	0,206	2,88576E-51	4,05295351	0,246733647	2,631067961		
COL12A1	2,10651E-49	2,010125868	0,504	0,197	4,44495E-45	4,028173622	0,248251464	2,558375635		
S100A16	5,46546E-63	2,007756015	0,577	0,252	1,15327E-58	4,021562147	0,248659591	2,28968254		
TNC	1,20429E-67	1,964017745	0,639	0,293	2,54118E-63	3,901469834	0,256313657	2,180887372		
COL8A1	2,42012E-60	1,958983909	0,522	0,168	5,1067E-56	3,887880589	0,257209546	3,107142857		
COL6A1	2,01681E-83	1,904860859	0,78	0,536	4,25567E-79	3,744727811	0,267042106	1,455223881		
POSTN	3,83097E-28	1,892523488	0,277	0,075	8,08373E-24	3,712840882	0,269335539	3,693333333		
SEM1	9,7043E-63	1,879455604	0,644	0,336	2,0477E-58	3,679361946	0,271786254	1,916666667		
NES	1,82782E-57	1,872988698	0,559	0,235	3,85689E-53	3,662906051	0,273007275	2,378723404		

In order to keep the number of pages of the doctoral thesis within limits, only the first page of this Supplementary Table is shown, the complete table can be viewed online in the supplements

Supplementary Table 6 – antibody information

1 st Antibodies					
Antigen	Species	catalog No	company	dilution	comment
S100	rabbit	#Z0311	DAKO	ready to use	o.n., 4°C
NGFR	mouse	#sc-13577	SantaCruz	1:100	o.n., 4°C
JUN	rabbit	#9165S	CellSignaling	1:300	o.n., 4°C
STAT3	rabbit	#9132	CellSignaling	1:200	o.n., 4°C
JUNB	rabbit	#3753	CellSignaling	1:200	o.n., 4°C
KLF4	rabbit	ab151733	abcam	1:200	o.n., 4°C
EGR1	rabbit	ab216964	abcam	1:200	o.n., 4°C
CCN3	rabbit	ab137677	abcam	1:200	o.n., 4°C
ELN	rabbit	ab21610	abcam	1:200	o.n., 4°C
2 nd Antibodies					
Antigen	Species	catalog No	company	dilution	comment
α rb AF488	goat	#A32731	Invitrogen	1:400	1 hr, RT
α ms AF594	donkey	#A21203	Invitrogen	1:400	1 hr, RT

Supplementary Table 7 – comparison_methods & materials

Dissociation	
source	
TT ¹	Whole Skin Dissociation Kit, human (Miltenyi Biotec, Germany) [37°C, 2h] + gentle MACS Octo Dissociator
XL ²	Whole Skin Dissociation Kit, human (Miltenyi Biotec, Germany) [37°C, over night] + gentle MACS Octo Dissociator
CCD ³	Dispase II (Sigma) [2h, 37°C] + epidermis peeled off + collagenase IV (YEASEN, China) [37°C, 2h]
MD ⁴	Whole Skin Dissociation Kit, human (Miltenyi Biotec, Germany) [37°C, 2.5h] + gentle MACS Octo Dissociator

enrichment		chemistry	
source	filtration	enrichment	chemistry
TT ¹	2x 70µm	No	Chromium Single Cell 3' version 1 (10X Genomics, USA)
XL ²	100µm, 40µm	Dead Cell Removal Kit (Miltenyi Biotec, Germany)	Chromium Single Cell 3' version 3 (10X Genomics, USA)
CCD ³	70µm	No	Chromium Single Cell 3' version2 (10X Genomics, USA)
MD	100µm, 40µm	Dead Cell Removal Kit (Miltenyi Biotec, Germany)	Chromium Single Cell 3' version 3.1 (10X Genomics, USA)

sequencing		cell ranger version	
source	sequencing	cell ranger version	
TT ¹	NextSeq (Illumina, USA)	NA	
XL ²	NovaSeq 6000 System (Illumina, USA)	Cell Ranger (v3.0.2, 10x Genomics)	
CCD ³	Hiseq X or Novaseq (Illumina, USA)	Cell Ranger (v2.1.0, 10x Genomics)	
MD ⁴	HiSeq 3000/4000 (Illumina, USA)	Cell Ranger (v3.0.2, 10x Genomics)	

Supplementary Table 7: Comparison_methods & materials.

1. Tabib, T.; Morse, C.; Wang, T.; Chen, W.; Lafyatis, R. SFRP2/DPF4 and FMO1/LSP1 Define Major Fibroblast Populations in Human Skin. *J Invest Dermatol* 2018, 138, 802-810.
2. Liu, X.; Chen, W.; Zeng, Q.; Ma, B.; Li, Z.; Meng, T.; Chen, J.; Yu, N.; Zhou, Z.; Long, X. Single-cell RNA-seq reveals lineage-specific regulatory changes of fibroblasts and vascular endothelial cells in keloids. *J Invest Dermatol* 2021.
3. Deng, C.C.; Hu, Y.F.; Zhu, D.H.; Cheng, Q.; Gu, J.J.; Feng, Q.L.; Zhang, L.X.; Xu, Y.P.; Wang, D.; Rong, Z.; et al. Single-cell RNA-seq reveals fibroblast heterogeneity and increased mesenchymal fibroblasts in human fibrotic skin diseases. *Nat Commun* 2021, 12, 3709.
4. Direeder, M.; Weiss, T.; Copic, D.; Vorstandlehner, V.; Laggner, M.; Mildner, M.; Klas, K.; Bormann, D.; Hasilik, W.; Radtke, C.; et al. Schwann cells contribute to keloid formation. *medRxiv* 2021, 2021.2008.2009.21261701.

Supplementary Table 8

			gene regulation in keloidal repair-like SCs compared to myelinating/nonmyelinating SCs				gene regulation after peripheral nerve lesion in rat compared to no lesion source: DOI: 10.1111/j.1471-4159.2005.03635.x						
			rel. expression level				rel. expression level						
GBN	human homolog	category	adj_Skin XL	Keloid XL	Keloid CCD	Keloid MD	Mean	5-8h	2d	4d	7d	14d	28d
M61875	CD44	A											
X61654	CD63	A											
AF049882	CD82	A											
X76489	CD9	A											
D83349	CDH22	A											
D25290	CDH6	A											
M92848	CEACAM1	A											
D87248	CNTN6	A											
L26525	DDR1	A											
U60096	ITGB4	A											
AF009133	KLRD1	A											
U41663	NLGN3	A											
D10831	SELL	A											
Y13714	SPARC	A											
U90448	CXCL5	A											
U54791	CXCR4	A											
U97142	GFRA1	A											
J04811	GHR	A											
M61177	MAPK3	A											
U66274	NPY5R	A											
M63837	PDGFRA	A											
D64045	PIK3R1	A											
M20637	PLCD1	A											
D38222	PTPRN	A											
L13151	RASA1	A											
AF084205	TAK1	A											
D14014	CCND1	B											
D16308	CCND2	B											
D16309	CCND3	B											
U05341	CDC20	B											
L11007	CDK4	B											
D64085	FGF5	B											
L32591	GADD45A	B											
X76453	PLAAT3	B											
M31177	THRA	B											
U72350	BCL2L1	B											
D26112	FAS	B											
L12458	LYZ	B											
X05137	NGFR	B											
Z54212	EMP1	B											
D85760	GNA12	B											
M31837	IGFBP3	B											
M69055	IGFBP6	B											
D50093	PRNP	B											
V01217	ACTB	B											
AF083269	ARPC1B	B											
L08505	DYNC1H1	B											
X67788	EZR	B											
U31367	MAL	B											
X60370	MAP1B	B											
U31463	MYH9	B											
X74815	MYO1E	B											
Z12152	NEFM	B											
X59601	PLEC	B											
X86789	SNCG	B											

Supplementary Table 8






			gene regulation in keloidal repair-like SCs compared to myelinating/nonmyelinating SCs				gene regulation after peripheral nerve lesion in rat compared to no lesion source: DOI: 10.1111/j.1471-4159.2005.03635.x						
			rel. expression level				rel. expression level						
GBN	human homolog	category	adj_Skin XL	Keloid XL	Keloid CCD	Keloid MD	Mean	5-8h	2d	4d	7d	14d	28d
M83107	TAGLN	B											
V01227	TUBA1A	B											
AJ002967	UTRN	B											
AF051425	CNMD	B											
AJ224879	COL2A1	B											
J04035	ELN	B											
AJ009698	EMB	B											
L34067	GPC1	B											
L14851	NRXN3	B											
D88250	C1S	B											
M15768	CD4	B											
U17035	CXCL10	B											
AF010464	IL7	B											
M34253	IRF1	B											
D10754	PSMB6	B											
M20035	PTMA	B											
X52498	TGFBI	B											
D42117	TNFRSF8	B											
L38644	KPNB1	B											
L20822	STX5	B											
D17615	YWHAZ	B											
U53184	LITAF	B											
AF014503	NUPR1	B											
J03628	S100A4	B											
K01934	THRSP	B											
L15079	ABCB4	B											
L06040	ALOX15	B											
M21730	ANXA5	B											
X55572	APOD	B											
M28647	ATP1A1	B											
M14512	ATP1A2	B											
J04629	ATP1B2	B											
D84450	ATP1B3	B											
X14209	COX4I1	B											
D10952	COX5B	B											
D13205	CYB5A	B											
U17697	CYP51A1	B											
J02773	FABP3	B											
U75581	FABP4	B											
U13253	FABP5	B											
U58829	FTH1	B											
M26161	KCNA1	B											
M12516	POR	B											
Y09164	SCN7A	B											
J04793	SLC4A1	B											
M95738	SLC6A11	B											
L38247	SYT4	B											
AJ004912	TMED10	B											
L12385	ARF6	B											
AF019109	SORT1	B											
U29339	ERBB3	C											
M25889	MBP	C											
K03242	MPZ	C											
AB019393	MYOC	C											
M34384	NES	C											

Supplementary Table 8

			gene regulation in keloidal repair-like SCs compared to myelinating/nonmyelinating SCs				gene regulation after peripheral nerve lesion in rat compared to no lesion source: DOI: 10.1111/j.1471-4159.2005.03635.x						
			rel. expression level				rel. expression level						
GBN	human homolog	category	adj_Skin XL	Keloid XL	Keloid CCD	Keloid MD	Mean	5-8h	2d	4d	7d	14d	28d
Z49858	PLLP	C											
M11185	PLP1	C											
M69139	PMP22	C											
Z29649	PRX	C											
M54919	S100B	C											
M24067	SERPINE1	C											
M27876	STMN1	C											
M12919	ALDOA	D											
D83479	CDO1	D											
D38495	CMA1	D											
M36320	CTSH	D											
S73583	ENPEP	D											
X79807	F10	D											
L03294	LPL	D											
U03763	PLA2G5	D											
M23697	PLAT	D											
L26043	PLIN1	D											
U50194	TPP2	D											
D90109	ACSL1	D											
M22413	CA3	D											
L33869	CP	D											
M95591	FDFT1	D											
M34477	FDPS	D											
M17701	GAPDH	D											
X62404	GPX5	D											
X62660	GSTA4	D											
J02592	GSTM2	D											
X02904	GSTP1	D											
M63983	HPRT1	D											
U62803	LCAT	D											
J03752	MGST1	D											
U25651	PFKM	D											
L02615	PKIA	D											
D90164	PPP1CB	D											
M33962	PTPN1	D											
D86373	SOAT1	D											
X74593	SORD	D											
M97662	UBP1	D											
U07683	UGT8	D											
X70685	H1-0	D											
M37584	H2AZ1	D											
M64986	HMGB1	D											
D84418	HMGB2	D											
M12156	HNRNPA1	D											
D13374	NME1	D											
X60790	PTBP1	D											
Z46372	TOP2A	D											
D49708	TRA2B	D											
M14864	CKM	D											
X15800	PKM	D											
AF017637	CPZ	D											
X61043	EEF1A1	D											
J02646	EIF2S1	D											
X54793	HSPD1	D											
M86870	PDIA4	D											

Supplementary Table 8

		gene regulation in keloidal repair-like SCs compared to myelinating/nonmyelinating SCs					gene regulation after peripheral nerve lesion in rat compared to no lesion source: DOI: 10.1111/j.1471-4159.2005.03635.x						
		rel. expression level					rel. expression level						
GBN	human homolog	category	adj_Skin XL	Keloid XL	Keloid CCD	Keloid MD	Mean	5-8h	2d	4d	7d	14d	28d
L25331	PLOD1	D											
X93352	RPL10A	D											
M20156	RPL18	D											
X06148	RPL5	D											
X52445	RPS24	D											
X59051	RPS29	D											
M84716	RPS3A	D											
C07039	RPSA	D											
M65149	CEBPD	E											
X14788	CREB1	E											
D17512	CRIP2	E											
U09229	CUX1	E											
J03179	DBP	E											
D31734	DLX5	E											
D10862	ID1	E											
D10863	ID2	E											
D10864	ID3	E											
X17163	JUN	E											
X63594	NFKBIA	E											
U17254	NR4A1	E											
AF008554	MAGT1	F											
AF025506	RABAC1	F											
U25264	SELENOW	F											

upregulation: 
rel. expression level UP ≥ 1.8: 
downregulation: 
rel. expression level DOWN ≥ 1.8: 
no regulation: 
GenBank accession number: GBN

Category according to Bosse et al. (2006):

- A: Cell communication
- B: Cellular physiological process
- C: Development
- D: Metabolism
- E: Transcription
- F: Miscellaneous

SC-Repair gene expression pattern

3 CHAPTER THREE: DISCUSSION

About 5000 years ago, Keloids have already been described as continuously spreading tumour-like pathology (Breasted, 1930). The term “keloid” has been formed later, about 200 years ago, accompanied by a more decent characterization of this pathology (Murray *et al.*, 1981). Since then, still no determinative cause for this fibrotic skin disease has been identified (Limandjaja *et al.*, 2020). Numerous hypotheses are still being discussed and challenged, including inflammatory, mechanic, hereditary and ethnical theories, amongst many others (Limandjaja *et al.*, 2020). A keloid is an extremely versatile disease that involves multiple cells with a pro-fibrotic state, including fibroblasts, endothelial cells and others (Broughton *et al.*, 2006; Kischer *et al.*, 1982; Lim *et al.*, 2019; Macarak *et al.*, 2021).

“All that glisters is not gold” (Shakespeare *et al.*, 1823)

Our scRNAseq analysis revealed novel insights in the cellular environment of keloids. In comparison with healthy skin and normal scars, increased numbers of fibroblasts and endothelial cells have been identified. These results correlate with previous findings of increased numbers of fibroblasts and microvessels in keloids (Limandjaja *et al.*, 2020). In addition, we observed an elevated number of cells associated with the neuronal system in keloids, the Schwann cells. A neuronal involvement in this pathology is not surprising, as patients frequently suffer from pruritus and pain. Nonetheless, the neuronal system and its potential pathologic involvement have been scarcely investigated so far. Studies based on staining of PGP9.5 describe a significantly lower nerve fibre density in keloids compared to healthy skin (Saffari *et al.*, 2018; Tey *et al.*, 2012). In contrast, Hochman *et al.* reported a significant increase of nerve fibres in keloids based on immunohistochemical staining of S100 to detect neuronal cells (Hochman *et al.*, 2008). These seemingly controversial results might be explained by the different biomarkers investigated. PGP9.5, also known as UCHL1, is a neuron-specific cytoplasmic protein and serves as a marker especially for small nerve fibres (Otsuki *et al.*, 2004; Van Acker *et al.*, 2016). S100 is a family of calcium binding proteins consisting of 24 members (Donato *et al.*, 2013). They can be subdivided in intracellular, intra- and extracellular subtypes according to their site of action, and are involved in cell proliferation and differentiation, programmed cell death, but also cell migration amongst others (Donato, 2003). Especially S100B has received attention in context with the neuronal system (Hachem *et al.*, 2005; Rickmann & Wolff, 1995). It is highly expressed in astrocytes, Schwann cells, melanocytes, Langerhans cells, adipocytes and chondrocytes and supports the cellular shape, homeostasis and the energy metabolism (Donato *et al.*, 2013) of the cells. In the peripheral nervous system, S100B has been shown to support the migration of injury-induced repair Schwann cells (Sbai *et al.*, 2010). Multiple studies proposed S100B as marker

for melanocytic tumors, breast cancer or neuronal damage, however a concrete qualification as marker for axons has not been reported (McIlroy *et al*, 2010; Mocellin *et al*, 2008; Muramatsu *et al*, 2003; Sindic *et al*, 1984). Already in 1985, S100B has been mentioned as factor associated with glial differentiation (Dhillon *et al*, 1985). The staining depicted in our study, using PGP9.5 to visualize neurons, corroborates the results of low neuronal density in keloids. In addition to the PGP9.5 staining, we further visualized neurofilaments to point out the accurate density of nerve fibres in keloids. Neurofilaments are about 10 nm-thick intermediate filaments specific for neurons (Schmitt & Geren, 1950). The highest amount of neurofilaments within a nerve cell was described in the axons, with low levels in the perikarya and dendrites (Burton & Wentz, 1992). Our staining of S100B additionally showed positivity of Schwann cells in the dermal area of the skin. Therefore, Hochman *et al*. presumably were the first to get a glimpse on Schwann cells in keloids. Together, these studies indicate a higher reliability of PGP9.5 or neurofilaments to determine the neuronal density in tissues, as the plain presence of glial cells does not always imply the presence of axons and therefore a connection with the neuronal system, as shown by our results.

“Love all, trust few, do wrong to none” (Shakespeare, 1813)

In 2021, the first scRNAseq works describing the cellular environment in keloids have been published (Deng *et al.*, 2021a; Liu *et al*, 2021; Xie *et al.*, 2021). These studies reported clusters of Schwann cells and neuronal cells but, in contrast to our findings, no significant difference in the amount of Schwann cells between keloids and the control groups (Deng *et al.*, 2021a; Liu *et al.*, 2021). We performed comprehensive bioinformatics analysis and found that the respective control conditions used were responsible for these contradictory findings. Deng *et al.* used normal scar as control condition for keloids (Deng *et al.*, 2021a). This comparison is eminently reasonable, as the keloid has been classified for multiple years as abnormal scar (Limandjaja *et al.*, 2020; Tan *et al.*, 2019). However, this comparison puts the keloid inevitably in a developmental connexion with normal, atrophic, or hypertrophic scars. This definition has been defused in the last years and keloids have been considered as fibrotic disorders of the skin and subcutaneous tissue rather than with scars. This rethinking relies on the fact that keloids also exhibit several cancer-like characteristics, including excessive, uncontrolled spreading into healthy tissue, regression failure and a high probability of recurrence after excision, that are untypical for all other scar types (Limandjaja *et al.*, 2020; Tan *et al.*, 2019). From the neoplastic point of view, the healthy skin would therefore serve as a better control for keloid research. Some studies, as the scRNAseq study conducted by Liu *et al.*, utilized “healthy” skin adjacent to keloids as control tissue (Jumper *et al.*, 2017; Liu *et al.*, 2021). However, as multiple studies already described significant alterations in the skin close to the keloid compared to keloid but also to keloid-independent skin, this study setting

would require an additional control-condition separate from keloids (Appleton *et al.*, 1996; Erdag *et al.*, 2008; Hahn *et al.*, 2013; Jiao *et al.*, 2017; Liu *et al.*, 2016). We further outlined this condition specific differences in our cross-study analysis.

“To be, or not to be, that is the question” (Shakespeare, 1954)

Our immunofluorescence confirmed increased amount of Schwann cells in keloids and uncovered their distinct spindle-shaped, elongated, narrow morphology aligned with the collagen bundles of the ECM. Their appearance closely resembles the shape of repair Schwann cells. However, repair Schwann cells are a well-defined subtype and characterized as Schwann cells arising from myelinating and non-myelinating Schwann cells, induced by an injury to support the neuronal repair and regeneration mechanisms (Jessen & Mirsky, 2016). The conversion of mature Schwann cells into repair Schwann cells implies several cellular changes, including dedifferentiation, activation, proliferation and cell migration towards the opposite nerve stump (Jessen & Mirsky, 2016). Keloidal Schwann cells exhibited similar features, as we detected several genes associated with Schwann cell precursors or immature Schwann cells, including nestin, SOX10 and NGFR. We further uncovered an upregulation of genes associated with cell migration and activation and a downregulation of genes involved in myelination in keloidal Schwann cells. However, the term “repair Schwann cell” is designated specifically for Schwann cells that express a defined panel of genes important for neuronal regeneration (Jessen & Mirsky, 2016). This includes c-JUN as major key factor, orchestrating the whole dedifferentiation process and the thereby acquired ability of repair Schwann cells to support functional recovery and to prevent neuronal death (Arthur-Farraj *et al.*, 2012). C-Jun and also STAT3 were reported to maintain the repair phenotype in Schwann cells (Arthur-Farraj *et al.*, 2012; Benito *et al.*, 2017). This is factors are required as long as the regeneration process lasts (Jessen & Mirsky, 2016). Further marker genes important for the functions of repair Schwann cells are BDNF, GDNF, SHH, OLIG1, and artemin (Arthur-Farraj *et al.*, 2012; Jessen & Mirsky, 2016). Keloidal Schwann cells, in contrast show many features similar to repair Schwann cells, but they do express c-JUN and STAT3 only in specific cluster areas and lack the remaining mentioned characteristic marker genes.

“Who can control his fate?” (Shakespeare, 1975)

As keloidal Schwann cells cannot be explicitly characterized as repair Schwann cells based on their transcriptional pattern, other potential options have to be considered. In the early investigation phase of repair Schwann cells, researchers discussed their findings with the possibility of more than one specific Schwann cell type arising from myelinating and non-

myelinating Schwann cells after damage (Jessen *et al.*, 2015). Comprehensive investigations of the function of repair Schwann cell with respect to their neuronal regeneration potential led to the strict definition of the repair subtype in association with the axonal recovery (Jessen & Mirsky, 2019b). Over time, the possibility of different repair-associated Schwann cell subtypes has been increasingly neglected. However, new insights on Schwann cells in conjunction with our results on keloidal Schwann cells revive this old discussion.

Neuronal damage and the subsequent regeneration have been associated with time-dependent changes in gene expression. In 2006, Bosse *et al.* performed a well-structured analysis of the transcriptional changes at different time points in the distal sciatic nerve induced by rupture (Bosse *et al.*, 2006). They investigated gene regulation after 5-8 hours, and on day 2, 4, 7, 14 and 28 following nerve crushes (Bosse *et al.*, 2006). Multiple cellular functions were associated with the regulated genes that have also been mentioned in context with repair Schwann cells, as morphogenesis, proliferation, and organization of cell structure (Bosse *et al.*, 2006). As Schwann cells represent the leading cell population in the peripheral neuronal repair mechanisms, the majority of genetic changes detected in this bulk sequencing analysis has been set in context with their injury-induced conversion (Bosse *et al.*, 2006). Juxtaposition of the temporally regulated genes with the according gene expression of keloidal Schwann cells revealed a set of concordant but also many divergent regulated genes. As the bulk sequencing analysis of Bosse *et al.* captured transcriptomic data from a cellular mix present in the distal nerve, it is not possible to assign these genetic changes to one specific dedifferentiation process of Schwann cells, which therefore leaves the possibility of more developmental tracks.

Another study reported a potential variability of activated Schwann cells after peripheral nerve injury (Clements *et al.*, 2017). Schwann cells from the distal stump revealed characteristic repair Schwann cell features (Clements *et al.*, 2017). Repair Schwann cells, intended for the bridge formation between the neuronal stumps, altered their expression pattern in the moment when they entered the interstice (Clements *et al.*, 2017). The bridge Schwann cells appeared to be more proliferative than the remaining repair Schwann cells. The repair Schwann cells on the other side revealed a genetic pattern associated with matrix production but also with immune signalling and inflammatory mechanisms (Clements *et al.*, 2017). These findings already indicate developmental differences of Schwann cells even in close contact to the disrupted nerve.

Strikingly, activated Schwann cells have also been detected in larger distance from the axon. The research group of Parfejevs *et al.* even described a direct involvement of peripheral glia cells (Schwann cells) in wound healing process (Parfejevs *et al.*, 2018). They showed a cellular reprogramming in addition with proliferation, and invasion of Schwann cells into the wound area (Parfejevs *et al.*, 2018). These Schwann cells originate from myelinating and

non-myelinating Schwann cells in the skin. They support a proper wound closure and induce a TGF- β 1-mediated differentiation of fibroblasts into myofibroblasts (Parfejevs *et al.*, 2018). TGF- β 1, one of the most powerful, pro-fibrotic proteins, has been identified to promote the proliferation and migration mechanisms of Schwann cells (Clements *et al.*, 2017; D'Antonio *et al.*, 2006). As extracellular TGF- β 1 increases after injury at the wound site, a potential promoting function in the invasion process of Schwann cells to this area is conceivable (Mahdavian Delavary *et al.*, 2011). Another indication for an involvement of Schwann cells in the healing process of skin wounds has been made by Reinisch *et al.* (Reinisch *et al.*, 2008). The authors showed a significantly lower amount of Schwann cells in patients suffering from diabetes mellitus (Reinisch *et al.*, 2008). It is therefore possible that the formation of diabetic foot ulcers is affected by the lack of Schwann cells. However, further studies on the involvement of Schwann cells in the healing process of (diabetic) skin wounds in humans are still required.

These findings indicate various Schwann cell subtypes arising from mature Schwann cells after injury. This assumption leads us further to question the actual terminology of “repair Schwann cells” so far associated with the neuronal regeneration, as Schwann cells involved in wound healing also contribute to a repair process. We therefore suggest a subcategorization of repair Schwann cells (e.g. fibrotic-repair Schwann cells, regenerative-repair Schwann cells, or bridging-repair Schwann cells).

“Our descent, then, is the origin of our evil passions” (Darwin, 1859)

Keloidal Schwann cells exhibit an unusual persistence in the tissue, whereas activated and dedifferentiated Schwann cells seem to disappear over time after injury. Walison *et al.* mentioned re-differentiation into mature Schwann cells or a so far not investigated second, EMT-mediated mechanism as potential fading options for Schwann cells located in the wound area (Silva *et al.*, 2018). This time-dependent decrease of Schwann cells at the wound site would be in line with our detected low amount of Schwann cells in mature scars. In contrast, repair Schwann cells closely located to the distal stump either differentiate back into their previous state induced by the contact of a vital axon or die (Sulaiman & Gordon, 2000). However, a conversion into another cell type might also be conceivable for regenerating-repair Schwann cells. These results indicate a pathologic mechanism that forces Schwann cells to persist in the tissue and/or hinders their re-differentiation, cellular conversion, or death.

The keloid is a continually growing pathologic tissue. As keloidal Schwann cells have been detected in the whole dermal area of the keloid, there has to be a solid source to provide this pathologic Schwann cells. One potential option might be the actively dividing Schwann cells detected within the keloid. However, the number of proliferating Schwann cells was rather

low and even not detectable in the keloid data generated by Deng et al. and Liu et al.. Another, more likely explanation might be that the spreading keloid constantly irritates the surrounding intact nerve fibres by alterations in tissue tension, the microenvironment and cellular composition, leading to a constant activation, dedifferentiation, and invasion of Schwann cells into the keloid area (Parfejevs *et al.*, 2018). Our finding of an increased number of keloidal Schwann cells in the surrounding skin adjacent to keloids further supports this theory.

From a developmental point of view, three options arise for keloidal Schwann cells. Pseudotime trajectories suggest that keloidal Schwann cells derive from myelinating and non-myelinating Schwann cells. This finding applies to both, repair and wound-invading Schwann cells. C-Jun and STAT3, as major factors in the development and for the maintenance of repair Schwann cells, are upregulated at the very branching point of the developmental track in the pseudotime and decrease in the direction of keloidal Schwann cells (Arthur-Farraj *et al.*, 2012; Benito *et al.*, 2017). This corresponds with the reported decrease of c-Jun following a long lack of axon contact in Schwann cells at the distal nerve stump (Gomez-Sanchez *et al.*, 2017). Keloidal Schwann cells could therefore arise from repair Schwann cells in consequence of missing attachment to the nerve system and persist due to the pathologic microenvironment in the keloid. This theory requires a former presence of nerve fibres in the keloid area, as repair Schwann cells only arise from mature Schwann cells in the distal nerve stump and also only close to the site of neuronal damage. These requirements might be given in flat keloids which spread horizontal into the healthy skin, but not in raising, bulging keloids at the earlobe with limited healthy tissue to expand. For validation of this theory, single cell data obtained from classical repair Schwann cells would be necessary to allocate them in the pseudotime trajectory. In contrast, the wound-invading Schwann cells might be a more reasonable source for keloidal Schwann cells, as they migrate through the tissue and therefore would be able to invade the neoplastic area of the keloid or even establish the pathologic spreading (Parfejevs *et al.*, 2018). This cellular migration is supposed to be triggered by the increased concentration of TGF- β 1 within the keloid (Clements *et al.*, 2017; Peltonen *et al.*, 1991). To proof this hypothetical relation, the transcriptional pattern of Schwann cells supporting a proper wound healing would be required. As third option, the keloidal Schwann cells could also arise as independent, pathologic subtype from mature Schwann cells triggered by genetic or external factors.

“It was the nightingale and not the lark” (Shakespeare, 2000)

In the last few years, scRNAseq uncovered multiple biological mechanisms. The method provides fundamental insights in the tissue composition and allows to identify so far unrecognized cellular subtypes. This promising approach has been applied to investigate

various tissue types in healthy and pathologic conditions. However, in case of the healthy skin varying factors of the method, cell isolation and the individual bioinformatics analyses, lead to considerable different results (He *et al*, 2020; Solé-Boldo *et al*, 2020; Tabib *et al*, 2018; Vorstandlechner *et al*, 2020). This scientific discrepancy has been solved by combined bioinformatic analysis of all skin datasets that resulted in a more precise idea of the actual cellular environment present in the tissue (Ascensión *et al*, 2021). This complex exploration has verified the results of the distinct studies, but also reported a more general cellular classification, detectable throughout all independent datasets (Ascensión *et al.*, 2021). Therefore, we aimed to strengthen the power of our findings through a screening including datasets generated by other research groups.

Extensive bioinformatics analysis of multiple datasets from healthy skin, normal scar, keloid and keloid adjacent skin, generated by four independent research groups allowed us to verify the keloidal Schwann cells as a keloid-specific cell type in a large number of distinct keloid types. It further paved the way to define a characteristic set of 21 genes to reliably distinguish keloidal Schwann cells from myelinating and non-myelinating Schwann cells. This set includes genes associated with matrix formation (*collagen type I alpha 1 [COL1A1]*, *collagen type VII alpha 1 [COL7A1]*, *elastin [ELN]*, *IGFBP5*, *LOXL2*, *MMP15*), cellular functions as differentiation and migration (*CCN3*, *cysteine and glycine rich protein 2 [CSR2]*, *insulin-like growth factor binding protein 3 [IGFBP3]*, *LY6/PLAUR domain-containing protein 1 [LYPD1]*, *SPARC like 1 [SPARCL1]*, *transforming growth factor beta induced [TGFB1]*, *tropomyosin 2 [TPM2]*), tumour functions (*protein phosphatase 1 regulatory inhibitor subunit 14b [PPP1R14B]*, *S100 calcium binding protein A16 [S100A16]*, *transgelin [TAGLN]*, *SH3 domain binding glutamate rich protein like 3 [SH3BGRL3]*), but also genes associated with the neuronal system and nerve development (*calbindin2 [CALB2]*, *integrin subunit beta 1 [ITGB1]*, *ectodermal-neural cortex 1 [ENC1]*, *nestin [NES]*) (Bernal & Arranz, 2018; Camp & Wijesinghe, 2009; Chen *et al*, 2014a; Chen *et al*, 2014b; Deng *et al*, 2021b; Fang *et al*, 2021; Guo *et al*, 2018; Karamanos, 2019; Lei *et al*, 2016; Lloyd-Burton & Roskams, 2012; Masuda *et al*, 2018; Min *et al*, 2016; Nie *et al*, 2021; Park *et al*, 2014; Shin *et al*, 2017; Vallet & Ricard-Blum, 2019; Watanabe *et al*, 2013; Yager & Nwomeh, 1999; Yasuoka *et al*, 2006a; Yasuoka *et al*, 2009; Yasuoka *et al*, 2006b). The identified genetic pattern provides an expressive picture of the keloidal Schwann cells and their functions and further empowers to identify the potential presence of this profibrotic Schwann cell type in other fibrotic pathologies, as scleroderma, pulmonary and cardiac fibrosis. Keloidal Schwann cells further express a large number of other matrix factors as *collagen type IV alpha 1 [COL4A1]*, *collagen type IV alpha 2 [COL4A2]*, *collagen type V alpha 1 [COL5A1]*, *collagen type V alpha 2 [COL5A2]*, *collagen type V alpha 3 [COL5A3]*, *collagen type VI alpha 1 [COL6A1]*, *collagen type VI alpha 2 [COL6A2]*, *collagen type VIII alpha 1 [COL8A1]*, *collagen*

type XII alpha 1 [COL12A1] and *tenascin* (Theocharis *et al.*, 2016). Some of these are exclusively expressed in keloidal Schwann cells compared to the remaining cell types. These findings suggest a crucial involvement of Schwann cells in the pathologic composition of the ECM in keloids.

Schwann cells as pathologic force have already been described in other diseases. In the human skin for example, the cutaneous neurofibromatosis 1 (NF1) is driven by Schwann cells (Mazuelas *et al.*, 2020). A combined analysis of Schwann cells from keloids, healthy skin and NF1 revealed almost no similarities between the detected Schwann cell populations. Pseudotime trajectory, however, set mature Schwann cells from the healthy skin as source for the aberrant Schwann cells in both pathologies. NF1-Schwann cells exhibited an inflammation-associated phenotype, whereas keloidal Schwann cells showed pro-fibrotic properties. These data highlight a decreased inflammatory component in keloid tissue that has also been proven in the general cellular setting. Inflammation has been mentioned as major impact factor on the extent of fibrosis, especially in hypertrophic scar formation (Niessen *et al.*, 1999; van der Veer *et al.*, 2009). Thereby, chronic inflammation has also been an often-discussed theory as driving force in keloids (Dong *et al.*, 2013). Our results, however, stand in contrast to this theory and at least show no pro-active inflammatory process induced by Schwann cells or inflammatory cells as dendritic cells, macrophages or T-cells.

“And where two raging fires meet together ...” (Shakespeare, 1998)

A high number of macrophages, as active cellular parts in inflammation and fibrosis, was detected in keloids. However, the majority of macrophages identified in our datasets were classified as M2 or at least M1/M2 intermediately polarized, indicating an involvement in the fibrotic pathomechanism of keloids. These findings confirm the previously reported general increase of macrophages with a high proportion of M2 macrophages in keloids (Bagabir *et al.*, 2012a; Boyce *et al.*, 2001; Jin *et al.*, 2018). M2 macrophages display a key regulator in the dermal wound healing, especially in the remodelling phase (Goerdts & Orfanos, 1999; Greenlee-Wacker, 2016). They support the production of ECM and are even able to differentiate into myofibroblasts (Mahdavian Delavary *et al.*, 2011; Wang *et al.*, 2016). Repair Schwann cells on the other side are known to attract and interact with macrophages to support myelin degradation, vascularization, and matrix formation at the site of neuronal damage (Jessen & Mirsky, 2019a). We were able to identify a pro-fibrotic interaction of Schwann cells and macrophages in keloids. This crosstalk of Schwann cells and macrophages is established by the secretion of several factors and thereby induces a pathology-supporting environment similar to a vicious circle. This process involves well-known proteins that typically occur in wound healing as CCL2, CCL3, TNF- α , MMP9, growth

arrest specific 6 (GAS6), but also CCN3, IGFBP3 and IGFBP5 as members of the characteristic expression pattern of keloidal Schwann cells.

One of the strongest regulated genes in keloidal Schwann cells that is also a member of the cell-type specific expression panel was IGFBP5. Staining of this factor revealed an extensive presence of IGFBP5 in the extracellular space of keloids, presumably established exclusively by keloidal Schwann cells. IGFBP5 has been described as an important pro-fibrotic factor in wound healing of the skin (Yasuoka *et al.*, 2009). It induces the invasion of fibroblasts, monocytes, NK cells and T cells to the site of injury (Yasuoka *et al.*, 2009). An overexpression of IGFBP5 was shown to induce an increase in dermal thickness and thickness of collagen bundles, both characteristic attributes of keloids (Yasuoka *et al.*, 2006a). Strikingly, this study further revealed that IGFBP5 induced a general increase in collagen, fibronectin and myofibroblasts in the skin, which are further prominent characteristics of keloids (Yasuoka *et al.*, 2006a). This insight alone suggests a significant contribution of the keloidal Schwann cells exclusively producing IGFBP5 to keloid formation. However, we identified several other factors involved in the pathologic characteristics of keloids. IGFBP3, another upregulated factor, has been shown to supply anti-inflammatory features (Min *et al.*, 2016). CCN3, as member of the specific keloidal Schwann cell pattern, is involved in the attraction of macrophages and additionally promotes the change of M1 macrophages into the M2 type (Chen *et al.*, 2014b). However, the potential effect of CCN3 in keloids should not be attributed to Schwann cells only, as keloidal melanocytes also exhibit increased levels of CCN3.

In 2009, Seki *et al.* showed a contribution of CCL2 in fibrotic process (Seki *et al.*, 2009). CCL2, also known as MCP-1, is an important factor in healing process of the skin by recruiting cells to the wound site, especially monocytes/macrophages (Werner & Grose, 2003). The significantly lower levels of CCL2 further might affect the attraction of M1 polarized macrophages to the keloid. CCL2 has also been discussed as factor affecting the extent of scarring (Ferreira *et al.*, 2006). However, this finding might depend rather on the cell types attracted by CCL2 than on a direct pro-fibrotic effect (Werner & Grose, 2003). This is also in line with the reported effect of CCL2 on the regulation of MMP9 (Robinson *et al.*, 2002). Robinson *et al.* uncovered the stimulating effects of CCL2, but also CCL3 and TNF- α , on the production of the ECM-degrading MMP9 in monocytes (Robinson *et al.*, 2002). Our findings of decreased levels of CCL2, CCL3 and TNF- α in keloidal cells, in addition with significantly lower levels of MMP9, suggest a contribution of this mechanism to the pathologic ECM composition. The low level of MMP9 in keloids further affects the status of Schwann cells, as an increase of MMP9 has been described to prevent Schwann cells from proliferation and dedifferentiation (Kim *et al.*, 2012). Reversely, a lack of MMP9 would therefore support the altered state of keloidal Schwann cells. Growth arrest-specific 6 protein

(GAS6) is another factor, that has been described in association with the cellular interaction of macrophages and Schwann cells (Stratton *et al*, 2018). GAS6 produced by macrophages promotes the re-differentiation of Schwann cells once neuronal repair is finished (Stratton *et al.*, 2018). Decreased level of GAS6 on a genetic as well as a protein level, suggest this protein as another key player in the pathologic cellular interplay of keloids.

Schwann cells in keloids further revealed a significant upregulation of tumor necrosis factor alpha-induced protein 6 (TNFAIP6). The product of TNFAIP6 is the hyaluronan-binding protein TNF-stimulated gene 6 (TSG-6) which has been shown to inhibit the migration of neutrophils, reduces the expression of neutrophil elastase and pro-inflammatory cytokines and inhibits the protease network, all features that lead to a decrease in inflammation (Getting *et al*, 2002; Lin *et al*, 2013; Nagyeri *et al*, 2011). TSG-6 additionally inhibits the STAT3 activity in macrophages to support a cellular M2 polarization (Mittal *et al*, 2016; Wan *et al*, 2020). An increase of TNFAIP6 in Schwann cells therefore might induce the reported reduced inflammation pattern and enhance M2 macrophage phenotype in keloids.

Together, these findings point out a pathologic intermezzo of Schwann cells and macrophages resulting in a pro-fibrotic, ECM and cell-state modifying vicious circle.

“We know what we are, but know not what we may be” (Shakespeare, 1954)

The macrophage subset analysis further identified a macrophage subcluster, expressing genes characteristic for macrophages as well as fibroblasts. Macrophages are known to have the potential to trans-differentiate into mesenchymal cells. The conversion can be induced by IGFBP5, which is also one of the main factors produced by keloidal Schwann cells (Yasuoka *et al.*, 2009). The finding of the MAC-FB cluster is equivalent to the SC-EC and SC-FB cell cluster, as scRNAseq analysis also identified specific Schwann cell cluster, with a transcriptional pattern typical for Schwann cells as well as for endothelial cells or fibroblasts. A potential of Schwann cells to convert into other cell types has already been reported (Jessen & Arthur-Farraj, 2019). Especially repair Schwann cells of the distal nerve stump revealed a high potential for EMT (Clements *et al.*, 2017). We managed to verify the detected intermediate Schwann cell types by staining. Additionally, the presence of SC-EC in the cutaneous neurofibromatosis type 1 datasets encouraged these findings. However, a high amount of Schwann cell seems to be required for a cluster formation of these specific cellular subtypes in scRNAseq analysis, as datasets of Deng *et al.* as well as Liu *et al.* did not reveal any SC-FB or SC-EC cluster in case of a source exclusive analysis. Additionally, characteristic genes for EMT and endoMT-like conversion as TWIST1, zinc finger e-box binding homeobox 1 (ZEB1), ZEB2, snail family transcriptional repressor 2 (SLUG), snail family transcriptional repressor 1 (SNAIL) were not expressed in the mentioned Schwann

cell- or macrophage-intermediate cell cluster (Thiery *et al*, 2009). However, these findings would correspond to the increased cellular plasticity in keloid tissue.

“There is nothing either good or bad ...” (Shakespeare, 1954)

The comparability of scRNAseq data sets and the findings still pose a challenging task. Different protocols for the preparation of single cells, together with changes in the sequencing method and the bioinformatic calculations in addition with donor variability affect the final data sets and the results and conclusions. Cellular heterogeneity of a certain tissue is also a varying component that should receive attention. In case of Schwann cells, a varying cellular density within the skin has been reported depending on the body site and potential pathologies (Reinisch & Tschachler, 2012). Already in 2017, van den Brink *et al.* elaborated on the detected cluster in their single cell analysis that is primarily a result of the dissociation protocol (van den Brink *et al*, 2017). Especially the duration of the dissociation step appeared to induce significant changes in the transcriptome of some cells, leading to a strong upregulation of IEG and HSP genes (van den Brink *et al.*, 2017). These changes have been interpreted as partial activation of cells that reside in a quiescent state in tissue (van den Brink *et al.*, 2017). Several further studies support the reported results of (Machado *et al*, 2017; van Velthoven *et al*, 2017; Wu *et al*, 2019; Wu *et al*, 2017) dissociation-induced alterations in the cellular transcriptome (Adam *et al*, 2017; Bakken *et al*, 2018; Lacar *et al*, 2016). Further important factors affecting the final single cell dataset are the tissue temperature during the dissociation step and the cellular condition prior the preservation of the transcriptome (fresh, cryopreserved or methanol-fixed) (Denisenko *et al*, 2020). However, depending on the cell type of interest, a faster and more intensive processing can also be recommended (Denisenko *et al.*, 2020). Cryopreservation of cells results in a decrease of epithelial cells, whereas methanol fixation leads to an increase leakage of ambient RNA (Denisenko *et al.*, 2020). All these findings indicate an individual adaption of protocols depending on the tissue type and intention of the study. The end result of this situation are multiple datasets, even for the same tissue type, due to individual approaches for preparation, dissociation and cellular preservation. (He *et al.*, 2020; Solé-Boldo *et al.*, 2020; Tabib *et al.*, 2018; Vorstandlechner *et al.*, 2020). However, as scRNAseq offers the opportunity to recombine published datasets to investigate new scientific questions, a standardisation of the tissue pre-processing step would be desirable but inevitably come along with limitations in certain cell type clusters. Machado *et al.* identified a genetic stress signature due to the dissociation step that allow to detect the biased results and to appropriately adapt the bioinformatics analysis (Machado *et al*, 2021).

The whole skin dissociation kit is one of the most frequently used enzyme mixture for skin dissociation in scRNAseq experiments (Ascensión *et al.*, 2021; Liu *et al.*, 2021;

Vorstandlechner *et al.*, 2021). As an alternative, tissue dissociation for two hours using dispase II and collagenase IV has been reported (Deng *et al.*, 2021a). Regarding an optimal single cell RNA seq analysis with focus on keloidal Schwann cells, our study suggests the application of the whole skin dissociation kit for about two hours to isolate keloidal Schwann cells from the tissue. Focusing on myelinating and non-myelinating Schwann cells, our findings suggest a prolonged dissociation time to detach the myelinating and non-myelinating Schwann cells more efficiently from their axons. This results further supports previous findings from Weiss *et al.* (Weiss *et al.*, 2018). The activation of Schwann cells located close and distal of the disrupted nerve occurs immediately after the neuronal damage, leading to a change in the transcriptional profile within hours (Rotshenker, 2011). We assume that the same transcriptional changes take place in the excised and dissociated skin tissue isolated for single cell analysis. Depending on the focus of the analysis, this situation confronts us with the fact that an isolation of a high amount of mature inactivated Schwann cells is almost impossible. Therefore, we must decide between a short-term tissue dissociation step with a low cellular yield and inactivated Schwann cells, or a long-term dissociation step with a high amount of Schwann cells but in an activated state. Nevertheless, the high numbers of keloidal Schwann cells in all datasets analysed here imply a much easier isolation of keloidal Schwann cells, probably due to their axon-independent presence in the tissue. The number of Schwann cells detected in normal scars varied between the tissue-specific and the comprehensive analysis. This could indicate an algorithmic phenomenon that cell types, present in a very low number are neglected in the cluster formation, while favouring the cell types present in large amounts. For the analysis of rare cell types, our study therefore suggests to involve at least one independent target cell-rich data set in the analysis for proper cluster formation. After cluster formation, the cell-rich dataset should be excluded from the analysis. However, cell characterisation must be proven afterwards as our results also displayed a certain amount of cluster contamination.

In addition to the dataset variations caused by the tissue pre-processing, the bioinformatics analysis of scRNAseq data is still not standardized (Slovin *et al.*, 2021). The average scRNAseq analysis usually consists of multiple consecutive steps as quality control, normalization, batch effect correction, visualization, unsupervised clustering but also cell cycle assignment, imputation and smoothing and projection. Following cluster annotation identification of differentially expressed genes comparing individual cluster combinations and subsets or pseudotime trajectory calculation can be performed (Andrews *et al.*, 2021). Andrews *et al.* mentioned at least two potential tools for each step (Andrews *et al.*, 2021). This indicates an almost unmanageable number of possible combinations for each analysis. In addition, multiple standard commands of each tool can be adopted and most of the tools are continuously developed. Varying UMAP plots or t-SNE graphs with varying numbers of

clusters, including over-clustering in the worst cases, and inconsistent distribution of detected cells are the consequence (Andrews *et al.*, 2021). For this reason, reported results, especially in case of excessive clustering or sub setting should be examined critically. However, the spatial assignment of the main cell types and major transcriptional differences seem to be independent from the analytic approach. To address this issue, Slovin *et al.* recently initiated a trial to standardize analysis or at least to provide up-to-date, ready-to-use pipelines for scRNAseq (Slovin *et al.*, 2021). Additionally, a verification of the transcriptional findings by a second method or on protein level is always recommendable. For our scRNAseq analysis, we applied Seurat as basic package, which is one of the best-established tools for scRNAseq that additionally provides feasible vignettes for the data set investigation.

3.1 Conclusion & future prospects

We provide evidence for the presence of a so far undescribed Schwann cell subtype in the tissue of keloids. These keloidal Schwann cells reside within the pathological tissue in a single cellular manner without any contact to axons. The transcriptional profile of keloidal Schwann cells uncovered their dedifferentiated state with features highly associated with matrix formation. However, the keloidal Schwann cells show characteristics typical for the neuro-regenerative “*repair Schwann cells*”, as a lack of specific cell markers was noticed. Additional comparison with cutaneous neurofibroma datasets clarified a clear distinction of keloidal Schwann cells to the pathologic Schwann cells involved in neurofibroma type 1.

In-depth analysis of keloidal Schwann cell and macrophages uncovered a potential interaction of both cell types, inducing a pathology-supporting state. We therefore suggest that the crosstalk of pro-fibrotic, keloidal Schwann cells and macrophages as a driving force in keloid formation and expansion. A comprehensive dataset evaluation obtained by three independent research groups, confirmed the increased number of pro-fibrotic Schwann cells in keloids and lead to the definition of a genetic panel specific for this cell type. Variable dataset combinations further highlight advantages and disadvantages of bioinformatics analysis of scRNAseq data and provides important information for the extraction of Schwann cells from skin tissue.

Our work describes pro-fibrotic Schwann cells as new key-players in keloid formation. Treatments targeting keloidal Schwann cells to induce a reduction or re-differentiation of these cells might therefore suggest a novel approach for the therapy of keloids. Based on our findings, the next step would be to compare the keloidal Schwann cells with repair Schwann cells gained from the peripheral nerve collected at different time points. ScRNAseq datasets of these Schwann cells would help to point out transcriptional similarities and differences between these subtypes und to allocate the repair Schwann cells in a common pseudotime trajectory. Furthermore, an establishment of keloidal Schwann cell cultures is essential for a better understanding of their features and to evaluate intercellular effects in co-culture with other cells. These *in vitro* models would further support identification and development of effective treatments.

4 CHAPTER FOUR: MATERIALS & METHODS

Materials and methods applied in this thesis are described in detail in the respective publications.

References

- Aarabi S, Bhatt KA, Shi Y, Paterno J, Chang EI, Loh SA, Holmes JW, Longaker MT, Yee H, Gurtner GC (2007) Mechanical load initiates hypertrophic scar formation through decreased cellular apoptosis. *Faseb j* 21: 3250-3261
- Abraira VE, Ginty DD (2013) The sensory neurons of touch. *Neuron* 79: 618-639
- Adam M, Potter AS, Potter SS (2017) Psychrophilic proteases dramatically reduce single-cell RNA-seq artifacts: a molecular atlas of kidney development. *Development* 144: 3625-3632
- Adameyko I, Lallemand F, Aquino JB, Pereira JA, Topilko P, Müller T, Fritz N, Beljajeva A, Mochii M, Liste I *et al* (2009) Schwann cell precursors from nerve innervation are a cellular origin of melanocytes in skin. *Cell* 139: 366-379
- Akaishi S, Ogawa R, Hyakusoku H (2008) Keloid and hypertrophic scar: neurogenic inflammation hypotheses. *Med Hypotheses* 71: 32-38
- Akaishi S, Ogawa R, Hyakusoku H (2010) Visual and pathologic analyses of keloid growth patterns. *Ann Plast Surg* 64: 80-82
- Akino K, Akita S, Yakabe A, Minoda T, Hayashi T, Hirano A (2008) Human mesenchymal stem cells may be involved in keloid pathogenesis. *Int J Dermatol* 47: 1112-1117
- Al-Attar A, Mess S, Thomassen JM, Kauffman CL, Davison SP (2006) Keloid pathogenesis and treatment. *Plast Reconstr Surg* 117: 286-300
- Alonso PE, Rioja LF, Pera C (2008) Keloids: A viral hypothesis. *Med Hypotheses* 70: 156-166
- Amadeu TP, Braune AS, Porto LC, Desmoulière A, Costa AM (2004) Fibrillin-1 and elastin are differentially expressed in hypertrophic scars and keloids. *Wound Repair Regen* 12: 169-174
- Andrews TS, Kiselev VY, McCarthy D, Hemberg M (2021) Tutorial: guidelines for the computational analysis of single-cell RNA sequencing data. *Nat Protoc* 16: 1-9
- Appleton I, Brown NJ, Willoughby DA (1996) Apoptosis, necrosis, and proliferation: possible implications in the etiology of keloids. *Am J Pathol* 149: 1441-1447
- Armstrong SJ, Wiberg M, Terenghi G, Kingham PJ (2007) ECM molecules mediate both Schwann cell proliferation and activation to enhance neurite outgrowth. *Tissue Eng* 13: 2863-2870
- Arthur-Farraj PJ, Latouche M, Wilton DK, Quintes S, Chabrol E, Banerjee A, Woodhoo A, Jenkins B, Rahman M, Turmaine M *et al* (2012) c-Jun reprograms Schwann cells of injured nerves to generate a repair cell essential for regeneration. *Neuron* 75: 633-647
- Ascensión AM, Fuertes-Álvarez S, Ibañez-Solé O, Izeta A, Araúzo-Bravo MJ (2021) Human Dermal Fibroblast Subpopulations Are Conserved across Single-Cell RNA Sequencing Studies. *J Invest Dermatol* 141: 1735-1744.e1735
- Aumailley M (2013) The laminin family. *Cell Adh Migr* 7: 48-55
- Bagabir R, Byers RJ, Chaudhry IH, Müller W, Paus R, Bayat A (2012a) Site-specific immunophenotyping of keloid disease demonstrates immune upregulation and the presence of lymphoid aggregates. *Br J Dermatol* 167: 1053-1066
- Bagabir R, Syed F, Paus R, Bayat A (2012b) Long-term organ culture of keloid disease tissue. *Exp Dermatol* 21: 376-381
- Bailey AJ, Bazin S, Sims TJ, Le Lous M, Nicoletis C, Delaunay A (1975) Characterization of the collagen of human hypertrophic and normal scars. *Biochim Biophys Acta* 405: 412-421
- Bakken TE, Hodge RD, Miller JA, Yao Z, Nguyen TN, Aevermann B, Barkan E, Bertagnolli D, Casper T, Dee N *et al* (2018) Single-nucleus and single-cell transcriptomes compared in matched cortical cell types. *PLoS One* 13: e0209648
- Balci DD, Inandi T, Dogramaci CA, Celik E (2009) DLQI scores in patients with keloids and hypertrophic scars: a prospective case control study. *J Dtsch Dermatol Ges* 7: 688-692
- Barrette B, Hébert MA, Filali M, Lafortune K, Vallières N, Gowing G, Julien JP, Lacroix S (2008) Requirement of myeloid cells for axon regeneration. *J Neurosci* 28: 9363-9376
- Battiston B, Geuna S, Ferrero M, Tos P (2005) Nerve repair by means of tubulization: literature review and personal clinical experience comparing biological and synthetic conduits for sensory nerve repair. *Microsurgery* 25: 258-267

Baum CL, Arpey CJ (2005) Normal cutaneous wound healing: clinical correlation with cellular and molecular events. *Dermatol Surg* 31: 674-686; discussion 686

Bayat A, Arscott G, Ollier WE, McGrouther DA, Ferguson MW (2005) Keloid disease: clinical relevance of single versus multiple site scars. *Br J Plast Surg* 58: 28-37

Bayat A, McGrouther DA, Ferguson MW (2003) Skin scarring. *Bmj* 326: 88-92

Bella H, Heise M, Yagi KI, Black G, McGrouther DA, Bayat A (2011) A clinical characterization of familial keloid disease in unique African tribes reveals distinct keloid phenotypes. *Plast Reconstr Surg* 127: 689-702

Benito C, Davis CM, Gomez-Sanchez JA, Turmaine M, Meijer D, Poli V, Mirsky R, Jessen KR (2017) STAT3 Controls the Long-Term Survival and Phenotype of Repair Schwann Cells during Nerve Regeneration. *J Neurosci* 37: 4255-4269

Bernal A, Arranz L (2018) Nestin-expressing progenitor cells: function, identity and therapeutic implications. *Cell Mol Life Sci* 75: 2177-2195

Bertheim U, Hellström S (1994) The distribution of hyaluronan in human skin and mature, hypertrophic and keloid scars. *Br J Plast Surg* 47: 483-489

Besn e I, Descombes C, Breton L (2002) Effect of age and anatomical site on density of sensory innervation in human epidermis. *Arch Dermatol* 138: 1445-1450

Bhattacharyya A, Oppenheim RW, Prevet e D, Moore BW, Brackenbury R, Ratner N (1992) S100 is present in developing chicken neurons and Schwann cells and promotes motor neuron survival in vivo. *J Neurobiol* 23: 451-466

Bijlard E, Kouwenberg CA, Timman R, Hovius SE, Busschbach JJ, Mureau MA (2017) Burden of Keloid Disease: A Cross-sectional Health-related Quality of Life Assessment. *Acta Derm Venereol* 97: 225-229

Boerboom A, Dion V, Chariot A, Franzen R (2017) Molecular Mechanisms Involved in Schwann Cell Plasticity. *Front Mol Neurosci* 10: 38

Bombaro KM, Engrav LH, Carrougher GJ, Wiechman SA, Faucher L, Costa BA, Heimbach DM, Rivara FP, Honari S (2003) What is the prevalence of hypertrophic scarring following burns? *Burns* 29: 299-302

Bosse F, Hasenpusch-Theil K, K ury P, M uller HW (2006) Gene expression profiling reveals that peripheral nerve regeneration is a consequence of both novel injury-dependent and reactivated developmental processes. *J Neurochem* 96: 1441-1457

Boyce DE, Ciampolini J, Ruge F, Murison MS, Harding KG (2001) Inflammatory-cell subpopulations in keloid scars. *Br J Plast Surg* 54: 511-516

Boyd JG, Gordon T (2003) Neurotrophic factors and their receptors in axonal regeneration and functional recovery after peripheral nerve injury. *Mol Neurobiol* 27: 277-324

Breasted JH (1930) Case Forty-five, Bulging Tumors on the Breast The Edwin Smith surgical papyrus. *The University of Chicago Press, Chicago, Illinois* Vol. 1: 463

Brennan A, Dean CH, Zhang AL, Cass DT, Mirsky R, Jessen KR (2000) Endothelins control the timing of Schwann cell generation in vitro and in vivo. *Dev Biol* 227: 545-557

Britsch S, Goerich DE, Riethmacher D, Peirano RI, Rossner M, Nave KA, Birchmeier C, Wegner M (2001) The transcription factor Sox10 is a key regulator of peripheral glial development. *Genes Dev* 15: 66-78

Brosius Lutz A, Chung WS, Sloan SA, Carson GA, Zhou L, Lovelett E, Posada S, Zuchero JB, Barres BA (2017) Schwann cells use TAM receptor-mediated phagocytosis in addition to autophagy to clear myelin in a mouse model of nerve injury. *Proc Natl Acad Sci U S A* 114: E8072-e8080

Broughton G, 2nd, Janis JE, Attinger CE (2006) The basic science of wound healing. *Plast Reconstr Surg* 117: 12s-34s

Brown BC, McKenna SP, Siddhi K, McGrouther DA, Bayat A (2008) The hidden cost of skin scars: quality of life after skin scarring. *J Plast Reconstr Aesthet Surg* 61: 1049-1058

Brown EJ (1995) Phagocytosis. *Bioessays* 17: 109-117

Buechler C, Ritter M, Ors o E, Langmann T, Klucken J, Schmitz G (2000) Regulation of scavenger receptor CD163 expression in human monocytes and macrophages by pro- and antiinflammatory stimuli. *J Leukoc Biol* 67: 97-103

Buraschi S, Neill T, Iozzo RV (2019) Decorin is a devouring proteoglycan: Remodeling of intracellular catabolism via autophagy and mitophagy. *Matrix Biol* 75-76: 260-270

Burd A (2006) Keloid epidemiology: population based studies needed. *J Plast Reconstr Aesthet Surg* 59: 105

Burd A, Huang L (2005) Hypertrophic response and keloid diathesis: two very different forms of scar. *Plast Reconstr Surg* 116: 150e-157e

Burnett MG, Zager EL (2004) Pathophysiology of peripheral nerve injury: a brief review. *Neurosurg Focus* 16: E1

Burton PR, Wentz MA (1992) Neurofilaments are prominent in bullfrog olfactory axons but are rarely seen in those of the tiger salamander, *Ambystoma tigrinum*. *J Comp Neurol* 317: 396-406

Butler PD, Longaker MT, Yang GP (2008) Current progress in keloid research and treatment. *J Am Coll Surg* 206: 731-741

Butzelaar L, Niessen FB, Talhout W, Schooneman DPM, Ulrich MM, Beelen RHJ, Mink van der Molen AB (2017) Different properties of skin of different body sites: The root of keloid formation? *Wound Repair Regen* 25: 758-766

Butzelaar L, Schooneman DP, Soykan EA, Talhout W, Ulrich MM, van den Broek LJ, Gibbs S, Beelen RH, Mink van der Molen AB, Niessen FB (2016) Inhibited early immunologic response is associated with hypertrophic scarring. *Exp Dermatol* 25: 797-804

Bux S, Madaree A (2012) Involvement of upper torso stress amplification, tissue compression and distortion in the pathogenesis of keloids. *Med Hypotheses* 78: 356-363

Camp AJ, Wijesinghe R (2009) Calretinin: modulator of neuronal excitability. *Int J Biochem Cell Biol* 41: 2118-2121

Carrino DA, Mesiano S, Barker NM, Hurd WW, Caplan AI (2012) Proteoglycans of uterine fibroids and keloid scars: similarity in their proteoglycan composition. *Biochem J* 443: 361-368

Causey G, Barton AA (1959) The cellular content of the endoneurium of peripheral nerve. *Brain* 82: 594-598

Chan CK, Rolle MW, Potter-Perigo S, Braun KR, Van Biber BP, Laflamme MA, Murry CE, Wight TN (2010) Differentiation of cardiomyocytes from human embryonic stem cells is accompanied by changes in the extracellular matrix production of versican and hyaluronan. *J Cell Biochem* 111: 585-596

Chen CH, Ho HH, Wu ML, Layne MD, Yet SF (2014a) Modulation of cysteine-rich protein 2 expression in vascular injury and atherosclerosis. *Mol Biol Rep* 41: 7033-7041

Chen PC, Cheng HC, Wang J, Wang SW, Tai HC, Lin CW, Tang CH (2014b) Prostate cancer-derived CCN3 induces M2 macrophage infiltration and contributes to angiogenesis in prostate cancer microenvironment. *Oncotarget* 5: 1595-1608

Chen Y, Jin Q, Fu X, Qiao J, Niu F (2019) Connection between T regulatory cell enrichment and collagen deposition in keloid. *Exp Cell Res* 383: 111549

Chen ZL, Yu WM, Strickland S (2007) Peripheral regeneration. *Annu Rev Neurosci* 30: 209-233

Chin MS, Lancerotto L, Helm DL, Dastouri P, Prsa MJ, Ottensmeyer M, Akaishi S, Orgill DP, Ogawa R (2009) Analysis of neuropeptides in stretched skin. *Plast Reconstr Surg* 124: 102-113

Chong Y, Kim CW, Kim YS, Chang CH, Park TH (2018) Complete excision of proliferating core in auricular keloids significantly reduces local recurrence: A prospective study. *J Dermatol* 45: 139-144

Chrysanthopoulou A, Mitroulis I, Apostolidou E, Arelaki S, Mikroulis D, Konstantinidis T, Sivridis E, Koffa M, Giatromanolaki A, Boumpas DT *et al* (2014) Neutrophil extracellular traps promote differentiation and function of fibroblasts. *J Pathol* 233: 294-307

Chua AW, Ma D, Gan SU, Fu Z, Han HC, Song C, Sabapathy K, Phan TT (2011) The role of R-spondin2 in keratinocyte proliferation and epidermal thickening in keloid scarring. *J Invest Dermatol* 131: 644-654

Clark RA (1983) Fibronectin in the skin. *J Invest Dermatol* 81: 475-479

Clark RA (1985) Cutaneous tissue repair: basic biologic considerations. I. *J Am Acad Dermatol* 13: 701-725

Clark RA, Lanigan JM, DellaPelle P, Manseau E, Dvorak HF, Colvin RB (1982) Fibronectin and fibrin provide a provisional matrix for epidermal cell migration during wound reepithelialization. *J Invest Dermatol* 79: 264-269

Clements MP, Byrne E, Camarillo Guerrero LF, Cattin AL, Zakka L, Ashraf A, Burden JJ, Khadayate S, Lloyd AC, Marguerat S *et al* (2017) The Wound Microenvironment Reprograms Schwann Cells to Invasive Mesenchymal-like Cells to Drive Peripheral Nerve Regeneration. *Neuron* 96: 98-114.e117

Cobbold CA (2001) The role of nitric oxide in the formation of keloid and hypertrophic lesions. *Med Hypotheses* 57: 497-502

Comper WD, Williams RP, Zamparo O (1990) Water transport in extracellular matrices. *Connect Tissue Res* 25: 89-102

Conway H, Gillette R, Smith JW, Findley A (1960) Differential diagnosis of keloids and hypertrophic scars by tissue culture technique with notes on therapy of keloids by surgical excision and decadron. *Plast Reconstr Surg Transplant Bull* 25: 117-132

Crowe R, Parkhouse N, McGrouther D, Burnstock G (1994) Neuropeptide-containing nerves in painful hypertrophic human scar tissue. *Br J Dermatol* 130: 444-452

D'Antonio M, Droggiti A, Feltri ML, Roes J, Wrabetz L, Mirsky R, Jessen KR (2006) TGFbeta type II receptor signaling controls Schwann cell death and proliferation in developing nerves. *J Neurosci* 26: 8417-8427

D'Orazio J, Jarrett S, Amaro-Ortiz A, Scott T (2013) UV radiation and the skin. *Int J Mol Sci* 14: 12222-12248

Daley JM, Brancato SK, Thomay AA, Reichner JS, Albina JE (2010) The phenotype of murine wound macrophages. *J Leukoc Biol* 87: 59-67

Dalkowski A, Schuppan D, Orfanos CE, Zouboulis CC (1999) Increased expression of tenascin C by keloids in vivo and in vitro. *Br J Dermatol* 141: 50-56

Darwin C (1859) *The Origin of Species*. London:John Murray: 371

De Felipe C, Hunt SP (1994) The differential control of c-jun expression in regenerating sensory neurons and their associated glial cells. *J Neurosci* 14: 2911-2923

Deckers J, Hammad H, Hoste E (2018) Langerhans Cells: Sensing the Environment in Health and Disease. *Front Immunol* 9: 93

Demling RH (2005) The burn edema process: current concepts. *J Burn Care Rehabil* 26: 207-227

Deng CC, Hu YF, Zhu DH, Cheng Q, Gu JJ, Feng QL, Zhang LX, Xu YP, Wang D, Rong Z *et al* (2021a) Single-cell RNA-seq reveals fibroblast heterogeneity and increased mesenchymal fibroblasts in human fibrotic skin diseases. *Nat Commun* 12: 3709

Deng M, Peng L, Li J, Liu X, Xia X, Li G (2021b) PPP1R14B Is a Prognostic and Immunological Biomarker in Pan-Cancer. *Front Genet* 12: 763561

Denisenko E, Guo BB, Jones M, Hou R, de Kock L, Lassmann T, Poppe D, Clément O, Simmons RK, Lister R *et al* (2020) Systematic assessment of tissue dissociation and storage biases in single-cell and single-nucleus RNA-seq workflows. *Genome Biol* 21: 130

Derderian CA, Bastidas N, Lerman OZ, Bhatt KA, Lin SE, Voss J, Holmes JW, Levine JP, Gurtner GC (2005) Mechanical strain alters gene expression in an in vitro model of hypertrophic scarring. *Ann Plast Surg* 55: 69-75; discussion 75

Dhillon AP, Rode J, Dhillon DP, Moss E, Thompson RJ, Spiro SG, Corrin B (1985) Neural markers in carcinoma of the lung. *Br J Cancer* 51: 645-652

Do DV, Ong CT, Khoo YT, Carbone A, Lim CP, Wang S, Mukhopadhyay A, Cao X, Cho DH, Wei XQ *et al* (2012) Interleukin-18 system plays an important role in keloid pathogenesis via epithelial-mesenchymal interactions. *Br J Dermatol* 166: 1275-1288

Donato R (2003) Intracellular and extracellular roles of S100 proteins. *Microsc Res Tech* 60: 540-551

Donato R, Cannon BR, Sorci G, Riuzzi F, Hsu K, Weber DJ, Geczy CL (2013) Functions of S100 proteins. *Curr Mol Med* 13: 24-57

Dong X, Mao S, Wen H (2013) Upregulation of proinflammatory genes in skin lesions may be the cause of keloid formation (Review). *Biomed Rep* 1: 833-836

Dong Z, Brennan A, Liu N, Yarden Y, Lefkowitz G, Mirsky R, Jessen KR (1995) Neu differentiation factor is a neuron-glia signal and regulates survival, proliferation, and maturation of rat Schwann cell precursors. *Neuron* 15: 585-596

Driskell RR, Jahoda CA, Chuong CM, Watt FM, Horsley V (2014) Defining dermal adipose tissue. *Exp Dermatol* 23: 629-631

Drummond PD, Dawson LF, Wood FM, Fear MW (2018) Up-regulation of $\alpha(1)$ -adrenoceptors in burn and keloid scars. *Burns* 44: 582-588

Duncan MR, Frazier KS, Abramson S, Williams S, Klapper H, Huang X, Grotendorst GR (1999) Connective tissue growth factor mediates transforming growth factor beta-induced collagen synthesis: down-regulation by cAMP. *Faseb j* 13: 1774-1786

Dunkin CSJ, Pleat JM, Gillespie PH, Tyler MPH, Roberts AHN, McGrouther DA (2007) Scarring occurs at a critical depth of skin injury: precise measurement in a graduated dermal scratch in human volunteers. *Plast Reconstr Surg* 119: 1722-1732

Dyachuk V, Furlan A, Shahidi MK, Giovenco M, Kaukua N, Konstantinidou C, Pachnis V, Memic F, Marklund U, Müller T *et al* (2014) Neurodevelopment. Parasympathetic neurons originate from nerve-associated peripheral glial progenitors. *Science* 345: 82-87

Eckes B, Nischt R, Krieg T (2010) Cell-matrix interactions in dermal repair and scarring. *Fibrogenesis Tissue Repair* 3: 4

Eggers R, Tannemaat MR, Ehlert EM, Verhaagen J (2010) A spatio-temporal analysis of motoneuron survival, axonal regeneration and neurotrophic factor expression after lumbar ventral root avulsion and implantation. *Exp Neurol* 223: 207-220

Eming SA, Krieg T, Davidson JM (2007) Inflammation in wound repair: molecular and cellular mechanisms. *J Invest Dermatol* 127: 514-525

English RS, Shenefelt PD (1999) Keloids and hypertrophic scars. *Dermatol Surg* 25: 631-638

Engrav LH, Covey MH, Dutcher KD, Heimbach DM, Walkinshaw MD, Marvin JA (1987) Impairment, time out of school, and time off from work after burns. *Plast Reconstr Surg* 79: 927-934

Erdag G, Qureshi HS, Patterson JW, Wick MR (2008) CD34-positive dendritic cells disappear from scars but are increased in pericicatrical tissue. *J Cutan Pathol* 35: 752-756

Esselman PC, Thombs BD, Magyar-Russell G, Fauerbach JA (2006) Burn rehabilitation: state of the science. *Am J Phys Med Rehabil* 85: 383-413

Fang D, Zhang C, Xu P, Liu Y, Mo X, Sun Q, Abdelatty A, Hu C, Xu H, Zhou G *et al* (2021) S100A16 promotes metastasis and progression of pancreatic cancer through FGF19-mediated AKT and ERK1/2 pathways. *Cell Biol Toxicol* 37: 555-571

Fang F, Huang RL, Zheng Y, Liu M, Huo R (2016) Bone marrow derived mesenchymal stem cells inhibit the proliferative and profibrotic phenotype of hypertrophic scar fibroblasts and keloid fibroblasts through paracrine signaling. *J Dermatol Sci* 83: 95-105

Fantin A, Vieira JM, Gestri G, Denti L, Schwarz Q, Prykhozhiy S, Peri F, Wilson SW, Ruhrberg C (2010) Tissue macrophages act as cellular chaperones for vascular anastomosis downstream of VEGF-mediated endothelial tip cell induction. *Blood* 116: 829-840

Ferreira AM, Takagawa S, Fresco R, Zhu X, Varga J, DiPietro LA (2006) Diminished induction of skin fibrosis in mice with MCP-1 deficiency. *J Invest Dermatol* 126: 1900-1908

Fhayli W, Boëté Q, Harki O, Briançon-Marjollet A, Jacob MP, Faury G (2019) Rise and fall of elastic fibers from development to aging. Consequences on arterial structure-function and therapeutical perspectives. *Matrix Biol* 84: 41-56

Foreman JC (1987a) Peptides and neurogenic inflammation. *Br Med Bull* 43: 386-400

Foreman JC (1987b) Substance P and calcitonin gene-related peptide: effects on mast cells and in human skin. *Int Arch Allergy Appl Immunol* 82: 366-371

Foreman JC (1988) The skin as an organ for the study of the pharmacology of neuropeptides. *Skin Pharmacol* 1: 77-83

Fuchs E (1990) Epidermal differentiation: the bare essentials. *J Cell Biol* 111: 2807-2814

Furlan A, Dyachuk V, Kastri ME, Calvo-Enrique L, Abdo H, Hadjab S, Chontorotzea T, Akkuratova N, Usoskin D, Kamenev D *et al* (2017) Multipotent peripheral glial cells generate neuroendocrine cells of the adrenal medulla. *Science* 357

Gabriel V (2011) Hypertrophic scar. *Phys Med Rehabil Clin N Am* 22: 301-310, vi

Gabriel VA (2009) Transforming growth factor-beta and angiotensin in fibrosis and burn injuries. *J Burn Care Res* 30: 471-481

Gamble HJ, Eames RA (1964) AN ELECTRON MICROSCOPE STUDY OF THE CONNECTIVE TISSUES OF HUMAN PERIPHERAL NERVE. *J Anat* 98: 655-663

Gao FL, Jin R, Zhang L, Zhang YG (2013) The contribution of melanocytes to pathological scar formation during wound healing. *Int J Clin Exp Med* 6: 609-613

Gao X, Gao M, Gorecka J, Langford J, Liu J, Luo J, Taniguchi R, Matsubara Y, Liu H, Guo L *et al* (2021) Human-Induced Pluripotent Stem-Cell-Derived Smooth Muscle Cells Increase Angiogenesis to Treat Hindlimb Ischemia. *Cells* 10

Garantziotis S, Savani RC (2019) Hyaluronan biology: A complex balancing act of structure, function, location and context. *Matrix Biol* 78-79: 1-10

Garg HG, Siebert JW, Garg A, Neame PJ (1996) Inseparable iduronic acid-containing proteoglycan PG(IdoA) preparations of human skin and post-burn scar tissues: evidence for elevated levels of PG(IdoA)-I in hypertrophic scar by N-terminal sequencing. *Carbohydr Res* 284: 223-228

Garratt AN, Britsch S, Birchmeier C (2000) Neuregulin, a factor with many functions in the life of a schwann cell. *Bioessays* 22: 987-996

Gauglitz GG, Korting HC, Pavicic T, Ruzicka T, Jeschke MG (2011) Hypertrophic scarring and keloids: pathomechanisms and current and emerging treatment strategies. *Mol Med* 17: 113-125

Getting SJ, Mahoney DJ, Cao T, Rugg MS, Fries E, Milner CM, Perretti M, Day AJ (2002) The link module from human TSG-6 inhibits neutrophil migration in a hyaluronan- and inter-alpha -inhibitor-independent manner. *J Biol Chem* 277: 51068-51076

Geyer SH, Nöhammer MM, Mathä M, Reissig L, Tinhofer IE, Weninger WJ (2014) High-resolution episcopic microscopy (HREM): a tool for visualizing skin biopsies. *Microsc Microanal* 20: 1356-1364

Giamarchi A, Padilla F, Crest M, Honore E, Delmas P (2006) TRPP2: Ca²⁺-permeable cation channel and more. *Cell Mol Biol (Noisy-le-grand)* 52: 105-114

Gibbons CH, Illigens BM, Wang N, Freeman R (2009) Quantification of sweat gland innervation: a clinical-pathologic correlation. *Neurology* 72: 1479-1486

Glass DA, 2nd (2017) Current Understanding of the Genetic Causes of Keloid Formation. *J Investig Dermatol Symp Proc* 18: S50-s53

Godwin ARF, Singh M, Lockhart-Cairns MP, Alanazi YF, Cain SA, Baldock C (2019) The role of fibrillin and microfibril binding proteins in elastin and elastic fibre assembly. *Matrix Biol* 84: 17-30

Goerdts S, Orfanos CE (1999) Other functions, other genes: alternative activation of antigen-presenting cells. *Immunity* 10: 137-142

Gomez-Sanchez JA, Carty L, Iruarrizaga-Lejarreta M, Palomo-Irigoyen M, Varela-Rey M, Griffith M, Hantke J, Macias-Camara N, Azkargorta M, Aurrekoetxea I *et al* (2015) Schwann cell autophagy, myelinophagy, initiates myelin clearance from injured nerves. *J Cell Biol* 210: 153-168

Gomez-Sanchez JA, Pilch KS, van der Lans M, Fazal SV, Benito C, Wagstaff LJ, Mirsky R, Jessen KR (2017) After Nerve Injury, Lineage Tracing Shows That Myelin and Remak Schwann Cells Elongate Extensively and Branch to Form Repair Schwann Cells, Which Shorten Radically on Remyelination. *J Neurosci* 37: 9086-9099

Granick M, Kimura M, Kim S, Daniali L, Cao X, Herbig U, Aviv A (2011) Telomere dynamics in keloids. *Eplasty* 11: e15

Greenlee-Wacker MC (2016) Clearance of apoptotic neutrophils and resolution of inflammation. *Immunol Rev* 273: 357-370

Gulamhuseinwala N, Mackey S, Meagher P, Powell B (2008) Should excised keloid scars be sent for routine histologic analysis? *Ann Plast Surg* 60: 186-187

Guo SK, Shen MF, Yao HW, Liu YS (2018) Enhanced Expression of TGFBI Promotes the Proliferation and Migration of Glioma Cells. *Cell Physiol Biochem* 49: 1097-1109

Gurtner GC, Werner S, Barrandon Y, Longaker MT (2008) Wound repair and regeneration. *Nature* 453: 314-321

Hachem S, Aguirre A, Vives V, Marks A, Gallo V, Legraverend C (2005) Spatial and temporal expression of S100B in cells of oligodendrocyte lineage. *Glia* 51: 81-97

Hacker S, Mittermayr R, Nickl S, Haider T, Lebherz-Eichinger D, Beer L, Mitterbauer A, Leiss H, Zimmermann M, Schweiger T *et al* (2016) Paracrine Factors from Irradiated Peripheral Blood Mononuclear Cells Improve Skin Regeneration and Angiogenesis in a Porcine Burn Model. *Sci Rep* 6: 25168

Hahn JM, Glaser K, McFarland KL, Aronow BJ, Boyce ST, Supp DM (2013) Keloid-derived keratinocytes exhibit an abnormal gene expression profile consistent with a distinct causal role in keloid pathology. *Wound Repair Regen* 21: 530-544

Hamill OP (2006) Twenty odd years of stretch-sensitive channels. *Pflugers Arch* 453: 333-351

Harris AK, Stopak D, Wild P (1981) Fibroblast traction as a mechanism for collagen morphogenesis. *Nature* 290: 249-251

Hasleton PS (1972) The internal surface area of the adult human lung. *J Anat* 112: 391-400

Hawthorne B, Simmons JK, Stuart B, Tung R, Zamierowski DS, Mellott AJ (2021) Enhancing wound healing dressing development through interdisciplinary collaboration. *J Biomed Mater Res B Appl Biomater* 109: 1967-1985

Hayakawa T, Hashimoto Y, Myokei Y, Aoyama H, Izawa Y (1979) Changes in type of collagen during the development of human post-burn hypertrophic scars. *Clin Chim Acta* 93: 119-125

He H, Suryawanshi H, Morozov P, Gay-Mimbrera J, Del Duca E, Kim HJ, Kameyama N, Estrada Y, Der E, Krueger JG *et al* (2020) Single-cell transcriptome analysis of human skin identifies novel fibroblast subpopulation and enrichment of immune subsets in atopic dermatitis. *J Allergy Clin Immunol* 145: 1615-1628

He S, Blombäck M, Bark N, Johnsson H, Wallén NH (2010) The direct thrombin inhibitors (argatroban, bivalirudin and lepirudin) and the indirect Xa-inhibitor (danaparoid) increase fibrin network porosity and thus facilitate fibrinolysis. *Thromb Haemost* 103: 1076-1084

He S, Yang Y, Liu X, Huang W, Zhang X, Yang S, Zhang X (2012) Compound Astragalus and Salvia miltiorrhiza extract inhibits cell proliferation, invasion and collagen synthesis in keloid fibroblasts by mediating transforming growth factor- β /Smad pathway. *Br J Dermatol* 166: 564-574

Helander HF, Fändriks L (2014) Surface area of the digestive tract - revisited. *Scand J Gastroenterol* 49: 681-689

Hendriks C, Drent M, De Kleijn W, Elfferich M, Wijnen P, De Vries J (2018) Everyday cognitive failure and depressive symptoms predict fatigue in sarcoidosis: A prospective follow-up study. *Respir Med* 138s: S24-s30

Hirata K, Kawabuchi M (2002) Myelin phagocytosis by macrophages and nonmacrophages during Wallerian degeneration. *Microsc Res Tech* 57: 541-547

Hochman B, Isoldi FC, Furtado F, Ferreira LM (2015) New approach to the understanding of keloid: psychoneuroimmune-endocrine aspects. *Clin Cosmet Investig Dermatol* 8: 67-73

Hochman B, Nahas FX, Sobral CS, Arias V, Locali RF, Juliano Y, Ferreira LM (2008) Nerve fibres: a possible role in keloid pathogenesis. *Br J Dermatol* 158: 651-652

Höke A (2006) Mechanisms of Disease: what factors limit the success of peripheral nerve regeneration in humans? *Nat Clin Pract Neurol* 2: 448-454

Holzer P (1998) Neurogenic vasodilatation and plasma leakage in the skin. *Gen Pharmacol* 30: 5-11

Hsu YC, Li L, Fuchs E (2014) Emerging interactions between skin stem cells and their niches. *Nat Med* 20: 847-856

Hu ZC, Tang B, Guo D, Zhang J, Liang YY, Ma D, Zhu JY (2014) Expression of insulin-like growth factor-1 receptor in keloid and hypertrophic scar. *Clin Exp Dermatol* 39: 822-828

Huang C, Akaishi S, Hyakusoku H, Ogawa R (2014) Are keloid and hypertrophic scar different forms of the same disorder? A fibroproliferative skin disorder hypothesis based on keloid findings. *Int Wound J* 11: 517-522

Huang C, Liu L, You Z, Wang B, Du Y, Ogawa R (2017) Keloid progression: a stiffness gap hypothesis. *Int Wound J* 14: 764-771

Huang C, Ogawa R (2013) Roles of lipid metabolism in keloid development. *Lipids Health Dis* 12: 60

Hübner G, Brauchle M, Smola H, Madlener M, Fässler R, Werner S (1996) Differential regulation of pro-inflammatory cytokines during wound healing in normal and glucocorticoid-treated mice. *Cytokine* 8: 548-556

Hunt TK, Hopf HW (1997) Wound healing and wound infection. What surgeons and anesthesiologists can do. *Surg Clin North Am* 77: 587-606

Hunzelmann N, Anders S, Sollberg S, Schönherr E, Krieg T (1996) Co-ordinate induction of collagen type I and biglycan expression in keloids. *Br J Dermatol* 135: 394-399

Iheanacho F, Vellipuram AR (2022) Physiology, Mechanoreceptors. In: *StatPearls*, StatPearls Publishing

Copyright © 2022, StatPearls Publishing LLC.: Treasure Island (FL)

Ikeda M, Naitoh M, Kubota H, Ishiko T, Yoshikawa K, Yamawaki S, Kurokawa M, Utani A, Nakamura T, Nagata K *et al* (2009) Elastic fiber assembly is disrupted by excessive accumulation of chondroitin sulfate in the human dermal fibrotic disease, keloid. *Biochem Biophys Res Commun* 390: 1221-1228

Imanaka-Yoshida K, Matsumoto KI (2018) Multiple Roles of Tenascins in Homeostasis and Pathophysiology of Aorta. *Ann Vasc Dis* 11: 169-180

Imhof BA, Aurrand-Lions M (2004) Adhesion mechanisms regulating the migration of monocytes. *Nat Rev Immunol* 4: 432-444

Ingber DE (1993) Cellular tensegrity: defining new rules of biological design that govern the cytoskeleton. *J Cell Sci* 104 (Pt 3): 613-627

Ingber DE, Madri JA, Jamieson JD (1986) Basement membrane as a spatial organizer of polarized epithelia. Exogenous basement membrane reorients pancreatic epithelial tumor cells in vitro. *Am J Pathol* 122: 129-139

Inoue R, Jensen LJ, Shi J, Morita H, Nishida M, Honda A, Ito Y (2006) Transient receptor potential channels in cardiovascular function and disease. *Circ Res* 99: 119-131

Iqbal SA, Sidgwick GP, Bayat A (2012) Identification of fibrocytes from mesenchymal stem cells in keloid tissue: a potential source of abnormal fibroblasts in keloid scarring. *Arch Dermatol Res* 304: 665-671

Jacinto A, Martinez-Arias A, Martin P (2001) Mechanisms of epithelial fusion and repair. *Nat Cell Biol* 3: E117-123

Jacob CI, Dover JS, Kaminer MS (2001) Acne scarring: a classification system and review of treatment options. *J Am Acad Dermatol* 45: 109-117

Jessen KR, Arthur-Farraj P (2019) Repair Schwann cell update: Adaptive reprogramming, EMT, and stemness in regenerating nerves. *Glia* 67: 421-437

Jessen KR, Brennan A, Morgan L, Mirsky R, Kent A, Hashimoto Y, Gavrilovic J (1994) The Schwann cell precursor and its fate: a study of cell death and differentiation during gliogenesis in rat embryonic nerves. *Neuron* 12: 509-527

Jessen KR, Mirsky R (2005) The origin and development of glial cells in peripheral nerves. *Nat Rev Neurosci* 6: 671-682

Jessen KR, Mirsky R (2008) Negative regulation of myelination: relevance for development, injury, and demyelinating disease. *Glia* 56: 1552-1565

Jessen KR, Mirsky R (2016) The repair Schwann cell and its function in regenerating nerves. *J Physiol* 594: 3521-3531

Jessen KR, Mirsky R (2019a) The Success and Failure of the Schwann Cell Response to Nerve Injury. *Front Cell Neurosci* 13: 33

Jessen KR, Mirsky R (2019b) The Success and Failure of the Schwann Cell Response to Nerve Injury. *Frontiers in Cellular Neuroscience* 13: 33

Jessen KR, Mirsky R, Lloyd AC (2015) Schwann Cells: Development and Role in Nerve Repair. *Cold Spring Harb Perspect Biol* 7: a020487

Jiao H, Zhang T, Fan J, Xiao R (2017) The Superficial Dermis May Initiate Keloid Formation: Histological Analysis of the Keloid Dermis at Different Depths. *Front Physiol* 8: 885

Jin Q, Gui L, Niu F, Yu B, Lauda N, Liu J, Mao X, Chen Y (2018) Macrophages in keloid are potent at promoting the differentiation and function of regulatory T cells. *Exp Cell Res* 362: 472-476

Jing C, Jia-Han W, Hong-Xing Z (2010) Double-edged effects of neuropeptide substance P on repair of cutaneous trauma. *Wound Repair Regen* 18: 319-324

Jonsson S, Wiberg R, McGrath AM, Novikov LN, Wiberg M, Novikova LN, Kingham PJ (2013) Effect of delayed peripheral nerve repair on nerve regeneration, Schwann cell function and target muscle recovery. *PLoS One* 8: e56484

Jumper N, Hodgkinson T, Paus R, Bayat A (2017) A Role for Neuregulin-1 in Promoting Keloid Fibroblast Migration via ErbB2-mediated Signaling. *Acta Derm Venereol* 97: 675-684

Kabashima K, Honda T, Ginhoux F, Egawa G (2019) The immunological anatomy of the skin. *Nat Rev Immunol* 19: 19-30

Karamanos NK (2019) Extracellular matrix: key structural and functional meshwork in health and disease. *Febs j* 286: 2826-2829

Karamanos NK, Piperigkou Z, Theocharis AD, Watanabe H, Franchi M, Baud S, Brézillon S, Götte M, Passi A, Vigetti D *et al* (2018) Proteoglycan Chemical Diversity Drives Multifunctional Cell Regulation and Therapeutics. *Chem Rev* 118: 9152-9232

Karamanos NK, Theocharis AD, Neill T, Iozzo RV (2019) Matrix modeling and remodeling: A biological interplay regulating tissue homeostasis and diseases. *Matrix Biol* 75-76: 1-11

Khallou-Laschet J, Varthaman A, Fornasa G, Compain C, Gaston AT, Clement M, Dussiot M, Levillain O, Graff-Dubois S, Nicoletti A *et al* (2010) Macrophage plasticity in experimental atherosclerosis. *PLoS One* 5: e8852

Khoo YT, Ong CT, Mukhopadhyay A, Han HC, Do DV, Lim IJ, Phan TT (2006) Upregulation of secretory connective tissue growth factor (CTGF) in keratinocyte-fibroblast coculture contributes to keloid pathogenesis. *J Cell Physiol* 208: 336-343

Khorshid FA (2005) Comparative study of keloid formation in humans and laboratory animals. *Med Sci Monit* 11: Br212-219

Kim Y, Remacle AG, Chernov AV, Liu H, Shubayev I, Lai C, Dolkas J, Shiryayev SA, Golubkov VS, Mizisin AP *et al* (2012) The MMP-9/TIMP-1 axis controls the status of differentiation and function of myelin-forming Schwann cells in nerve regeneration. *PLoS One* 7: e33664

Kioussi C, Gross MK, Gruss P (1995) Pax3: a paired domain gene as a regulator in PNS myelination. *Neuron* 15: 553-562

Kiprono SK, Chaula BM, Masenga JE, Muchunu JW, Mavura DR, Moehrle M (2015) Epidemiology of keloids in normally pigmented Africans and African people with albinism: population-based cross-sectional survey. *Br J Dermatol* 173: 852-854

Kirkness MW, Lehmann K, Forde NR (2019) Mechanics and structural stability of the collagen triple helix. *Curr Opin Chem Biol* 53: 98-105

Kischer CW (1984) Comparative ultrastructure of hypertrophic scars and keloids. *Scan Electron Microsc*: 423-431

Kischer CW, Hendrix MJ (1983) Fibronectin (FN) in hypertrophic scars and keloids. *Cell Tissue Res* 231: 29-37

Kischer CW, Thies AC, Chvapil M (1982) Perivascular myofibroblasts and microvascular occlusion in hypertrophic scars and keloids. *Hum Pathol* 13: 819-824

Komi DEA, Khomtchouk K, Santa Maria PL (2020) A Review of the Contribution of Mast Cells in Wound Healing: Involved Molecular and Cellular Mechanisms. *Clin Rev Allergy Immunol* 58: 298-312

Koo JY, Smith LL (1991) Psychologic aspects of acne. *Pediatr Dermatol* 8: 185-188

Krieg T, Aumailley M (2011) The extracellular matrix of the dermis: flexible structures with dynamic functions. *Exp Dermatol* 20: 689-695

Kwan PO, Tredget EE (2017) Biological Principles of Scar and Contracture. *Hand Clin* 33: 277-292

Kwon YK, Bhattacharyya A, Alberta JA, Giannobile WV, Cheon K, Stiles CD, Pomeroy SL (1997) Activation of ErbB2 during wallerian degeneration of sciatic nerve. *J Neurosci* 17: 8293-8299

Lacar B, Linker SB, Jaeger BN, Krishnaswami SR, Barron JJ, Kelder MJE, Parylak SL, Paquola ACM, Venepally P, Novotny M *et al* (2016) Nuclear RNA-seq of single neurons reveals molecular signatures of activation. *Nat Commun* 7: 11022

Ladin DA, Hou Z, Patel D, McPhail M, Olson JC, Saed GM, Fivenson DP (1998) p53 and apoptosis alterations in keloids and keloid fibroblasts. *Wound Repair Regen* 6: 28-37

Lansman JB (1988) Endothelial mechanosensors. Going with the flow. *Nature* 331: 481-482

Lawrence T, Natoli G (2011) Transcriptional regulation of macrophage polarization: enabling diversity with identity. *Nat Rev Immunol* 11: 750-761

Lazarus GS, Cooper DM, Knighton DR, Percoraro RE, Rodeheaver G, Robson MC (1994) Definitions and guidelines for assessment of wounds and evaluation of healing. *Wound Repair Regen* 2: 165-170

Le AD, Zhang Q, Wu Y, Messadi DV, Akhondzadeh A, Nguyen AL, Aghaloo TL, Kelly AP, Bertolami CN (2004) Elevated vascular endothelial growth factor in keloids: relevance to tissue fibrosis. *Cells Tissues Organs* 176: 87-94

Lee KS, Song JY, Suh MH (1991) Collagen mRNA expression detected by in situ hybridization in keloid tissue. *J Dermatol Sci* 2: 316-323

Lee SS, Yosipovitch G, Chan YH, Goh CL (2004) Pruritus, pain, and small nerve fiber function in keloids: a controlled study. *J Am Acad Dermatol* 51: 1002-1006

Lee YS, Hsu T, Chiu WC, Sarkozy H, Kulber DA, Choi A, Kim EW, Benya PD, Tuan TL (2016) Keloid-derived, plasma/fibrin-based skin equivalents generate de novo dermal and epidermal pathology of keloid fibrosis in a mouse model. *Wound Repair Regen* 24: 302-316

Lei H, Li J, Zhao Z, Liu L (2016) Inhibition of Ectodermal-Neural Cortex 1 Protects Neural Cells from Apoptosis Induced by Hypoxia and Hypoglycemia. *J Mol Neurosci* 59: 126-134

Leppert W, Malec-Milewska M, Zajackowska R, Wordliczek J (2018) Transdermal and Topical Drug Administration in the Treatment of Pain. *Molecules* 23

Levenson SM, Geever EF, Crowley LV, Oates JF, 3rd, Berard CW, Rosen H (1965) THE HEALING OF RAT SKIN WOUNDS. *Ann Surg* 161: 293-308

Lim KH, Itinteang T, Davis PF, Tan ST (2019) Stem Cells in Keloid Lesions: A Review. *Plast Reconstr Surg Glob Open* 7: e2228

Limandjaja GC, Niessen FB, Scheper RJ, Gibbs S (2020) The Keloid Disorder: Heterogeneity, Histopathology, Mechanisms and Models. *Front Cell Dev Biol* 8: 360

Limandjaja GC, van den Broek LJ, Waaijman T, Breetveld M, Monstrey S, Scheper RJ, Niessen FB, Gibbs S (2018) Reconstructed human keloid models show heterogeneity within keloid scars. *Arch Dermatol Res* 310: 815-826

Limandjaja GC, van den Broek LJ, Waaijman T, van Veen HA, Everts V, Monstrey S, Scheper RJ, Niessen FB, Gibbs S (2017) Increased epidermal thickness and abnormal epidermal differentiation in keloid scars. *Br J Dermatol* 176: 116-126

Lin JY, Fisher DE (2007) Melanocyte biology and skin pigmentation. *Nature* 445: 843-850

Lin QM, Zhao S, Zhou LL, Fang XS, Fu Y, Huang ZT (2013) Mesenchymal stem cells transplantation suppresses inflammatory responses in global cerebral ischemia: contribution of TNF- α -induced protein 6. *Acta Pharmacol Sin* 34: 784-792

Liu JY, Hu JH, Zhu QG, Li FQ, Sun HJ (2006) Substance P receptor expression in human skin keratinocytes and fibroblasts. *Br J Dermatol* 155: 657-662

Liu Q, Wang X, Jia Y, Long X, Yu N, Wang Y, Chen B (2016) Increased blood flow in keloids and adjacent skin revealed by laser speckle contrast imaging. *Lasers Surg Med* 48: 360-364

Liu X, Chen W, Zeng Q, Ma B, Li Z, Meng T, Chen J, Yu N, Zhou Z, Long X (2021) Single-cell RNA-seq reveals lineage-specific regulatory changes of fibroblasts and vascular endothelial cells in keloids. *J Invest Dermatol*

Liu X, Chen W, Zeng Q, Ma B, Li Z, Meng T, Chen J, Yu N, Zhou Z, Long X (2022) Single-Cell RNA-Sequencing Reveals Lineage-Specific Regulatory Changes of Fibroblasts and Vascular Endothelial Cells in Keloids. *J Invest Dermatol* 142: 124-135.e111

Lloyd-Burton S, Roskams AJ (2012) SPARC-like 1 (SC1) is a diversely expressed and developmentally regulated matricellular protein that does not compensate for the absence of SPARC in the CNS. *J Comp Neurol* 520: 2575-2590

Losquadro WD (2017) Anatomy of the Skin and the Pathogenesis of Nonmelanoma Skin Cancer. *Facial Plast Surg Clin North Am* 25: 283-289

Lovvorn HN, 3rd, Cheung DT, Nimni ME, Perelman N, Estes JM, Adzick NS (1999) Relative distribution and crosslinking of collagen distinguish fetal from adult sheep wound repair. *J Pediatr Surg* 34: 218-223

Lu F, Gao J, Ogawa R, Hyakusoku H, Ou C (2007) Biological differences between fibroblasts derived from peripheral and central areas of keloid tissues. *Plast Reconstr Surg* 120: 625-630

Lu WS, Zheng XD, Yao XH, Zhang LF (2015) Clinical and epidemiological analysis of keloids in Chinese patients. *Arch Dermatol Res* 307: 109-114

Lubetzki C, Sol-Foulon N, Desmazières A (2020) Nodes of Ranvier during development and repair in the CNS. *Nat Rev Neurol* 16: 426-439

Lucas T, Waisman A, Ranjan R, Roes J, Krieg T, Müller W, Roers A, Eming SA (2010) Differential roles of macrophages in diverse phases of skin repair. *J Immunol* 184: 3964-3977

Lund T, Onarheim H, Reed RK (1992) Pathogenesis of edema formation in burn injuries. *World J Surg* 16: 2-9

Lunn ER, Perry VH, Brown MC, Rosen H, Gordon S (1989) Absence of Wallerian Degeneration does not Hinder Regeneration in Peripheral Nerve. *Eur J Neurosci* 1: 27-33

Ma KH, Hung HA, Svaren J (2016) Epigenomic Regulation of Schwann Cell Reprogramming in Peripheral Nerve Injury. *J Neurosci* 36: 9135-9147

Ma X, Chen J, Xu B, Long X, Qin H, Zhao RC, Wang X (2015) Keloid-derived keratinocytes acquire a fibroblast-like appearance and an enhanced invasive capacity in a hypoxic microenvironment in vitro. *Int J Mol Med* 35: 1246-1256

Macarak EJ, Wermuth PJ, Rosenbloom J, Uitto J (2021) Keloid disorder: Fibroblast differentiation and gene expression profile in fibrotic skin diseases. *Exp Dermatol* 30: 132-145

Machado L, Esteves de Lima J, Fabre O, Proux C, Legendre R, Szegedi A, Varet H, Ingerslev LR, Barrès R, Relaix F *et al* (2017) In Situ Fixation Redefines Quiescence and Early Activation of Skeletal Muscle Stem Cells. *Cell Rep* 21: 1982-1993

Machado L, Geara P, Camps J, Dos Santos M, Teixeira-Clerc F, Van Herck J, Varet H, Legendre R, Pawlotsky JM, Sampaolesi M *et al* (2021) Tissue damage induces a conserved stress response that initiates quiescent muscle stem cell activation. *Cell Stem Cell* 28: 1125-1135.e1127

Mackman N, Tilley RE, Key NS (2007) Role of the extrinsic pathway of blood coagulation in hemostasis and thrombosis. *Arterioscler Thromb Vasc Biol* 27: 1687-1693

Madison KC (2003) Barrier function of the skin: "la raison d'être" of the epidermis. *J Invest Dermatol* 121: 231-241

Maeda D, Kubo T, Kiya K, Kawai K, Matsuzaki S, Kobayashi D, Fujiwara T, Katayama T, Hosokawa K (2019) Periostin is induced by IL-4/IL-13 in dermal fibroblasts and promotes RhoA/ROCK pathway-mediated TGF- β 1 secretion in abnormal scar formation. *J Plast Surg Hand Surg* 53: 288-294

Mahdavian Delavary B, van der Veer WM, van Egmond M, Niessen FB, Beelen RH (2011) Macrophages in skin injury and repair. *Immunobiology* 216: 753-762

Mak K, Manji A, Gallant-Behm C, Wiebe C, Hart DA, Larjava H, Häkkinen L (2009) Scarless healing of oral mucosa is characterized by faster resolution of inflammation and control of myofibroblast action compared to skin wounds in the red Duroc pig model. *J Dermatol Sci* 56: 168-180

Manou D, Caon I, Bouris P, Triantaphyllidou IE, Giaroni C, Passi A, Karamanos NK, Vignetti D, Theocharis AD (2019) The Complex Interplay Between Extracellular Matrix and Cells in Tissues. *Methods Mol Biol* 1952: 1-20

Marin V, Montero-Julian FA, Grès S, Boulay V, Bongrand P, Farnarier C, Kaplanski G (2001) The IL-6-soluble IL-6R α autocrine loop of endothelial activation as an intermediate between acute and chronic inflammation: an experimental model involving thrombin. *J Immunol* 167: 3435-3442

Marneros AG, Norris JE, Olsen BR, Reichenberger E (2001) Clinical genetics of familial keloids. *Arch Dermatol* 137: 1429-1434

Marshall CD, Hu MS, Leavitt T, Barnes LA, Lorenz HP, Longaker MT (2018) Cutaneous Scarring: Basic Science, Current Treatments, and Future Directions. *Adv Wound Care (New Rochelle)* 7: 29-45

Martin P (1997) Wound healing--aiming for perfect skin regeneration. *Science* 276: 75-81

Martini R, Fischer S, López-Vales R, David S (2008) Interactions between Schwann cells and macrophages in injury and inherited demyelinating disease. *Glia* 56: 1566-1577

Masuda S, Matsuura K, Shimizu T (2018) Inhibition of LYPD1 is critical for endothelial network formation in bioengineered tissue with human cardiac fibroblasts. *Biomaterials* 166: 109-121

Matsumura H, Engrav LH, Gibran NS, Yang TM, Grant JH, Yunusov MY, Fang P, Reichenbach DD, Heimbach DM, Isik FF (2001) Cones of skin occur where hypertrophic scar occurs. *Wound Repair Regen* 9: 269-277

Mazuelas H, Carrió M, Serra E (2020) Modeling tumors of the peripheral nervous system associated with Neurofibromatosis type 1: Reprogramming plexiform neurofibroma cells. *Stem Cell Res* 49: 102068

McDonald D, Cheng C, Chen Y, Zochodne D (2006) Early events of peripheral nerve regeneration. *Neuron Glia Biol* 2: 139-147

McIlroy M, McCartan D, Early S, P OG, Pennington S, Hill AD, Young LS (2010) Interaction of developmental transcription factor HOXC11 with steroid receptor coactivator SRC-1 mediates resistance to endocrine therapy in breast cancer [corrected]. *Cancer Res* 70: 1585-1594

Meenakshi J, Jayaraman V, Ramakrishnan KM, Babu M (2005) Ultrastructural differentiation of abnormal scars. *Ann Burns Fire Disasters* 18: 83-88

Meier C, Parmantier E, Brennan A, Mirsky R, Jessen KR (1999) Developing Schwann cells acquire the ability to survive without axons by establishing an autocrine circuit involving insulin-like growth factor, neurotrophin-3, and platelet-derived growth factor-BB. *J Neurosci* 19: 3847-3859

Melis P, van Noorden CJ, van der Horst CM (2006) Long-term results of wounds closed under a significant amount of tension. *Plast Reconstr Surg* 117: 259-265

Meszaros AJ, Reichner JS, Albina JE (1999) Macrophage phagocytosis of wound neutrophils. *J Leukoc Biol* 65: 35-42

Meyer D, Birchmeier C (1995) Multiple essential functions of neuregulin in development. *Nature* 378: 386-390

Midwood KS, Chiquet M, Tucker RP, Orend G (2016) Tenascin-C at a glance. *J Cell Sci* 129: 4321-4327

Mildner M, Hacker S, Haider T, Gschwandtner M, Werba G, Barresi C, Zimmermann M, Golabi B, Tschachler E, Ankersmit HJ (2013) Secretome of peripheral blood mononuclear cells enhances wound healing. *PLoS One* 8: e60103

Miller SJ, Burke EM, Rader MD, Coulombe PA, Lavker RM (1998) Re-epithelialization of porcine skin by the sweat apparatus. *J Invest Dermatol* 110: 13-19

Min HK, Maruyama H, Jang BK, Shimada M, Mirshahi F, Ren S, Oh Y, Puri P, Sanyal AJ (2016) Suppression of IGF binding protein-3 by palmitate promotes hepatic inflammatory responses. *Faseb j* 30: 4071-4082

Mindos T, Dun XP, North K, Doddrell RD, Schulz A, Edwards P, Russell J, Gray B, Roberts SL, Shivane A *et al* (2017) Merlin controls the repair capacity of Schwann cells after injury by regulating Hippo/YAP activity. *J Cell Biol* 216: 495-510

Mine S, Fortunel NO, Pagon H, Asselineau D (2008) Aging alters functionally human dermal papillary fibroblasts but not reticular fibroblasts: a new view of skin morphogenesis and aging. *PLoS One* 3: e4066

Mittal M, Tiruppathi C, Nepal S, Zhao YY, Grzych D, Soni D, Prockop DJ, Malik AB (2016) TNF α -stimulated gene-6 (TSG6) activates macrophage phenotype transition to prevent inflammatory lung injury. *Proc Natl Acad Sci U S A* 113: E8151-e8158

Mocellin S, Zavagno G, Nitti D (2008) The prognostic value of serum S100B in patients with cutaneous melanoma: a meta-analysis. *Int J Cancer* 123: 2370-2376

Mogha A, Harty BL, Carlin D, Joseph J, Sanchez NE, Suter U, Piao X, Cavalli V, Monk KR (2016) Gpr126/Adgrg6 Has Schwann Cell Autonomous and Nonautonomous Functions in Peripheral Nerve Injury and Repair. *J Neurosci* 36: 12351-12367

Molan P, Rhodes T (2015) Honey: A Biologic Wound Dressing. *Wounds* 27: 141-151

Monk KR, Feltri ML, Taveggia C (2015) New insights on Schwann cell development. *Glia* 63: 1376-1393

Monstrey S, Hoeksema H, Verbelen J, Pirayesh A, Blondeel P (2008) Assessment of burn depth and burn wound healing potential. *Burns* 34: 761-769

Monstrey S, Middelkoop E, Vranckx JJ, Bassetto F, Ziegler UE, Meaume S, Téot L (2014) Updated scar management practical guidelines: non-invasive and invasive measures. *J Plast Reconstr Aesthet Surg* 67: 1017-1025

Moon JH, Kwak SS, Park G, Jung HY, Yoon BS, Park J, Ryu KS, Choi SC, Maeng I, Kim B et al (2008) Isolation and characterization of multipotent human keloid-derived mesenchymal-like stem cells. *Stem Cells Dev* 17: 713-724

Morris JK, Lin W, Hauser C, Marchuk Y, Getman D, Lee KF (1999) Rescue of the cardiac defect in ErbB2 mutant mice reveals essential roles of ErbB2 in peripheral nervous system development. *Neuron* 23: 273-283

Morton LM, Phillips TJ (2016) Wound healing and treating wounds: Differential diagnosis and evaluation of chronic wounds. *J Am Acad Dermatol* 74: 589-605; quiz 605-586

Mosteller RD (1987) Simplified calculation of body-surface area. *N Engl J Med* 317: 1098

Mukhopadhyay A, Fan S, Dang VD, Khoo A, Ong CT, Lim IJ, Phan TT (2010) The role of hepatocyte growth factor/c-Met system in keloid pathogenesis. *J Trauma* 69: 1457-1466

Muramatsu Y, Kurosaki R, Watanabe H, Michimata M, Matsubara M, Imai Y, Araki T (2003) Expression of S-100 protein is related to neuronal damage in MPTP-treated mice. *Glia* 42: 307-313

Murao N, Seino K, Hayashi T, Ikeda M, Funayama E, Furukawa H, Yamamoto Y, Oyama A (2014) Treg-enriched CD4+ T cells attenuate collagen synthesis in keloid fibroblasts. *Exp Dermatol* 23: 266-271

Murdamoothoo D, Schwenzer A, Kant J, Rupp T, Marzeda A, Midwood K, Orend G (2018) Investigating cell-type specific functions of tenascin-C. *Methods Cell Biol* 143: 401-428

Murphrey MB, Miao JH, Zito PM (2022) Histology, Stratum Corneum. In: *StatPearls*, StatPearls Publishing

Copyright © 2022, StatPearls Publishing LLC.: Treasure Island (FL)

Murray JC (1994) Keloids and hypertrophic scars. *Clin Dermatol* 12: 27-37

Murray JC, Pollack SV, Pinnell SR (1981) Keloids: a review. *J Am Acad Dermatol* 4: 461-470

Mustoe TA, Cooter RD, Gold MH, Hobbs FD, Ramelet AA, Shakespeare PG, Stella M, Téot L, Wood FM, Ziegler UE (2002) International clinical recommendations on scar management. *Plast Reconstr Surg* 110: 560-571

Nagyeri G, Radacs M, Ghassemi-Nejad S, Trynieszewska B, Olasz K, Hutás G, Gyorfy Z, Hascall VC, Glant TT, Mikecz K (2011) TSG-6 protein, a negative regulator of inflammatory arthritis, forms a ternary complex with murine mast cell tryptases and heparin. *J Biol Chem* 286: 23559-23569

Nave KA (2010) Myelination and the trophic support of long axons. *Nat Rev Neurosci* 11: 275-283

Nedelec B, Ghahary A, Scott PG, Tredget EE (2000) Control of wound contraction. Basic and clinical features. *Hand Clin* 16: 289-302

Nguyen AV, Soulika AM (2019) The Dynamics of the Skin's Immune System. *Int J Mol Sci* 20

Nie Z, Cheng D, Pan C, Wei Z, Wang C, Wang C (2021) SH3BGRL3, transcribed by STAT3, facilitates glioblastoma tumorigenesis by activating STAT3 signaling. *Biochem Biophys Res Commun* 556: 114-120

Niessen FB, Spauwen PH, Schalkwijk J, Kon M (1999) On the nature of hypertrophic scars and keloids: a review. *Plast Reconstr Surg* 104: 1435-1458

Nishiguchi MA, Spencer CA, Leung DH, Leung TH (2018) Aging Suppresses Skin-Derived Circulating SDF1 to Promote Full-Thickness Tissue Regeneration. *Cell Rep* 24: 3383-3392.e3385

Nobes CD, Hall A (1995) Rho, rac, and cdc42 GTPases regulate the assembly of multimolecular focal complexes associated with actin stress fibers, lamellipodia, and filopodia. *Cell* 81: 53-62

Nobes CD, Hall A (1999) Rho GTPases control polarity, protrusion, and adhesion during cell movement. *J Cell Biol* 144: 1235-1244

Noble J, Munro CA, Prasad VS, Midha R (1998) Analysis of upper and lower extremity peripheral nerve injuries in a population of patients with multiple injuries. *J Trauma* 45: 116-122

Nolano M, Provitera V, Caporaso G, Stancanelli A, Leandri M, Biasiotta A, Cruccu G, Santoro L, Truini A (2013) Cutaneous innervation of the human face as assessed by skin biopsy. *J Anat* 222: 161-169

Nussenzweig V, Seligmann M, Pelmont J, Grabar P (1961) [The products of degradation of human fibrinogen by plasmin. I. Separation and physicochemical properties]. *Ann Inst Pasteur (Paris)* 100: 377-389

Ogawa R (2011) Mechanobiology of scarring. *Wound Repair Regen* 19 Suppl 1: s2-9

Ogawa R (2017) Keloid and Hypertrophic Scars Are the Result of Chronic Inflammation in the Reticular Dermis. *Int J Mol Sci* 18

Ogawa R (2022) The Most Current Algorithms for the Treatment and Prevention of Hypertrophic Scars and Keloids: A 2020 Update of the Algorithms Published 10 Years Ago. *Plast Reconstr Surg* 149: 79e-94e

Ogawa R, Akaishi S (2016) Endothelial dysfunction may play a key role in keloid and hypertrophic scar pathogenesis - Keloids and hypertrophic scars may be vascular disorders. *Med Hypotheses* 96: 51-60

Ohura T, Takahashi M, Ohura N, Jr. (2008) Influence of external forces (pressure and shear force) on superficial layer and subcutis of porcine skin and effects of dressing materials: are dressing materials beneficial for reducing pressure and shear force in tissues? *Wound Repair Regen* 16: 102-107

Okamoto A, Lovett M, Payan DG, Bunnett NW (1994) Interactions between neutral endopeptidase (EC 3.4.24.11) and the substance P (NK1) receptor expressed in mammalian cells. *Biochem J* 299 (Pt 3): 683-693

Ong CT, Khoo YT, Tan EK, Mukhopadhyay A, Do DV, Han HC, Lim IJ, Phan TT (2007) Epithelial-mesenchymal interactions in keloid pathogenesis modulate vascular endothelial growth factor expression and secretion. *J Pathol* 211: 95-108

Orgill DP, Manders EK, Sumpio BE, Lee RC, Attinger CE, Gurtner GC, Ehrlich HP (2009) The mechanisms of action of vacuum assisted closure: more to learn. *Surgery* 146: 40-51

Osso LA, Chan JR (2017) Architecting the myelin landscape. *Curr Opin Neurobiol* 47: 1-7

Otsuki T, Yata K, Takata-Tomokuni A, Hyodoh F, Miura Y, Sakaguchi H, Hatayama T, Hatada S, Tsujioka T, Sato Y *et al* (2004) Expression of protein gene product 9.5 (PGP9.5)/ubiquitin-C-terminal hydrolase 1 (UCHL-1) in human myeloma cells. *Br J Haematol* 127: 292-298

Pang X, Boucher W, Triadafilopoulos G, Sant GR, Theoharides TC (1996) Mast cell and substance P-positive nerve involvement in a patient with both irritable bowel syndrome and interstitial cystitis. *Urology* 47: 436-438

Papalexi E, Satija R (2018) Single-cell RNA sequencing to explore immune cell heterogeneity. *Nat Rev Immunol* 18: 35-45

Parfejevs V, Debbache J, Shakhova O, Schaefer SM, Glausch M, Wegner M, Suter U, Riekstina U, Werner S, Sommer L (2018) Injury-activated glial cells promote wound healing of the adult skin in mice. *Nat Commun* 9: 236

Park GH, Lee SJ, Yim H, Han JH, Kim HJ, Sohn YB, Ko JM, Jeong SY (2014) TAGLN expression is upregulated in NF1-associated malignant peripheral nerve sheath tumors by hypomethylation in its promoter and subpromoter regions. *Oncol Rep* 32: 1347-1354

Parkinson DB, Bhaskaran A, Arthur-Farraj P, Noon LA, Woodhoo A, Lloyd AC, Feltri ML, Wrabetz L, Behrens A, Mirsky R *et al* (2008) c-Jun is a negative regulator of myelination. *J Cell Biol* 181: 625-637

Parrinello S, Napoli I, Ribeiro S, Wingfield Digby P, Fedorova M, Parkinson DB, Doddrell RD, Nakayama M, Adams RH, Lloyd AC (2010) EphB signaling directs peripheral nerve regeneration through Sox2-dependent Schwann cell sorting. *Cell* 143: 145-155

Peltonen J, Hsiao LL, Jaakkola S, Sollberg S, Aumailley M, Timpl R, Chu ML, Uitto J (1991) Activation of collagen gene expression in keloids: co-localization of type I and VI collagen and transforming growth factor-beta 1 mRNA. *J Invest Dermatol* 97: 240-248

Plikus MV, Guerrero-Juarez CF, Ito M, Li YR, Dedhia PH, Zheng Y, Shao M, Gay DL, Ramos R, Hsi TC *et al* (2017) Regeneration of fat cells from myofibroblasts during wound healing. *Science* 355: 748-752

Quan TE, Cowper S, Wu SP, Bockenstedt LK, Bucala R (2004) Circulating fibrocytes: collagen-secreting cells of the peripheral blood. *Int J Biochem Cell Biol* 36: 598-606

Quintes S, Brinkmann BG, Ebert M, Fröb F, Kungl T, Arlt FA, Tarabykin V, Huylebroeck D, Meijer D, Suter U *et al* (2016) Zeb2 is essential for Schwann cell differentiation, myelination and nerve repair. *Nat Neurosci* 19: 1050-1059

Ramos C, Montaña M, Cisneros J, Sommer B, Delgado J, Gonzalez-Avila G (2007) Substance P up-regulates matrix metalloproteinase-1 and down-regulates collagen in human lung fibroblast. *Exp Lung Res* 33: 151-167

Ravanti L, Kähäri VM (2000) Matrix metalloproteinases in wound repair (review). *Int J Mol Med* 6: 391-407

Ray S, Ju X, Sun H, Finnerty CC, Herndon DN, Brasier AR (2013) The IL-6 trans-signaling-STAT3 pathway mediates ECM and cellular proliferation in fibroblasts from hypertrophic scar. *J Invest Dermatol* 133: 1212-1220

Reed CC, Iozzo RV (2002) The role of decorin in collagen fibrillogenesis and skin homeostasis. *Glycoconj J* 19: 249-255

Reina MA, Boezaart AP, Tubbs RS, Zsimevich Y, Fernández-Domínguez M, Fernández P, Sala-Blanch X (2020) Another (Internal) Epineurium: Beyond the Anatomical Barriers of Nerves. *Clin Anat* 33: 199-206

Reinisch CM, Traxler H, Piringer S, Tangl S, Nader A, Tschachler E (2008) Rarefaction of the peripheral nerve network in diabetic patients is associated with a pronounced reduction of terminal Schwann cells. *Diabetes Care* 31: 1219-1221

Reinisch CM, Tschachler E (2012) The dimensions and characteristics of the subepidermal nerve plexus in human skin--terminal Schwann cells constitute a substantial cell population within the superficial dermis. *J Dermatol Sci* 65: 162-169

Reinke JM, Sorg H (2012) Wound repair and regeneration. *Eur Surg Res* 49: 35-43

Reynolds ML, Fitzgerald M, Benowitz LI (1991) GAP-43 expression in developing cutaneous and muscle nerves in the rat hindlimb. *Neuroscience* 41: 201-211

Rickmann M, Wolff JR (1995) S100 protein expression in subpopulations of neurons of rat brain. *Neuroscience* 67: 977-991

Robinson SC, Scott KA, Balkwill FR (2002) Chemokine stimulation of monocyte matrix metalloproteinase-9 requires endogenous TNF-alpha. *Eur J Immunol* 32: 404-412

Robson MC, Steed DL, Franz MG (2001) Wound healing: biologic features and approaches to maximize healing trajectories. *Curr Probl Surg* 38: 72-140

Rockwell WB, Cohen IK, Ehrlich HP (1989) Keloids and hypertrophic scars: a comprehensive review. *Plast Reconstr Surg* 84: 827-837

Rodrigues M, Kosaric N, Bonham CA, Gurtner GC (2019) Wound Healing: A Cellular Perspective. *Physiol Rev* 99: 665-706

Romanovsky AA (2014) Skin temperature: its role in thermoregulation. *Acta Physiol (Oxf)* 210: 498-507

Rönkkö H, Göransson H, Siironen P, Taskinen HS, Vuorinen V, Röttä M (2011) The capacity of the distal stump of peripheral nerve to receive growing axons after two and six months denervation. *Scand J Surg* 100: 223-229

Roosterman D, Goerge T, Schneider SW, Bunnnett NW, Steinhoff M (2006) Neuronal control of skin function: the skin as a neuroimmunoendocrine organ. *Physiol Rev* 86: 1309-1379

Rotshenker S (2011) Wallerian degeneration: the innate-immune response to traumatic nerve injury. *J Neuroinflammation* 8: 109

Saffari TM, Bijlard E, Van Bodegraven EAM, Mureau MAM, Hovius SER, Huygen F (2018) Sensory perception and nerve fibre innervation in patients with keloid scars: an investigative study. *Eur J Dermatol* 28: 828-829

Sakurai M, Miyasaka Y (1986) Neural fibrosis and the effect of neurolysis. *J Bone Joint Surg Br* 68: 483-488

Sano H, Hokazono Y, Ogawa R (2018) Distensibility and Gross Elasticity of the Skin at Various Body Sites and Association with Pathological Scarring: A Case Study. *J Clin Aesthet Dermatol* 11: 15-18

Santoro MM, Gaudino G (2005) Cellular and molecular facets of keratinocyte reepithelization during wound healing. *Exp Cell Res* 304: 274-286

Sbai O, Devi TS, Melone MA, Feron F, Khrestchatisky M, Singh LP, Perrone L (2010) RAGE-TXNIP axis is required for S100B-promoted Schwann cell migration, fibronectin expression and cytokine secretion. *J Cell Sci* 123: 4332-4339

Scherberich A, Tucker RP, Degen M, Brown-Luedi M, Andres AC, Chiquet-Ehrismann R (2005) Tenascin-W is found in malignant mammary tumors, promotes alpha8 integrin-dependent motility and requires p38MAPK activity for BMP-2 and TNF-alpha induced expression in vitro. *Oncogene* 24: 1525-1532

Schmitt FO, Geren BB (1950) The fibrous structure of the nerve axon in relation to the localization of "neurotubules". *J Exp Med* 91: 499-504

Scholzen T, Armstrong CA, Bunnett NW, Luger TA, Olerud JE, Ansel JC (1998) Neuropeptides in the skin: interactions between the neuroendocrine and the skin immune systems. *Exp Dermatol* 7: 81-96

Scott JR, Muangman P, Gibran NS (2007) Making sense of hypertrophic scar: a role for nerves. *Wound Repair Regen* 15 Suppl 1: S27-31

Scott JR, Muangman PR, Tamura RN, Zhu KQ, Liang Z, Anthony J, Engrav LH, Gibran NS (2005) Substance P levels and neutral endopeptidase activity in acute burn wounds and hypertrophic scar. *Plast Reconstr Surg* 115: 1095-1102

Scott PG, Dodd CM, Ghahary A, Shen YJ, Tredget EE (1998) Fibroblasts from post-burn hypertrophic scar tissue synthesize less decorin than normal dermal fibroblasts. *Clin Sci (Lond)* 94: 541-547

Seddon HJ, Medawar PB, Smith H (1943) Rate of regeneration of peripheral nerves in man. *J Physiol* 102: 191-215

Seifert O, Bayat A, Geffers R, Dienus K, Buer J, Löfgren S, Matussek A (2008) Identification of unique gene expression patterns within different lesional sites of keloids. *Wound Repair Regen* 16: 254-265

Seifert O, Mrowietz U (2009) Keloid scarring: bench and bedside. *Arch Dermatol Res* 301: 259-272

Seki E, de Minicis S, Inokuchi S, Taura K, Miyai K, van Rooijen N, Schwabe RF, Brenner DA (2009) CCR2 promotes hepatic fibrosis in mice. *Hepatology* 50: 185-197

Sen CK, Gordillo GM, Roy S, Kirsner R, Lambert L, Hunt TK, Gottrup F, Gurtner GC, Longaker MT (2009) Human skin wounds: a major and snowballing threat to public health and the economy. *Wound Repair Regen* 17: 763-771

Senba E, Kashiba H (1996) Sensory afferent processing in multi-responsive DRG neurons. *Prog Brain Res* 113: 387-410

Shah JM, Omar E, Pai DR, Sood S (2012) Cellular events and biomarkers of wound healing. *Indian J Plast Surg* 45: 220-228

Shakespeare W (1813) *All's well that ends well*. [London] : [Thomas Tegg], [1813]

Shakespeare W (1975) *Othello* : 1622. Oxford : Clarendon Press, 1975.

Shakespeare W (1998) *The taming of the shrew*. Second revised edition / with new and updated critical essays and a revised bibliography. New York : Signet Classic, 1998.

Shakespeare W (2000) *Romeo and Juliet, 1597*. Oxford : published for the Malone Society by Oxford University Press, 2000.

Shakespeare W, Reed I, Johnson S, Steevens G (1823) *Measure for measure. Comedy of errors. Merchant of Venice. As you like it*. Collins & Hannay

Shakespeare Wa (1954) *The tragedy of Hamlet, Prince of Denmark*. [London] : The Folio Society, 1954.

Shamash S, Reichert F, Rotshenker S (2002) The cytokine network of Wallerian degeneration: tumor necrosis factor- α , interleukin-1 α , and interleukin-1 β . *J Neurosci* 22: 3052-3060

Shi J, Wang H, Guan H, Shi S, Li Y, Wu X, Li N, Yang C, Bai X, Cai W *et al* (2016) IL10 inhibits starvation-induced autophagy in hypertrophic scar fibroblasts via cross talk between the IL10-IL10R-STAT3 and IL10-AKT-mTOR pathways. *Cell Death Dis* 7: e2133

Shi Q, Zhao L, Xu C, Zhang L, Zhao H (2019) High Molecular Weight Hyaluronan Suppresses Macrophage M1 Polarization and Enhances IL-10 Production in PM(2.5)-Induced Lung Inflammation. *Molecules* 24

Shim J, Oh SJ, Yeo E, Park JH, Bae JH, Kim SH, Lee D, Lee JH (2022) Integrated analysis of single-cell and spatial transcriptomics in keloids: Highlights on fibro-vascular interactions in keloid pathogenesis. *J Invest Dermatol*

Shin H, Kim D, Helfman DM (2017) Tropomyosin isoform Tpm2.1 regulates collective and amoeboid cell migration and cell aggregation in breast epithelial cells. *Oncotarget* 8: 95192-95205

Shirshin EA, Gurfinkel YI, Priezzhev AV, Fadeev VV, Lademann J, Darvin ME (2017) Two-photon autofluorescence lifetime imaging of human skin papillary dermis in vivo: assessment of blood capillaries and structural proteins localization. *Sci Rep* 7: 1171

Siepmann T, Frenz E, Penzlin AI, Goelz S, Zago W, Friehs I, Kubasch ML, Wienecke M, Löhle M, Schrepf W *et al* (2016) Pilomotor function is impaired in patients with Parkinson's disease: A study of the adrenergic axon-reflex response and autonomic functions. *Parkinsonism Relat Disord* 31: 129-134

Siepmann T, Gibbons CH, Illigens BM, Lafo JA, Brown CM, Freeman R (2012) Quantitative pilomotor axon reflex test: a novel test of pilomotor function. *Arch Neurol* 69: 1488-1492

Silva WN, Leonel C, Prazeres P, Sena IFG, Guerra DAP, Heller D, Diniz IMA, Fortuna V, Mintz A, Birbrair A (2018) Role of Schwann cells in cutaneous wound healing. *Wound Repair Regen* 26: 392-397

Silver FH, Siperko LM, Seehra GP (2003) Mechanobiology of force transduction in dermal tissue. *Skin Res Technol* 9: 3-23

Simader E, Traxler D, Kasiri MM, Hofbauer H, Wolzt M, Glogner C, Storck A, Mildner M, Gouya G, Geusau A *et al* (2017) Safety and tolerability of topically administered autologous, apoptotic PBMC secretome (APOSEC) in dermal wounds: a randomized Phase 1 trial (MARSYAS I). *Sci Rep* 7: 6216

Sindic CJ, Freund M, Van Regemorter N, Verellen-Dumoulin C, Masson PL (1984) S-100 protein in amniotic fluid of anencephalic fetuses. *Prenat Diagn* 4: 297-302

Singer AJ, Clark RA (1999) Cutaneous wound healing. *N Engl J Med* 341: 738-746

Singh Malik D, Mital N, Kaur G (2016) Topical drug delivery systems: a patent review. *Expert Opin Ther Pat* 26: 213-228

Slovin S, Carissimo A, Panariello F, Grimaldi A, Bouché V, Gambardella G, Cacchiarelli D (2021) Single-Cell RNA Sequencing Analysis: A Step-by-Step Overview. *Methods Mol Biol* 2284: 343-365

Smack DP, Korge BP, James WD (1994) Keratin and keratinization. *J Am Acad Dermatol* 30: 85-102

Smith MM, Melrose J (2015) Proteoglycans in Normal and Healing Skin. *Adv Wound Care (New Rochelle)* 4: 152-173

Sogabe Y, Akimoto S, Abe M, Ishikawa O, Takagi Y, Imokawa G (2002) Functions of the stratum corneum in systemic sclerosis as distinct from hypertrophic scar and keloid functions. *J Dermatol Sci* 29: 49-53

Sokabe M, Naruse K, Sai S, Yamada T, Kawakami K, Inoue M, Murase K, Miyazu M (1997) Mechanotransduction and intracellular signaling mechanisms of stretch-induced remodeling in endothelial cells. *Heart Vessels Suppl* 12: 191-193

Sokabe M, Sachs F (1990) The structure and dynamics of patch-clamped membranes: a study using differential interference contrast light microscopy. *J Cell Biol* 111: 599-606

Solé-Boldo L, Raddatz G, Schütz S, Mallm JP, Rippe K, Lonsdorf AS, Rodríguez-Paredes M, Lyko F (2020) Single-cell transcriptomes of the human skin reveal age-related loss of fibroblast priming. *Commun Biol* 3: 188

Sommerlad BC, Creasey JM (1978) The stretched scar: a clinical and histological study. *Br J Plast Surg* 31: 34-45

Sontheimer RD (2014) Skin is not the largest organ. *J Invest Dermatol* 134: 581-582

Sorg H, Krueger C, Vollmar B (2007) Intravital insights in skin wound healing using the mouse dorsal skin fold chamber. *J Anat* 211: 810-818

Sorushanova A, Delgado LM, Wu Z, Shologu N, Kshirsagar A, Raghunath R, Mullen AM, Bayon Y, Pandit A, Raghunath M *et al* (2019) The Collagen Suprafamily: From Biosynthesis to Advanced Biomaterial Development. *Adv Mater* 31: e1801651

Steen KH, Reeh PW, Anton F, Handwerker HO (1992) Protons selectively induce lasting excitation and sensitization to mechanical stimulation of nociceptors in rat skin, in vitro. *J Neurosci* 12: 86-95

Stewart HJ, Brennan A, Rahman M, Zoidl G, Mitchell PJ, Jessen KR, Mirsky R (2001) Developmental regulation and overexpression of the transcription factor AP-2, a potential regulator of the timing of Schwann cell generation. *Eur J Neurosci* 14: 363-372

Stoll G, Müller HW (1999) Nerve injury, axonal degeneration and neural regeneration: basic insights. *Brain Pathol* 9: 313-325

Stone RC, Pastar I, Ojeh N, Chen V, Liu S, Garzon KI, Tomic-Canic M (2016) Epithelial-mesenchymal transition in tissue repair and fibrosis. *Cell Tissue Res* 365: 495-506

Stout RD, Watkins SK, Suttles J (2009) Functional plasticity of macrophages: in situ reprogramming of tumor-associated macrophages. *J Leukoc Biol* 86: 1105-1109

Stratton JA, Holmes A, Rosin NL, Sinha S, Vohra M, Burma NE, Trang T, Midha R, Biernaskie J (2018) Macrophages Regulate Schwann Cell Maturation after Nerve Injury. *Cell Rep* 24: 2561-2572.e2566

Strodtbeck F (2001) Physiology of wound healing. *Newborn and Infant Nursing Reviews* 1: 43-52

Suarez E, Syed F, Alonso-Rasgado T, Mandal P, Bayat A (2013) Up-regulation of tension-related proteins in keloids: knockdown of Hsp27, $\alpha\beta 1$ -integrin, and PAI-2 shows convincing reduction of extracellular matrix production. *Plast Reconstr Surg* 131: 158e-173e

Sulaiman OA, Gordon T (2000) Effects of short- and long-term Schwann cell denervation on peripheral nerve regeneration, myelination, and size. *Glia* 32: 234-246

Sun LM, Wang KH, Lee YC (2014) Keloid incidence in Asian people and its comorbidity with other fibrosis-related diseases: a nationwide population-based study. *Arch Dermatol Res* 306: 803-808

Sunderland S (1951) A classification of peripheral nerve injuries producing loss of function. *Brain* 74: 491-516

Sunderland S, Bradley KC (1952) The perineurium of peripheral nerves. *Anat Rec* 113: 125-141

Suttho D, Mankhetkorn S, Binda D, Pazart L, Humbert P, Rolin G (2017) 3D modeling of keloid scars in vitro by cell and tissue engineering. *Arch Dermatol Res* 309: 55-62

Szpadarska AM, Zuckerman JD, DiPietro LA (2003) Differential injury responses in oral mucosal and cutaneous wounds. *J Dent Res* 82: 621-626

Tabib T, Morse C, Wang T, Chen W, Lafyatis R (2018) SFRP2/DPP4 and FMO1/LSP1 Define Major Fibroblast Populations in Human Skin. *J Invest Dermatol* 138: 802-810

Tammela T, Zarkada G, Wallgard E, Murtomäki A, Suchting S, Wirzenius M, Waltari M, Hellström M, Schomber T, Peltonen R *et al* (2008) Blocking VEGFR-3 suppresses angiogenic sprouting and vascular network formation. *Nature* 454: 656-660

Tan S, Khumalo N, Bayat A (2019) Understanding Keloid Pathobiology From a Quasi-Neoplastic Perspective: Less of a Scar and More of a Chronic Inflammatory Disease With Cancer-Like Tendencies. *Front Immunol* 10: 1810

Tan VL, Andrawos A, Ghabriel MN, Townsend GC (2014) Applied anatomy of the lingual nerve: relevance to dental anaesthesia. *Arch Oral Biol* 59: 324-335

Tang D, Kang R, Coyne CB, Zeh HJ, Lotze MT (2012) PAMPs and DAMPs: signal 0s that spur autophagy and immunity. *Immunol Rev* 249: 158-175

Taylor G, Lehrer MS, Jensen PJ, Sun TT, Lavker RM (2000) Involvement of follicular stem cells in forming not only the follicle but also the epidermis. *Cell* 102: 451-461

Teichert M, Milde L, Holm A, Stanicek L, Gengenbacher N, Savant S, Ruckdeschel T, Hasanov Z, Srivastava K, Hu J *et al* (2017) Pericyte-expressed Tie2 controls angiogenesis and vessel maturation. *Nat Commun* 8: 16106

Tey HL, Maddison B, Wang H, Ishiju Y, McMichael A, Marks M, Willford P, Maruzivab D, Ferdinando D, Dick J *et al* (2012) Cutaneous innervation and itch in keloids. *Acta Derm Venereol* 92: 529-531

Theocharis AD, Skandalis SS, Gialeli C, Karamanos NK (2016) Extracellular matrix structure. *Adv Drug Deliv Rev* 97: 4-27

Thiery JP, Aclouque H, Huang RY, Nieto MA (2009) Epithelial-mesenchymal transitions in development and disease. *Cell* 139: 871-890

Thomas AJ, Erickson CA (2009) FOXD3 regulates the lineage switch between neural crest-derived glial cells and pigment cells by repressing MITF through a non-canonical mechanism. *Development* 136: 1849-1858

Thomas AM, Harding KG, Moore K (1999) The structure and composition of chronic wound eschar. *J Wound Care* 8: 285-287

Tonnesen MG, Feng X, Clark RA (2000) Angiogenesis in wound healing. *J Investig Dermatol Symp Proc* 5: 40-46

Touchi R, Ueda K, Kurokawa N, Tsuji M (2016) Central regions of keloids are severely ischaemic. *J Plast Reconstr Aesthet Surg* 69: e35-41

Trace AP, Enos CW, Mantel A, Harvey VM (2016) Keloids and Hypertrophic Scars: A Spectrum of Clinical Challenges. *Am J Clin Dermatol* 17: 201-223

Tsao JW, Brown MC, Carden MJ, McLean WG, Perry VH (1994) Loss of the compound action potential: an electrophysiological, biochemical and morphological study of early events in axonal degeneration in the C57BL/Ola mouse. *Eur J Neurosci* 6: 516-524

Tsujita-Kyutoku M, Uehara N, Matsuoka Y, Kyutoku S, Ogawa Y, Tsubura A (2005) Comparison of transforming growth factor-beta/Smad signaling between normal dermal fibroblasts and fibroblasts derived from central and peripheral areas of keloid lesions. *In Vivo* 19: 959-963

Tuan TL, Nichter LS (1998) The molecular basis of keloid and hypertrophic scar formation. *Mol Med Today* 4: 19-24

Tucker RP, Degen M (2019) The Expression and Possible Functions of Tenascin-W During Development and Disease. *Front Cell Dev Biol* 7: 53

Tulandi T, Al-Sannan B, Akbar G, Ziegler C, Miner L (2011) Prospective study of intraabdominal adhesions among women of different races with or without keloids. *Am J Obstet Gynecol* 204: 132.e131-134

Ud-Din S, Bayat A (2014) New insights on keloids, hypertrophic scars, and striae. *Dermatol Clin* 32: 193-209

Ulrich D, Ulrich F, Unglaub F, Piatkowski A, Pallua N (2010) Matrix metalloproteinases and tissue inhibitors of metalloproteinases in patients with different types of scars and keloids. *J Plast Reconstr Aesthet Surg* 63: 1015-1021

Vallet SD, Ricard-Blum S (2019) Lysyl oxidases: from enzyme activity to extracellular matrix cross-links. *Essays Biochem* 63: 349-364

Van Acker N, Ragé M, Sluydts E, Knaapen MW, De Bie M, Timmers M, Fransen E, Duymelinck C, De Schepper S, Anand P *et al* (2016) Automated PGP9.5 immunofluorescence staining: a valuable tool in the assessment of small fiber neuropathy? *BMC Res Notes* 9: 280

van den Brink SC, Sage F, Vértesy Á, Spanjaard B, Peterson-Maduro J, Baron CS, Robin C, van Oudenaarden A (2017) Single-cell sequencing reveals dissociation-induced gene expression in tissue subpopulations. *Nat Methods* 14: 935-936

van der Bijl I, de Korte D, Middelkoop E (2021) Variation in platelet-rich plasma compositions used for wound healing indications. *Wound Repair Regen* 29: 284-287

van der Veer WM, Bloemen MC, Ulrich MM, Molema G, van Zuijlen PP, Middelkoop E, Niessen FB (2009) Potential cellular and molecular causes of hypertrophic scar formation. *Burns* 35: 15-29

van Velthoven CTJ, de Morree A, Egnér IM, Brett JO, Rando TA (2017) Transcriptional Profiling of Quiescent Muscle Stem Cells In Vivo. *Cell Rep* 21: 1994-2004

Verhaegen PD, van Zuijlen PP, Pennings NM, van Marle J, Niessen FB, van der Horst CM, Middelkoop E (2009) Differences in collagen architecture between keloid, hypertrophic scar, normotrophic scar, and normal skin: An objective histopathological analysis. *Wound Repair Regen* 17: 649-656

Vindin H, Mithieux SM, Weiss AS (2019) Elastin architecture. *Matrix Biol* 84: 4-16

Vorstandlechner V, Laggner M, Copic D, Klas K, Direder M, Chen Y, Golabi B, Haslik W, Radtke C, Tschachler E *et al* (2021) The serine proteases dipeptidyl-peptidase 4 and urokinase are key molecules in human and mouse scar formation. *Nat Commun* 12: 6242

Vorstandlechner V, Laggner M, Kalinina P, Haslik W, Radtke C, Shaw L, Lichtenberger BM, Tschachler E, Ankersmit HJ, Mildner M (2020) Deciphering the functional heterogeneity of skin fibroblasts using single-cell RNA sequencing. *Faseb j* 34: 3677-3692

Wajchenberg BL (2000) Subcutaneous and visceral adipose tissue: their relation to the metabolic syndrome. *Endocr Rev* 21: 697-738

Wallis S, Lloyd S, Wise I, Ireland G, Fleming TP, Garrod D (2000) The alpha isoform of protein kinase C is involved in signaling the response of desmosomes to wounding in cultured epithelial cells. *Mol Biol Cell* 11: 1077-1092

Wan YM, Wu HM, Li YH, Xu ZY, Yang JH, Liu C, He YF, Wang MJ, Wu XN, Zhang Y (2020) TSG-6 Inhibits Oxidative Stress and Induces M2 Polarization of Hepatic Macrophages in Mice With Alcoholic Hepatitis via Suppression of STAT3 Activation. *Front Pharmacol* 11: 10

Wang J, Dodd C, Shankowsky HA, Scott PG, Tredget EE (2008) Deep dermal fibroblasts contribute to hypertrophic scarring. *Lab Invest* 88: 1278-1290

Wang J, Jiao H, Stewart TL, Shankowsky HA, Scott PG, Tredget EE (2007) Increased TGF-beta-producing CD4+ T lymphocytes in postburn patients and their potential interaction with dermal fibroblasts in hypertrophic scarring. *Wound Repair Regen* 15: 530-539

Wang ML, Rivlin M, Graham JG, Beredjikian PK (2019) Peripheral nerve injury, scarring, and recovery. *Connect Tissue Res* 60: 3-9

Wang S, Meng XM, Ng YY, Ma FY, Zhou S, Zhang Y, Yang C, Huang XR, Xiao J, Wang YY *et al* (2016) TGF- β /Smad3 signalling regulates the transition of bone marrow-derived macrophages into myofibroblasts during tissue fibrosis. *Oncotarget* 7: 8809-8822

Wang X, Liu K, Ruan M, Yang J, Gao Z (2018) Gallic acid inhibits fibroblast growth and migration in keloids through the AKT/ERK signaling pathway. *Acta Biochim Biophys Sin (Shanghai)* 50: 1114-1120

Wang Z, Fong KD, Phan TT, Lim IJ, Longaker MT, Yang GP (2006) Increased transcriptional response to mechanical strain in keloid fibroblasts due to increased focal adhesion complex formation. *J Cell Physiol* 206: 510-517

Wang ZC, Zhao WY, Cao Y, Liu YQ, Sun Q, Shi P, Cai JQ, Shen XZ, Tan WQ (2020) The Roles of Inflammation in Keloid and Hypertrophic Scars. *Front Immunol* 11: 603187

Watanabe Y, Broders-Bondon F, Baral V, Paul-Gilloteaux P, Pingault V, Dufour S, Bondurand N (2013) Sox10 and Itgb1 interaction in enteric neural crest cell migration. *Dev Biol* 379: 92-106

Webster HD, Martin R, O'Connell MF (1973) The relationships between interphase Schwann cells and axons before myelination: a quantitative electron microscopic study. *Dev Biol* 32: 401-416

Wei JCJ, Edwards GA, Martin DJ, Huang H, Crichton ML, Kendall MAF (2017) Allometric scaling of skin thickness, elasticity, viscoelasticity to mass for micro-medical device translation: from mice, rats, rabbits, pigs to humans. *Scientific Reports* 7: 15885

Weiner JA, Chun J (1999) Schwann cell survival mediated by the signaling phospholipid lysophosphatidic acid. *Proc Natl Acad Sci U S A* 96: 5233-5238

Weiss T, Taschner-Mandl S, Ambros PF, Ambros IM (2018) Detailed Protocols for the Isolation, Culture, Enrichment and Immunostaining of Primary Human Schwann Cells. *Methods Mol Biol* 1739: 67-86

Weiss T, Taschner-Mandl S, Bileck A, Slany A, Kromp F, Rifatbegovic F, Frech C, Windhager R, Kitzinger H, Tzou CH *et al* (2016) Proteomics and transcriptomics of peripheral nerve tissue and cells unravel new aspects of the human Schwann cell repair phenotype. *Glia* 64: 2133-2153

Werner S, Grose R (2003) Regulation of wound healing by growth factors and cytokines. *Physiol Rev* 83: 835-870

Wilgus TA (2007) Regenerative healing in fetal skin: a review of the literature. *Ostomy Wound Manage* 53: 16-31; quiz 32-13

Wipff PJ, Rifkin DB, Meister JJ, Hinz B (2007) Myofibroblast contraction activates latent TGF-beta1 from the extracellular matrix. *J Cell Biol* 179: 1311-1323

Woldeyesus MT, Britsch S, Riethmacher D, Xu L, Sonnenberg-Riethmacher E, Abou-Rebyeh F, Harvey R, Caroni P, Birchmeier C (1999) Peripheral nervous system defects in erbB2 mutants following genetic rescue of heart development. *Genes Dev* 13: 2538-2548

Wolfram D, Tzankov A, Pülzl P, Piza-Katzer H (2009) Hypertrophic scars and keloids--a review of their pathophysiology, risk factors, and therapeutic management. *Dermatol Surg* 35: 171-181

Wong R, Geyer S, Weninger W, Guimberteau JC, Wong JK (2016) The dynamic anatomy and patterning of skin. *Exp Dermatol* 25: 92-98

Woo YC, Park SS, Subieta AR, Brennan TJ (2004) Changes in tissue pH and temperature after incision indicate acidosis may contribute to postoperative pain. *Anesthesiology* 101: 468-475

Woodhoo A, Alonso MB, Droggiti A, Turmaine M, D'Antonio M, Parkinson DB, Wilton DK, Al-Shawi R, Simons P, Shen J *et al* (2009) Notch controls embryonic Schwann cell differentiation, postnatal myelination and adult plasticity. *Nat Neurosci* 12: 839-847

Wu H, Kirita Y, Donnelly EL, Humphreys BD (2019) Advantages of Single-Nucleus over Single-Cell RNA Sequencing of Adult Kidney: Rare Cell Types and Novel Cell States Revealed in Fibrosis. *J Am Soc Nephrol* 30: 23-32

Wu YE, Pan L, Zuo Y, Li X, Hong W (2017) Detecting Activated Cell Populations Using Single-Cell RNA-Seq. *Neuron* 96: 313-329.e316

Wynn TA (2004) Fibrotic disease and the T(H)1/T(H)2 paradigm. *Nat Rev Immunol* 4: 583-594

Xie J, Chen L, Cao Y, Wu D, Xiong W, Zhang K, Shi J, Wang M (2021) Single-Cell Sequencing Analysis and Weighted Co-Expression Network Analysis Based on Public Databases Identified That TNC Is a Novel Biomarker for Keloid. *Front Immunol* 12: 783907

Xu JC, Xiao MF, Jakovcevski I, Sivukhina E, Hargus G, Cui YF, Irintchev A, Schachner M, Bernreuther C (2014) The extracellular matrix glycoprotein tenascin-R regulates neurogenesis during development and in the adult dentate gyrus of mice. *J Cell Sci* 127: 641-652

Yager DR, Nwomeh BC (1999) The proteolytic environment of chronic wounds. *Wound Repair Regen* 7: 433-441

Yagi Y, Muroga E, Naitoh M, Isogai Z, Matsui S, Ikehara S, Suzuki S, Miyachi Y, Utani A (2013) An ex vivo model employing keloid-derived cell-seeded collagen sponges for therapy development. *J Invest Dermatol* 133: 386-393

Yamaoka J, Di ZH, Sun W, Kawana S (2007) Erratum to "changes in cutaneous sensory nerve fibers induced by skin-scratching in mice". *J Dermatol Sci* 47: 172-182

Yan L, Cao R, Wang L, Liu Y, Pan B, Yin Y, Lv X, Zhuang Q, Sun X, Xiao R (2015) Epithelial-mesenchymal transition in keloid tissues and TGF-β1-induced hair follicle outer root sheath keratinocytes. *Wound Repair Regen* 23: 601-610

Yasuoka H, Jukic DM, Zhou Z, Choi AM, Feghali-Bostwick CA (2006a) Insulin-like growth factor binding protein 5 induces skin fibrosis: A novel murine model for dermal fibrosis. *Arthritis Rheum* 54: 3001-3010

Yasuoka H, Yamaguchi Y, Feghali-Bostwick CA (2009) The pro-fibrotic factor IGFBP-5 induces lung fibroblast and mononuclear cell migration. *Am J Respir Cell Mol Biol* 41: 179-188

Yasuoka H, Zhou Z, Pilewski JM, Oury TD, Choi AM, Feghali-Bostwick CA (2006b) Insulin-like growth factor-binding protein-5 induces pulmonary fibrosis and triggers mononuclear cellular infiltration. *Am J Pathol* 169: 1633-1642

Young WG, Worsham MJ, Joseph CL, Divine GW, Jones LR (2014) Incidence of keloid and risk factors following head and neck surgery. *JAMA Facial Plast Surg* 16: 379-380

Yu D, Shang Y, Yuan J, Ding S, Luo S, Hao L (2016) Wnt/ β -Catenin Signaling Exacerbates Keloid Cell Proliferation by Regulating Telomerase. *Cell Physiol Biochem* 39: 2001-2013

Yu WM, Feltri ML, Wrabetz L, Strickland S, Chen ZL (2005) Schwann cell-specific ablation of laminin gamma1 causes apoptosis and prevents proliferation. *J Neurosci* 25: 4463-4472

Yunna C, Mengru H, Lei W, Weidong C (2020) Macrophage M1/M2 polarization. *Eur J Pharmacol* 877: 173090

Zhang GY, Gao WY, Li X, Yi CG, Zheng Y, Li Y, Xiao B, Ma XJ, Yan L, Lu KH *et al* (2009) Effect of camptothecin on collagen synthesis in fibroblasts from patients with keloid. *Ann Plast Surg* 63: 94-99

Zhang J, Qiao Q, Liu M, He T, Shi J, Bai X, Zhang Y, Li Y, Cai W, Han S *et al* (2018) IL-17 Promotes Scar Formation by Inducing Macrophage Infiltration. *Am J Pathol* 188: 1693-1702

Zhang Q, Qiao Q, Gould LJ, Myers WT, Phillips LG (2010) Study of the neural and vascular anatomy of the anterolateral thigh flap. *J Plast Reconstr Aesthet Surg* 63: 365-371

Zhao B, Guan H, Liu JQ, Zheng Z, Zhou Q, Zhang J, Su LL, Hu DH (2017) Hypoxia drives the transition of human dermal fibroblasts to a myofibroblast-like phenotype via the TGF- β 1/Smad3 pathway. *Int J Mol Med* 39: 153-159

Zimmerman A, Bai L, Ginty DD (2014) The gentle touch receptors of mammalian skin. *Science* 346: 950-954

Zollinger AJ, Smith ML (2017) Fibronectin, the extracellular glue. *Matrix Biol* 60-61: 27-37

Curriculum Vitae

Dr. med. univ. Martin Leopold Direder

Date of Birth: October 15th, 1993
Nationality: Austria
E-Mail: martin.direder@meduniwien.ac.at

Education

since 2022	Resident, Department of Orthopedics and Trauma-Surgery, Medical University of Vienna
since 2020	PhD Studies, Vascular Biology, Medical University of Vienna
2019 – 2020	MDPhD Studies, Vascular Biology, Medical University of Vienna
2014 – 2020	Medical studies, Medical University of Vienna & Panepistimio Patron
2013 – 2014	Civilian service, Austrian Red Cross, Tulln
2013	Matura, Priv. HTL für Lebensmitteltechnologie Hollabrunn, course module: Fleischwirtschaft with Apprenticeship certificate: Fleischverarbeiter*in mit Gewerbeberechtigung

Clinical Training

2020	Clinical Clerkship in Endocrinology and Metabolism, Medical University of Vienna
2019 – 2020	Clinical Clerkship in Plastic, Reconstructive and Aesthetic Surgery, Medical University of Vienna
2019	Clinical Clerkship in Traumatology, Medical University of Vienna
2018	Clinical Clerkship in Psychiatry, Klinikum rechts der Isar, TUM, Munich
2017	Clinical Clerkship in Traumatology, University Hospital Krems
2017	Clinical Clerkship in Emergency and Intensive Care Medicine, University Hospital Krems
2017	Clinical Clerkship in Pediatric Surgery, SMZ Ost-Danube Hospital, Wien
2016	Clinical Clerkship in Internal Medicine, University Hospital Tulln
2016	Clinical Clerkship in General Medicine, Medical Centre Ziersdorf
2015	Clinical Clerkship in Orthopaedics, University Hospital Krems

Professional Career

2019 – 2020	Long-term clinical training, Traumatic Surgery, Medical University of Vienna, Mentor: Dr. ⁱⁿ Anna Antoni
2017 – 2019	Long-term clinical training, II. Orthopedics Department, Herz-Jesu Hospital Vienna
2017 – 2019	Research associate, Thoracic Surgery, Applied Immunology Laboratory
2017	Physician assistant, Momentum Surgery, Prim. Dr. Werner Anderl, Mödling
2015 – 2017	Sales, Fleischhauerei Kolobratnik, Kirchberg/Wagram
2014 – 2016	Summer job, Österreichische Post AG, Frauendorf an der Au
2013	Internship, Fleischwaren Berger GesmbH & Co KG, Sieghartskirchen
2012	Internship, Die Käsemacher, Vitis
2011	Internship, Bäckerei Peter Burger, Großweikersdorf

2010	Internship, Zuckerforschung Tulln GesmbH
2009	Internship, Butcher's shop Kolobratnik, Kirchberg/Wagram

Awards and Qualifications

2022	ESDR 2022 Scholarship Award by the European Society of Dermatological Research
2022	NK and Irene Cheung Family Scholarship
2019 – 2020	MDFPhD Excellence Programme, Medical University of Vienna
2013	Löffler-Müller-Grant for excellent performance
2013	Nomination DLG Sensorik Award 2013 Diploma thesis „Beschreibende Prüfung von Fleischerzeugnissen – Free - Choice Profiling – Hollabrunner Modell“
2011 – 2012	Head boy of the Priv. HTL für Lebensmitteltechnologie Hollabrunn
2011	Löffler-Müller-Grant for excellent performance
2011	Quality Management Training (with distinction)
2011	Business English Certificate Preliminary
2010	Löffler-Müller-Grant for excellent performance
2009	Löffler-Müller-Grant for excellent performance

Teaching Activity

2022 WS	Lecturer: TS Applied Immunology and Tissue Regeneration, Medical University of Vienna
2022 WS	Lecturer: JC Current Topics in Applied Immunology, Medical University of Vienna
2022 SS	Lecturer: TS Applied Immunology and Tissue Regeneration, Medical University of Vienna
2022 SS	Lecturer: JC Current Topics in Applied Immunology, Medical University of Vienna
2017 SS	Tutor: Organ Morphologie, Medical University of Vienna

Memberships of scientific societies

Österreichische Gesellschaft für Unfallchirurgie (ÖGU)
 Österreichische Gesellschaft für Dermatologie und Venerologie (ÖGDV)

Oral presentations

Direder, M.; „Schwann cells – an unexpected key player in keloid formation“; oral presentation: Plenary session, 51st annual ESDR meeting, Amsterdam, 30.09.2022

Direder, M.; “A unique Schwann cell subtype with repair-like and pro-fibrotic properties contributes to keloid formation“; Oral presentation: Joint session, Keystone Symposia: “Tissue Fibrosis and Repair: Mechanisms, Human Disease and Therapies” & “Resolution of Inflammation”, Keystone, 14.06.2022

Direder, M.; „An unexpected role of Schwann cells in Keloid formation “; oral presentation: 48. ADF-Tagung der Arbeitsgemeinschaft Dermatologische Forschung (ADF). virtual, 23.-26.02.2022

Direder, M.; „An unexpected role of Schwann cells in Keloid formation“; oral presentation: Skin Science Seminar, 25.03.2022, virtual, Department of Dermatologie, Medical University of Vienna

Direder, M.; „Schwann cells – Key players in the formation of Keloids?“; oral presentation: 6th Science Days dedicated to Dermatology Research in Austria der Österreichischen Gesellschaft für Dermatologie und Venerologie (ÖGDV). Mondsee, 26.06.2021

Direder, M.; „Schwann cells_The neglected cells in Keloid“; oral presentation: Skin Science Seminar, 30.04.2021, virtual, Department of Dermatologie, Medical University of Vienna

Poster presentations

Direder, M.; Weiss, T.; Copic, D.; Vorstandlechner, V.; Klas, K.; Laggner, M.; Wielscher, M.; Bormann, D.; Ankersmit, H. J.; Mildner, M.; „Schwann cells - an unexpected key player in keloid formation“; Poster: 51st annual ESDR meeting, Amsterdam, 28.-01.09.2022

Direder, M.; Weiss, T.; Wielscher, M.; Pfisterer, K.; Laggner, M.; Copic, D.; Klas, K.; Vorstandlechner, V.; Ankersmit, H. J.; Mildner, M.; „A unique Schwann cell subtype with repair-like and pro-fibrotic properties contributes to keloid formation“; Poster: Keystone Symposia: “Tissue Fibrosis and Repair: Mechanisms, Human Disease and Therapies” & “Resolution of Inflammation”, Keystone, 12.-16.06.2022

Direder, M.; Weiss, T.; Copic, D.; Vorstandlechner, V.; Klas, K.; Laggner, M.; Wielscher, M.; Radtke, C.; Golabi, B.; Ankersmit, H. J.; Mildner, M.; “An unexpected role of Schwann cells in Keloid formation“; Poster: 48. ADF-Tagung der Arbeitsgemeinschaft Dermatologische Forschung (ADF). virtuell, 23.-26.02.2022

Direder, M.; Weiss, T.; Copic, D.; Vorstandlechner, V.; Laggner, M.; Mildner, C.S.; Klas, K.; Bormann, D.; Haslik, W.; Radtke, C.; et al.; „Schwann cells – Key players in the formation of Keloids?“; Poster: 6th Science Days dedicated to Dermatology Research in Austria der Österreichischen Gesellschaft für Dermatologie und Venerologie (ÖGDV). Mondsee, 26.06.2021

Language Skills and Additional Qualifications

German (native language), English (C1),
IT-skills in R with focus on Single Cell Analysis, Adobe Illustrator, Microsoft Office, GraphPad Prism, SPSS

Social Engagement

since 2019	Archivist, Musikverein Kirchberg/Wagram
2015 – 2019	Chairman, Musikverein Kirchberg/Wagram
since 2013	Temporary Organist, Parish Wagram-Au
since 2012	Paramedic, Red Cross Austria
since 2010	Firefighter, Voluntary Fire Brigade Unterstockstall
since 2007	Member, Musikverein Kirchberg/Wagram

Publication List:

- 1 **Direder, M.**, T. Weiss, D. Copic, V. Vorstandlechner, M. Laggner, K. Pfisterer, C. S. Mildner, K. Klas, D. Bormann, W. Haslik, C. Radtke, M. Farlik, L. Shaw, B. Golabi, E. Tschachler, K. Hoetzenecker, H. J. Ankersmit and M. Mildner (2022). "Schwann cells contribute to keloid formation." **Matrix Biol. (IF:11.583)**
- 2 **Direder, M.**, M. Wielscher, T. Weiss, M. Laggner, D. Copic, K. Klas, D. Bormann, V. Vorstandlechner, E. Tschachler, H. J. Ankersmit and M. Mildner (2022). "The transcriptional profile of keloidal Schwann cells." **Exp. Mol Med. (IF:12.153)**
- 3 Mildner, C. S., D. Copic, M. Zimmermann, M. Lichtenauer, **M. Direder**, K. Klas, D. Bormann, A. Gugerell, B. Moser, K. Hoetzenecker, L. Beer, M. Gyöngyösi, H. J. Ankersmit and M. Laggner (2022). "Secretome of Stressed Peripheral Blood Mononuclear Cells Alters Transcriptome Signature in Heart, Liver, and Spleen after an Experimental Acute Myocardial Infarction: An In Silico Analysis." **Biology (Basel) 11(1). (IF:5.079)**
- 4 Laggner, M., M. T. Lingitz, D. Copic, **M. Direder**, K. Klas, D. Bormann, A. Gugerell, B. Moser, C. Radtke, S. Hacker, M. Mildner, H. J. Ankersmit and T. Haider (2022). "Severity of thermal burn injury is associated with systemic neutrophil activation." **Sci Rep 12(1): 1654. (IF:4.380)**
- 5 Copic D., D. Bormann, **M. Direder**, H. J. Ankersmit (2022). "Alpha-Gal specific humoral immune response and reported clinical consequence for cardiac valve replacement in patients below 65 years: moving beyond conjecture." **Eur J Cardiothorac Surg. (IF:4.191)**
- 6 Copic D., **M. Direder**, K. Schossleitner, M. Laggner, K. Klas, D. Bormann, H. J. Ankersmit, M. Mildner (2022). "Paracrine factors of stressed peripheral blood mononuclear cells activate pro-angiogenic and anti-proteolytic processes in whole blood cells and protect the endothelial barrier." **Pharmaceutics: under review. (IF:6.525)**
- 7 Laggner, M., G. Sánchez Acosta, C. Kitzmüller, D. Copic, F. Gruber, L. M. Altenburger, V. Vorstandlechner, A. Gugerell, **M. Direder**, K. Klas, D. Bormann, A. Peterbauer, A. Shibuya, B. Bohle, H. J. Ankersmit, M. Mildner (2022). "The secretome of irradiated peripheral blood mononuclear cells attenuates activation of mast cells and basophils." **EBioMedicine: (IF:8.143)**
- 8 Klas, K.; A. S. Ondracek, T. M. Hofbauer, A. Mangold, K. Pfisterer, M. Laggner, D. Copic, M. Direder, D. Bormann, H. J. Ankersmit, M. Mildner (2022). „The Effect of Paracrine Factors Released by Irradiated Peripheral Blood Mononuclear Cells on Neutrophil Extracellular Trap Formation." **Antioxidants (Basel): (IF:7.675)**
- 9 Rossiter, H., D. Copic, **M. Direder**, F. Gruber, S. Zoratto, M. Marchetti-Deschmann, C. Kremslehner, M. Sochorová, I. M. Nagelreiter, V. Mlitz, M. Buchberger, B. Lengauer, B. Golabi, S. Sukseree, M. Mildner, L. Eckhart and E. Tschachler (2021). "Autophagy protects murine preputial glands against premature aging, and controls their sebum phospholipid and pheromone profile." **Autophagy: 1-15. (IF:16.016)**
- 10 Vorstandlechner, V., M. Laggner, D. Copic, K. Klas, **M. Direder**, Y. Chen, B. Golabi, W. Haslik, C. Radtke, E. Tschachler, K. Hötzenecker, H. J. Ankersmit and M. Mildner (2021). "The serine proteases dipeptidyl-peptidase 4 and urokinase are key molecules in human and mouse scar formation." **Nat Commun 12(1): 6242. (IF:14.919)**
- 11 Klas, K., D. Copic, **M. Direder**, M. Laggner, P. S. Prucksamas, F. Gruber, H. J. Ankersmit and M. Mildner (2021). "Transcriptional Differences in Lipid-Metabolizing Enzymes in Murine Sebocytes Derived from Sebaceous Glands of the Skin and Preputial Glands." **Int J Mol Sci 22(21): 11631. (IF:5.924)**

Veraar, C., S. Schwarz, J. Thanner, **M. Direder**, P. M. Boehm, L. Harnoncourt, J. Ortmayr, C.

- 12 Veraar, J. Mascherbauer, W. Klepetko, M. Dworschak, H. J. Ankersmit and B. Moser (2021). "Transient perioperative inflammation following lung transplantation and major thoracic surgery with elective extracorporeal support: a prospective observational study." **Ann Transl Med** 9(5): 385. (IF:3.932)